All Dissertations   Dissertations

12-2011

EFFECT OF RELATIVE HUMIDITY AND TEMPERATURE CONTROL ON IN-CABIN THERMAL COMFORT STATE

Ali Alahmer
Clemson University, aal@clemson.edu

EFFECT OF RELATIVE HUMIDITY AND TEMPERATURE CONTROL ON IN-
CABIN THERMAL COMFORT STATE

_____

A Thesis
Presented to
the Graduate School of
Clemson University

_____

In Partial Fulfillment
of the Requirements for the Degree
Doctor of Philosophy
Mechanical Engineering

_____

by
Ali I. Alahmer
December, 2011

_____

Accepted by:
Dr. Mohammed A. Omar, Committee Chair
Dr. Mica Grujicic
Dr. Young Haung
Dr. Mohammed Daqaq

ABSTRACT

This dissertation discusses the effect of manipulating the relative humidity RH levels inside vehicular cabins on the thermal comfort and human occupants' thermal sensation. Three different techniques are used to investigate this effect. Firstly, thermodynamic and psychometric analyses are used to incorporate the effect of changing RH along with the dry bulb temperature on the human comfort window. Specifically, the study computes the effect of changing the relative humidity on the amount of heat rejected from the passenger compartment and the effect on occupants comfort zone. A practical system implementation is also discussed in terms of an evaporative cooler design. Secondly, a 3-D finite difference simulation is used to predict the RH effects on the thermal sensation metrics. The study uses the Berkeley and the Fanger models to investigate the human comfort using four specific perspectives; (i) the effect on other environmental conditions, (ii) the effect on the body segments temperature variation within the cabin, (iii) the cabin local sensation (LS) and comfort (LC) for the different body segments; in addition to the overall sensation (OS) and overall comfort (OC), (iv) the human sensation is also measured by the Predicted Mean Value (PMV) and the Predicted Percentage Dissatisfied (PPD) indices during the summer and the winter periods following the Fanger model calculations. Thirdly, the analysis and modeling of the vehicular thermal comfort parameters is conducted using a set of designed experiments aided by thermography measurements. The experiments employed a full size climatic chamber to host the test vehicle, to accurately assess the transient and steady

state temperature distributions of the test vehicle cabins. The experimental and simulation work show that controlling the RH levels along with the Dry Bulb Temperature helps the A/C system achieve the human comfort zone faster than the case if the RH value is not controlled. Also, the results show that changing the RH along with Dry Bulb Temperature inside vehicular cabins can improve the air conditioning efficiency by reducing the amount of heat removed. Finally, this work has developed the passenger thermal-comfort psychometric zones during summer and winter periods using Berkeley and Fanger models.

DEDICATION

       This thesis is dedicated to my parents, who gave me the greatest support throughout my education.

       Also, to the vest of my family, brothers and sisters with my sincere love.

ACKNOWLEDGMENTS

TABLE OF CONTENTS

<div align="right">**Page**</div>

Table of Contents (Continued)

Page

LIST OF TABLES

List of Tables (Continued)

Table   **Page**

LIST OF FIGURES

Figure **Page**

Figure   **Page**

Figure   **Page**

Figure **Page**

List of Figures (Continued)

Figure **Page**

CHAPTER ONE

INTRODUCTION

1.1 Motivation

Today's demands for better performance have produced an increase for vehicle environments requirement. Vehicular climatic control or Heating Ventilation and Air Conditioning (HVAC) systems operate on the in-cabin air through adjusting its dry bulb temperature to reach the thermal-comfort zone for human occupants. However, it relies on adjusting the cabin environment temperature while relying on the passengers to exchange heat with their environment to reach the desired steady state conditions. This approach is not optimal and will lead to increased loads on the HVAC system (compressor, fan, etc), hence leading to increased fuel consumption. Numerically, in the United States alone approximately 26 billion liters of fuel are consumed annually for cooling vehicle passenger compartments [1]. This number along with the growing demands for better vehicular energy utilization, and more efficient performing vehicles, have led to an increased interest in revising the current approach to mobile enclosures HVAC, through investigating and analyzing its sub-systems, its control strategies, and design. To provide an example, reducing the heat loads (mainly solar) that enter the passenger compartments through improved glazing, is becoming an important issue in the early stages of vehicle design. Additionally, new vehicles such as the Prius utilize a solar panel module to reject the stagnant hot air in the cabin before the conditioning starts.

1.2 Problem Statement

Current in-cabin thermal comfort control is based solely on dry bulb temperature manipulation is not optimal due to suffer from following distinct challenges [2]; its fast transient behavior that complicates predicting the optimum settings to achieve thermal comfort. Such transient behavior is due mainly to the short trip durations, where 85% of trips involve an average distance fewer than 18 km and with time durations from 15 to 30 minutes. Hence, through this period the passengers do not achieve the adequate heat transfer to be in the thermal comfort range [3]. Also the Non-uniformities associated with the cabin thermal environment due to the air temperature distribution, the solar flux, and the radiation heat flux from the cabin surrounding interior-trim surfaces, complicate the conditioning process. Furthermore, the multiple governing parameters of the cabin thermal comfort such as the solar incidence angle, the glass/glazing properties, the surrounding radiant heat and air velocity, affect the HVAC system performance [4, 5]. Finally, the variation in passengers' thermal loads in terms of; thermal sensation, clothing, number of passenger, metabolism rate, hinders the system robustness.

1.3 Research Objectives

The main objectives of this dissertation through optimize in-cabin climate control strategy by;

- Investigate the effect of changing the relative humidity on the amount of heat rejected from the passenger compartment and the effect of relative humidity on occupants comfort zone.

- Investigate the effect of manipulating Relative Humidity RH along with temperature on the in-cabin local and overall thermal sensation and comfort state.

- In addition, investigate the effect of changing RH on other environmental conditions such as the Dew Point Temperature (DPT, the humidity (H), the vapor pressure (vp) and the humidity ratio (ω) in the cabin.

- Lastly, develop the passenger thermal comfort zones during summer and winter periods by using Berkeley and Fanger models.

1.4 Research Significance

This study will be a significant endeavor in promoting a good work. At which, the potential extending building condition regime to in-cabin conditioning is not well investigated, so this research manipulate the relative humidity and temperature control on in-cabin to achieve the optimal thermal comfort because thermal comfort state can be achieved faster through manipulating both RH and temperature. Furthermore, the controlled manipulation of RH inside vehicle cabin has distinct advantages for respiratory health system. Finally, Controlling RH inside vehicle cabin can also effect on the cabin smell and odor.

1.5 Research Approach

To investigate the effect of relative humidity and dry bulb temperature control on in cabin human comfort, the following steps will be implemented:

- Firstly, Literature review – in this phase, a comprehensive review of the different models developed to predict vehicular cabins thermal comfort, in addition to the different experimental techniques were used related to this thesis was carried out. Those materials are mostly obtained from different books, internet, articles, and journals. The collected materials are studied and reviewed so that this thesis can provide new solution to an identified problem that is not addressed in the previous works.

- Secondly, psychometric and thermodynamic analysis will be conducted to incorporate the RH effect and temperature on thermal comfort. Also, a practical system implementation is also discussed in terms of an evaporative cooler design.

- Next, develop and validate a comprehensive 3-D finite difference thermal comfort model for vehicle cabin by capturing the relative humidity, velocity and temperature fields under actual and artificial scenarios. Also, the control of RH on thermal comfort will be assist terms standard thermal comfort indices (PMV, PPD) and Berkeley model.

- The experiments will be conducted to extract the boundary condition and vehicle conditioning system parameters.

- Lastly, develop the passenger thermal comfort envelopes during summer and winter periods by using Berkeley and Fanger models.

1.6 Thesis Organization

This thesis is divided into eight chapters. Chapter one presents the overview of the dissertation and highlights the motivation, objectives and approaches of the dissertation. A comprehensive review of the different models developed to predict vehicular cabins thermal comfort, in addition to the different experimental techniques used is presented in chapter two. In chapter three discuss a human thermal environment which includes basic parameters, the heat balance equation for human body and mathematical models to predict thermal comfort. In next three chapters, three key techniques were used in this dissertation to validate our research. So, chapter four presents the thermodynamic and psychometric analysis to investigate the effect of changing RH along with the dry bulb temperature on human comfort follow with a practical implementation in term of evaporative cooling. Chapter five uses two simulation models Berkeley and Fanger models to study human comfort upon controlling RH along with the dry bulb temperature (DBT). The design for thermal sensation and comfort states in vehicles cabins using experimental and simulation techniques are presented in chapter six. The develop of passenger thermal comfort envelopes during summer and winter periods by using Berkeley and Fanger models is offered in chapter seven. Finally, chapter eight summarizes the entire dissertation and shows the conclusion and future work.

CHAPTER TWO

VEHICULAR THERMAL HUMAN COMFORT; A COMPREHENSIVE

REVIEW

This chapter provides a comprehensive review of the different models developed to predict vehicular cabins thermal comfort, in addition to the different experimental techniques used. The review classifies the in-cabin modeling into; human physiological and psychological perspectives in addition to the compartment zone and the human thermal manikin modeling. While the experimental approaches are mainly; the subjective observers, the thermal manikins, and the Infrared Thermography. Additionally the chapter discusses and analyzes each of the thermal indices that are typically used in assessing the in-cabin conditions such as the Predicted Mean Value (PMV) index and the Predicted Percentage Dissatisfied (PPD). The chapter also highlights the main attributes of vehicular thermal comfort, in terms of its fast transient behavior, the in-homogeneity in the thermal fields associated with the high localized air velocity, solar loads and flux, in addition to the inherent variations related to the trip durations.

2.1 Introduction

Human thermal comfort is defined by The American Society of Heating Refrigeration and Air Conditioning Engineers (ASHRAE), as the state of mind that expresses satisfaction with the surrounding environment (ASHRAE Standard 55) [6]. The principal factors affecting human thermal comfort depends upon four physical

environmental variables; the air temperature, its relative humidity, the mean radiant temperature, and the relative air velocity; in addition to two independent but related parameters, which are the active level provided by metabolism and the thermal insulation value provided the clothing.

Maintaining thermal comfort for occupants in buildings or other enclosures, even in extreme climatic conditioning requirements and irrespective of the environmental outside conditions, has been the main focus for the Heating Ventilation and Air Conditioning (HVAC) design engineers and systems developers. On the other hand, the thermal comfort of vehicular occupants is gaining more importance due to the rising focus on comfortable mobility, in addition to the fact that, the time that people spend in vehicles (private or public transport) has grown substantially. Moreover comfortable vehicular climate control in many cases not only help to reduce the driver stress but also guarantee good visibility by avoiding the fogging phenomenon, hence contributing to safer driving experience. In addition, today's demand for better vehicular energy utilization and more efficient performance, have led to an increased interest in investigating and analyzing the system and design requirements for good indoor and vehicle environments. For example, the need to reduce the heat loads that enter passenger compartments has become an important issue in the early stages of vehicle design, also achieving an improved thermal comfort system will lead to substantial cost reductions. To provide a quantitative example, in the United States alone approximately 26 billion liters of fuel are consumed annually for cooling vehicle passenger compartments [1]. This cost can be reduced by improving climate control systems design.

The evaluation of the thermal comfort inside vehicle cabins has been studied in depth for a long time. Currently, there are international standards that resulted from studies based on subjective evaluations (human observers' vote) and quantified through specific indices. One of these indices is the Predicted Mean Value (PMV) index, which predicts the mean response of the thermal vote of a large group of people exposed to the same environment; the PMV is derived from the physics of heat transfer combined with an empirical fit to human sensation. The PMV establishes thermal strain based on a steady-state heat transfer between the human body and thermal comfort ratings from panel subject. However, the PMV has been proposed and established for homogenous conditions only and when applied in non-homogenous conditions as the case in vehicular cabins, it did not provide accurate predictions. Another proposed index is the Predicted Percentage Dissatisfied (PPD), which calculates a prediction of the number of thermally dissatisfied people.

The main characteristics of the vehicular in-cabin environments that complicate the human thermal comfort determination and predictions are due to its thermal transient values and time gradients, especially the cooling rate after a hot soak. Additionally, the non-uniform thermal environment associated with the high localized air velocity, the in-cabin air temperature distribution, the solar flux, and the radiation heat flux from surrounding interior surface, all further complicate such predictions [4]. Furthermore, unlike air conditioned buildings, the vehicle in-cabin climate is dominated by thermal transient conditions than steady-state conditions; 85% of the trips, in fact, involve an average distance fewer than 18 km and with durations from 15 to 30 minutes. This further

stresses the fact that the characterization of the vehicular in-cabin thermal behavior over the first 30 minutes is especially significant [3]. Other challenges include the psychological as well as physiological differences among the passengers.

Finally, the vehicular in-cabin environments is affected by a large number of parameters that include the different interior trim surface air temperatures, the air velocity and its profiles over the different geometries, the relative humidity, the solar intensity and its reflections over the different material types and surface finishes in the cabin, the angles of incidence, the type of clothes, etc. Also many of these parameters are dependent with unknown relationships [4]. This not only complicates any modeling effort but also any experimental work.

So to overcome these difficulties, the current climate comfort control strategy has been based on controlling the temperature of panel surfaces (radiating component), that are directly facing passengers, and diffusing the conditioned air through it (convective component). The automotive Original Equipment Manufacturers OEMs have also been dedicating more research and development efforts to investigate and test more efficient approaches and instruments to predict the thermal sensation of the driver and the passengers under both transients and steady state conditions.

2.2 Literature Review

Recently, the emphasis on thermal comfort for vehicular occupants has been increasing and becoming one of the competitive technologies and main features in the automobile design. Several researchers have analyzed the in-cabin thermal comforts from

different perspectives and modeling schemes; human thermal physiological modeling, human thermal psychological modeling, compartment zone modeling, and the human thermal manikin model. Also, some researchers investigated the use of thermal imagery via infrared detectors to visualize and help predict the in-cabin surfaces' temperature. Some of these studies have also integrated all of these models to provide a complete picture of in-cabin human comfort conditions.

2.2.1   Human Thermal Physiological Model

A number of models have been developed during the past few years in order to describe human thermal response to the variations in its surrounding conditions. Models have been developed to simulate the human body response, by discreatizing the human body into major segments. Each of these segments consists of four body layers; the core, the muscle, the fat, and the skin tissue, in addition to clothing layer [4, 5]. Other discreatization segmented the human body into human tissue system and thermoregulatory system. The human tissue systems represent the human body including the physiological and the thermal properties of the tissue. While the thermoregulatory system controls the physiological response such as vasomotor control, sweating and shivering [7]. Doherty et al. evaluated two different physiological comfort models; the J.B. Pierce two-node model of human thermoregulation and the Fanger comfort equation PMV model, in addition these two models are also used to estimate the psychological response. Doherty's evaluation was based on the ability of each of these two models to predict the physiological variables under thermal comfort under a specific range of air

temperatures and exercise intensity levels [8]. However, to estimate physiological variables that control the thermal comfort and thermal sensation, the heat transfer exchange rate between each of the body segments and their surrounding environment should be accurately measured, also the convection coefficients of heat transfer are not easily extracted due to the body shape complexity and the heterogeneity of body tissues. Other factors include the two processes of heat exchange; the evaporation of sweat from skin surface and the heat convection from an internal source to the skin. Finally the physical training rate that depends on the fat body mass, the gender, the age, and the type of exercise and time of day [7].

The most famous and widely referenced physiological models also include; the model presented by Han et al. that consists of 16 body segments and studies the effects of the solar load for various solar incidence angles, glass properties, surrounding radiant heat, air velocity, and air temperature on the thermal comfort of the occupants [5]. Another model was proposed by Martinho et al. to evaluate the thermal comfort in a vehicle cabin using the equivalent temperature index. Two methods were used to calculate equivalent temperature for all objects and body segments [9]; the first is based on an empirical equation derived by Madson et al. in which the thermal comfort parameters within the cabin are measured from a laboratory model without the presence of the thermal manikin. While the second relied on measurements that were taken using real scale thermal manikin that divided the body into 16 segments. Same cabin conditions were applied for the two methods [10].

Kaynakli and Kilic presented two studies; the first presented a theoretical and experimental analysis of the in-cabin thermal comfort during the heating period by dividing the human body into 16 segments, with the change of temperature measured and calculated in both experimental and theoretical basis. The air temperature, velocity and relative humidity inside the automobile were acquired experimentally through multiple sensors distributed across the passenger compartment [11]. While, Kaynakli's second study discussed a model for thermal interactions between the human body and the interior environmental condition inside the automobile. Also the effects of both heating and cooling processes were analyzed. The model used depends on the heat balance equation for human body (segmented into 16 parts), with empirical equations defining the sweat rate and mean skin temperature [12]. The National Renewable Laboratory (NREL) improved the current models by increasing the number of body segments; the model was developed using a finite element analysis environment. Their physiological model consisted of 126 segments, the skin temperature, the sweat rates, and the breathing rate. Then these data are transmitted to the manikin to predict the body's response to the environment. Also, this model calculated the conduction heat transfer based on temperature gradient between tissue nodes [7].

2.2.2 Human Thermal Psychological Model

This modeling approach depends on the physiological response of people to the environment conditions, which is then related to the thermal sensation to these responses. The inner workings of this model rely on a thermal comfort index that uses the

12

temperature data from a physiological model to predict the local and global thermal comfort as a function of local skin and core temperatures and their rates of changes. Also, this model is basically based on integrating the relevant factors from the environment (temperature, air velocity, relative humidity ...etc) that in a way to present the thermal sensation response of human occupants. Examples of such modeling studies include the work by Kaynakli et al. who presented a numerical model for the heat and mass transfer between the human body and its environment. This study was only limited to steady state conditions, while the total sensible and latent heat losses, skin temperature, wittedness, predicted mean vote PMV and predicted percent of dissatisfied PPD values were calculated via simulation [13].

Other psychological models used the Virtual Thermal Comfort Engineering (VTCE) model as a function of air velocity, humidity, direct solar flux, level of activity, and clothing type for each individual. The VTCE models are used to perform sensitivity analyses for the effects of the various vehicle cabin thermal environments on the occupant thermal comfort; including discharge temperature, air velocity, breath level temperature, solar intensity and solar angles. This thermal comfort model was based on automotive OEM's comfort scale for both summer and winter, using a Sport Utility Vehicle (SUV) cabin environment [4]. A different model developed by Han et al. used the Equivalent Homogenous Temperature (EHT) tool to predict the thermal comfort level. The ETH is defined as "the uniform temperature of the imaginary enclosure with air velocity equal to zero in which a person will exchange the same dry heat by radiation and convection as in the actual non-uniform environment" [14].

Mattiello et al. presented a Computational Fluid Dynamics (CFD) virtual design approach of the breathable panels and their position in order to optimize the thermal comfort for different air flow conditions. The model used the standard thermal comfort index that is the Predicted Mean Vote (PMV) to evaluate the virtual comfort environment [15]. For the multi-zone or comparative assessment and transient pull down situation, Kulkarni et al. developed an experimental technique based on previous conditions to predict thermal comfort inside a cabin, while still using the Predicted Mean Vote (PMV) to predict thermal comfort zone [16].

Another variation from this study utilized subjective measurements through a questionnaire. An example of such subjective based measurements or questionnaire based is the model presented by Cengiz et al. that consisted of 15 questions and the participant were required to answer these questions every 5 min for 1 h. The questionnaire consisted of four parts: thermal sensation on ten different areas on the bodies, body moisture on two areas, others on the seat and sweat level. The evaluation of thermal comfort for the whole human body is based on PMV [17]. Another subjective modeling example is from the work by Shek et al. where he presented a subjective questionnaire survey that investigated the satisfaction of the passenger's sensation votes in terms of comfort and air quality. The physical parameters of thermal and air quality measurement were collected in a bus, while the questionnaire collected the subjective response and sensation votes from the occupants. Then a correlation is compiled to connect the objective and the subjective data, while showing its effects on the individuals. Then a model is built to

14

evaluate the percentage of dissatisfaction under passengers' sensation votes towards thermal comfort and air quality [18].

2.2.3   Compartment Zone Model

The purpose of the heating, ventilation and air condition is to provide a comfortable thermal environment for all passengers especially in extreme climate condition. Hence, it is necessary to understand the thermal aspects of human body as discussed in previous sections, with addition to understanding the passenger compartment parameters such as the velocity of conditioned air that flow to the passengers, the temperature distribution inside the cabin, the relative humidity and pressure variation inside the compartment. So the thermal environment in a car is more difficult to control and evaluate compared to buildings' environment due to complexity of shape and size that create thermal asymmetry; in addition to the transient conditions and the in-homogeneous air temperature and velocity fields. So, to predict accurate thermal comfort for vehicular cabins, the operating condition and the environmental parameters should be accurately determined. One approach is to simulate the passenger compartment and then investigate the effect of changing each of the environment conditions on the thermal sensation of a human body.

Chakroun et al. presented a study of the air temperature variations and its effect on the thermal comfort inside a car parked in the sun during the summer months in Kuwait. Also, they studied the effect of using different combinations of internal covering (including covering the front windshield, and the four side windows, and covering both

windshields and the four side windows) on the air temperature inside that car. Also, they developed an effective idea to reduce the inside air temperature of the parked vehicle by installing a solar power ventilating fan [19]. Mezrhab et al. developed a numerical model that studies the behavior of thermal comfort inside passenger cars' compartment' according to change solar radiation, type of glazing, and car color and the radiative properties of vehicle interior materials. This model is based on the nodal and the finite difference methods. The model considers following parameters; the transient mode, combination of heat transfer mode as conduction, convection and radiation. Also it is coupled with two spectral bands (short wave and long wave radiation) and two solar fluxes (beam and diffusion) [20]. Further studies of the air flow and its temperature fields inside a passenger compartment were also proposed by Zhang et al. Zhang's used a 3-D model in a commercial software FLUENT environment to simulate 3-D temperature distributions and the flow field within the compartment, with and without passengers. Furthermore, two scenarios were implemented; the first test run with an outside temperature of 43 $^{\circ}$C , relative humidity 15% and sun load of 1kW/m^2. The vehicle is first operated on 32 km/h for one hour and then 0 km/h for one hour with natural wind speed of 10 km. The total test duration time was 120min, with the temperature data being recorded for head, foot; knee…etc. every 5 min. While, in the second scenario, the test was carried out with an outside temperature of 38 ℃, relative humidity 40% and sun load is 1 kW/m^2. The vehicle is first operated on 50 km/h for 20 min., then 80 km/h for 20 min. The air conditioning system started to work when the test began; the total test duration time lasted for 162 min, with a recording frequency of 5 minutes. The measured

and the predicted transient temperatures were compared and found to be in good agreement [21]. Additionally, Zhang's modeling included another set of simulations for variety of cases; some cases included the investigation of the flow fields with four persons in the cabin and without any person in the cabin. Other cases analyzed the effect of decreasing the cooling load by decreasing the inlet air temperature or decreasing the inlet air flow rate. Additionally, Zhang's modeling investigated the effect of the boundary conditions by changing; the outside environment temperature, the outside wind speed, the insulation of the vehicle different surfaces, the penetrating radiation into compartment, the air flow around the passengers' feet, and finally the air flow from the left inlet leaving towards driver feet. The main findings from Zhang's comprehensive studies can be summarized as; the decrease in the cooling load can be achieved by increasing the inlet air temperature, the thermal comfort in the compartment is dependent on the number of the persons in it and their seating arrangement, in addition to the outside temperature effect which plays a vital role on the cooling load. Also, changing the material of the windows to reduce its transmissivity can lead to a decrease in the cooling load, finally to improve the uniformity of temperature field around the driver's feet, the inlet air direction should be kept horizontal [22].

The unique attributes of the Zhang et al. model over previous models, is in the fact that it investigated the relationship between the thermal sensation and thermal comfort experimentally under uniform and non-uniform, steady and dynamic conditions. Also, its main conclusions proved that under steady and uniform conditions, the thermal sensation are linearly correlated to the thermal comfort; while, under steady and non-

17

uniform conditions, the thermal sensation changes with space. Finally, under the dynamic condition, the thermal sensation changes with time [23].

Han et al. provided an assessment of the various environmental thermal loads on the passenger thermal comfort using a 3-D model in a RadTherm environment to compute the effect of the solar load and temperature variation on the passenger compartment; when coupled with 3-D flow fields using Fluent simulation to help predict the air velocities around an occupant during soak and cool-down periods. These studies presented sensitivity analyses of the various vehicle cabin thermal environments including the glass properties, the vehicle body insulation, and the vehicle interior thermal mass for a compact size vehicle [24, 25]. Then the cabin thermal environment was further coupled with a human physiological model [4, 5] to predict the local and the overall thermal comfort levels based on local skin and core temperatures and their change time rate. Figure 2.1 shows a flow chart that presented these interaction models and their relationships.
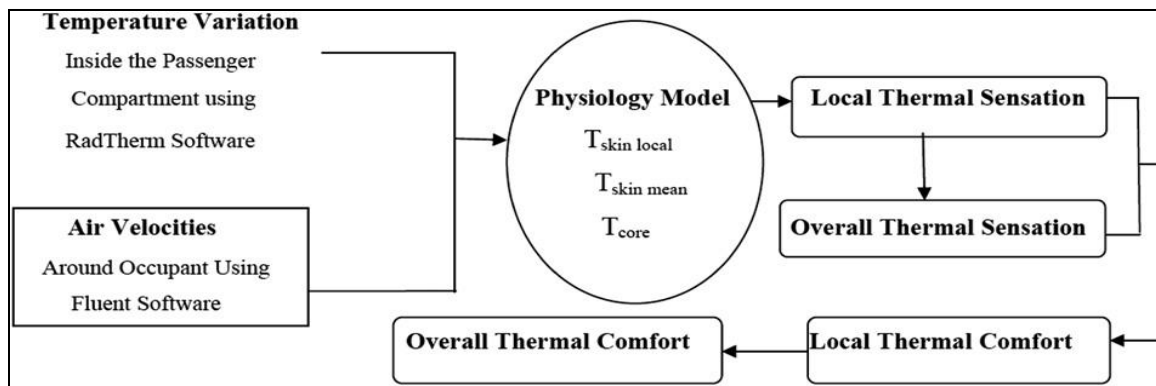
Figure 2.1: Flow chart that presented interaction models and their relationships.

Huang et al. developed 3-D flow and thermal analyses for passenger compartment by generating a Virtual Thermal Comfort Engineering (VTCE) model, which has the capability to predict the local human comfort for a passenger in non uniform conditions as related to variations in; air temperature, surface temperature, relative air velocity, relative humidity and two personal parameters that were presented by the level of activity and the clothing of the passenger. The sensitivity analysis for this model is conducted based on OEM's comfort scale for summer and winter condition [26]. Another perspective model presented by Karimi et al. is based on establishing a transient physical model for the thermal interactions between an automobile passenger in winter and summer conditions and the cabin environment for heated/ ventilated seated. Also the experimental studies were conducted under the same condition to validate a model prediction [27]. Fountain et al. have investigated the influence of high humidity levels on human comfort; specifically the response of sedentary human to high humidity exposure (RH between 60% - 90%) at a temperature range of $20 – 26 \, ^{o}$C. The study findings indicated the RH effect but did not quantify it independent of other contributing factors [28]. Guerra presented another perspective study to show the effect of changing the relative humidity on the performance of an automobile air conditioning system; by using an evaporative cooling scheme [29]. The effect of manipulating the relative humidity of in-cabin environment on the thermal comfort and human occupants' thermal sensation with introducing, a practical system implementation is also discussed in terms of an evaporative cooler design is discussed by Alahmer at el. , the results show that changing the RH along with dry bulb temperature inside vehicular cabins can improve the air

conditioning efficiency by reducing heat removed and improved the human comfort sensations [30].

2.2.4 Thermal Manikin Model

Thermal manikins are widely used to resolve the problem of having a human passenger under extreme conditions for a long time. Thermal manikins today comprise one-segment, easy-to use, low-cost equipment, as well as high-tech, sophisticated, multi-purpose models [31]. Also, the thermal manikin has a capability to integrate the physiological and the psychological models at the same time. Hence, the increasing interest from the automobile industry and the clothing manufacturers for this kind of versatile evaluation instrument. Currently, there are two major areas of application for manikins' research; (a) the first is based on the determination of clothing heat transfer characteristics and (b) the assessment of the impact of thermal environments on the human body [32]. So, to predict the thermal responses of humans accurately, the thermal manikin has been incorporated with the physiological and psychological studies. Also, the following prosperities should be available in a thermal manikin to provide accurate simulation predictions the of human body; the correct body shape and size; the control of heat emission; the control of the heat distribution across the skin surfaces; the emission from the skin; the perspiration control and distribution across the skin; and the control of pose and movement and the control of the core [32].

The evaluation of thermal comfort using a thermal manikin with controlled skin temperature was conducted by Tanabe et al.; the manikin based equivalent temperature

was proposed and a PMV index was used as method of calculation [33]. Nilsson developed three different climate evaluations; firstly the human subjective measurements, such as: Predicted Mean Vote (PMV), Predicted Percentage Dissatisfied (PPD) and an adaptive model. Secondly; manikin measurements, where two slightly different manikins were used, with both manikins seated. The manikin surface was divided into independently temperature-regulated segments, with each zone of the manikin surface layer is densely covered with resistance wires, embedded in a hard plastic shell, on which surface temperature sensors were positioned. Every zone was regulated to a constant temperature ($34.0\pm0.1°C$) and the power required was recorded with a personal computer. The heat loss measurements took several factors into account; such as air temperature, air speed, radiation and clothing, in its estimation of the climate. Once heated, the manikin responds to a step change and equilibrates at the new power consumption within approx. 20 minutes. The variation between double determinations in percentage of their average value is less than a few percentages. Finally, a computer model developed a virtual manikin (MANIKIN 3) based on a CFD code with 18 zones; this code was done using CFX and STAR-CD environments. Also, he presented the definition of equivalent temperature, and identified and compared the different expressions used in determining t_{eq} [34, 35].

The National Renewable Energy Laboratory (NREL) developed a system that consists of three main tools to predict the human thermal comfort in non-uniform transient thermal environments. These tools consisted of a finite element model of a human physiology, a psychological model to predict local and global thermal comfort,

21

and finally a thermal manikin that consisted of 150 individual zones on the skin surface. Each segment is an integrated device of heating, temperature sensing, sweating distribution and dispensing. The main characteristic of this manikin is that it had a high degree of sensory spatial resolution and a fast time response and a feedback loop to continuously react and adjust to the thermal environment [36]. Similar approach was presented by Rugh et al. [2005] where he built a thermal comfort manikin, physiological and psychological models to assess the comfort in transient non homogenous environments; the manikin consisted of 120 individual controlled zones of the human body, and incorporated the basic processes such as heating, sweating and breathing. The model received heat losses data from the manikin and then it predicted the human physiological response while the skin temperature was used to predict the thermal sensation and thermal comfort.

The manikin based modeling efforts as stated above had been validated against other models, and appeared to be in good agreement to models that used human subjects except for the head and feet [37]. Mahmoud et al. developed a 3D simulation of two different manikins (Maria & Till) to study the influence of the different shapes on the flow patterns, the temperature distribution, the equivalent temperature, and the comfort assessment by using PMV and PPD thermal indices [38]. Other proposed thermal manikins' modeling relied on the use of virtual thermal manikins as the work by Curran et al. who presented two scenarios: one using air temperature and the other using equivalent temperature for a homogenous space. In this experiment two virtual thermal manikins placed in a simulated aircraft cabin; with one used to determine the equivalent

temperature and the other used to predict human thermal comfort for simulated cabin environment [39].

2.2.5 IR Thermography to Predict Surface Temperature

Because the Infrared IR thermography is non-invasive, non contact and relatively forward imaging approach, it has been used to measure the temperature variation on the human skin temperature. Hence, the application of sensing routine utilizing IR thermographic detectors enables the real-time measurement of solid surfaces temperature within the cabin in addition to clothes and visible body parts of the human subjects. Additionally, automated infrared imaging system can be used to overcome the limitation of using conventional thermocouple and visual observation methods due to complexity of implementation and the inherent ambiguity of visual observation [40].

However, there are a limited number of published manuscripts that discuss the use of IR Thermal imaging to measure and evaluate the thermal conditions inside the cabin, even though the IR thermography is a promising tool to measure and/or predict the climatic conditions inside the passenger compartment and has been used to measure surface temperature in [41] during transient conditions.

Burch et al. described several automotive applications of infrared IR sensor with focus on their use for automotive climatic control analysis. Additionally, he proposed a different method for measuring ambient air temperature by using a thin (0.15 mm) layer of polyethylene plastic mounted perpendicular to the air stream [42]. Korukçu et al. reported the use of the IR thermal imaging using un-cooled thermal detectors to measure

the temperature of the front panel and that of the facial skin during the heating and the cooling periods. Also the study mounted several thermocouples junctions to the surfaces measured by the thermal cameras; the temperature acquisition was done at a frequency of 10 seconds. The experiment validated the use of the thermal imagers by showing that the acquired temperature profiles (spatial and temporal) from the thermal imagers and the thermocouples are in agreement [43]. Table 2.1 summarizes all the discussed models; classified according to their modeling approach. Surveying the published literature shows the limited knowledge and studies that discuss extending the practices, mainly changing both RH and dry-bulb temperature, found in conditioning big enclosures (buildings) into vehicular cabins.

Table 2.1: Summary of proposed thermal comfort models.

Model	Reference	Description
Physiological Model	Han et al.,2001 [5]	16 body segments, effect of solar load for various solar incidence angles, glass properties, surrounding radiant heat, air velocity, air temperature on thermal comfort.
	Martinho et al.,2004 [9]	16 body segments, evaluate thermal comfort using equivalent temperature index.
	Kaynakli et al.,2005 [11]	16 body segments, heating period, theoretical and experiments analysis in cabin thermal comfort.
	Kaynakli et al., 2005 [12]	16 body segments, heating and cooling period, interaction between the human body and the interior condition inside automobile, define the sweat rate and mean skin temperature.

Psychological Model	Kulkarni et al.,2004 [16]	Experimental technique for the multi-zone or comparative assessment and transient pull down situation, using Fanger comfort equation PMV.
	Cengiz et al.,2007 [17]	Subjective questionnaire, 15 questions based on thermal sensation on ten different areas on the bodies, body moisture on two areas, others on the seat and sweat level. Using Fanger comfort equation PMV.
	Shek et al.,2008 [18]	Subjective questionnaire, investigated the satisfaction of the passenger's sensation votes in terms of comfort and air quality.
Compartment Zone Model	Chakroun et al.,1997 [19]	Effect air temperature variations on the thermal comfort inside a car parked in the sun during the summer months. Effect of using different combinations of internal covering.
	Mezrhab et al.,2006 [20]	Numerical model based on the nodal and the finite difference methods. Effect of change solar radiation, type of glazing, and car color and the radiative properties of vehicle interior materials on thermal comfort.
	H. Zhang et al. ,2009 [21,22]	3-D FLUENT to simulate 3-D temperature distributions and the flow field in cabin with and without passengers.

		Y. Zhang et al.,2009 [23]	Relationship between the thermal sensation and thermal comfort experimentally under uniform and non-uniform, steady and dynamic conditions.
		Han et al. 2009,2010 [24,25]	3-D RadTherm environment and Fluent simulation, compute the effect of the solar load and temperature variation on the passenger compartment.
		Huang et al.,2005 [26]	3-D flow and thermal analyses for passenger compartment by generating VTCE model, summer and winter condition
		Karimi et al.,2003 [27]	Transient physical model for the thermal interactions between an automobile passenger in winter and summer conditions.
		Alahmer et al., 2011 [30]	Manipulating the Relative Humidity RH of in-cabin environment on the thermal comfort and human occupants' thermal sensation, A practical system in terms of an evaporative cooler design.
Combination	Physiological and Psychological Models	Doherty et al.,1988 [8]	Two different physiological comfort models; the J.B. Pierce two node model of human thermoregulation and the Fanger comfort equation PMV model.
	Physiological and Manikin Models	Rugh et al.,2004 [7]	126 Segments, define skin temperature, sweat rate, and the breathing rate. Calculating the conduction heat transfer based on temperature gradient.

	Psychological and Compartment zone models	Mattiello et al.,2001 [15]	Computational Fluid Dynamics CFD virtual design approach of the breathable panels and their position, using Fanger comfort equation PMV.
	Psychological and Compartment zone model	Tanabe et al.,1994 [33]	Thermal manikin based on equivalent temperature and PMV to evaluation of thermal comfort.
	Compartment zone and Manikin models	Curran et al.,2009 [39]	Two virtual thermal manikins placed in a simulated aircraft cabin; one used to determine the equivalent temperature and the other used to predict human thermal comfort for simulated cabin environment.
		Mahmoud et al.,2003 [38]	3D simulation of two different manikins (Maria and Till) to study the influence of the different shapes on the flow patterns, the temperature distribution, the equivalent temperature, and the comfort assessment by using PMV and PPD thermal indices.
	Physiological , Psychological and Thermal Manikin Models	Nilsson,2004,2007 [34, 35]	Three different climate evaluations; the human subjective measurements (PMV, PPD), adaptive model and two slightly different manikin measurements. A computer model developed a virtual manikin (MANIKIN 3) based on a CFD code with 18 zones. Definition of equivalent temperature.

		McGuffin,2002 [36]	Tools consisted of a finite element to predict local and global thermal comfort. Thermal manikin consisted of 150 individual zones on the skin surface. Each segment is an integrated device of heating, temperature sensing, sweating distribution and dispensing.
		Rugh et al.,2008 [37]	A thermal comfort manikin consisted of 120 individual controlled zones of the human body, and incorporated the heating, sweating and breathing. Physiological and psychological models transient non homogenous environments.
	Compartment zone and IR thermography models	Burch et al.,1993 [42]	Measuring ambient air temperature by using a thin (0.15 mm) layer of polyethylene plastic mounted perpendicular to the air stream.
		Korukçu et al.,2009 [43]	Un-cooled thermal detectors to measure the temperature of the front panel and that of the facial skin during the heating and the cooling periods.

2.3 Summary

This chapter introduced a comprehensive review of the different modeling and experimental approaches that address the thermal comfort for vehicular cabins. The review classified the published work into the two modeling efforts; the human

physiological and the psychological models. The physiological models aimed at stimulating the human body response by discreatizing the body into segments, with each segment comprised of four main layers; the core, the fat, the muscle group, and skin tissue. On the other hand, the psychological depends on the psychological response of number of observers to the surrounding environment, which is then related to the thermal sensation. Additionally the current study discussed the different experimental approaches used to capture the different parameters affecting the in-cabin conditions mainly; the air velocity, the relative humidity, the solar loads, and the air temperature. In addition to discussing the use of the thermal manikins in comparison to actual human subjects for testing the different scenarios; the studies reviewed reveals that the thermal manikins can provide accurate predictions of the human thermal sensation that is comparable with using human subjects. Also, the development of virtual thermal manikins is discussed. The chapter discussed the use of the Infrared IR thermal imaging techniques to capture the temperature fields of the different objects within the cabin and the air flow too.

The presented study investigated the different challenges that exist in predicting and evaluating the thermal comfort for vehicular cabins when compared with thermal comfort in buildings i.e. static enclosures. These challenges are mainly related to the fast transient behaviors involved especially the cases of cooling the cabin after a hot soak condition, in addition to the non-uniformities in the thermal environment associated with the high localized air velocity, air temperature distribution, solar flux, and radiation heat flux from surrounding interior surfaces; in addition to other variations related to trip durations (driving distances) and passenger clothing levels.

CHAPTER THREE

HUMAN THERMAL ENVIRONMENTS

The main objective of heating, ventilation and air conditioning is to provide comfort to the occupants removing or adding heat and humidity of the occupied space [44]. Similarly, the main objective of the study of the thermal comfort conditions is generally able to determine the conditions for achieving human internal thermal neutrality with minimal power consumption. To do this, there arises the need to study the human body's response to certain environmental conditions [44, 45].

Human Thermal Environments is a branch of the discipline Ergonomics, concerned with the thermal comfort (i.e. whether a person feels too cold, hot...etc.) of human beings in any, but especially in their working environment. Convective, conductive, radiative and insulating properties of the human body and the environment in which it finds itself are all variables whose effects are closely considered in this science. The aim of the discipline is to manipulate these variables in the environment and/or the clothing of the individual to achieve 'thermal comfort', the state in which the individual is content with their perceived thermal state.

This chapter highlights the overview of human thermal environment parameters that effect on human comfort, the heat balance equation for human body, mathematical models to predict thermal comfort and the most widely thermal comfort indices used.

3.1 In-Cabin Thermal Comfort and its Controlling Factors

Providing satisfactory thermal environment inside a vehicular cabin is rather complex, because of the subjective nature of human response and the multitude of interacting variables. There are six main factors affecting the in-cabin thermal comfort, which can be perceived as both environmental and personal. The environmental factors include four variables that influence the environment around the human body and therefore its ability to transfer heat. These variables are mainly; (i) the Air Temperature termed as T_a and defined as the temperature of the air surrounding the occupant that determines the net heat flow between the human body and its environment. This factor is considered important because of its narrow range within the comfort zone. (ii) The Mean Radiant Temperature T_r arises from the fact that the net exchange of radiant energy between two objects is approximately proportional to their temperature difference multiplied by their ability to emit and absorb heat (emissivity). Also the T_r can defined as the temperature of a uniform enclosure with which a small black sphere at the test point would have the same radiation exchange as it does with real environment. The use of the sphere in the definition is to show the average in three dimensions. T_r also has the strongest influence on the thermo-physiological comfort indices mainly the PMV (Predicted Mean Vote). (iii) Relative Air Velocity; defines the air movement across skin layer or clothing surface, convecting heat. The air velocity controls the heat convection coefficients which in turn can manipulate the rate of heat transfer without any change in air temperature. Air velocities inside vehicular compartments tend to have small values, ranging from 0.1 and 0.4 m/s [32]. The maximum air velocity allowed inside a vehicle

cabin is considered a function of the air temperature as determined by the convection heat exchange. (iv) Humidity is defined as the amount of water vapor in a given space; while the humidity ratio or specific humidity is defined as the weight of water vapor per unit weight of dry air. Relative humidity (RH) is the ratio between the actual amount of water vapor in the air and the maximum amount of water vapor that the air can hold at that air temperature. Although human tolerance to relative humidity variations is much higher than that for temperature variations [32], the relative humidity is still important.

The personal or human factors are two, which depend on the nature of the passenger state or level of activity. The first personal factor is Clothing Thermal Resistance; which describes the thermal resistance or insulation level between the human body and its environment, with the clothing insulation typically quantified in terms of its "Clo" values (1 Clo = 0.155 $m^2.^oC/W$ insulation value). Table 3.1 presents an estimation of some types of clothing insulation. The second personal factor is the Activity level that is the work or metabolic rate that controls the generated heat inside the human body as we carry out physical activity. Hence, the metabolic rate depends on the activity level and the fitness level. The estimate of metabolic rate for basic activity is depicted in table 3.2. Although the personal and the environmental factors might be independent, together they contribute to the thermal comfort state; as one of these variables changes, others need to be adjusted to maintain the thermal equilibrium.

Table 3.1: Clothing Levels and Insulation.

Description	Thermal Insulation range (Clo)
Winter Outdoor Clothing	2 –3
Normal Indoor Clothing	1.2 -1.5
Summer Indoor Clothing	0.8 -1.2
Indoor 'Lightweight' Clothing	0.3-0.5

Table 3.2: Estimate of metabolic rate for basic activity.

Basic Activity	Estimate of metabolic rate
Lying Down	0.8 met - 47 W/m^2
Sitting Quietly	1.0 met - 58 W/m^2
Seated Office Work	1.2 met - 70 W/m^2
Light Work	1.6 met - 93 W/m^2
Medium Work	2.0 met - 117 W/m^2
Heavy Work	3.0 met - 175 W/m^2

3.2 Heat Balance Equation for Human Body

The human body heat balance equation can be presented by inspecting three main terms; the heat generation in the human body, the heat transfer, and the heat storage. Figure 3.1 display the schematics for a total body heat balance in a vehicle cabin environment [14]. Mathematically, the relation between the body's heat production and all its other heat gains and losses can be computed through equation (3.1);

$$M - W = E \pm R \pm C \pm K \pm S \tag{3.1}$$

Where, M is the metabolic rate of body that provides energy, W is the rate of mechanical works, E is the rate of heat loss through evaporation, R is the radiation Rate, C is the convection rate, K is the conduction rate, and S is the body heat storage rate, all have the same unit Wm^{-2}.

33

Discussing each term briefly can highlight its contribution and impact; first (i) the metabolic rate is the energy released per unit time by the oxidation processes in the human body and is dependent on the amount of muscular activity. Usually the metabolism rate is measured by a unit of "met", and is proportional to the body weight, activity level, body surface area, health, sex, age, amount of clothing, surrounding thermal and atmospheric condition. Typically, the metabolic rate for a normal adult with a surface area of 1.7 m^2 during a vehicle drive is evaluated at 1.4 met or an equivalent of 80W/m^2.

Secondly, (ii) the mechanical work deals with the external mechanical efficiency η of the human body in other words it can be defined as the ratio W/M, with a range of 0 to 0.2; so a human body is considered as a mechanical system with low efficiency; with the legs being more efficient than the arms [46]. (iii) The evaporation is similar to the heat transfer by convection but it requires an initial change of state from liquid to vapor at the skin surface in addition to the study of the vapor boundary layer at the skin then into ambient air. Also, the evaporation is considered a cooling mechanism. So, it plays a significant role in the body's heat balance especially if the ambient temperature is continuously increasing, or when the body is gaining heat from its environment. Also, evaporation heat losses increase at high activity levels when the metabolic heat production rises as shown in figure 3.2 [47]. The (iv) radiation term describes the net exchange of radiant energy between two bodies across an open space. During a vehicle cool down or warm up period, the radiation heat load –especially from solar loads- can

have a big effect on the occupant thermal comfort. The heat losses through radiation can be expressed for a clothed body and bare skin as in equation (3.2) from [14];

$$R = \sigma \, F_{i,j}\{\epsilon_{cl}f_{cl}[(T_{cl} + 273)^4 - (T_r + 273)^4] + \epsilon_{sk}(1 \qquad\qquad (3.2)$$

$$- f_{cl})[(T_{sk} + 273)^4 - (T_r + 273)^4]$$

Where, ϵ_{cl} is the emittance of the cloth, ϵ_{sk} is the emittance of the skin, σ is the Stefan-Boltzman constant, $F_{i,j}$ is the view factor between surface i and j, f_{cl} is the clothing area factor which is defined as the ratio of the surface area of the clothed body to the surface area of the naked body, T_{cl} is the temperature of the cloth, T_{sk} is the temperature of the skin and T_r is the temperature of the surrounding surfaces. (v) The convection term describes the movement of molecules within fluids to transfer heat. The heat losses by convection can be expressed for a clothed body and the skin in equation (3.3) [14];

$$C = f_{cl}h_c(T_{cl} - T_a) + (1 - f_{cl})h_c(T_{sk} - T_a) \qquad\qquad (3.3)$$

Where, h_c is the convection heat transfer coefficient and T_a is the air temperature around the body. The magnitude of h_c depends on the type of convection. When the air velocity inside the vehicle is high then a forced convection correlation is applied. On the other hand, if the air is low, free convection correlation is used; one main consideration for vehicular cabins is the limited are velocity ranges allowed. (vi) The conduction term typically describe the heat losses when the occupant is seated, as heat is exchanged between the body and the vehicle seat. However, the term C_k is difficult to evaluate due to the variations in the clothing and seat finishes and material types so it is usually ignored as a separate item, but taken into account in the clothing thermal resistance.

Lastly, is the (vii) Storage rate, the body always produces heat, so the metabolic rate *M* is always positive; so if there is a net heat gain, the storage term will be positive and the body temperature will rise. On the other hand, if there is a net heat loss, then the storage will be negative and body temperature will decrease. But the body heat storage term *S* is typically small because the body has a limited thermal storage capacity. Therefore, as a body becomes warmer, the body reacts by increasing the blood flow to the skin surface and increasing sweating and respiration, thereby maintaining the desired body temperature. Table 3.3 indicates the environmental and the human factors that influence each of the major terms in the body heat balance equation; equation (3.1).
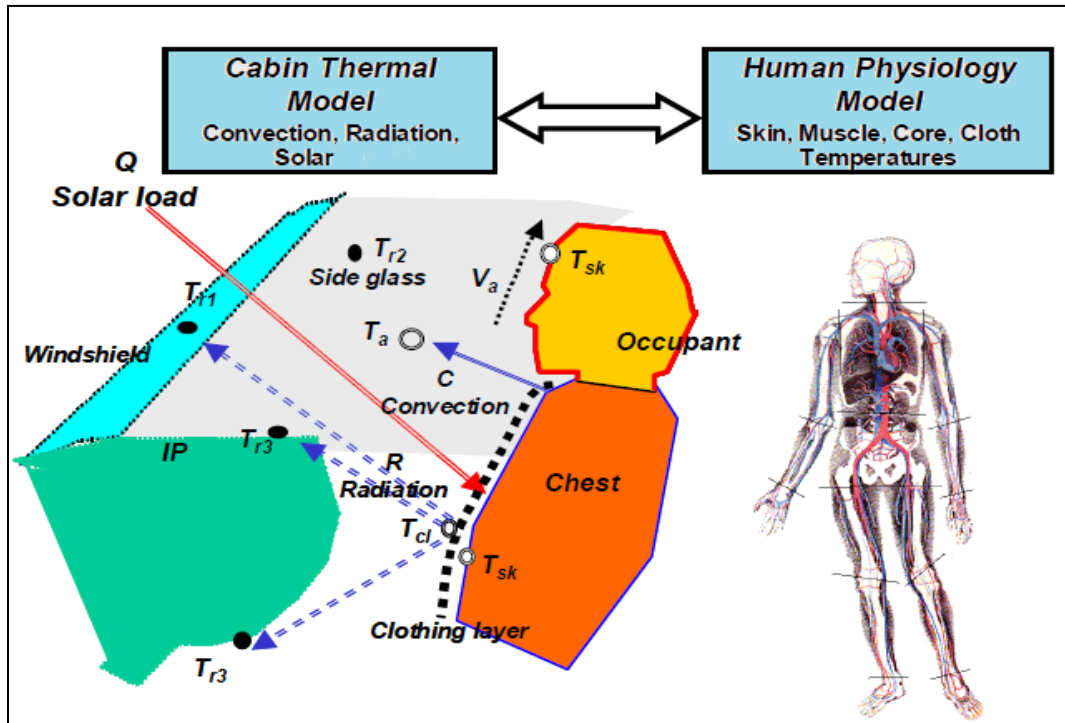
Figure 3.1: schematics for total body heat balance in a vehicle cabin environment [14].
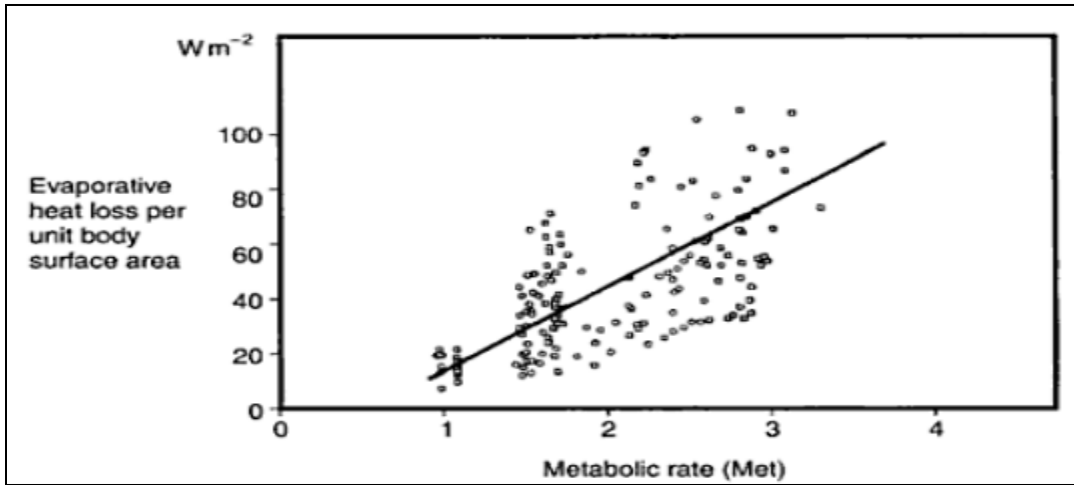
Figure 3.2: Evaporative heat losses as a function of the activity level for persons in thermal comfort [47].

Table 3.3: Factors influence on the heat balance equation.

Factor	Environment	Human
Metabolism (M)	• Little effect	• Activity • Weight • Surface area • Age • Sex
Environment (E)	• Wet-bulb temperature • Dray-bulb temperature • Velocity	• Ability to produce sweat • Surface area • Clothing
Radiation (R)	• Temperature difference between bodies • Emissivity of surfaces	• Surface area • Clothing
Convection (C)	• Dray-bulb temperature • Velocity	• Clothing • Mean body surface temperature • Surface area

3.3 Mathematical Models for Predicting Thermal Comfort

Many researchers have been tried to predict the thermal sensation of people in their environment based on numbers of factors such as the personal, environmental and physiological variables that influence thermal comfort. From the research done, some mathematical models that simulate occupants' thermal response to their environment have been developed. The most notable models have been developed by P.O. Fanger (it is called Fanger Comfort Model), the J. B. Pierce Foundation (it is called the Pierce Two-Node Model). The main similarity of the two models is that two model apply an energy balance to a person and use the energy exchange mechanisms along with experimentally derived physiological parameters to predict the thermal sensation and the physiological response of a person due to their environment. The models differ somewhat in the physiological models that represent the human passive system (heat transfer through and from the body) and the human control system (the neural control of shivering, sweating and skin blood flow). The models also differ in the criteria used to predict thermal sensation.

3.3.1   Fanger Model

Fanger (1970) defined thermal comfort as "The condition of mind which expresses satisfaction with the thermal environment". Fanger's model can be predicted the thermal comfort if all the values of all six parameters that discussed previously are known, and also based on three conditions for a person to be in thermal comfort: the body

is in heat transfer; sweat limit within comfort limits; and mean skin temperature is within comfort limits [48- 50].

The heat balance equation for a body-environment according to Fanger definition:

$$H = E_d - E_{SW} - E_{re} - L = K = R + C \qquad (3.4)$$

Where; H is internal heat production in the human body, E_d is heat loss by water vapor diffusion through skin, E_{SW} is heat loss by evaporation of sweat from skin surface, E_{re} is latent respiration heat loss, L is dry respiration heat loss, K is heat transfer from skin to outer surface of clothes, R is heat transfer by radiation from clothing surface and C is heat transfer by convection from clothing surface + others.

The equations for components of the heat balance equation was used by Fanger

$$H = M - W \qquad (3.5)$$

$$E_d = 3.05\text{x}10^{-3} \ (256 \ T_s - 3373 - P_a) \qquad (3.6)$$

$$E_{sw}: E_{rsw,req} \ (\text{for human comfort}) \ = 0.42 \ (M - W - 58.15) \qquad (3.7)$$

$$L = \ 0.0014M \ (34 - T_a) \qquad (3.8)$$

$$E_{re} = 1.72\text{x}10 - 5M \ (5867 - \ P_a) \qquad (3.9)$$

$$K = \frac{(\ T_s - T_{cl})}{0.155 \ I_{cl}} \qquad (3.10)$$

$$R = 3.96\text{x}10^{-8} f_{cl}[(T_{cl} + 273)^4 - (T_r + 273)^4] \qquad (3.11)$$

$$C = f_{cl}h_c(T_{cl} - T_a) \qquad (3.12)$$

Where; P_a is partial pressure of water vapor in air (kPa), I_{cl} is intrinsic clothing insulation (clo or m^2 °C W^{-1}). The unit of all above components is Wm^{-2}.

Nevins (1971) [51] provided the following equations, which also shown represented graphically in figure 3.2 and 3.3.

$$T_{sk,req} = 35.7 - 0.0275\,(M - W)\ \degree C \tag{3.13}$$

$$E_{rsw,req} = 0.42\,(M - W - 58.15)\ Wm^{-2} \tag{3.14}$$

Where; $T_{sk,req}$ is skin temperature required for comfort ($\degree C$) and $E_{rsw,req}$ is sweat rate required for comfort (Wm^{-2}).
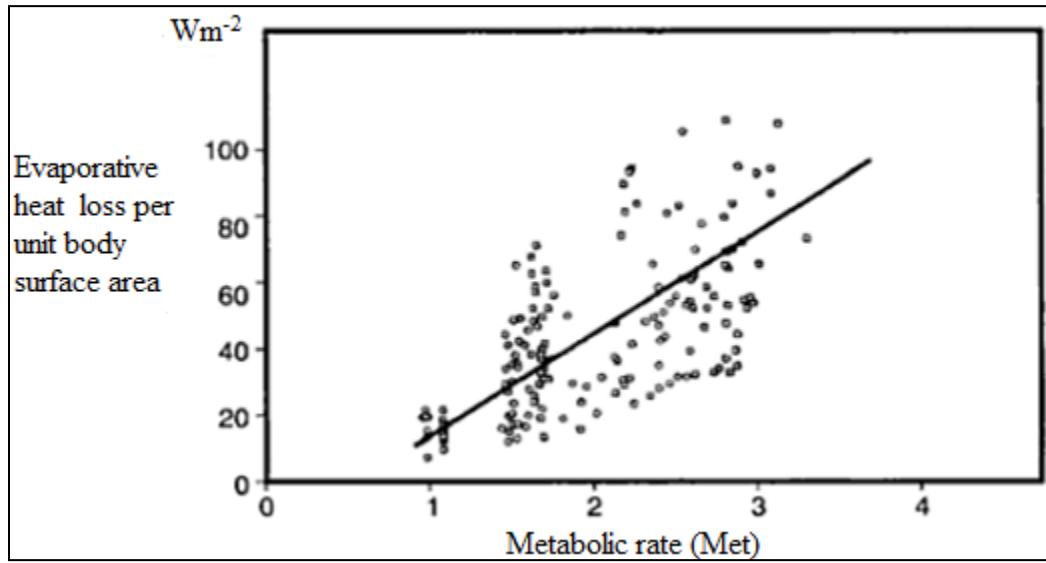
Figure 3.3: Mean skin temperature as a function of the activity level for persons in thermal comfort [47].

By substituting equation (3.5) into equation (3.14) terms into heat balance equation (3.4):

$$E_{st} = (M - W)$$

$$- 3.05\,[5.73 - 0.007(M - W) - P_a] - 0.42[(M - W) - 58.15]$$

$$-\quad 0.00173\,M\,(5.87 - P_a) - 0.014\,M(34 - T_a) \tag{3.15}$$

$$= 3.96 \times 10^{-8} f_{cl}[(T_{cl} + 273)^4 - (T_r + 273)^4] + f_{cl} h_c (T_{cl} - T_a)$$

Where; E_{st} is the rate of increase of energy stored within the human body.

$$T_{cl} = 35.7 - 0.0275(M - W) - 0.155I_{cl}[(M - W)$$

$$- 3.05(5.73 - 0.007(M - W) - P_a)$$

$$- 0.42[(M - W) - 58.15] - 0.00173 \, M \, (5.87 - P_a) \tag{3.16}$$

$$- 0.014 \, M(34 - T_a)$$

$$h_c = \max(\, 2.38(T_{cl} - T_a)^{0.25}, 12.1\sqrt{v}) \tag{3.17}$$

$$f_{cl} = 1.0 + 0.2I_{cl} \quad for \, I_{cl} < 0.5$$

$$= 1.05 + 0.1I_{cl} for \, I_{cl} > 0.5 \tag{3.18}$$

The above equations describe human thermal comfort. Heat is generated in the body it is transferred through clothing; and then lost at the skin to the environment. If the storage term E_{st} is nearly zero, then thermal comfort is achieved. Also, the six basic parameters (T_a, T_r, RH, v, clo, met) obviously appears in above equations complex because they are iterative.

3.4.1.1 Predicted Mean Vote Index (PMV)

The comfort equations (3.15 & 3.16) are one of the earliest and still the most widely used as an index to predict the thermal sensation for a give combination of activity level, clothing value and other thermal environmental parameters [52]. The PMV equation is given by:

$$PMV = [0.303 \exp\{-0.036 \, M + 0.028\} \times E_{st} \tag{3.19}$$

The table 3.4 describes seven-points thermal sensation scale was used by Fanger based on PMV index of a large group of persons.

Table 3.4: Thermal sensation scale was used by Fanger.

Sign	Value	Description
+	3	Hot
+	2	Warm
+	1	Slightly warm
	0	Neutral
-	1	Slightly cool
-	2	Cool
-	3	cold

3.4.1.2 Predicted Percentage of Dissatisfied (PPD)

The purpose of PMV index to predict the mean value of thermal vote of a large group of people faced the same environment conditions. This "mean vote" is indeed an expression for the general degree of discomfort for the group as a whole. But indusial votes are scattered around this mean value. So, PPD was introduced to predict the number of people likely to feel uncomfortably warm or cold. The PPD an index that establishes a quantitative prediction of the percentage of thermally dissatisfied people determined from PMV [52]. When the PMV value has been determine, the PPD can be found from figure 3.4 or determine from the equation:

$$PPD = 100 - 95 \exp\{-(0.03353 \times PMV^4 + 0.2179 \times PMV^2)\} \tag{3.20}$$

Fanger model has limitation related to: PMV has been established for homogenous condition, distinction between local and whole-body thermal comfort.
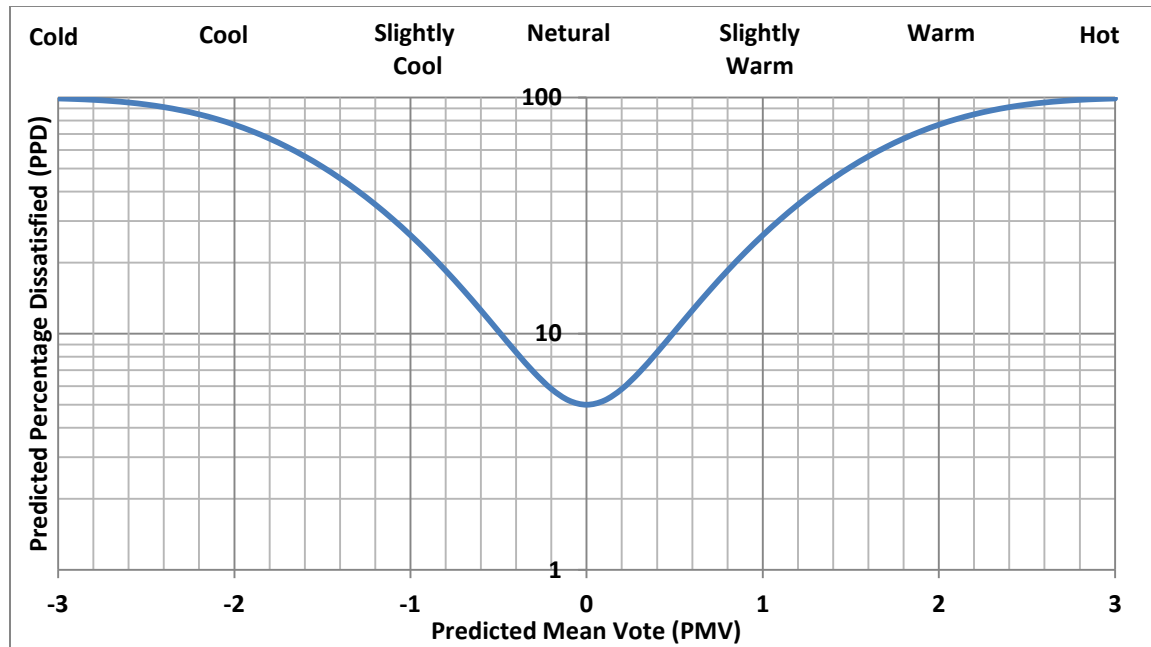
Figure 3.4: The Predicted Percentage of Dissatisfied (PPD) persons as a function of the predicted mean vote (PMV) index.

3.4.2   Pierce Two Node Model

In parallel with work of Fanger (1970), workers at the John B. Pierce Foundation at Yale University conducted a research into determine indices of thermal comfort. The Pierce two-node model depends on using finite difference to estimate physiological parameters for any given thermal environment, that are subjected to metabolic rate and clothing insulation level. The Pierce two node model resented geometry by as two concentric cylinders, tile inner cylinder representing the body core and the thin, outer cylinder representing the skin shell as depicted in figure 3.5. Skin blood flow rate per unit skin surface area play role as boundary line between the two nodes changes [8].

The total body surface area is traditionally estimated from simplified equation of DuBois (1916) [47, 53]:

$$A_D = 0.202 \times W^{0.425} \times H^{0.725} \tag{3.21}$$

Where; A_D is Dubois surface area (m^2), W is weight of body (kg) and H is height of body (m). A standard value of 1.8 m^2 is sometimes used for a 70 kg man of height 1.73m.

The heat balance equation according to ASHRAE (1989 a) [54]:

$$M - W = Q_{sk} + Q_{res} = (C + R + E_{sk}) + (C_{res} + E_{res}) \tag{3.22}$$

For normal conditions heat exchange by conduction is often assumed to be negligible.

Where; Q_{sk} is total rate of heat loss from the skin, Q_{res} is total rate of heat loss through respiration, C is rate of convective heat loss from the skin, R is rate of radiative heat loss from the skin, E_{sk} is rate of total evaporative heat loss from the skin, C_{res} is rate of convective heat loss from respiration and E_{res} is rate of evaporative heat loss from respiration. All above terms have a same unit $\frac{W}{m^2}$.

Note that $E_{sk} = E_{rsw} + E_{dif}$ $\tag{3.23}$

Where; E_{rsw} is rate of evaporative heat loss from the skin through sweating and E_{dif} is rate of evaporative heat loss from the skin through moisture diffusion.

From a practical approach, there are three types of energy, heat production within body (M-W), heat loss at the skin (C+R+E_{sk}) and heat loss due to respiration (C_{res}+ E_{res}). So, the next goal is to quantify components of the heat balance equation in terms of parameters which can be determined by measuring or estimating.

Heat production within the body (M-W) is related to activity of the person. In general, oxygen is taken into the body by breathing air then is transported by the blood to

the cells of the body where it is used to burn food and generates the energy. Depending on the activity level, there is estimate of metabolic rate as shown in table 3.2.

The sensible heat loss (R+C) according to ASHRAE (1989 a) [54] gives as following:

$$C = f_{cl}h_c(T_{cl} - T_a) \tag{3.24}$$

$$R = f_{cl}h_r(T_{cl} - T_r) \tag{3.25}$$

$$C + R = f_{cl}h(T_{cl} - T_\circ) \tag{3.26}$$

$$f_{cl} = \frac{1}{1 + 0.155hI_{cl}} \tag{3.27}$$

Where f_{cl} is clothing area factor (ND) and I_{cl} is clothing insulation (clo).

There is an approximation equation to estimate clothing insulation value indoor which given by McCullough and Jones (1984) [55]:

$$f_{cl} = 1 + 0.31I_{cl} \tag{3.28}$$

The combined effects of air and mean radiant temperature can be combined into a single index; the operative temperature. The operative temperature (T_o) is defined as the uniform temperature of an imaginary enclosure in which man will exchange the same dry heat by radiation and convection as in the actual environment.

$$T_0 = \frac{(h_r T_r + h_c T_a)}{h_r + h_c} \tag{3.29}$$

$$h = h_r + h_c \tag{3.30}$$

The actual heat transfer through clothing (conduction, convection, radiation) is combined into single thermal resistance value R_{cl}. So,

$$C + R = \frac{(T_{sk} - T_{cl})}{R_{cl}} \tag{3.31}$$

Combining equations (3.26 & 3.31) to remove T_{cl}, it will lead

$$C + R = \frac{(T_{sk} - T_0)}{(R_{cl} + \frac{1}{f_{cl}h})} \tag{3.32}$$

Now; Air temperature T_a, mean radiant temperature T_r and the thermal resistance of clothing R_{cl}, are all basic parameters which must be measured or estimated to define environmental human comfort. Mean skin temperature can be estimated as constant value around 33ºC for comfort and 36ºC under heat stress. For a seated person, Mitchell (1974) [47] gives:

$$h_c = 8.3v^{0.6} \quad \text{For } 0.2 < v < 4 \tag{3.33}$$

$$h_c = 3.1 \quad \quad \text{For } 0 < v < 0.2 \tag{3.34}$$

Where; v is the air velocity ($\frac{m}{s}$). The radiative heat transfer coefficient h_r can be given by

$$h_r = 4\epsilon\sigma \frac{A_r}{A_D} \left[273.2 + \frac{T_{cl} + T_r}{2}\right]^3 \tag{3.35}$$

Where; ε is emissivity (ND) and assumed it between 0.95 to 1 and $\frac{A_r}{A_D}$ is ratio between radiating area of the body and DuBois surface body area, it can be estimated as 0.7 for a sitting person and 0.73 for a standing person (Fanger, 1967). T_r is a basic parameter and T_{cl} can be calculated by using iteration techniques. ASHRAE (1989 a) [54] suggests a value of $h_r = 4.7 \frac{W}{m^2 k}$ for most typical indoor condition.

The evaporative heat loss from the skin (E_{sk}) can be evaluated according to ASHRAE (1989 a) [54]:

$$E_{sk} = \frac{w(P_{sk,s} - P_a)}{(R_{e,cl} + \frac{1}{f_{cl}h_e})} \tag{3.37}$$

Where; P_a is water vapor pressure in the ambient air (kPa) and $P_{sk,s}$ is water vapor pressure at the skin, normally assumed to be that if saturated water vapor at skin temperature, T_{sk}, (kPa), $R_{e,cl}$ is evaporative heat transfer resistance of the clothing surface,$(\frac{m^2 kPa}{W})$; h_e is convection evaporative heat transfer coefficient at the clothing surface,$(\frac{W}{m^2 kPa})$ and w is skin wittedness, the fraction of wetted skin area, (ND).

The saturated vapor pressure, P_{sat} (mb) at a temperature T (ºC) is given by Antoine's equation or it can be found from thermodynamic tables.

$$P_{sat} = \exp\left(18.956 - \frac{4030.18}{T + 235}\right) \tag{3.38}$$

The table 3.5 is used to estimate the evaporative heat transfer resistance based on an air layer resistance of 0.014 $\frac{m^2 kPa}{W}$ for range of clothing ensembles.

Table 3.5: Evaporative heat transfer resistance based on an air layer resistance of 0.014 $\frac{m^2 kPa}{W}$ for range of clothing ensembles.

Ensemble	Evaporative resistance of clothing $R_{e,cl}$ $(\frac{m^2 kPa}{W})$
Men's business suit	0.033
Women's business suit	0.028
Men's summer casual	0.013
Jeans and shirt	0.020
Summer shorts and shirt	0.01
Women's casual	0.014
Women's shorts and tank top	0.009
Athletic sweat suit	0.017
Sleepwear and rope	0.024
Overalls and shirt	0.024
Insulated coverall and long underwear	0.037
Work shirt and trousers	0.025
Wool coverall	0.031
cotton coverall	0.027

Usually, the Lewis number is used to determine the value of convective heat transfer coefficient. The Lewis number is defined as the ratio of mass transfer coefficient by evaporation to heat transfer coefficient by convection with no radiation. At sea level for air:

$$LR = \frac{h_e}{h_c} = 16.5 \; K \; kPa^{-1} \rightarrow h_e = 16.5 * h_c \left(\frac{W}{m^2 K}\right) \tag{3.39}$$

The Lewis relation (LR) is not affected by the size and shape of the body, nor by air speed or temperature. It is affected by physical properties of the gases (air and water vapor).

The skin wettedness is the ratio of observed skin evaporation loss to the maximum; this index is considered as particularly suitable for predicting discomfort in hot environmental conditions. It varies from a value of 0.06 when only natural diffusion of water through the skin occurs (E_{dif}) to 1 when skin is completely wet and maximum evaporation occurs (E_{max}).

E_{max} can be calculated by letting w=1 in equation (3.37). Skin wettedness can be calculated from

$$w = 0.06 + 0.94 \frac{E_{rsw}}{E_{max}} \tag{3.40}$$

Where; $E_{rsw} = M_{rsw} \times h_{fg}$ (3.41)

Where; h_{fg} is heat of vaporization of water ($\frac{kJ}{kg}$). It can be founded from thermodynamic tables. M_{rsw} is rate at which sweat is secreted ($\frac{kg}{sm^2}$).

E_{max} can be determined from basic parameter and equation (3.37). Skin evaporation and skin wettedness are often calculated from heat balance equation in terms of wettedness required (w_{req}) or evaporation required (E_{req}) to maintain the body in heat balance. It can be determined by calculating E_{rsw} by using equation (3.41).

$$M_{rsw} = 4.7 \times 10^{-5} \times W_{SIG_b} \exp\left(\frac{W_{SIG_{sk}}}{10.7}\right) \tag{3.42}$$

49

Where; W_{SIG_b} is mean body temperature component of sweating controller signal (ND) and $W_{SIG_{sk}}$ is mean skin temperature component of sweating controller signal (ND).

$$W_{SIG_b} = T_b - T_{b,n} \ for \ T_b > T_{b,n} \tag{3.43}$$

$$W_{SIG_{sk}} = T_{sk} - T_{sk,n} \ for \ T_{sk} > T_{sk,n} \tag{3.44}$$

Where; T_b is mean body temperature (°C), $T_{b,n}$ is mean body temperature for a person in thermal neutrality (°C) and $T_{sk,n}$ is mean skin temperature for a person in thermal neutrality =33.7 °C.

$$T_b = \propto T_{sk} + (1-\propto)T_{cr} \tag{3.45}$$

$$T_{b,n} = \propto T_{sk,n} + (1-\propto)T_{cr,n} \tag{3.46}$$

Where; $\propto$ is relative mass of skin to core (ND), T_{cr} is mean core temperature (°C) and $T_{cr,n}$ is mean core temperature for a person in thermal neutrality=36.8 °C.

The mean body temperature equation means a weighted of skin and core temperature, with weighting $\propto$ depends on degree of vasodilatation. Typical values for $\propto$ are 0.2 for thermal equilibrium while sedentary, 0.1 in vasodilatation and 0.33 for vasoconstriction. The mean body temperature in neutrality $T_{b,n}$ is

$$T_{b,n} = 0.2 \times 33.7 + 0.8 \times 36.8 = 36.18°C$$

There are two types of heat loss from respiration. Firstly, convective heat loss from respiration (C_{res}) is resulted from cool air being inhaled, then heated to core temperature in the lungs and then heat transfer in exhaled air to the environment. In addition, inhaled air is moistened to saturation by the lungs. Secondly, evaporative heat loss from respiration (E_{res}) is due to body inhaled, this will lead a heat transfer from the body core to outside environment.

The total heat loss from respiration is given by ASHRAE (1989 a) [54]:

$$C_{res} = \frac{0.0014\ M(34 - T_a)}{A_D} \tag{3.47}$$

$$E_{res} = \frac{0.0173\ M(5.87 - P_a)}{A_D} \tag{3.48}$$

A_D is defined in equation (3.21). All other values are basic parameters.

Where; 34°C is exhaled air temperature, 5.87 kPa is the saturation vapor pressure at lung temperature: 35°C and P_a is vapor pressure of ambient temperature in kPa.
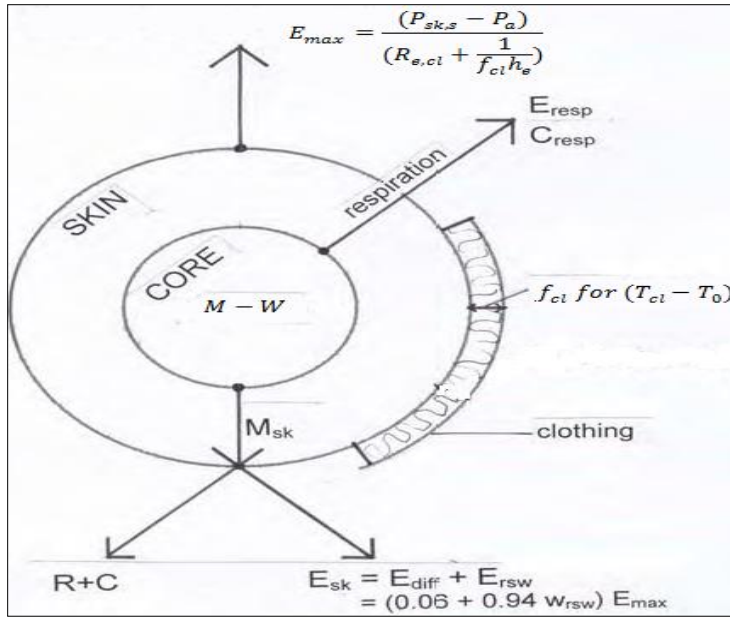
Figure 3.5: Two node model representation.

3.4.3   Berkeley Model

It is one of the most sophisticated thermal comfort models in existence. It is capable of analyzing human thermoregulation and comfort responses in non-uniform and

transient conditions. The model has been under development at UC Berkeley since the early 90s.

The Berkeley model [56-61] has been developed to simulate the human body response, by discreatizing it into major finite segments. Each of these segments consists of four body layers; the core, the muscle, the fat, and the skin tissue, in addition to a clothing layer [4, 5]. So, the Berkeley model investigates the physiological response through examining the local sensation and the local comfort of each body segment. The body thermal sensation in a given environment depends on the skin temperature (cold through hot). However, the thermal comfort depends on the desired physiological state (uncomfortable through comfortable). Table 3.6 describes the nine-point scale for thermal sensation and comfort as used by Berkeley model.

So, the sensation and comfort are interrelated but their interaction is of a complex nature, which includes the environment and the dynamic physiological conditions. The local sensation is calculated from the body segment skin temperatures, average skin temperature (T_{sk}), core temperature (T_{cr}), the rate of change of skin temperature (dT_{sk}/dt) and rate of change of core temperature (dT_{cr}/dt). The overall sensation (OS) is a complex combination of these local sensation values. On the other hand, the local comfort (LC) is calculated from local sensation values (LS) as well as the overall sensation (OS) value, at the same time the overall comfort (OC) is a combination of the local comfort value as sown in figure 3.6 [62, 63].

The major advantages of using the Berkeley model can be summarized through; it provides a powerful tool to analyze and understand the human physiological response

under different boundary conditions. It also generates the human's overall comfort prediction as well as the comfort of each body segment (local sensation). Additionally, the model can demonstrate how the changes in the clothing layer can affect the comfort and the sensation results. The Berkley model also adopts full radiant, convective and conductive heat transfer mechanisms including the localized thermoregulatory response such as the perspiration, the respiration, and the blood flow changes.

Table 3.6: Sensation and comfort vote description for Berkeley model.

Berkeley Model			
Sensation		Comfort	
4	Very hot	4	Very comfortable
3	Hot	3	
2	Warm	2	
1	Slightly warm	1	Just comfortable
0	Neutral	0	
-1	Slightly cool	-1	Just uncomfortable
-2	cool	-2	Very uncomfortable
-3	Cold	-3	
-4	Very cold	-4	
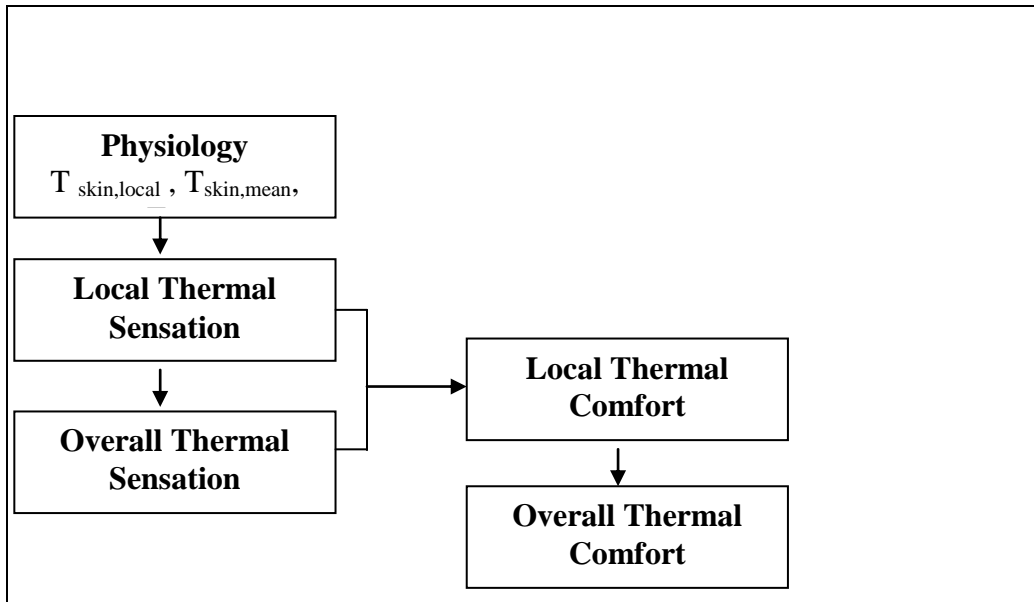
Figure 3.6: Flow chart demonstrates relations between sensation and comfort [62].

3.4.4 Other Human Comfort Indices

The indicator of human thermal comfort is technically called the thermal comfort index. A thermal comfort index method uses a model that provides a single number that represents the degree of discomfort caused by an environment. The model is based upon research and integrates the relevant factors of the environment (temperatures, air flows, humidity, etc) surrounding a person in a way representing the comfort response of the person.

A number of thermal comfort indices have been studied for the design of HVAC systems. Below, the most widely thermal comfort indices used [64]:

3.4.4.1 Equivalent Temperature (T_{eq})

The equivalent temperature (T_{eq}) is the temperature of an imaginary enclosure with the mean radiant temperature equal to air temperature and still air in which a person has the same heat exchange by convection and radiation as in the actual conditions. The advantages of using T_{eq} are expressing the effects of combined thermal influences in a single figure, easy to interpret and explain [33, 34]. It is particularly useful for differential assessment of the climatic conditions. On the other side the drawback of using equivalent temperature index is not take into account humidity, thus it is unsuitable for temperatures higher than about 24°C, as at such levels humidity becomes increasingly important. Bedford produced equation based on regression analysis to measure T_{eq}.

$$T_{eq} = 0.522T_{db} + 0.478Tr - 0.21 \times v \times (37.8 - T_{db}) \tag{3.49}$$

3.4.4.2 New Effective Temperature Scale (ET*)

The 2-node model was introduced in 1970 specifically to formulate a new effective temperature scale. It is used to determine the heat flow between the environment, skin and core body areas on a minute by minute basis. Starting from an initial condition at time=0, the model iterates until equilibrium has been reached (60 minutes is a typical time). The final mean skin temperature and skin wettedness are then associated with an effective temperature. The model represents the human body as two concentric cylinders, a core cylinder and a thin skin cylinder surrounding it. Clothing and sweat are assumed to be evenly distributed over the skin surface. At time "zero", the cylinder is exposed to a uniform environment, and the model produces a minute-by-

minute simulation of the human thermoregulatory system. After reach an equilibrium

state, the final surface temperature (ET*), standard effective temperature (SET*), and

other indices. ET* is define as the temperature of an environment at 50% relative

humidity in which a person experiences the same amount heat loss as radiation,

convection and evaporation in the actual environment.

ET* lines coincide with dry bulb temperature (T_{db}) values at the 50% RH curve.

Radiation is taken into account by using operating temperature (T_0) on the horizontal

scale instead of T_{db}. The ET* lines are shown on the psychometric chart for the following

conditions: clothing: 0.6 clo, activity: 1 met, air movement =< 0.2 m/s, exposure time: 60

min. The figure 3.7 depicts Psychometric chart showing constant ET* line.
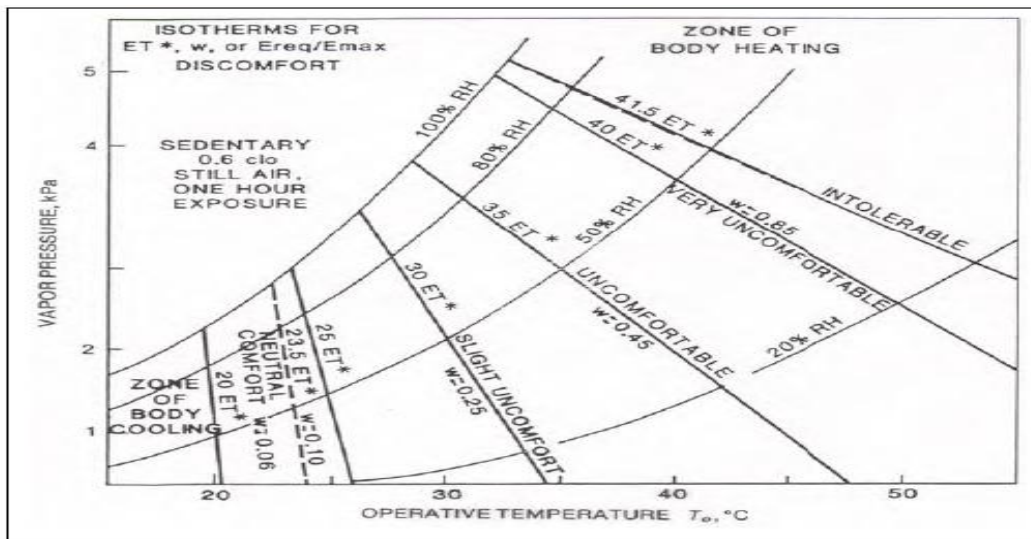
Figure 3.7: Psychometric chart showing constant ET* line.

3.4.4.3 Standard Effective Temperature (SET*)

SET* numerically represents the thermal strain experienced by the cylinder

relative to a "standard" person in a "standard" environment. The advantage of using

SET* is to allow thermal comparisons between environments at any combination of the physical input variables, but there is a drawback of requiring "standard" people. It was developed based on a laboratory study with a large number of subjects, empirical functions between two comfort indices, and skin temperature and skin wettedness. These functions are used in the 2-Node model to produce predicted values of the votes of populations exposed to the same conditions as the cylinder. The measurement SET* depends on predict the average body temperature (T_b) by using the two node model. The T_b was measured for a wide range of metabolic rates, clothing levels, air velocity, air pressure, air temperature, mean radiant temperature and humidity. For standard conditions (1.1 met) it is taken as 36.35°C and the following tables 3.7& 3.8 gives some regulations.

Table 3.7: SET index for standard condition 1.1 met and T_b is 36.35ºC.

SET	10	14	18	22	26	30	34	38	42
T_b	33.90	34.55	35.63	36.27	36.44	36.55	36.67	36.78	36.97

Table 3.8: SET index is related to comfort votes, sensation and physiology.

SET	Vote	Sensation	Physiology
> 37.5	> 3	very hot, great discomfort	Increasing failure of evaporative regulation.
37.5-34.5	+2 to +3	hot, very unacceptable	profuse sweating
34.5-30	+1 to +2	warm, uncomfortable, unacceptable	sweating
30-25.6	+0.5 to+1	slightly warm, slightly unacceptable	slight sweat, vasodilatation
25.6-22.2	-0.5,+0.5	comfortable, acceptable	physiological thermal neutrality
22.2-17.5	-1 to -0.5	slightly cool, slightly unacceptable	initial vasoconstriction
17.5-14.5	-2 to -1	cool, unacceptable	slow body cooling
14.5-10	-3 to -2	cold, very unacceptable	beginning of shivering

3.4.4.4 Predicted Thermal Sensation (TSENS)

TSENS "Predicted Thermal Sensation" is a predicted vote on the seven-point thermal sensation scale as shown in table 3.9:

Table 3.9: Predicted thermal sensation scale.

Vote	+3	+2	+1	0	-1	-2	-3
Sensation	Hot	Warm	Slightly warm	Neutral	Slightly cold	Cool	Cold

By application to the data collected by the Rohles-Nevins [65] study a thermal sensation index

(TSENS) was created with a regression equation giving:

$$TSENS = 0.245SET^* + 0.0165PSET^* - 6.741 \qquad (3.50)$$

Where SET* is the standard effective temperature and PSET* is the corresponding water vapor pressure at this temperature.

3.4.4.5 Predicted Thermal Discomfort (DISC)

"Predicted Thermal Discomfort" is used to predict a vote on a scale of thermal discomfort. It is similar to TSENS except that it accounts for discomfort due to sweating in warm conditions. In non-sweating conditions, DISC=TSENS. The table 3.10 presents the Prediction of thermal discomfort scale.

Table 3.10: Predicted thermal discomfort scale.

Vote	4.7	3.7	2.7	1.3	0-0.3
Sensation	Intolerable	Very uncomfortable	Uncomfortable	Slightly uncomfortable	Comfortable

3.4.4.6 Thermal Sensation Vote (TS)

TS is an equation that predicts thermal sensation vote using a linear function of air temperature and partial vapor pressure. The TS equation is:

$$TS = 0.245T_a + 0.248P - 6.475 \qquad (3.51)$$

Ta is the air temperature in degrees Celsius and p is the partial vapor pressure in kPa. The TS equation arises from a study similar to the PMV-PPD study described above.

3.5 Summary

The complex interaction of air temperature, mean radiant temperature, air velocity and humidity makes up the human thermal environment. To achieve a satisfactory thermal environment it is useful to be able to predict what the effect of a particular combination of thermal conditions will be on human occupants. So, this chapter introduced a comprehensive background of the human thermal environment, basic definitions, main factors affecting on thermal comfort, human heat balance equation in terms of heat generation and heat exchange with the environment. Then presents the most popular and widely used comfort models to estimate local and overall sensation and comfort, Fanger model in terms of PMV and PPD indices, pierce two node model and Berkeley model. Finally, some important indices widely used in comfort and thermal sensation such as T_{eq}, ET*, SET*, TSENS, DISC and TS.

CHAPTER FOUR

THERMODYNAMIC AND PSYCHOMETRIC ANALYSES

This chapter discusses the effect of manipulating the Relative Humidity RH of in-cabin environment on the thermal comfort and human occupants' thermal sensation. The study uses thermodynamic and psychometric analyses, to incorporate the effect of changing RH along with the dry bulb temperature on human comfort. Specifically, the study computes the effect of changing the relative humidity on the amount of heat rejected from the passenger compartment and the effect of relative humidity on occupants comfort zone. A practical system implementation is also discussed in terms of an evaporative cooler design. The results show that changing the RH along with dry bulb temperature inside vehicular cabins can improve the air conditioning efficiency by reducing the heat removed while improving the Human comfort sensations as measured by the Predicted Mean Value PMV and the Predicted Percentage Dissatisfied PPD indices.

4.1 Introduction

About 26 billion liters of fuel are used annually to cool vehicle passenger compartments in the United States. Europe would use about 6.9 billion liters if all its vehicles were equipped with air conditioners. Japan uses about 1.7 billion liters to air condition its vehicles [1, 7]. These numbers along with the growing demands for better vehicular energy utilization, and more efficient performing vehicles, have led to an

increased interest in revising the current approach to mobile enclosures HVAC, through investigating and analyzing its sub-systems, its control strategies, and design.

However, it relies on adjusting the cabin environment temperature while relying on the passengers to exchange heat with their environment to reach the desired steady state conditions. This approach is not optimal and will lead to increased loads on the HVAC system (compressor, fan, etc), hence leading to increased fuel consumption.

So, there is a continuing need for sophisticated tools to evaluate the effectiveness of advanced climate control systems. And the effort spent by car manufacturers to increase the thermal comfort in cabs has leaded to the research and development of innovative methods and instruments able to predict the thermal sensation of driver and passengers under both transients and steady state conditions.

4.2 Approach - Thermodynamics and Psychometric Analysis

Proposed research aims at investigating the effect of controlling RH along with dry-bulb temperature on the amount and rate of heat rejected from the cabin which controls the amount of fuel expended to run the Air Conditioning (AC) system and the time duration needed to provide satisfactory thermal comfort to cabin occupants, respectively.

This chapter will discuss both the thermal sensation and the thermal comfort zone, when the RH control is described. The thermal comfort will be analyzed based on the international accepted standards for vehicular cabins; mainly the Predicted Mean Value

PMV index. The theory of Fanger model with PMV and PPD indices is briefly discussed in chapter 3.

On the other hand, the thermal comfort zone study will include an analytical approach covering the Psychometry and thermodynamic calculations needed to study the RH effect and temperature on thermal comfort.

4.2.1   Thermodynamic Analysis

To start the relevant calculations, the mathematical definitions of the terms (RH, etc) used are first discussed. The relative humidity RH is defined as the ratio of the mole fraction of the vapor in the mixture to the mole fraction of vapor in a saturated mixture at the same temperature and total pressure, as in equation (4.1).

$$RH = \frac{P_v}{P_g} \tag{4.1}$$

Where, P_v is the partial pressure of the vapor as it exists in the mixture, and P_g is the saturation pressure of the vapor at the same temperature. At the same time, the humidity ratio ω of an air-water vapor mixture is defined as the ratio of the mass of water vapor m_v to the mass of dry air m_a, which can expressed in equation (4.2) or (4.3) when the equation of state is used;

$$\omega = \frac{m_v}{m_a} \tag{4.2}$$

$$\omega = 0.622 \frac{P_v}{P_a} \tag{4.3}$$

Hence, an expression to relate the relative humidity RH to the humidity ratio ω, can be described in equation (4.4);

$$RH = \frac{\omega P_a}{0.622 P_g} \tag{4.4}$$

First, the thermodynamic analyses [66-68] are conducted to investigate the RH effect on the amount of hear rejected. This is done by applying first law of thermodynamics to gas-vapor mixture as in figure 4.1, then assuming that of rate of work $\dot{W}_{cv} = 0$, and ignoring all the kinetic and potential energy effects, the rate of heat transfer reduces at steady state to the expression in equation (4.5)

$$\dot{Q}_{c.v.} + \sum \dot{m}_i h_i = \sum \dot{m}_e h_e \tag{4.5}$$

Where; $\dot{Q}_{c.v.}$: rate of heat transfer , $\dot{m}_i$: inlet mass flow rate, h_i:specific inlet enthalpy, $\dot{m}_e$: exit mass flow rate and h_e:specific exit enthalpy.
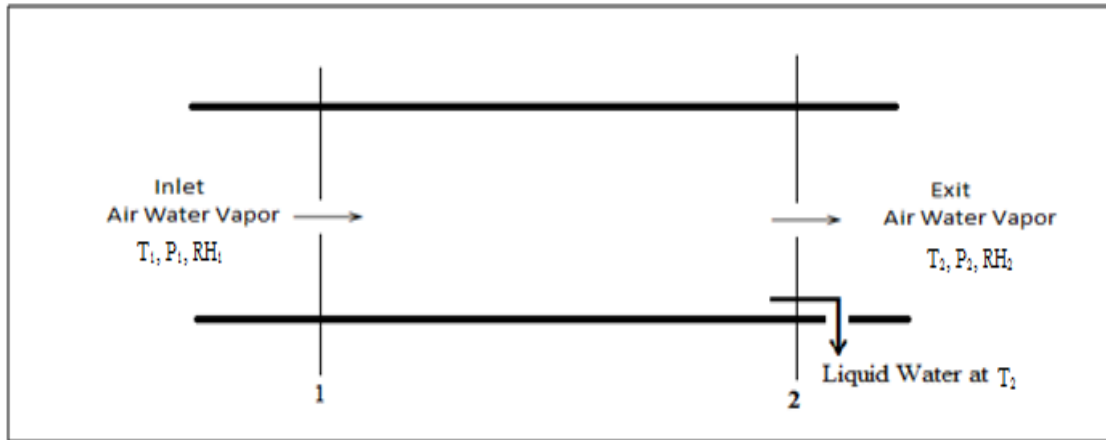
Figure 4.1: Schematic for air conditioning process.

Noting that the continuity equations for the mixture are in equations (4.6) and

(4.7):

$$\dot{m}_a = \dot{m}_{a1} = \dot{m}_{a2} \tag{4.6}$$

$$\dot{m}_{v1} = \dot{m}_{v2} + \dot{m}_{l2} \tag{4.7}$$

Where; $\dot{m}_{a1}$: inlet mass of dry air, $\dot{m}_{a2}$: exit mass of dry air, $\dot{m}_{v1}$:inlet mass of vapor air,

$\dot{m}_{v2}$:exit mass of vapor air and $\dot{m}_{l2}$:mass of water condensation at exit.

Then the first law of thermodynamic can be described in equation (4.8);

$$\dot{Q}_{c.v.} + \dot{m}_a h_{a1} + \dot{m}_{v1} h_{v1} = \dot{m}_a h_{a2} + \dot{m}_{v2} h_{v2} + (\dot{m}_{v1} - \dot{m}_{v2})h_{l2} \tag{4.8}$$

Furthermore, dividing equation (4.8) by $\dot{m}_a$ and substituting $\dot{m}_v = \omega \dot{m}_a$, then the first

law of thermodynamic expression can be written in the forms in (4.9) and (4.10);

$$\frac{\dot{Q}_{c.v.}}{\dot{m}_a} + h_{a1} + \omega_1 h_{v1} = h_{a2} + \omega_2 h_{v2} + (\omega_1 - \omega_2)h_{l2} \tag{4.9}$$

$$\frac{\dot{Q}_{c.v.}}{\dot{m}_a} = Cp_a(T_2 - T_1) + \omega_2 h_{v2} - \omega_1 h_{v1} + (\omega_1 - \omega_2)h_{l2} \tag{4.10}$$

With Cp_a being the Specific heat at constant pressure for dry air ($\frac{KJ}{Kg.K}$).

The previous analysis gives how relative humidity is affect on the amount of heat

rejection. So, the application of effect relative humidity on the air conditioning system is

evaporative cooler.

4.2.2 Psychometric Processes

Psychrometric chart presents the properties of atmospheric air at a specified

pressure and two independent intensive properties. The psychrometric chart is a plot of

absolute humidity versus dry-bulb temperature and shows lines of constant relative humidity, wet bulb temperature, specific volume, and enthalpy for the atmospheric air. So given the values of any two psychometric properties, all the others can be found without computation. The chart arrangement is as follows.

a. Lines of constant dry bulb temperature (DBT) are vertical.

b. Lines of constant dew point temperature (DPT), vapor pressure (vp) and humidity ratio (ω) are horizontal.

c. Lines of constant enthalpy (H) and wet bulb temperature (WBT) are diagonal, down to the right.

d. The saturation line of 100% relative humidity curves, down to the left. The temperatures in that line are the coinciding of dew point, dry bulb and wet bulb temperatures in saturated air.

e. Curves of constant relative humidity (RH) are located below the saturation line and generally parallel to it.

f. Lines of constant specific volume (v) are widely located downward to right more steeply than wet bulb lines.

All constant lines are depicted in psychometric char in figure 4.2.
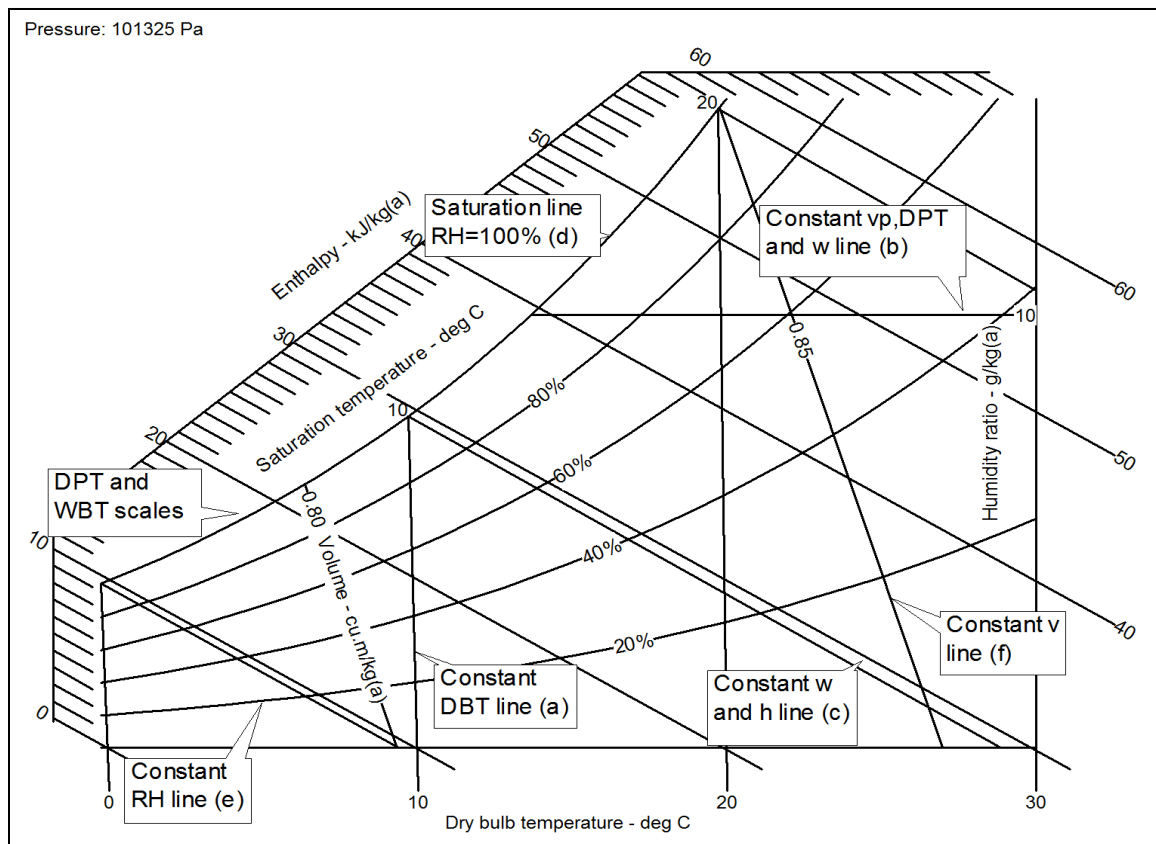
Figure 4.2: Schematic of psychometric chart shows all constant lines.

Maintaining a living space or an industrial facility at the desired temperature and humidity requires some processes called air-conditioning processes. These processes include simple heating (raising the temperature), simple cooling (lowering the temperature), humidifying (adding moisture), and dehumidifying (removing moisture). Sometimes two or more of these processes are needed to bring the air to a desired temperature and humidity level. Various air-conditioning processes are illustrated on the psychrometric chart in figure 4.3, which simple heating and cooling processes appears horizontal lines on this chart since the moisture content of the air remains constant (ω= constant) during these processes.
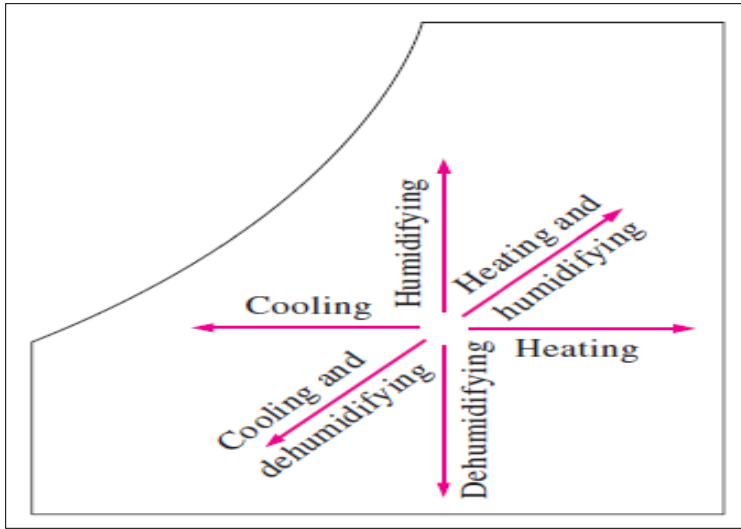
Figure 4.3: Various air conditioning process [67].

4.3 Practical Application- Evaporative Cooling

The evaporative cooling process is shown schematically and on a psychrometric chart in figure 4.4. Hot, dry air at state 1 enters the evaporative cooler, where it is sprayed with liquid water. Part of the water evaporates during this process by absorbing heat from the airstream. As a result, the temperature of the airstream decreases and its humidity increases (state 2). In the saturating case, the air leaves the evaporative cooler saturated at state 2. This is the lowest temperature that can be achieved by this process. The evaporative cooling process is adiabatic saturation process since the heat transfer between the airstream and the surroundings is usually negligible. Therefore, the evaporative cooling process follows a line of constant wet-bulb temperature on the psychrometric chart. Since the constant-wetbulb- temperature lines almost coincide with the constant-enthalpy lines, the enthalpy of the airstream can also be assumed to remain constant. That is,

$$
\left.\begin{array}{l}
T_{wb} \cong constant \\[1.5em]
h \cong constant
\end{array}\right\}
\qquad (4.11)
$$
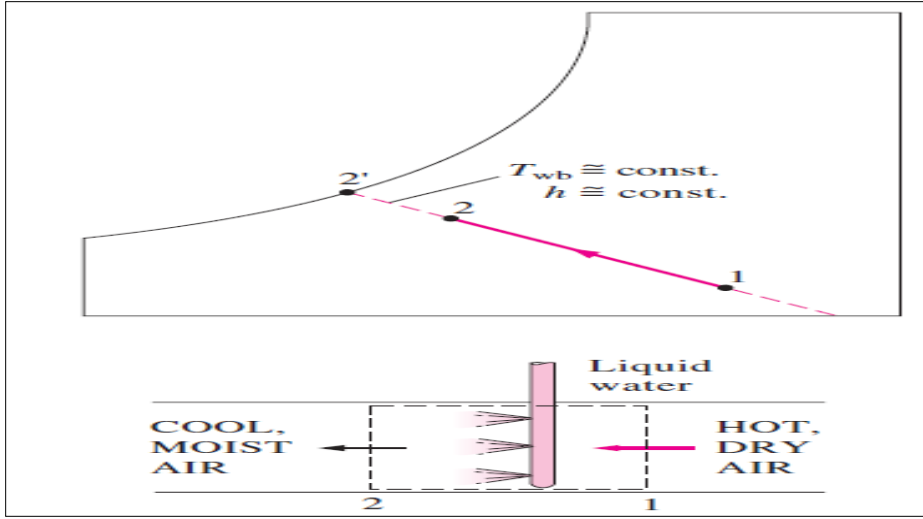
Figure 4.4: Evaporative cooling process [67].

4.4 Analysis

The expression in equations (4.9) and (4.10) can then be used to describe the RH effect on the amount of heat rejected in an AC system that manipulates its RH and dry-bulb temperature. So, the vehicle's cabin final RH effect can be directly plotted as for different initial dry-bulb temperatures as shown in figure 4.5. Inspecting this figure shows that when the final relative humidity increases; the amount of heat rejected or released decreases. Specifically, at an initial relative humidity, initial dry bulb temperature and final dry bulb temperature of 80%, 45°C and 25°C respectively. The amount of heat transfer rejected for final relative humidity RH values of 30%, 40%, 50% and 60% are 137.38, 132.3, 127.18 and 122.03 kJ/ kg, respectively. Also, the effect of changing the initial relative humidity on the amount of heat rejected can be seen in figure 4.6. This

figure shows that as the initial relative humidity value increases, the amount of heat transfer released also increases. For example, at an initial dry bulb temperature, final dry bulb temperature and final relative humidity values of 50ºC, 25ºC and 40% respectively; the amount of heat rejected when initial relative humidity are 70%, 80% and 90% are 156.2, 180.14 and 204.74 kJ/ kg respectively. So, the energy efficient value of RH for the case of a combined process of cooling and dehumidification with initial conditions of hot and humid air is found to be 60%. The effect of the initial conditions on the amount of heat removed and the thermal sensation can be displayed in table 4.1, which shows two initial conditions scenarios; hot and humid initial condition (Ta=50 ºC, RH=80%) and hot and dry initial conditions (Ta=50 ºC, RH=10%). For each scenario, there are six different processes; each with the same initial values but with different final conditions. At the end, each process will provide the same thermal sensation value as computed by the PMV index (PMV=0.1), knowing that process has a different amount of heat removed. These six processes starting with the hot and humid, and hot and dry initial conditions are displayed in figures 4.7, 4.8 respectively. From these two figures, the heat removed under hot and dry initial condition is less than the case of hot and humid initial conditions. For example, the heat removed from process A under hot, humid conditions and hot, dry are 172.03 kJ/ kg and 14.61 kJ/ kg, respectively. Also from these two figures, the low ambient temperature and high humidity is more energy efficient than a high ambient temperature and low humidity for both scenarios. For example, the heat removed from process A (low Ta 25ºC and high RH 60%) is less than process F (high Ta 26 ºC and low

RH 23%) for both different initial conditions. So, a HVAC system will reach a final state with low Ta and high RH faster than high Ta and low RH, because it rejects less heat.
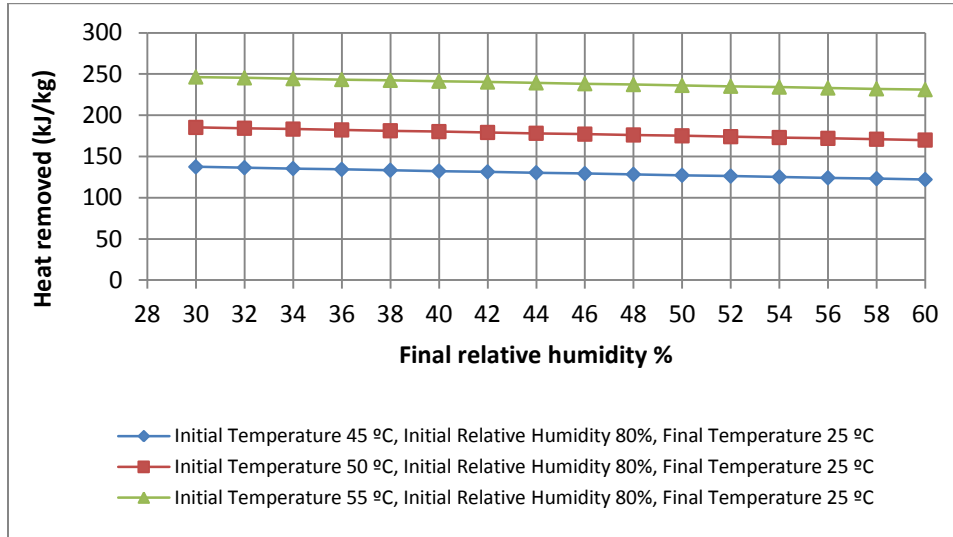
Figure 4.5: Heat transfer removed versus final relative humidity for different initial temperature.
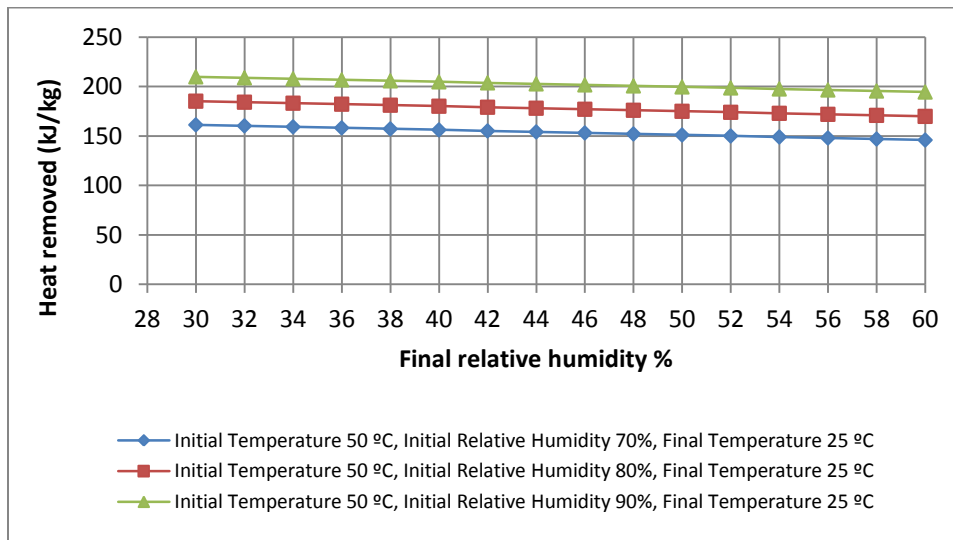
Figure 4.6: Heat transfer removed versus final relative humidity for different initial relative humidity.

Table 4.1: Heat removed for the same PMV with different final RH and air temperature at hot, humid initial condition and hot, dry initial condition.

Process Name	PMV=0.1									
	Hot and Humid Initial Condition					Hot and Dry Initial Condition				
	Initial Condition		Final Condition		Heat Removed	Initial Condition		Final Condition		Heat Removed
	Ta (° C)	RH %	Ta (° C)	RH %	Q (KJ/Kg)	Ta (° C)	RH %	Ta (° C)	RH %	Q (kJ/kg)
A	50	80	25	60	172.03	50	10	25	60	14.61
B	50	80	25.2	52	175.68	50	10	25.2	52	18.26
C	50	80	25.4	44	179.41	50	10	25.4	44	21.98
D	50	80	25.6	37	182.68	50	10	25.6	37	25.26
E	50	80	25.8	30	186.03	50	10	25.8	30	28.6
F	50	80	26	23	189.44	50	10	26	23	32.02
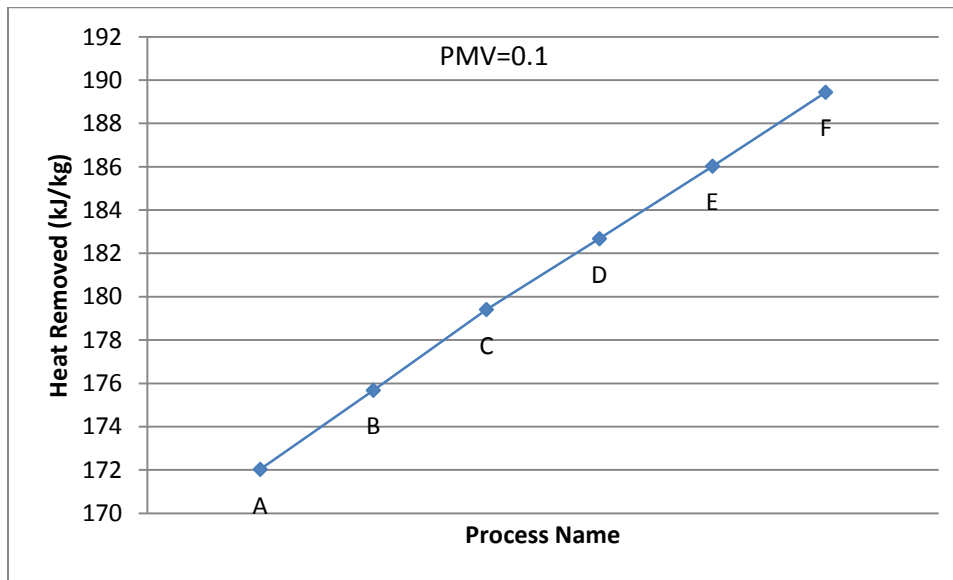
Figure 4.7: Heat removed for the same PMV with different final RH and air temperature at hot and humid initial condition.
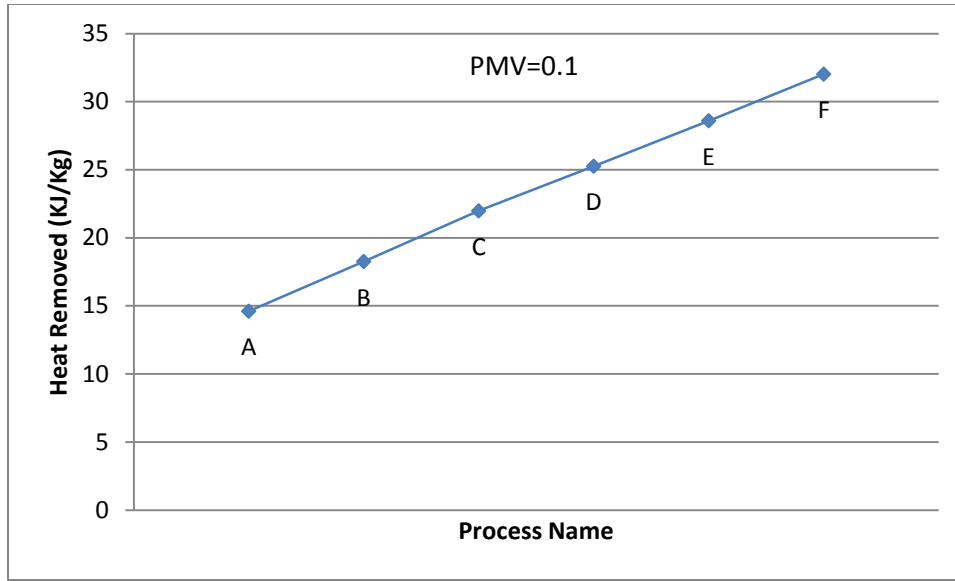
Figure 4.8: Heat removed for the same PMV with different final RH and air temperature at hot and dry initial condition.

The psychometric analysis provides more details on the actual process of changing the RH value, during the conditioning process. This analysis not only provides the time duration needed to achieve thermal comfort range but also, describes the actual implementation associated efficiencies. Changing the RH for a vehicular AC system can be done through an evaporative cooling system, with one type shown schematically from [29] in figure 4.9 along with its psychometric trace. Following the psychometric trace; the ambient air enters through desiccant (state 1) under adiabatic and dehumidification process $(1 \rightarrow 2)$ and air becomes hot and dry at state (2). Then the hot air enters to the heat exchanger, heat is removed by the air leaving the heat exchanger under constant humidity ratio $(2 \rightarrow 3)$. In this analysis another heat exchanger will be used to achieve the temperature at state (3). The warm air exit from heat exchanger (state 3) is cooled and humidified by sprayed water inside the evaporator under adiabatic saturation process

$(3 \rightarrow 4)$. The cold humid air (state 4) is entered to the passenger compartment and absorbed the heat (state 5) under constant humidity ratio $(4 \rightarrow 5)$. Usually the waste heat exit from heat exchanger used to get rid of the moisture trap inside the desiccant's layers.
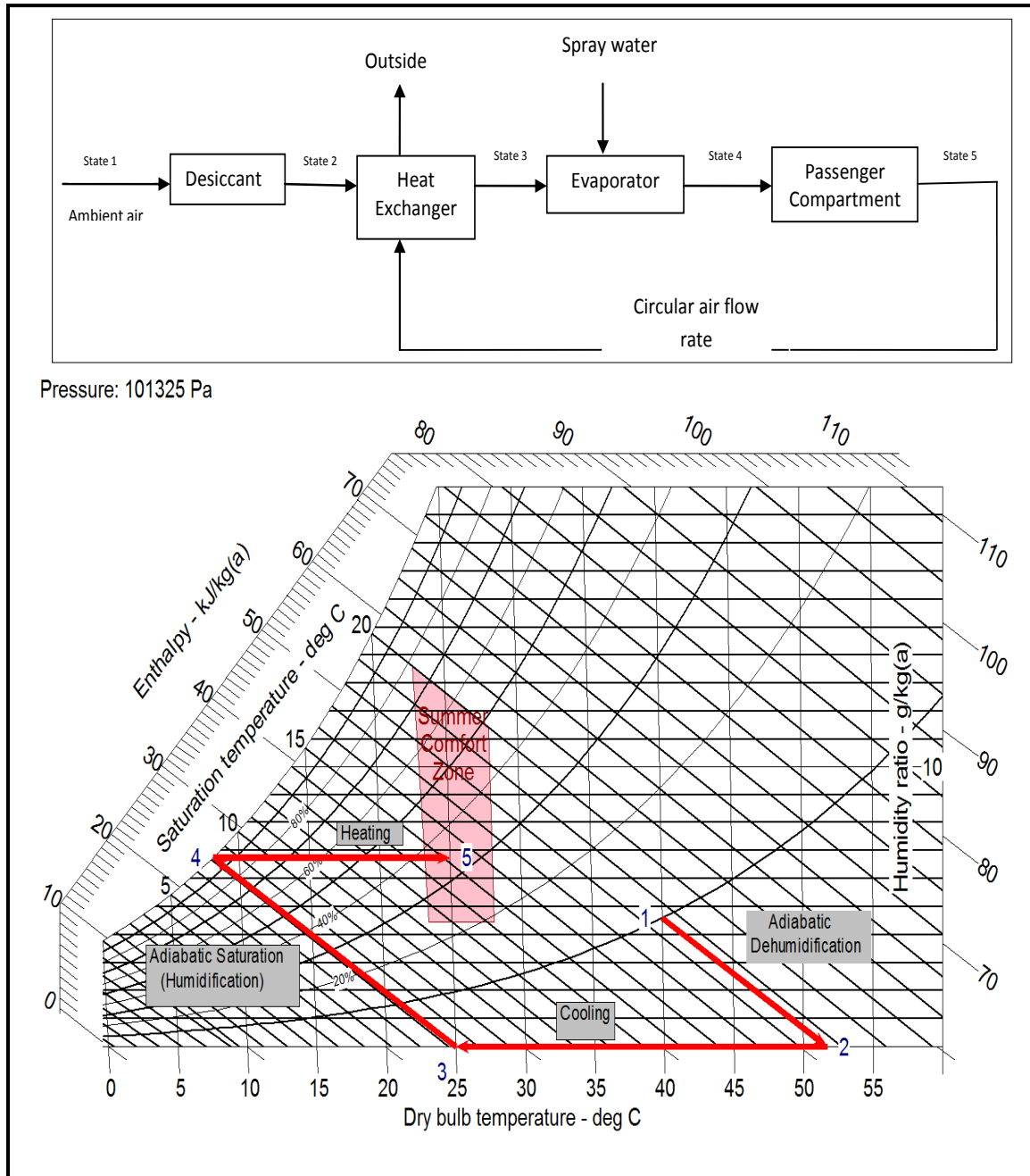
Figure 4.9: Evaporative cooling system representation.

One can further discuss the performance of the evaporative cooling system through analyzing its sub-systems sensitivities and behavior. Specifically, the effect of desiccant, the heat-exchanger, and the evaporation process performances can be analyzed. For the desiccant performance, it is affected by the air humidity leaving the desiccant (state 2) that also changes the adiabatic dehumidification process $(1 \rightarrow 2)$. Figure 4.10 displays the changes of the final humidity ratio of state 2, showing that when the desiccant performance decreases, the humidity ratio increases. Additionally, as the circular mass flow rate increases, the humidity ratio increases because the mass flow rate changes when the humidity ratio changes as shown in figure 4.11, while the water spray requirements do not change considerably as shown in figure 4.12.
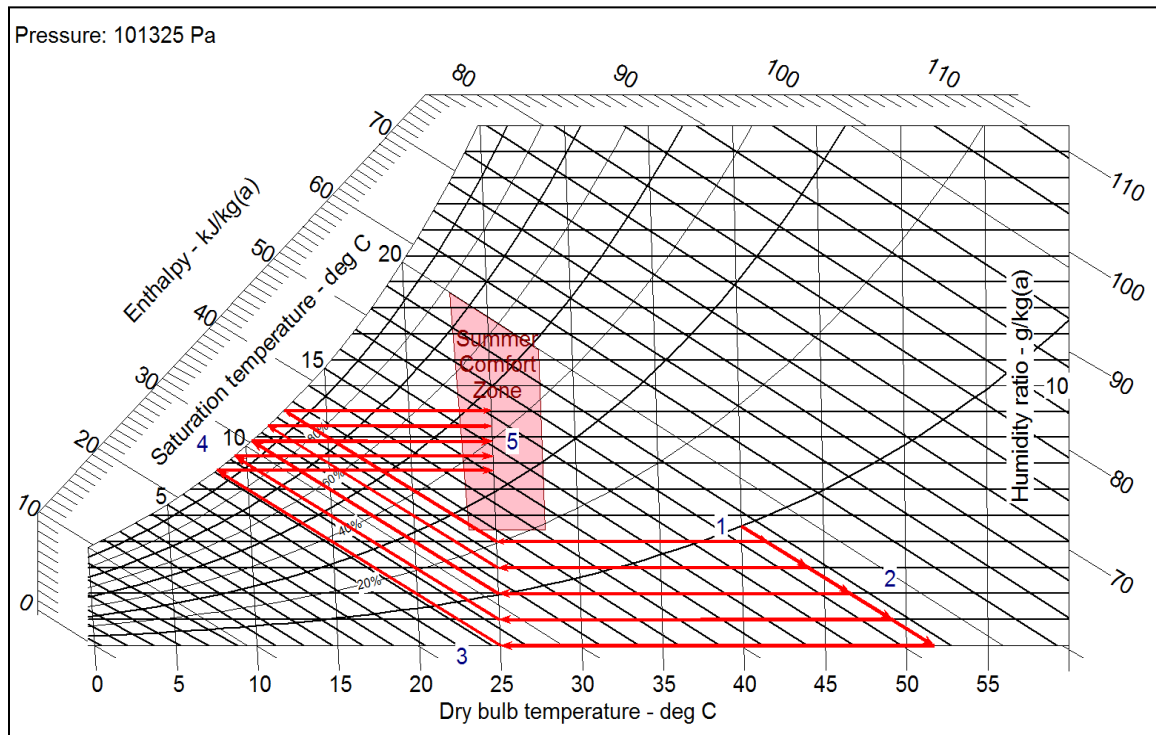
Figure 4.10: Psychometric chart shows effect of desiccant performance on evaporative cooling system.

74
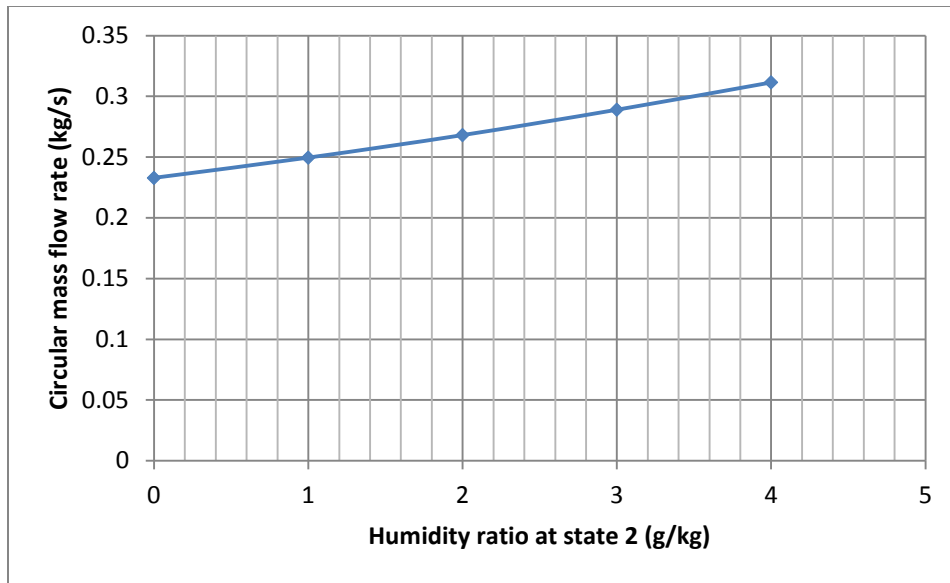
Figure 4.11: Effect of desiccant performance on the mass flow rate of evaporative cooling system**.**
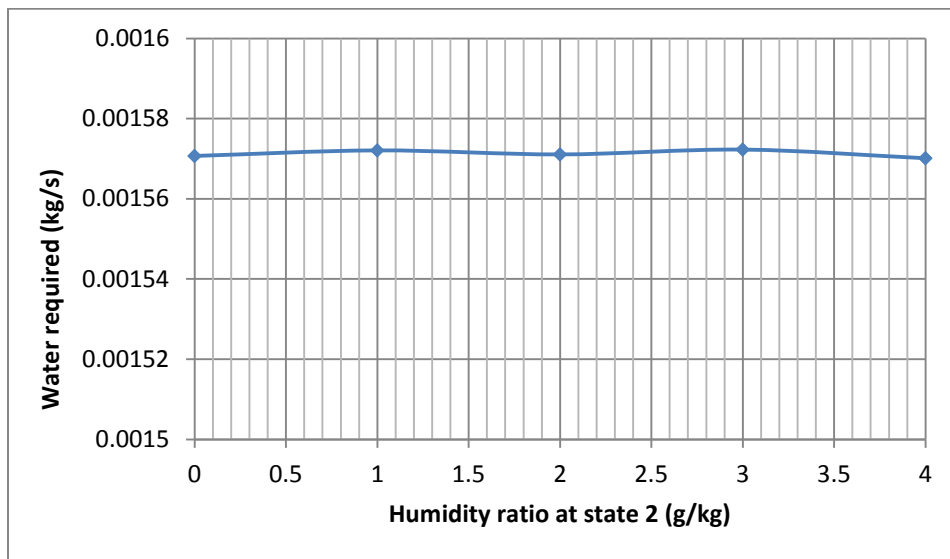
Figure 4.12: Effect of desiccant performance on the water sprayed required for evaporative cooling system.

The performance of the heat exchanger plays a vital role to determine the exit air-stream temperature at (state 3), which is then delivered to the evaporator. The change of the air-stream temperature (state 3) as it leaves the heat exchanger is shown in figure

4.13, showing that as the heat exchanger efficiency decreases, the air temperature leaving the heat exchanger increases, leading to an increase in the circular mass flow rate as in figure 4.14. Also, the sprayed water requirement will increase, shown in figure 4.15.
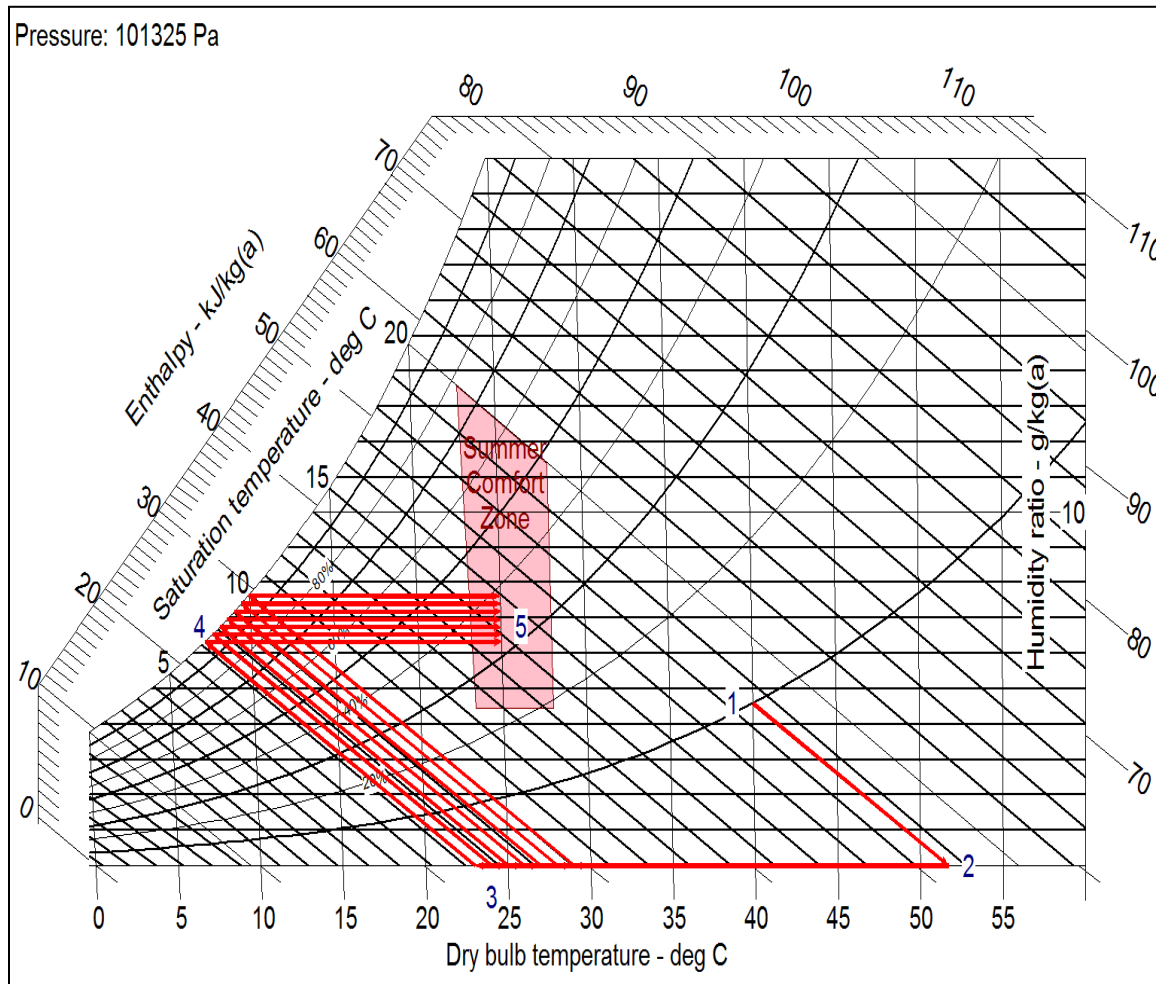
Figure 4.13: Psychometric chart shows effect of heat exchanger performance on evaporative cooling system.
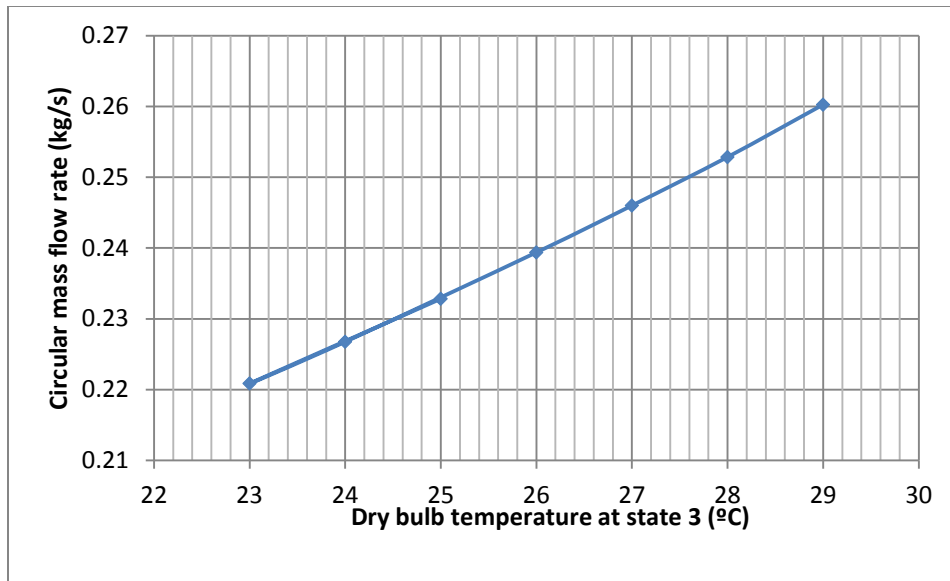
Figure 4.14: Effect of heat exchanger performance on the mass flow rate of evaporative cooling system**.**
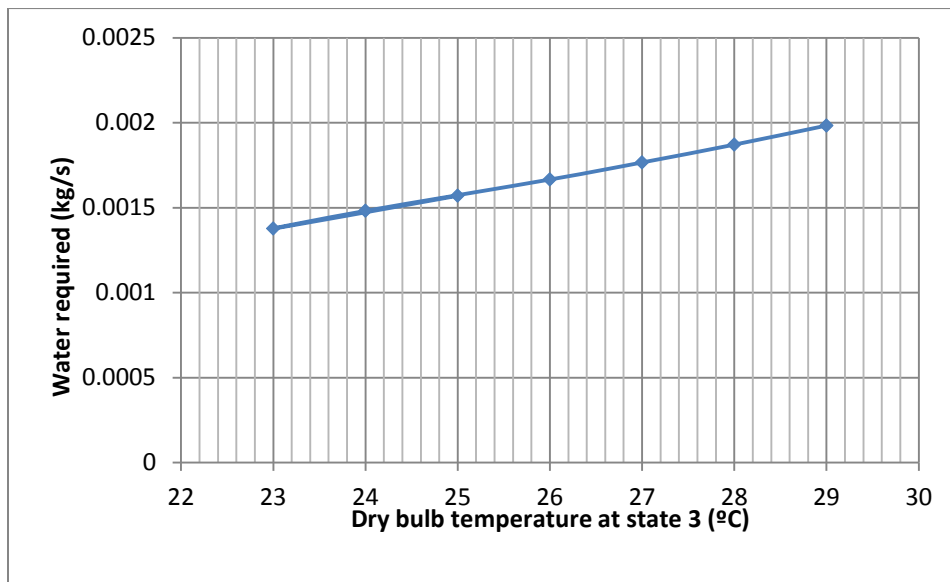
Figure 4.15: Effect of heat exchanger performance on sprayed water required for evaporative cooling system.

Lastly, the change of air stream exits from evaporator without being saturation (state 4) that leaves evaporator is shown in figure 4.16. The effect of the evaporative cycle performance on the evaporative cooling system can be investigated through studying the water-added temperature and its saturation efficiency. So, when increasing the performance of the evaporator increases, the delivered, un-saturated air-stream from evaporator decreases; thus the circular mass flow rate decreases as can be depicted in figure 4.17, while the water spray requirement is does not change as in figure 4.16.
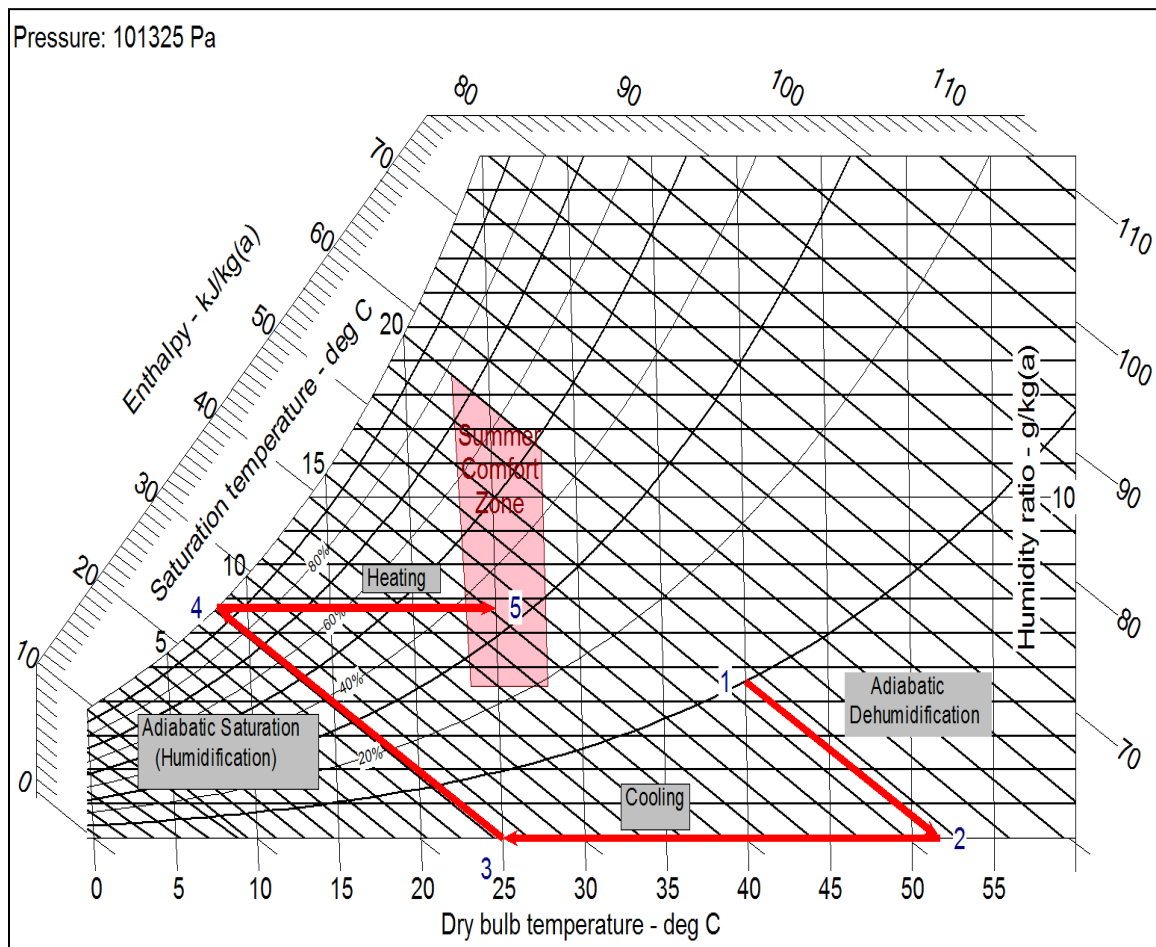
Figure 4.16: Psychometric chart shows effect of evaporative performance on evaporative cooling system.
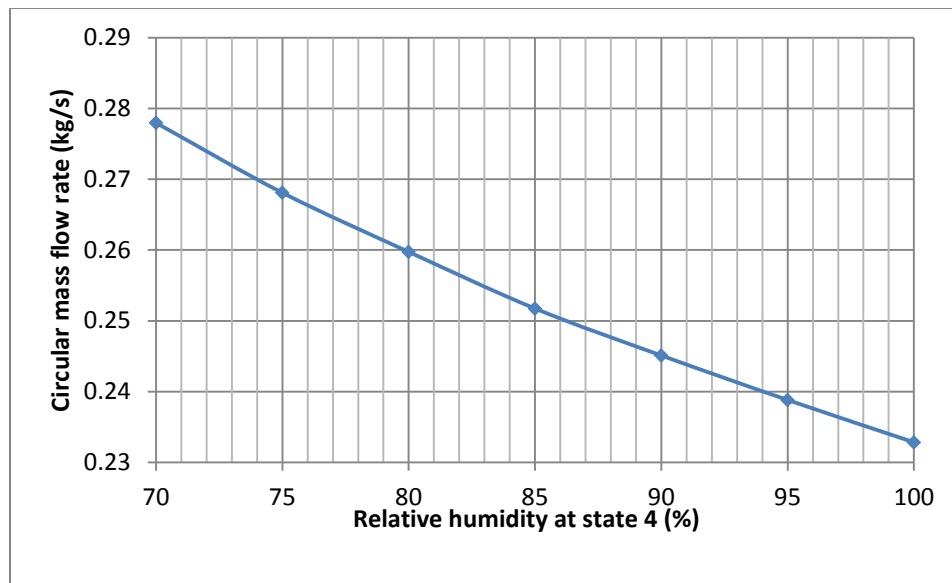
Figure 4.17: Effect of evaporative performance on the mass flow rate for evaporative cooling system.
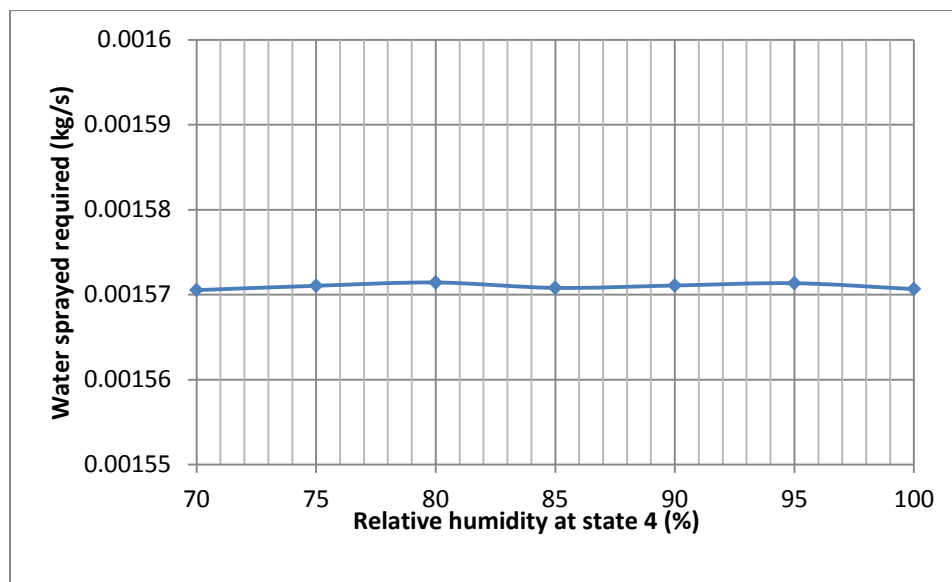
Figure 4.18: Effect of evaporative performance on sprayed water required for evaporative cooling system.

Guerra (1994) [29] presented a comprehensive study of evaporative air conditioner for automotive application. According to this study, the main advantages and limitations of evaporative cooling can be summarized in table 4.2, and the comparison of the evaporative cooling system to vapor compression cooling system was shown in table 4.3.

Table 4.2: The advantages and limitations of evaporative cooling system in automotive applications [29].

Evaporative cooling system	
Advantages	**Limitations**
- It uses water, an environmentally safe substance compared to the refrigerant.	- The water was used to operating system has to be replaced regularly.
- Using the waste of heat combustion to dry desiccant, so it will save the engine power.	- The water has to be carried will increase the automobile weight that will lead to reduce the fuel economy.
- It has a few components that it will make a high reliability, compact and easy to maintain.	- In the winter, it has to be drained to prevent damage of the components.
- It is quit because it does not need a compressor.	- Compared to compressor cooling system, it is low efficiency.
- It has a low operating pressure.	- Evaporative cooling is especially well suited for climates where the air is hot and humidity is low.
- It has a winter heater capability.	

Table 4.3: The comparison between the evaporative cooling system and vapor compressor cooling system; (↑ increase, ↓ decrease) [29].

	Evaporative Cooling	Vapor Compression
Fuel Consumption	↓	↑
Cost	↑	↓
Cooling Capacity	↓	↑
System Care	↑	↓
Environment Safety	↑	↓
Weight	↑	↓
Volume	↑	↓

So, combining the results from the psychometric and thermodynamic analyses, along with the PMV and PPD metrics, one can understand the effect of RH on in-cabin thermal comfort conditions and sensation. Figure 4.19 displays the changing of dry bulb temperature and relative humidity effects on the PMV index, with the relative humidity being the vertical axis, and dry bulb temperature the horizontal axis, and the diagonal lines represent the PMV index different values. According to the PMV index scale; humans will be thermally comfortable, if the PMV index ranges from -0.5 to 0.5. From the figure, occupants will be more comfortable at higher temperatures with a lower humidity. As the temperature drops, higher humidity levels are required to attain the PMV comfort range. The PPD as defined by equation 3.20 is dependent on the PMV value and can be represented graphically in figure 4.20.
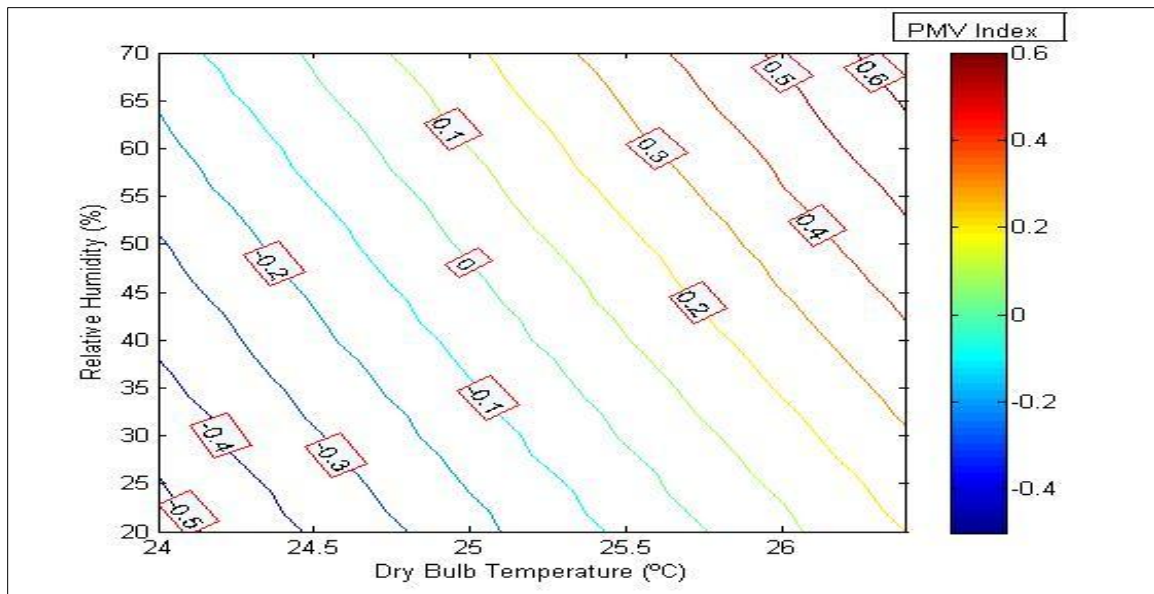
Figure 4.19: Effect of changing RH and dry bulb temperature on PMV index when relative air velocity 0.1 m/s, metabolic rate 1 met and insulation level 0.7 clo.
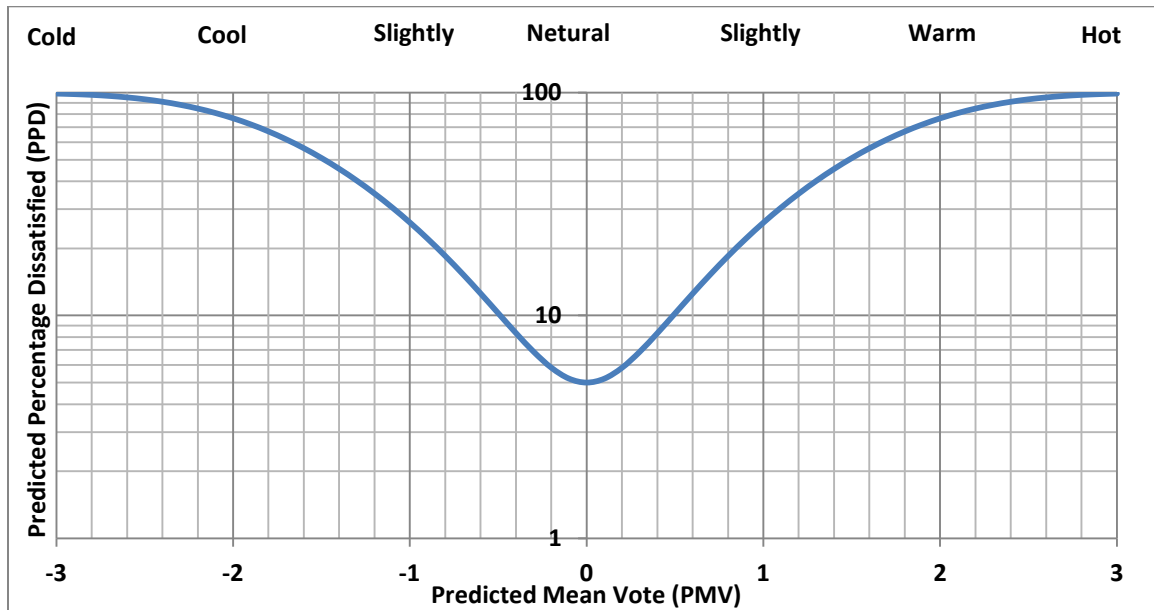
Figure 4.20: The Predicted Percentage of Dissatisfied (PPD) persons as a function of the Predicted mean vote (PMV) index.

4.5 Summary

This chapter analyzed the effect of controlling the RH along with dry-bulb temperature on the Thermal comfort zone and sensation, in vehicular cabins. The Psychometric and thermodynamic analyses investigated an actual embodiment of a system capable of RH manipulation through an evaporative cooling design. Additionally, the effect of each sub-system has been studied to quantify its effect on the sprayed water requirement, which affects the ultimate system size and accompanying accessories (tanks, etc). The thermal comfort has been also computed through the PMV and PPD indices using the Fanger model The study results can be summarized into following point;

- Increasing the final relative humidity inside the passenger compartment reduces the amount of heat rejected thus making the AC system more efficient in terms of fuel consumption.

- Starting the AC system under hot and dry air is more energy efficient than under hot and humid conditions.

- Controlling the RH inside the cabin should take into consideration the initial RH value, because, as higher initial relative humidity values leads to higher amount of heat rejection.

- Evaporative cooling system can be used to control the RH inside vehicles' cabin; however the sprayed water requirements will determine its packaging and weight constraints for automotive applications. The water requirements have been found in-sensitive to the evaporative cooler and desiccant performances, but dependant on the amount of heat to be rejected.

CHAPTER FIVE

ANALYSIS OF VEHICULAR CABINS' THERMAL SENSATION AND

COMFORT STATE USING BERKELEY AND FANGER MODELS

This chapter discusses the effect of manipulating the Relative Humidity (RH) along with the Dry Bulb Temperature (DBT) on vehicular cabins' environment in terms of the overall thermal comfort and human occupants' thermal sensation. The study uses the Berkeley and the Fanger models to investigate the human comfort through analyzing the (RH) effect from three specific perspectives; firstly its effect on other environmental conditions such as the Dew Point Temperature (DPT), the Enthalpy (H), the vapor pressure (vp) and the humidity ratio (ω) in the cabin. This will be done during the summer and winter periods. Secondly, the cabin local sensation (LS) and comfort (LC) will be analyzed for different body segments mainly; the head, chest, back, hands and feet with the addition of the overall sensation (OS) and the overall comfort (OC). This will be done using a thermal manikin based on the Berkeley model. Thirdly, the human sensation will be measured by the Predicted Mean Value (PMV) and the Predicted Percentage Dissatisfied (PPD) indices during the summer and the winter periods using the Fanger model calculations. From this study and according to the Berkeley model; the RH value should be controlled and synced with the cooling process such that at the early stage (rapid transient) low RH value should be enforced; while a high RH value is needed in the steady state phase. During the start of the heating process (winter conditions), the RH value does not play a major role due to low temperature in the passenger

compartment. However, at later periods until the end of the heating process, a low RH value is needed to achieve the needed comfort level. According to Fanger model, in the summer period as the RH value increases, the A/C can achieve the human comfort zone ($PMV = \mp\, 0.5$) in lesser time than if the RH value is not controlled. While in the winter period, as the RH value decreases, the A/C reaches the human comfort zone faster.

So, this study shows that controlling the relative humidity along with (DBT) enables the cabin to reach the comfort zone faster than the sole control of the cabin (DBT), in both the cooling and the heating processes i.e. summer and winter conditions respectively.

5.1 Introduction

Comfort is defined as the absence of discomfort. People feel thermally uncomfortable when they are too hot or too cold or when they are exposed to extreme hot or cold conditions. So, the positive comfort conditions are those that do not distract by causing unpleasant sensation of temperature, humidity, or other aspects of the surrounding environment. Thermal Comfort climate is defined as "that state of mind which expresses satisfaction with the thermal environment" (ASHRAE 55, 2004) [6]. However, thermal comfort is still evaluated based on subjective procedures –each person senses it differently-. In other words, the thermal comfort of people can be determined by surveying a sample of individuals and their responses to their environment. So, thermal comfort is very difficult to objectively quantify because it relies on a wide range of environmental and personal factors that decides on what will make people feel thermally

comfortable. These factors constitute what is known as the human thermal environment, which relies on physiological and psychological variations from person to person. However, extensive laboratory and field data have been collected to provide statistical information or thresholds to define the conditions that a specified percentage of occupants (human subjects) will find thermally comfortable, so that vehicles' designers try to provide average conditions of comfort through the Air Conditioning A/C system.

The principal factors that affect human thermal comfort depend upon four physical environmental variables, which are: the air temperature, relative humidity, mean radiant temperature, and the relative air velocity, in addition to two personal related parameters that are the activity level as provided by the metabolic rate and the thermal insulation (clothing) value. Several models have been developed during the past few years in order to describe human thermal response to the variations in its surrounding conditions, best summarized by Alahmer et al. in [2].

This chapter discusses and analyzes the effect of controlling the relative humidity inside vehicular cabins on the thermal comfort state using the Berkeley thermal manikin approach and the Fanger based indices.

5.2 Methodology

The virtual thermal Berkeley manikin is used in this study to predict the thermal comfort in different vehicle cabin environments. This manikin integrates a human thermal physiological model to predict the body core and skin temperatures for twenty one parts of the human body. The thermal sensation and comfort votes are calculated

using the Berkeley comfort model and the Fanger model too. The sensation and comfort are then reported on the nine-point Berkeley scale for the Berkeley model and the seven-point thermal sensation scale for the Fanger model based on PMV index. On both scales, the higher positive sensation value indicates hotter feeling. On the other side the higher negative sensation value indicates cooler feeling, while a zero sensation indicates a neural thermal sensation. The higher comfort value indicates a better or more comfortable feeling as shown in table 3.4 and 3.6. The Berkeley comfort manikin is placed inside a vehicle cabin with a homogeneous environment over a range of relative humidity of (20-60%) as shown in figure 5.1. The manikin is simulated wearing short sleeve with long trousers with approximate clothing insulation value of 0.5 clo or 0.078 $\frac{m^2 K}{W}$ for summer period, and wearing long thick sleeve, long thick trousers, hand-wear and footwear with approximate clothing insulation value of 1 clo (0.155 $\frac{m^2 K}{W}$) for the winter period. The metabolic rate is set at 1.4 met (81 $\frac{W}{m^2}$) [14, 69] which would be for a seated human metabolic rate. The measured discharge temperatures at A/C outlets are specified as the boundary conditions for the finite differencing processor, which is relied on using a RadTherm solver package. The major five steps that the Berkeley model utilizes are; (i) firstly importing a human geometry into a finite differencing platform [63] that includes the Berkeley sub-routine. Secondly, (ii) meshing the human geometry to discreatize it depending on the resolution needed. (iii) Setting the biological material properties and the thickness values to each individual part. (iv) Setting the environmental boundary conditions including the environmental variables, the clothing properties, the surface

87

conditions, and the convection settings. (v) Finally, solving the heat transfer equations using the finite differencing algorithm.
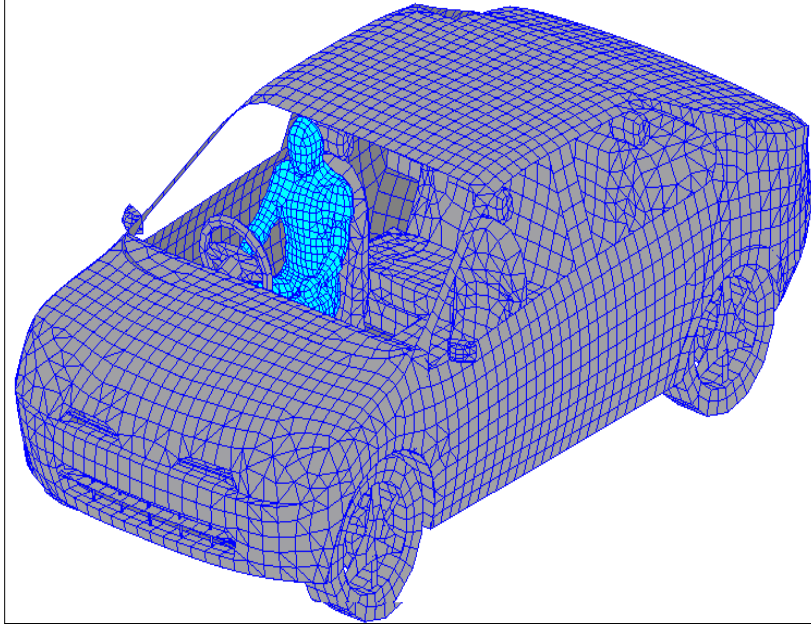
Figure 5.1: Schematic of a manikin was placed inside Vehicular cabin under a different environmental condition.

5.3 Analysis

5.3.1   Environmental Conditions for the Cabin during the Summer Period

The analysis of all the physical and the thermal properties of cabin air and water vapor mixtures using the psychometric chart for different values of relative humidity during the summer period is shown in figure 5.2. The variation in dry bulb temperature (DBT) inside the cabin environment with time is displayed in figure 5.3a. As shown in this figure, as time passes, the DBT decreases for different values of RH. At the beginning of the cooling process, the DBT decreases sharply until time reaches 5 min mark with DBT 35.4, 35.1, 34.7, 34.5 and 34.2 $^{\circ}$C at 20, 30, 40, 50 and 60% of RH

respectively. Then the DBT decreases slowly with time until it reaches the steady state phase after 25 min mark with DBT 30.2, 29.2, 28.1, 27.5 and 26.7 $^{\circ}$C at 20, 30, 40, 50 and 60% of RH.

The variation in dew point temperature (DPT) inside the cabin with time is further displayed in figure 5.3b, which indicates that as time passes, the DPT decreases for different values of RH. At the beginning of the cooling process the DPT decreases sharply until time reaches the 4 min mark with DPT 9.6, 15.5, 19.7, 23 and 26 $^{\circ}$C at 20, 30, 40, 50 and 60% of RH respectively. Then the DPT decreases slowly with time which is mainly due to the decrease in the DBT value in this period until it reaches the steady state phase after 20 min mark with DPT 5.2, 10.4, 13.6, 16.7 and 19.1 $^{\circ}$C at 20, 30, 40, 50 and 60% of RH respectively.

The variation in the specific enthalpy (H) inside the cabin with time is also shown in figure 5.3c, which indicates that as time passes, the H decreases for different values of RH. At the beginning of the cooling process, the H decreases sharply until time reaches 4 min mark with H 55.5, 64.4, 72.6, 81 and 90.4 kJ/kg at 20, 30, 40, 50 and 60% of RH respectively. Then the H decreases slowly with time till it reaches the steady state phase value after passing 20 min with H 44.9, 50.1, 53.6, 58.8 and 63.4 kJ/ kg at 20, 30, 40, 50 and 60% RH.

The variation in the vapor pressure (vp) inside the cabin with time is shown in figure 5.3d. As shown in this figure, while the time passes, the vp decreases for different values of RH. At the beginning of the cooling process, the vp decreases sharply until time reaches 4 min mark with vp 1.2, 1.8, 2.3, 2.8 and 3.4 kPa at 20, 30, 40, 50 and 60% of

RH respectively. Then the vp decreases slowly with time until it reaches the steady state phase after passing 20 min mark with vp 0.89, 1.26, 1.56, 1.9, and 2.2 kPa at 20, 30, 40, 50 and 60% of RH.

Lastly, the variation in the humidity ratio (ω) inside the cabin with time is shown in figure 5.3e. As shown in this figure, as the time passes, the ω decreases for different values of RH. At the beginning of the cooling process, the ω decreases sharply until time reaches 4 min mark with ω being 7.5, 11.07, 14.4, 17.8 and 21.5 g of water vapor/ kg of dry air at 20, 30, 40, 50 and 60% of RH respectively. Then the ω decreases slowly with time until it reaches the steady state phase after passing 20 min with ω 5.5, 7.86, 9.75, 11.95 and 13.97 g of water vapor/ kg of dry air at 20, 30, 40, 50 and 60% of RH.
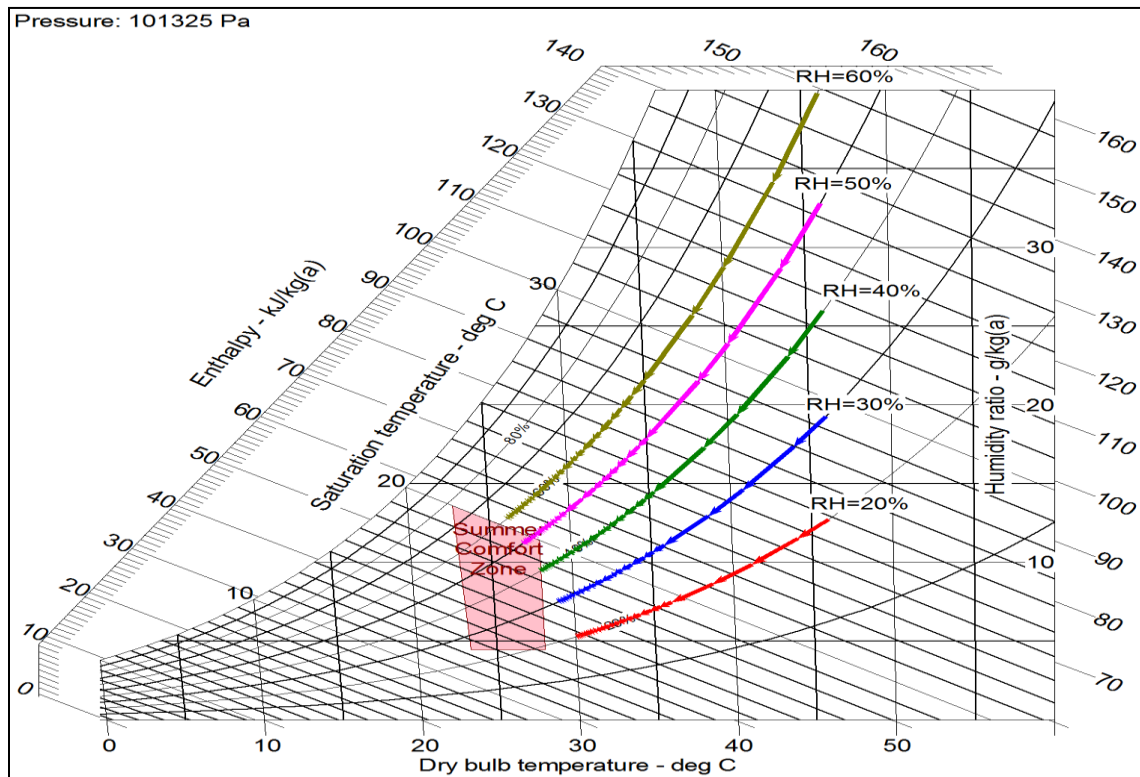
Figure 5.2: Psychometric chart of the cabin during the summer period for different RH values.
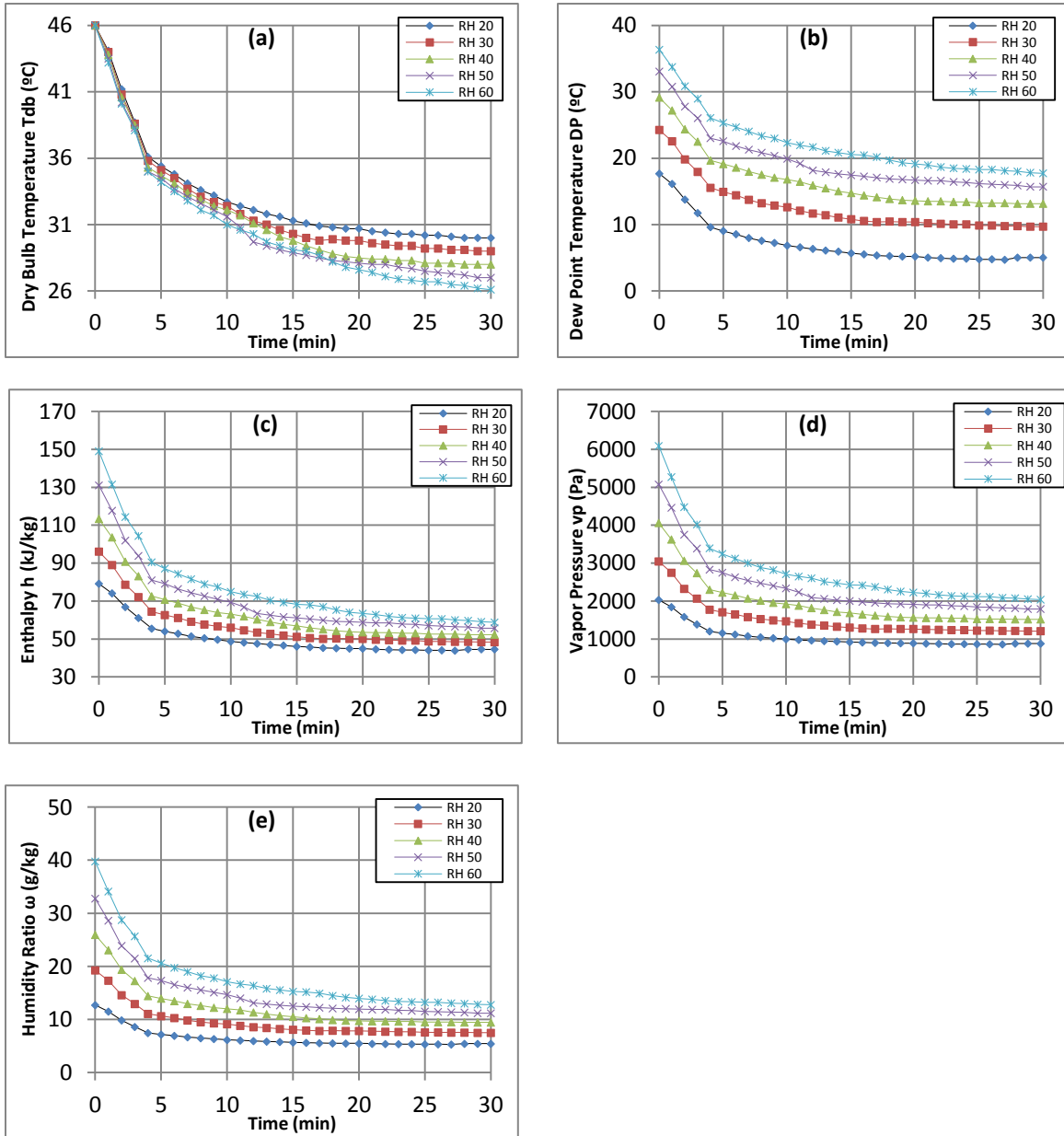
Figure 5.3: Different environmental conditions' variation versus time inside the cabin during the summer period for different values of relative humidity; (a) Dry bulb temperature, (b) Dew point temperature, (c) Enthalpy, (d) Vapor pressure, (e) Humidity ratio.

5.3.2 Skin Temperature Variation, Local and Overall Sensation-Comfort at Summer Period

The skin temperature variation for different body segments such as the head, chest, back, R hand, L hand, R foot and L foot versus time for different relative humidity scenarios, during the summer period are displayed in figure 5.4; with the schematic of temperature variation at the end of cooling process under different relative humidity scenarios being shown in figure 5.5. At the beginning of the cooling process, the skin temperature for different body segments increases for short period (less than 3 min) because of the big difference between the skin temperature and the vehicular compartment. Then the skin temperature decreases sharply till the 18 min mark, because the compartment temperature decreases sharply due to the air conditioning process, then the skin temperature decreases slowly with time until it reaches the steady state value as depicted in figure 5.4. The amount of the temperature difference between starting and ending of the cooling process depends on the human segment and relative humidity. At relative humidity of 40%, the amount of temperature difference (during cooling process) are 0.713, 0.754, 0.036, 0.937, 0.921, 0.357and 0.435 ^{o}C for the head, chest, back, R hand, L hand, R foot and L foot respectively. Thusly, the RH effect on the skin temperature is clear especially for the unclothed segments such as the hand and the foot; at the beginning of the cooling process, as the RH increases the skin temperature of all segments increase. For example, as time reaches 3 min, the skin temperature of the R foot is around 30.75, 30.8, 30.9, 31 and 31.6 ^{o}C at 20, 30, 40, 50 and 60% of RH respectively. Then the decreasing rate of skin temperature change is accelerated during an increasing

trend of RH. For example, at the end of cooling process, the skin temperature of the R foot is around 29.3, 29.1, 28.9, 28.7, and 28.5 °C at 20, 30, 40, 50 and 60% of RH respectively.
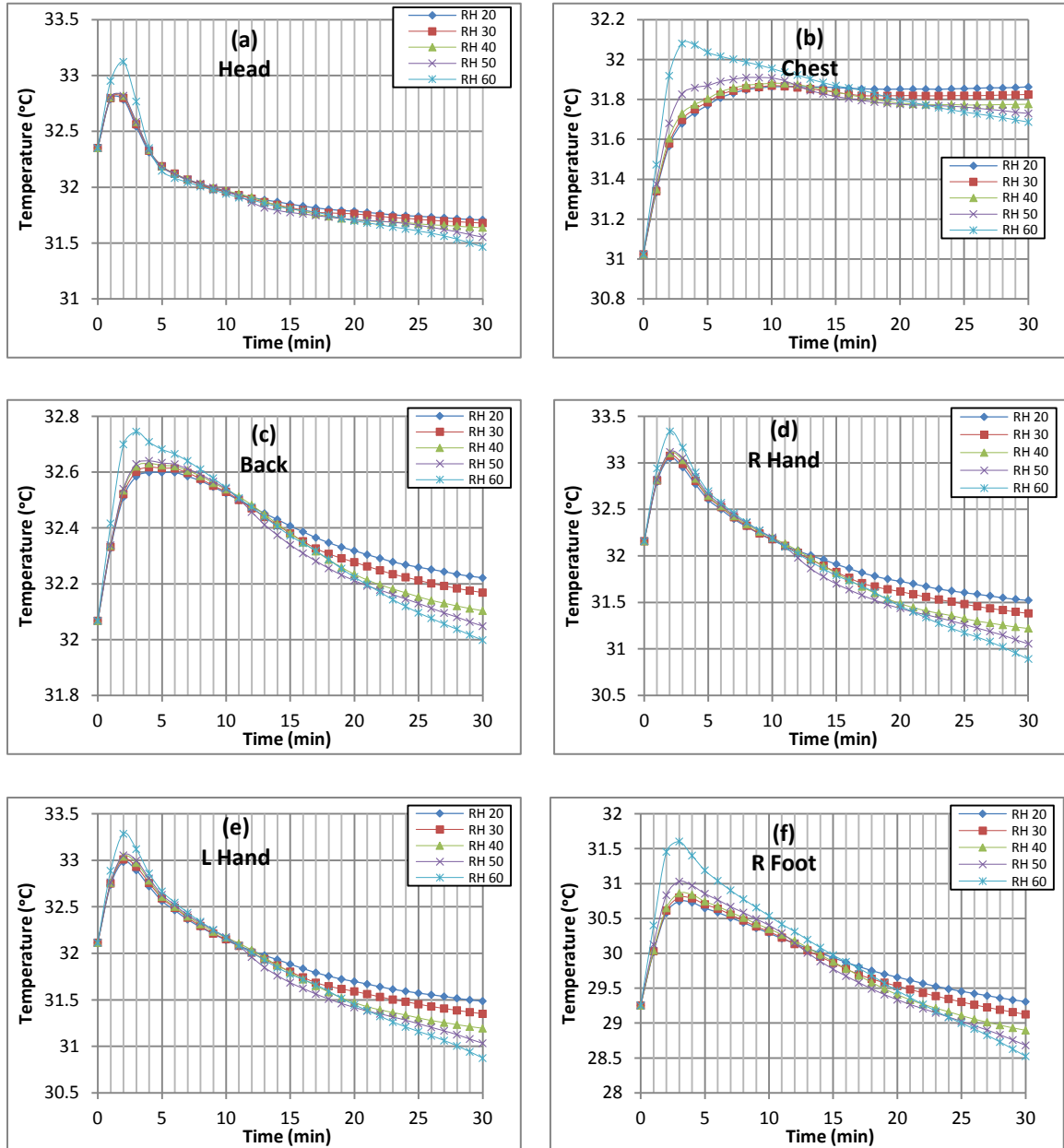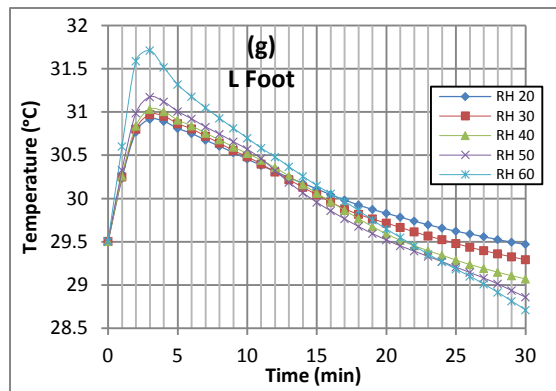
Figure 5.4: Temperature variation versus time for different human segments at summer period at different relative humidity; (a) Head (b) Chest (c) Back (d) Right hand (e) Left hand (f) Right foot (g) Left foot.
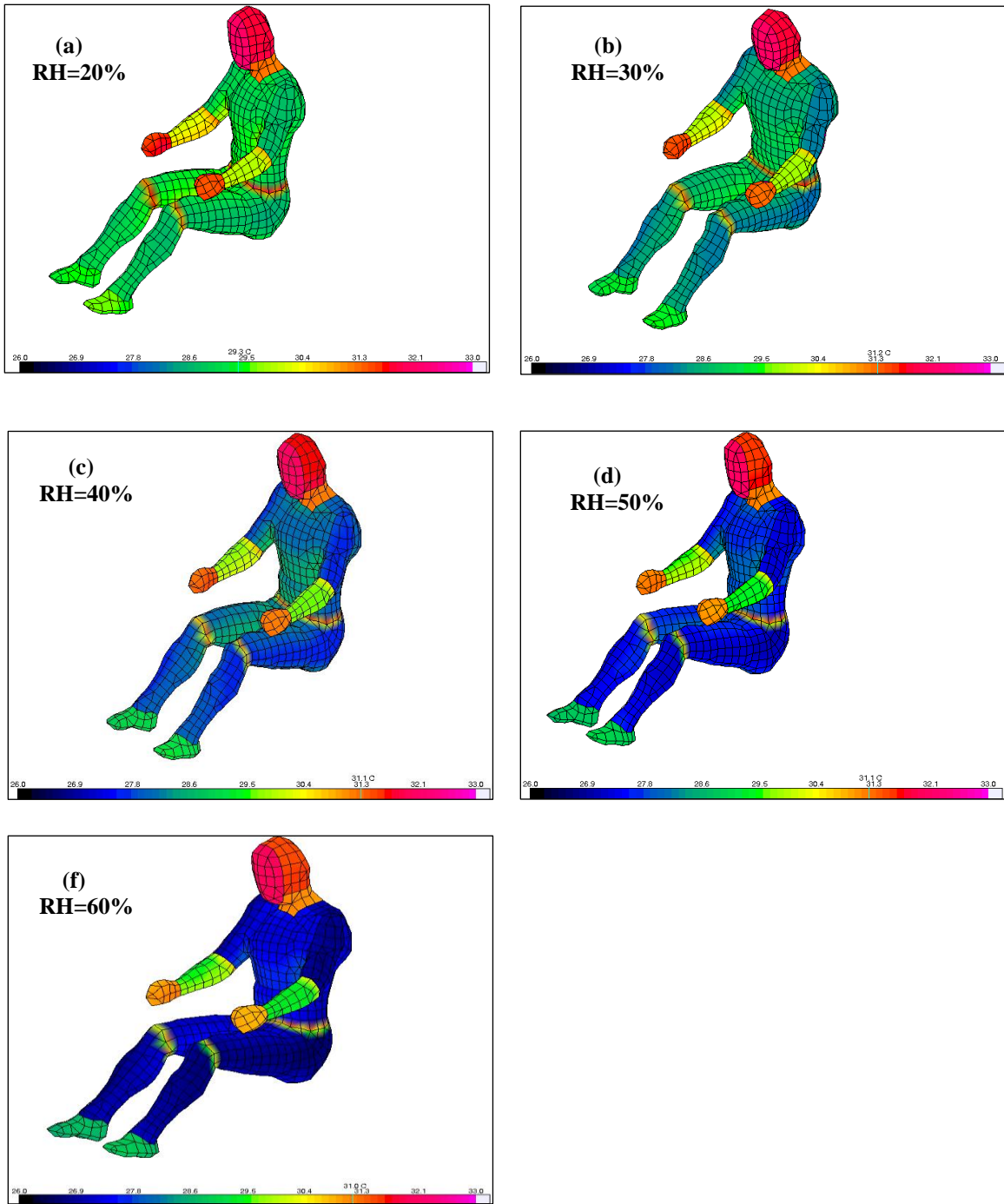
Figure 5.5: Schematic of body temperature variation on in cabin at end of cooling process for different relative humidity; (a) RH=20%, (b) RH=30%, (c) RH=40%, (d) RH=50%, (e) RH=60%.

The main difference between the temperature sensation and the thermal comfort is the fact that the temperature sensation is considered as a rational experience that can be described as being directed towards an objective world in terms of "cold" and "warm". Thermal comfort on the other hand is an emotional experience, which can be characterized in terms of "comforted or pleasant" and "uncomforted or unpleasant" [70]. The overall sensation and comfort variations of the Berkeley model against time for the different relative humidity scenarios, during the summer period are presented in figure 5.6. In the early stage, the thermal sensation increases until reach maxima and the thermal comfort decreases until reaches minima. As time passes, the temperature of air surrounding the body decreases and the body becomes more neutral (i.e. more comfortable). At beginning of cooling process; the higher the value of RH, the feeling of "hot" conditions become more dominant and the more uncomfortable body feels. But at ending of cooling process; the higher the RH value, the more comfortable the body feels. The local sensation and comfort vote versus for the different body segments are pictorially displayed in figure 5.7; which shows the same behavior for the overall sensation and comfort versus time. The RH has more influential effect at beginning of the cooling process, when the RH increases, the feeling of "hot" and "uncomfortable" increases. But at the end of cooling process; the effect of an increasing RH value on the comfort level becomes neglected for the hands and the feet, with small negative effect on head and small positive effect on the chest and the back.
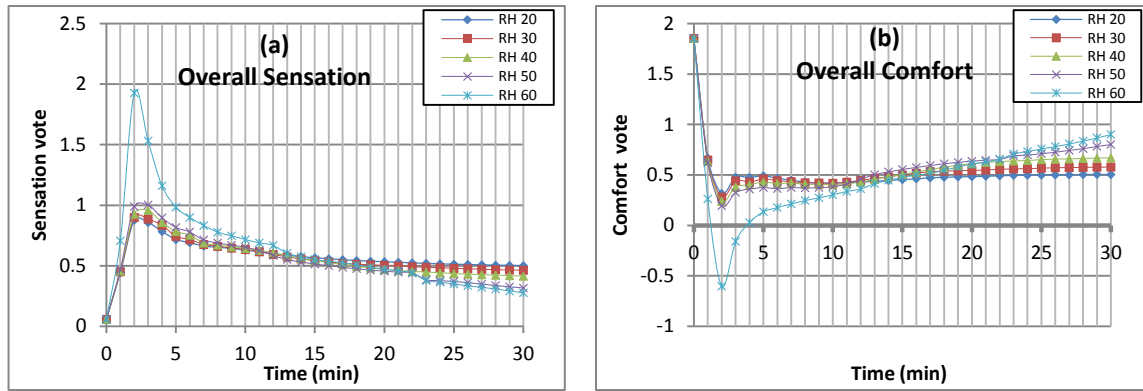
Figure 5.6: Overall sensation and comfort variation versus time at summer period for different RH; (a) Overall sensation (b) Overall comfort.

98
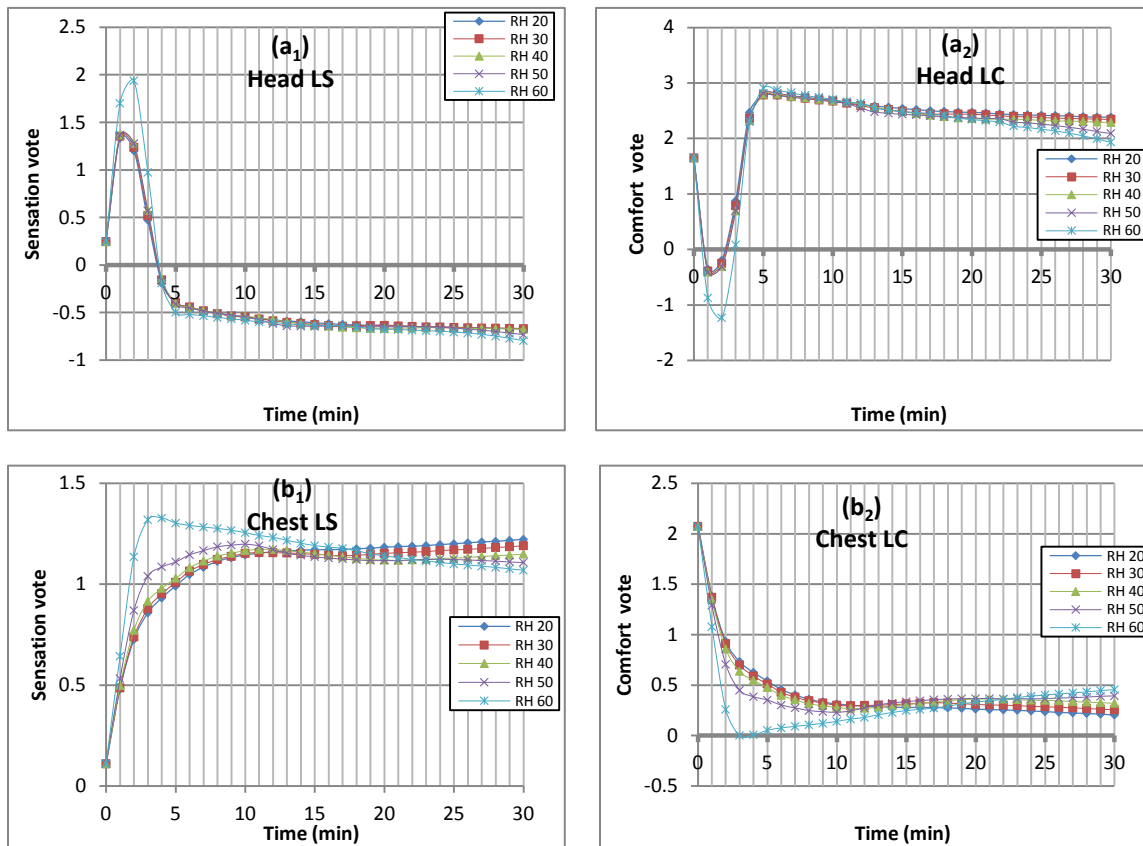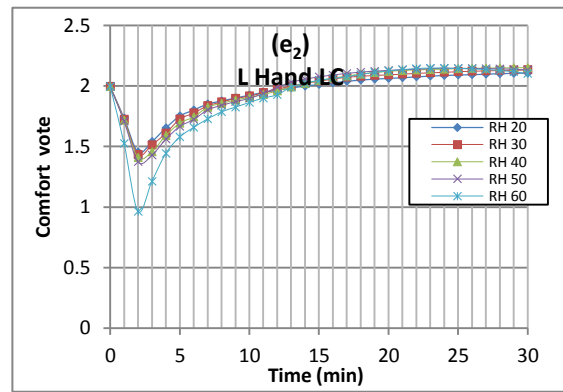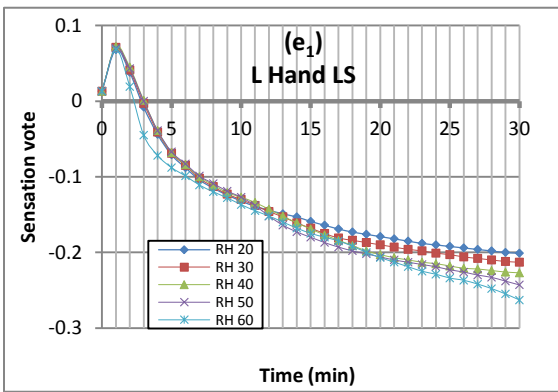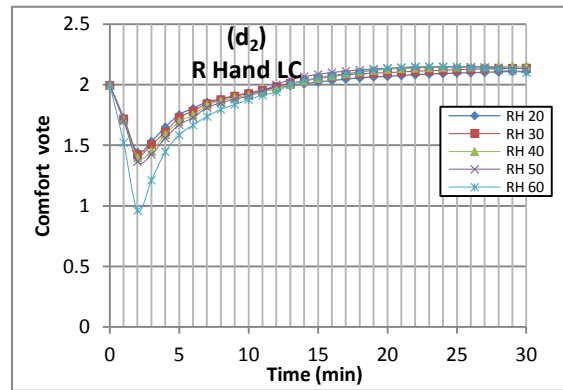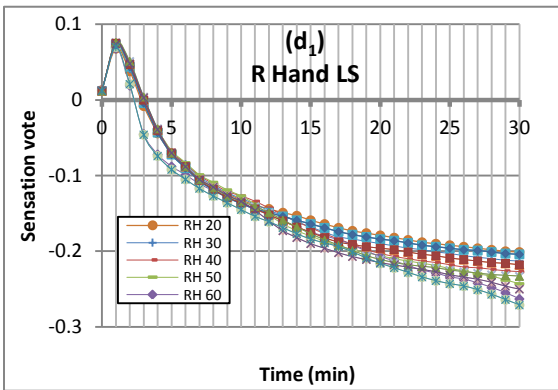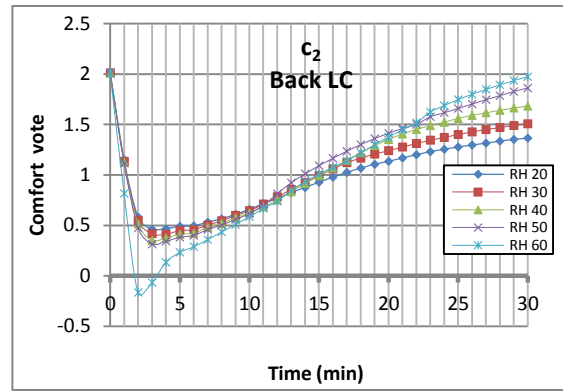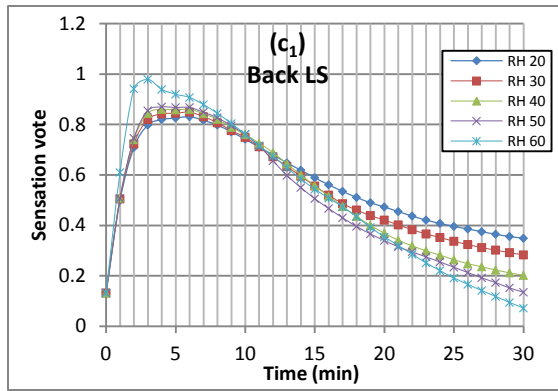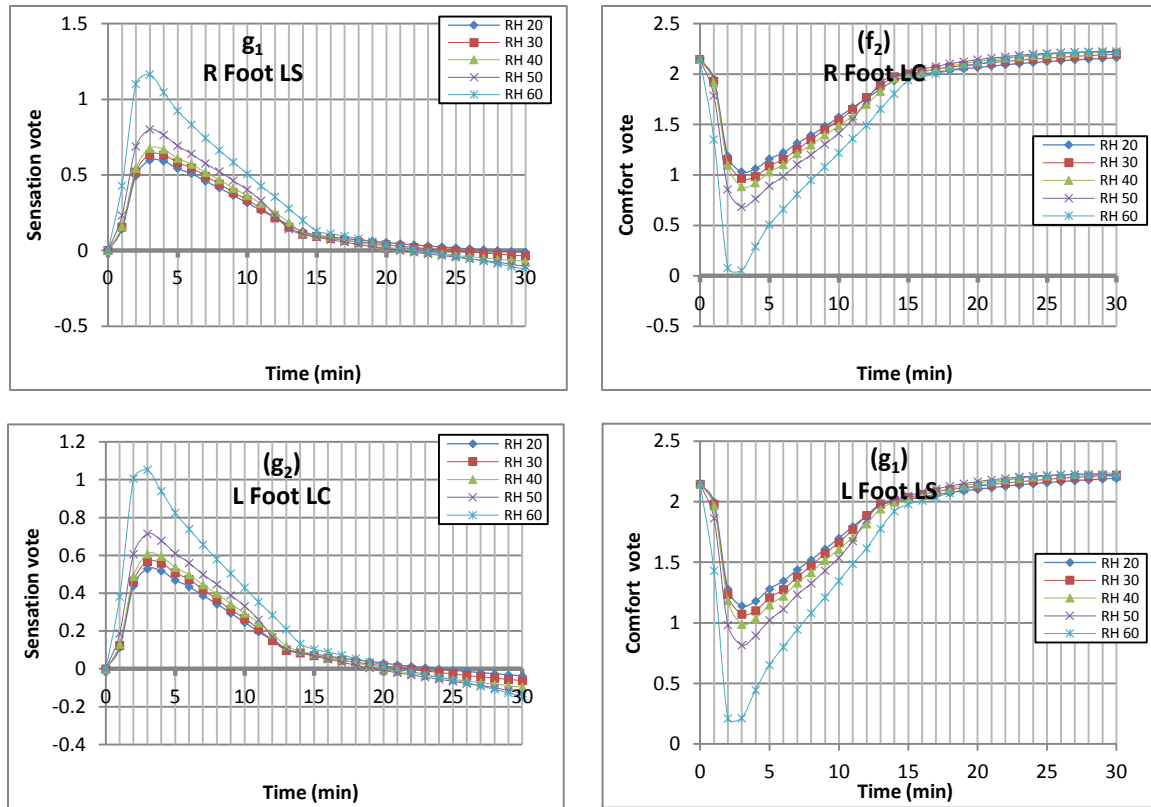
Figure 5.7: Local sensation (LS) and Local comfort (LC) variation versus time for different human segments at summer period at different RH; (a_1) Head LS (a_2) Head LC (b_1) Chest LS (b_2) Chest LC(c_1) Back LS(c_2) Back LS (d_1)Right hand LS(d_2) Right hand LS(e_1)Left hand LS (e_2)Left hand LC(f_1)Right foot LS(f_2) Right foot LC(g_1) Left foot LC(g_2) Left foot LS.

According to the Fanger model, the variation in the PMV and PPD indices with time for the different relative humidity scenarios at the summer period are presented in figure 5.8. As shown in this figure, the RH has no effect on the PMV value at the beginning of the cooling process. But as the time reaches 12 min, the RH effect becomes more pronounced on the predicted thermal sensation. So, as the RH value increases, the A/C can achieve the human comfort zone ($PMV = \mp 0.5$) faster than the case if the RH

value is not controlled. The environmental conditions inside the cabin become more comfortable as the time reaches 29, 19, 17 and 18 min when the RH values are 30, 40, 50 and 60% respectively. But at an RH value of 20%, the environmental condition inside the cabin does not reach the comfortable zone during the cooling process as judged by the PMV index. At end of the cooling process, the percentage of people feeling uncomfortable (according to PPD) is 19, 10, 5, 6 and 11% at 20, 30, 40, 50 and 60% of RH respectively.
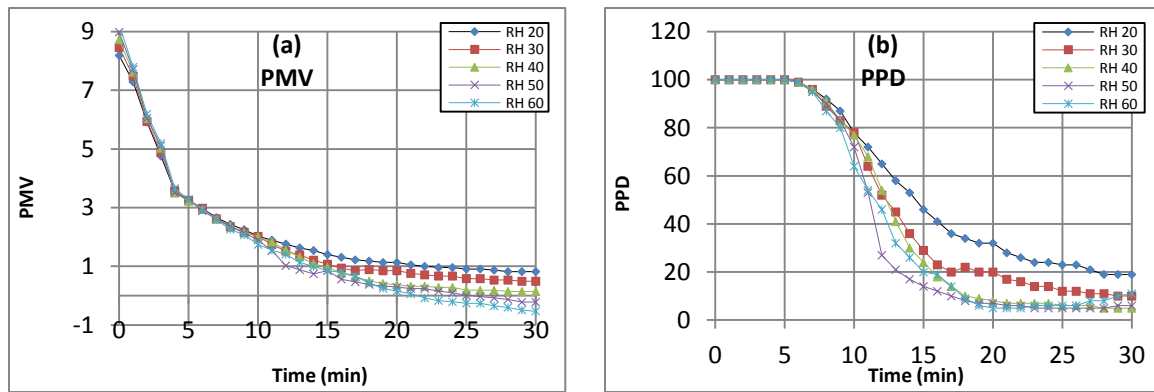
Figure 5.8: PMV and PPD versus time on in cabin at summer period for different RH; (a) PMV (b) PPD.

5.3.3   Environmental Conditions for the Cabin during the Winter Period

The analysis of all the physical and the thermal properties of cabin air and water vapor mixtures using the Psychometric chart for different values of relative humidity during the winter period is shown in figure 5.9.

The variation in the dry bulb temperature (DBT) inside the cabin environment with time is displayed in figure 5.10a. As shown in this figure, as the time passes, the

DBT increases for different values of RH. At the beginning of the heating process, the DBT increases sharply until time reaches 15 min mark with DBT 24.7, 22.4, 20.8, 19.3 and 19.2 $^\circ$ C at 20, 30, 40, 50 and 60% of RH respectively. Then the DBT increases slowly with time until it reaches the steady state phase after 25 min mark with DBT 25.7, 24.6, 23.4, 22.3 and 21.5°C at 20, 30, 40, 50 and 60% of RH.

The variation in the dew point temperature (DPT) inside the cabin with time is further displayed in figure 5.10b, which indicates that as time passes, the DPT increases for different values of RH. At the beginning of the heating process the DPT increases sharply until time reaches the 10 min mark with DPT -1.52, 2.5, 5, 7.4 and 9.8°C at 20, 30, 40, 50 and 60% of RH respectively. Then the DPT increases slowly with time which is mainly due to the increase in DBT value in this period until it reaches the steady state phase after 20 min mark with DPT is 0.92, 4.9, 8.4, 10 and 12.6°C at 20, 30, 40, 50 and 60% of RH respectively.

The variation in the specific enthalpy (H) inside the cabin with time is also shown in figure 5.10c. Which indicates that as time passes, the H increases for different values of RH. At the beginning of the heating process, the H increases sharply until time reaches 15 min mark with H 34.7, 34.8, 36.5, 37.1 and 40.5 kJ/kg at 20, 30, 40, 50 and 60% of RH respectively. Then the H increases slowly with time till it reaches the steady state phase after passing 25 min mark with H 36.3, 39.3, 41.8, 43.8 and 46.09 kJ/kg at 20, 30, 40, 50 and 60% of RH.

The variation in the vapor pressure (vp) inside the cabin with time is shown in figure 5.10d. From this figure, as the time passes, the vp decreases for different values of

RH. At the beginning of the heating process, the vp increases sharply until time reaches 12 min mark with vp 0.58, 0.77, 0.92, 1.07 and 1.28 kPa at 20, 30, 40, 50 and 60% of RH respectively. Then the vp increases slowly with time until it reaches the steady state phase after passing 25 min mark with vp 0.66, 0.93, 1.16, 1.35 and 1.55 kPa at 20, 30, 40, 50 and 60% of RH.

Lastly, the variation in the humidity ratio (ω) inside the cabin with time is shown in figure 5.10e. As shown in this figure, as the time passes, the ω increases for different values of RH. At the beginning of the heating process, the ω increases sharply until time reaches 13 min mark with ω being 3.7, 4.8, 5.7, 6.6 and 8 g of water vapor/ kg of dry air at 20, 30, 40, 50 and 60% of RH respectively. Then the ω increases slowly with time until it reaches the steady state phase after passing 22 min mark with ω 4.1, 5.6, 7.1, 8 and 9.4 g of water vapor/ kg of dry air at 20, 30, 40, 50 and 60% of RH.
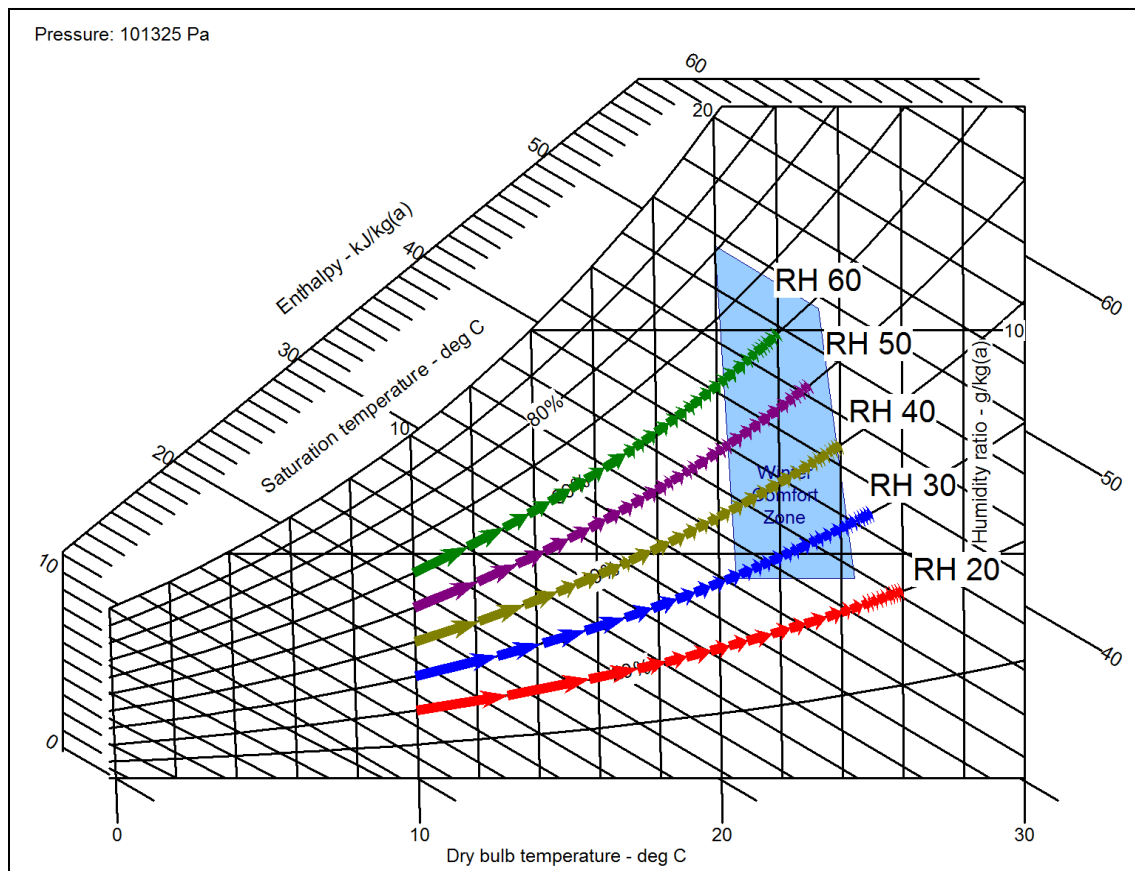
Figure 5.9: Psychometric chart of the cabin during winter period for different RH values.
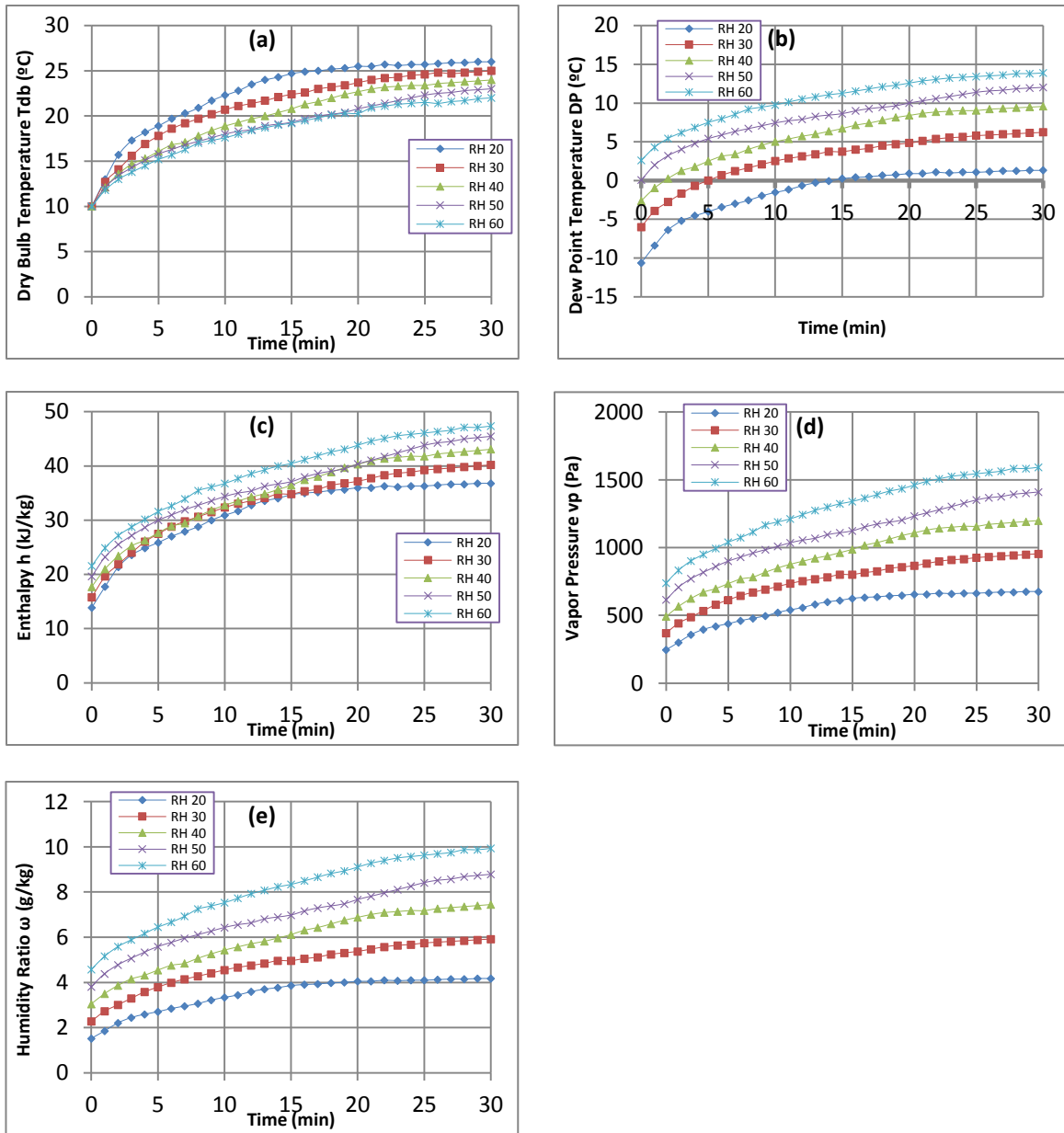
Figure 5.10: Different environmental conditions variation versus time inside the cabin during winter period for different values of relative humidity; (a) Dry bulb temperature, (b) Dew point temperature, (c) Enthalpy, (d) Vapor pressure, (e) Humidity ratio.

5.3.4 Skin Temperature Variation, Local and Overall Sensation-Comfort at Winter Period

The skin temperature variation for different body segments such as the head, chest, back, R hand, L hand, R foot and L foot versus a time for different relative humidity scenarios during the winter period are displayed in figure 5.11; with the schematic of temperature variation at the end of heating process under different relative humidity scenarios being shown in figure 5.12. At the beginning of the heating process, the skin temperature for different body segments decreases because of the big difference between the skin temperature and vehicular compartment temperature. From the figure 5.11; the rate of skin temperature increases, it will depend on the RH inside the vehicular compartment until reaches steady state phase. Also, if the RH inside the vehicular compartment increases, the rate of skin temperature change will decrease. The amount of the temperature difference between starting and ending heating process depends on the body segments and relative humidity. Now, the effect of RH on skin temperature is obviously clear for all body segments especially for clothed segment as chest and back. At the beginning of heating process; as the RH inside vehicular compartment increases the rate skin temperature change increases. For example, at time reaches 6 min mark, the skin temperature of the chest is around 30.34, 30.26, 30.16, 30.14 and 30.11 °C at 20, 30, 40, 50 and 60% of RH respectively. Then the rate of skin temperature change is accelerated at the RH decreases. For example, at the end of heating process, the skin temperature of the chest being 31.2, 31.05, 30.92, 30.78 and 30.71 °C at 20, 30, 40, 50 and 60% of RH respectively.
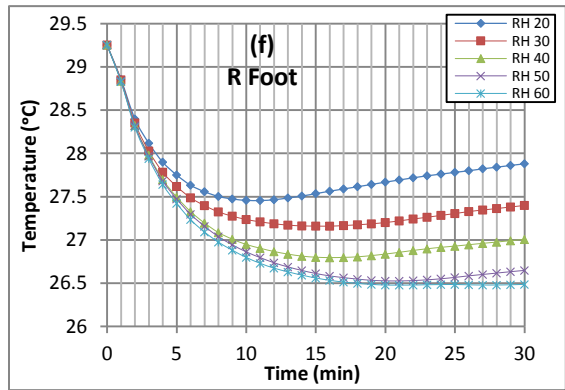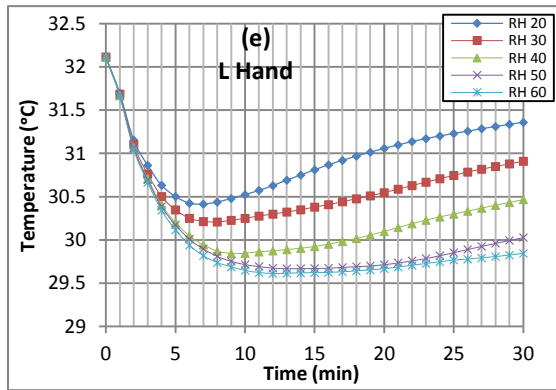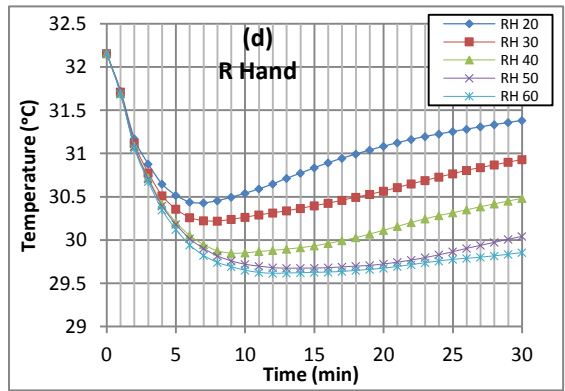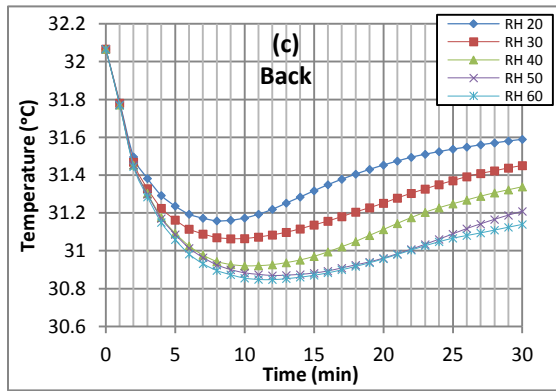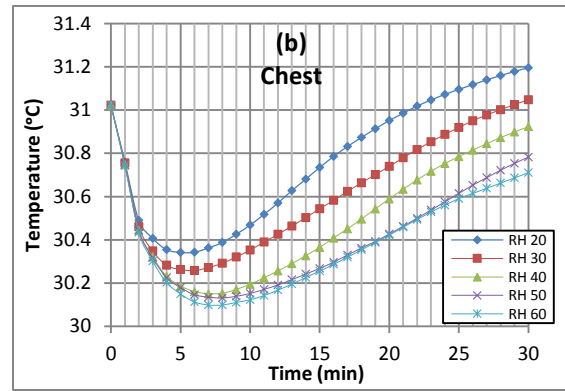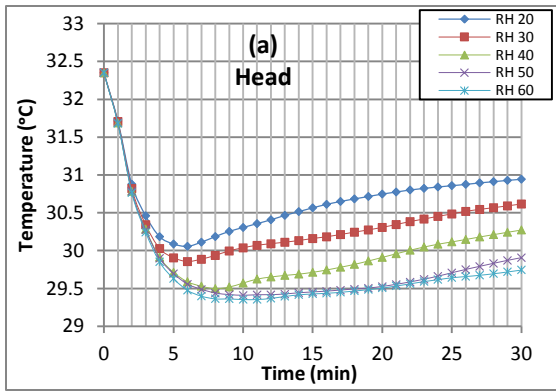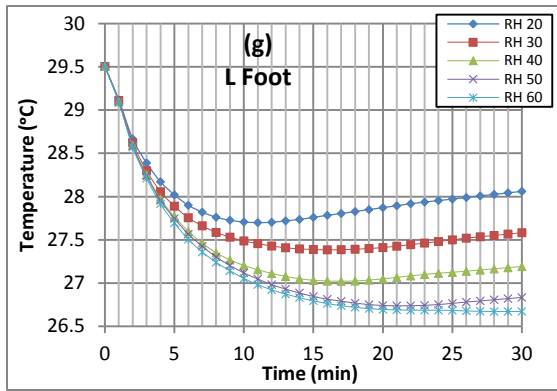
Figure 5.11: Temperature variation versus time for different human segments at winter period at different relative humidity; (a) Head (b) Chest (c) Back (d) Right hand (e) Left hand (f) Right foot (g) Left foot.
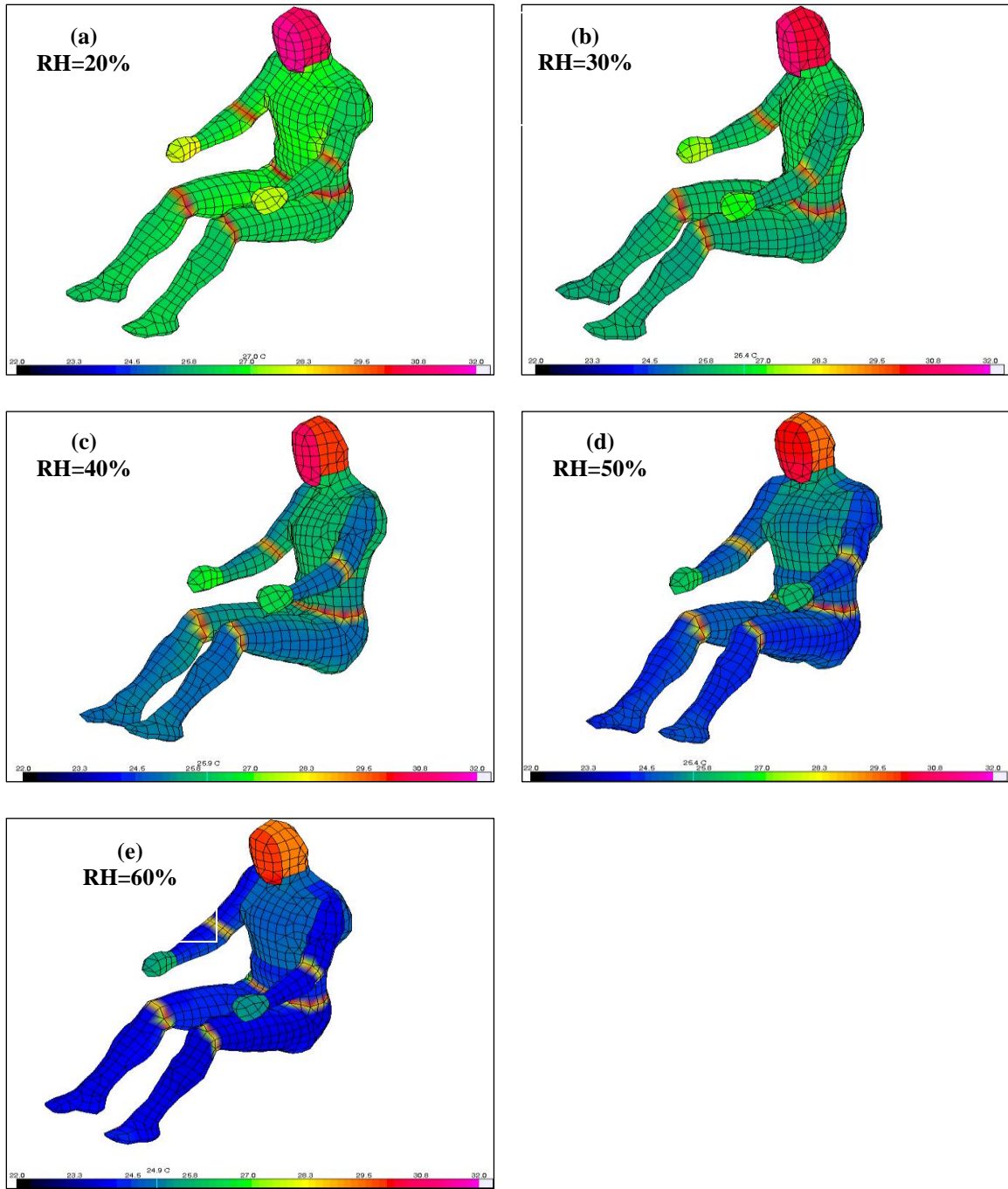
Figure 5.12: Schematic of body temperature variation on in cabin at end of heating process for different relative humidity; (a) RH=20%, (b) RH=30%, (c) RH=40%, (d) RH=50%, (e) RH=60%.

The overall sensation and comfort variation of the Berkeley model against time for the different relative humidity scenarios, during the winter period are depicted in figure 5.13. In the early stage, the thermal sensation and thermal comfort decreases until reach minima. As time passes, the temperature of air surrounding the body increases and the body become more neutral (i.e. more comfortable). At beginning of the heating process; the body feels cold and uncomfortable, and at the end of heating process the body becomes more comfortable the body feels especially at lower RH. The local sensation and comfort vote versus for different human segment are shown in figure 5.14. And they have a same behavior of overall sensation and comfort versus time. The RH is more influential effect during heating process for all body segments. As the RH inside vehicular compartment increases, the feeling of uncomforting will also increase.
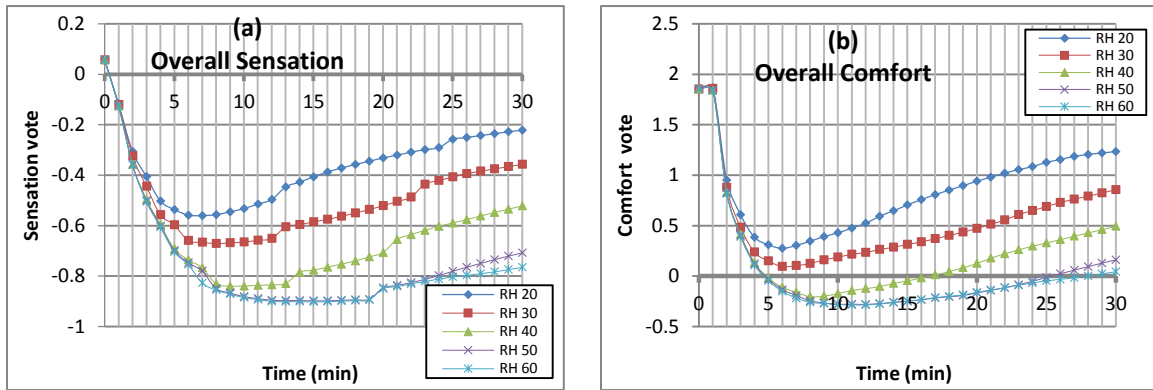
Figure 5.13: Overall sensation and comfort variation versus time at winter period for different RH; (a) Overall sensation (b) Overall comfort.

109
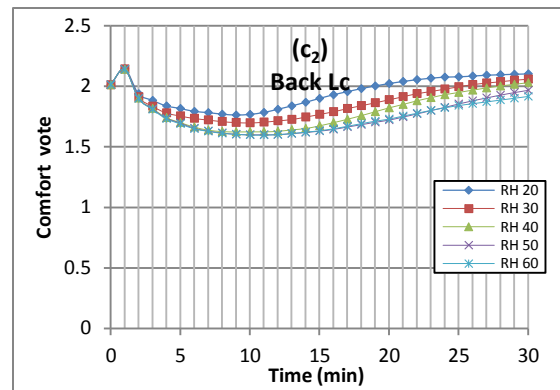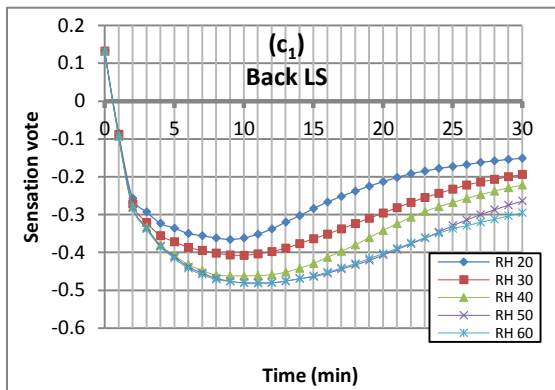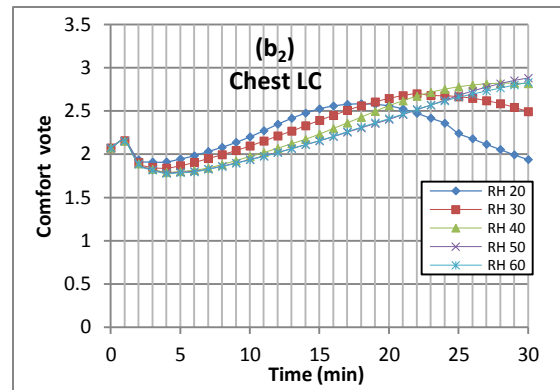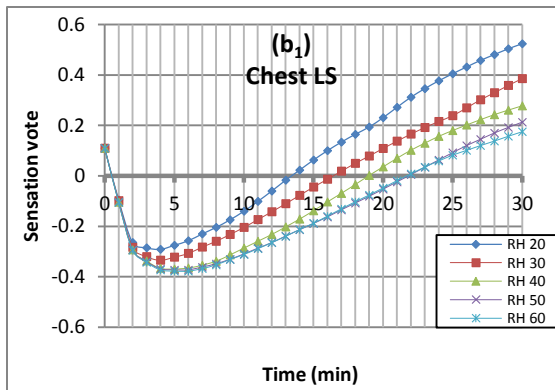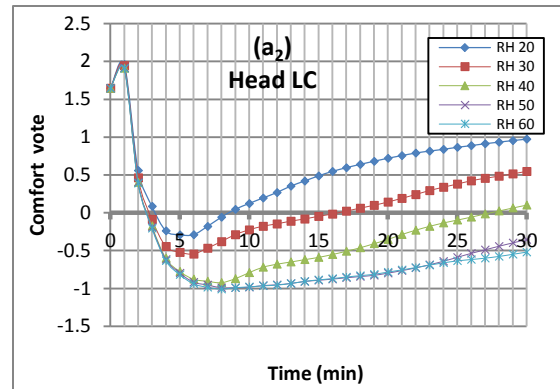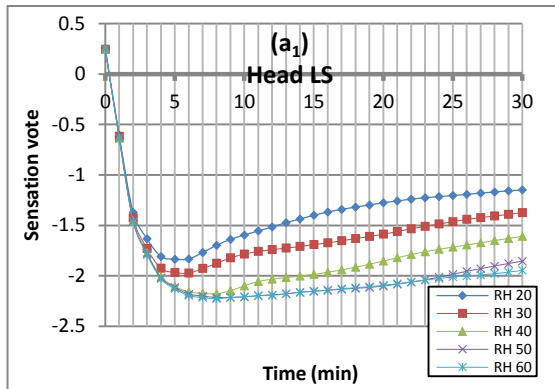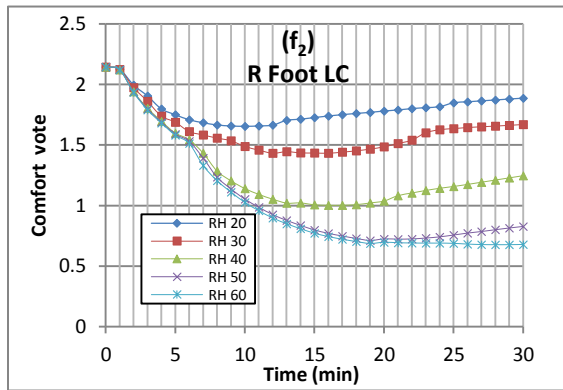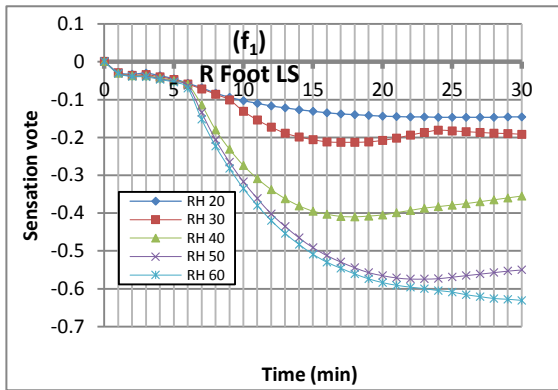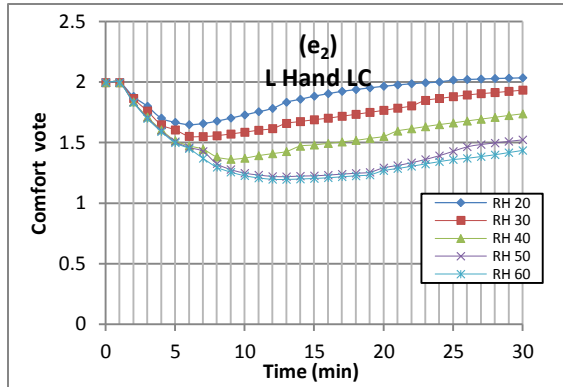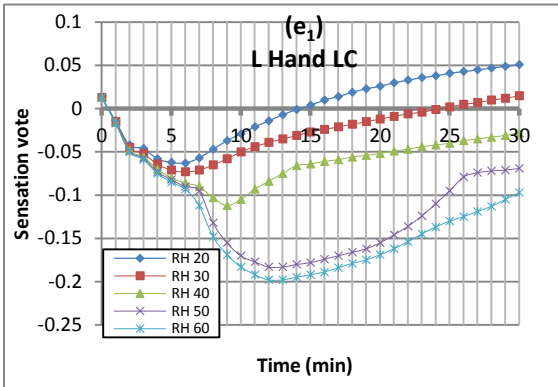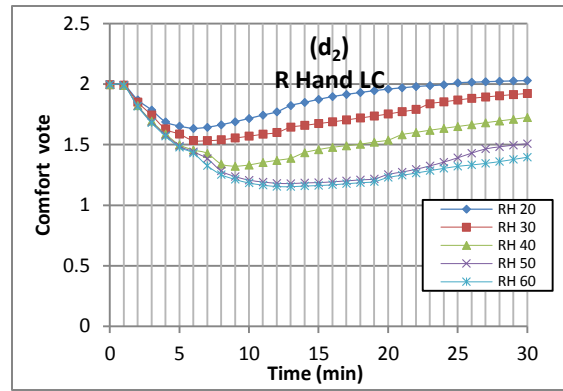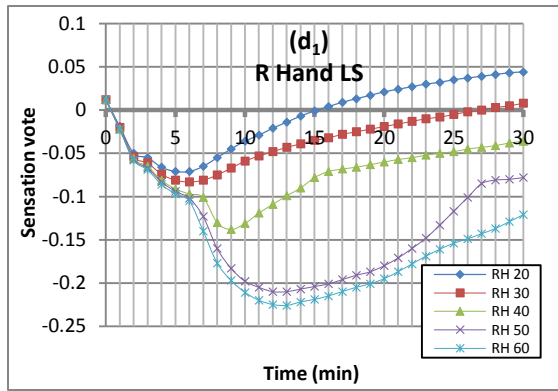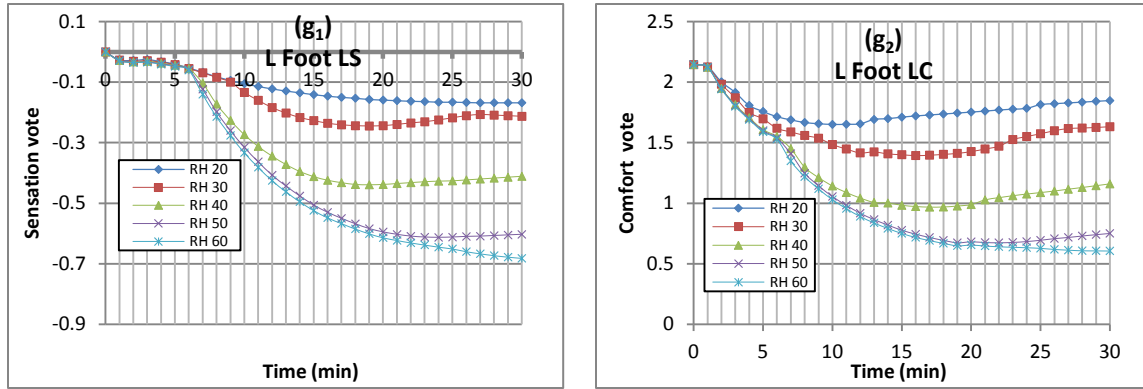
Figure 5.14: Local sensation (LS) and Local comfort (LC) variation versus time for different human segments at winter period at different RH; (a_1) Head LS (a_2) Head LC (b_1) Chest LS (b_2) Chest LC(c_1) Back LS(c_2) Back LS (d_1)Right hand LS(d_2) Right hand LS(e_1)Left hand LS (e_2)Left hand LC(f_1)Right foot LS(f_2) Right foot LC(g_1) Left foot LC(g_2) Left foot LS.

According to the Fanger model, the variation in the PMV and PPD indices with time for the different relative humidity scenarios at the winter period are presented in figure 5.15. As shown in this figure, the RH is effecting on comfortable predicted thermal sensation. So, as the RH decreases, it accelerates to reach human comfort zone ($PMV = \mp 0.5$). The environmental conditions inside the cabin become more comfortable at time being 13, 20, 23 and 30min at 20, 30, 40 and 50 % of RH respectively. But at 60% of RH, the environmental condition inside the cabin did not reach the comfortable zone during heating process according to PMV index. At end of the heating process the percentage of people feeling uncomfortable is 5, 5, 6, 10 and 16% at 20, 30, 40, 50 and 60% of RH respectively.
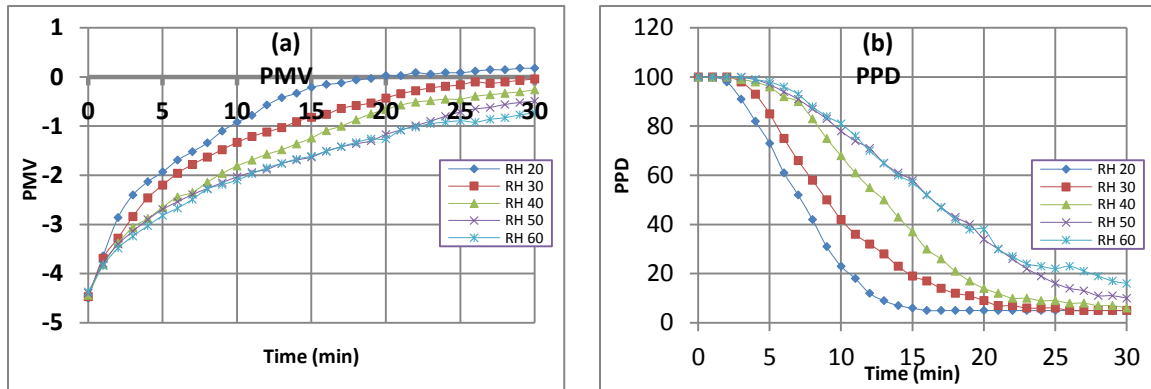
Figure 5.15: PMV and PPD versus time on in cabin at winter period for different RH; (a) PMV (b) PPD.

5.4 Discussion

5.4.1   Environmental Conditions Inside the Cabin during the Summer Period

The variations in the cabin environmental conditions during the summer period are depicted in figure 5.3 and analyzed in section 5.3.1. These conditions are mainly; dry bulb temperature (DBT), dew point temperature (DPT), specific enthalpy (H), vapor pressure (vp), and the humidity ratio (ω). All of these factors -during summer period- go into three stages, specifically the (i) rapid transient response that is due to rapid changes and interactions between the cabin different heat sources, so that the heat removed by the Air Conditioning system (A/C) is more than the heat generated within the cabin; thusly leading to a rapid decrease in the cabin temperature; this stage typically lasts for few minutes. The cabin main heat generation sources are mainly (1) the outside temperature surrounding the vehicle, (2) the Sun loading in terms of the green-house effect as shown in table 5.1 from [71]. (3) The vehicle occupants also add heat to the compartment because of the human body's thermoregulatory system which evaporates perspiration to

cool down. (4) Lastly, other heating sources include in-cabin electronics and infotainment systems. (ii) The second stage is described by another transient response that is slower that the first stage due to lesser amounts of heat being removed from the cabin. (iii) Lastly, a steady state or an equilibrium state, where the heat added from the generation sources is equal to the heat removed by the A/C system.

To investigate the relative humidity effect on the human thermal parameters (the five factors mentioned above) during the summer period, two scenarios will be discussed. The first case is when the RH value increases inside the cabin, the rate of change (a decline in this case) of the DBT increases, as can be seen in figure 5.3a. This can be explained by the airstream thermal energy that is absorbed through evaporating water. This phenomenon is similar to the evaporative cooler principle, where part of the sprayed water evaporates absorbing the airstream thermal energy, as a result, the air temperature decreases and its humidity increases [30, 67]. The second case is when the RH increases inside the cabin, thusly decreasing the changing the rate of the following environmental conditions; DPT, H, vp, and ω; as displayed in figures 5.3b, 5.3c, 5.3d and 5.3e, respectively. This is due to the inter-relationships between RH, DBT and the other environmental conditions; as depicted in the psychometric relationship chart in figure 5.2. In more words, the DPT is dependent on the RH value, where a high RH indicates a DPT value that is similar the DBT. So for an RH of 100%, the DPT is equal to the current temperature DBT and the air is fully saturated. However, when the DPT remains constant while the DBT increases, the RH decreases because the air is not fully saturated, hence the DPT is lower than the DBT as in figures 5.2 and 5.3b. For the specific enthalpy H

which expresses the air energy content, it is strongly dependent on the DBT and the RH. So any increase in the DPT and the RH values will lead to increase in the H, as pictorially shown in figures 5.2 and 5.3c. Similarly, the vapor pressure vp increases as the DBT increases; as shown in figures 5.2 and 5.3d. For the humidity ratio ω, it is related to the partial vapor pressure according to ($\omega = 0.622\frac{P_v}{P_g}$), where P_v is the partial pressure of the vapor as it exists the mixture, and P_g is the vapor saturation pressure at the same temperature. Because, the water vapor pressure value is small when compared to the atmospheric pressure, the relation between the ω and the saturation pressure is almost linear. Also, ω depends on the DPT and RH, so that an increase in the DPT and the RH leads to higher ω value, as displayed in figures 5.2 and 5.3e.

Usefully, table 5.2 summarizes the effect of changing the RH value on the cabin's environmental parameters during summer and winter periods.

Table 5.1: Compared the temperature inside close automobile to outside temperature (prepared by the Animal Protection Institute) [71].

Time	Outside Temperature (ºC)	Inside Closed Automobile Temperature(ºC)
9:15 AM	28.9	37.7
10:00 AM	31.1	39.4
10:30 AM	32.2	42.2
11:00 AM	33.3	42.8
12:00 PM	35	45
1:00 PM	38.3	45.6
2:00 PM	43.3	50.6
3:40 PM	44.4	53.9
4:00 PM	46.1	55.6

Table 5.2: Describe the effect of changing RH on other environmental parameters on in cabin during summer and winter period (↑ increase, ↓ decrease).

Rate of Drop						
Period	RH	DBT	DPT	H	vp	ω
Su mer	↑	↑	↓	↓	↓	↓
Rate of Grow						
Period	RH	DBT	DPT	H	vp	ω
Winter	↑	↓	↑	↑	↑	↑

5.4.2 Skin Temperature Variation, Local and Overall Sensation/Comfort at Summer Period

The skin temperature variation with time, for different body segments during the summer period, are depicted in figures 5.4, 5.5 and described in section 5.3.2. The skin segment temperature-time history passes through three stages; (i) it increases at the beginning of the cooling process, usually it take few minutes. This increase is due to the big difference between the skin temperature and the vehicle's compartment within a highly non-homogenous thermal environment composed of solar flux, and radiation heat flux from surrounding and interior surfaces. So, in warmer conditions active perspiration is required to achieve thermal balance, so RH plays an important role in this stage [72]. (ii) In the second stage, the skin temperature decreases by few degrees (considered a sharp decrease) because the compartment temperature drops due to the heat removed by the A/C. Lastly, (iii) the skin temperature decreases slowly until it reaches the steady state value following the change in the compartment temperature.

In general, the relative humidity has little effect on the temperature of un-clothed body segments during the cooling process as in figure 5.4. The results agree with Wiley and Newburgh [73] who found no change in skin temperature when subjects were exposed to a varying relative humidity value from 20 to 80% at a room temperature of 28ºC. Also, Winslow et al in [74] showed that the skin temperature was in general the same for both low and high humidity values.

The overall, local sensation and comfort variations from the Berkeley model versus time, and during the summer period are presented in figures 5.6, 5.7 and described

in section 5.3.2. In the early time period and due to the high cabin temperatures, the heat is transferred from the cabin environment to the passenger body through conduction, convection and radiation. But the conduction heat losses to the seat, back support and steering wheel is rather low in comparison to the total value of convective and radiative heat losses because the areas of body segments in contact with solid surfaces are smaller than other body surfaces [12]. Because of the total heat losses, the body will have a significant thermal load i.e. TS will start at a high value. Then, the thermal load decreases as the cabin temperature cools down, when body temperature rises above room temperature, the blood vessels in the skin dilate, bringing more heat-carrying blood to the surface. This results in a higher skin temperature and, consequently, an increased heat loss. At the same time, sweat glands are stimulated, opening the pores of the skin to the passage of body fluids which evaporate on the surface of the skin and thereby cool the body down. This evaporative perspiration is responsible for a great deal of heat loss. A minor amount of heat is also lost continuously by the water evaporating from the lungs and the respiratory tracts [67, 75, 76]. After that, the overall thermal sensation TS is improved (decreases) with the decrease in the inside temperature and the temperature of the interior surfaces, as shown in figure 5.6. So, as time passes, the temperature of the air surrounding the body decreases and the body becomes more neutral (i.e. more comfortable) because the body thermal inertia is around zero, then neutrality or thermal comfort is achieved. To investigate the RH effect on thermal sensation and thermal comfort, two stages are identified and analyzed. The first stage starts the cooling process, with a high RH value, and then the feeling of "uncomfortably hot" is more dominant;

118

because at this early stage, the cabin temperature is nearly the same for the different RH values. In the second stage, this usually starts from the low transient period and continues till the end of cooling process. The higher the RH value, the more comfortable the body feels because the cabin temperature is lower at a higher relative humidity. The local sensation and comfort exhibit the same of behavior, overall sensation and comfort are displayed in figure 5.7.

The Fanger model predication in summer period in terms of PMV is shown in figure 5.8. As the RH value increases, the cabin reaches the human comfort zone $(PMV = \mp 0.5)$ in lesser time, due to the decrease in the body thermal load. Hence, the A/C can achieve the human comfort zone faster than the case if the RH value is not controlled.

5.4.3   Environmental Conditions for the Cabin during Winter Period

The variation in the cabin environmental conditions during the winter period are depicted in figure 5.10 and analyzed in section 5.3.3, these conditions pass through three stages specifically; (i) the rapid transient response period, through which the heat losses to the outside is lower than the heat added (by the cabin heated air), leading to a rapid increase in the cabin temperature. (ii) The second phase is the slow transient response period while the (iii) third period is the steady state or equilibrium state, at which the heat added to the cabin is equal to the heat lost to the outside.

To investigate the effect of relative humidity on the human thermal environment parameters during the winter period, one can analyze two cases. The first case is when

the RH value is set to increase, leading to a decline in the rate of change of these environmental parameters. The DBT is an example of this case, so as the RH increases, the rate of DBT change decreases as displayed in figure 5.10a. The second case is when the RH increases inside the cabin, while the rate of change for the other environmental conditions (other than DBT) increases, as depicted in figures 5.10b, 5.10c, 5.10d and 5.10e. This is due to the inter-relationship between the RH, the DBT and the remaining environmental conditions, as in the psychometric chart in figure 5.9.

5.4.4   Skin Temperature Variation, Local and Overall Sensation/Comfort during Winter Period

The skin temperature-time history for the different body segments during the winter period, are depicted in figures 5.11, 5.12 and described in section 5.3.4. The skin segment temperature variation goes into three stages; (i) the decreases in skin temperature at the beginning of the heating process, during which a highly non-uniform thermal conditions surround the occupant body. This decrease is mainly due to the large difference between the skin temperature and the vehicle compartment temperature. (ii) The second stage exhibits an increase in skin temperature but at different rates for each segment; lastly, (iii) the steady state or equilibrium state.

The RH effect on the skin temperature during the heating process is clear for all the body segments, especially for the clothed segments such as the chest and the back, shown in figure 5.11. This is due to the difference in the body surrounding temperature for the different RH values, depicted in figure 10a. So, the rise in skin temperature is

related to the temperature surrounding the occupant body.

The overall, local sensation and comfort variations with time from the Berkeley model, during the winter period, are presented in figures 5.13, 5.14 and previously described in section 5.3.4. At the early stages and due to the low temperatures, the heat is transferred from the passenger body to cabin environment by conduction, convection and radiation. Because of this, the body will have a significant cooling load i.e. TS will start at a high value. Then, the cooling load decreases as the cabin temperature increases. When the body loses more heat to a cold environment than it produces, it decreases the heat loss by constricting the outer blood vessels, thereby reducing blood flow to the outer surface of the skin. This converts the skin surface to a layer of insulation between the interior of the body and the environment. It has about the same effect as putting on a light sweater. If the body is still losing heat, then the control device increases heat production by calling for involuntary muscular activity or shivering [67, 75, 76].

After that the overall thermal sensation TS is improved (i.e. increased) due to heating system as in figure 5.13. So, as time passes, the air temperature surrounding the body increases and the body becomes more neutral (i.e. more comfortable), then neutrality or thermal comfort is achieved. To investigate the effect of relative humidity on the thermal sensation and the thermal comfort, two stages are discussed. The first stage starts the heating process; the humidity does not play any role due to low cabin temperature. Second stage, usually it is starts from the low transient period until the end of the heating process, here the lower the RH value, the more comfortable the body feels because the cabin temperature at a low relative humidity is more comfortable for all body

121

segments. The local sensation and comfort exhibit the same behavior of overall sensation and comfort. Table 5.3 presents the RH values that correspond to the best comfort levels as achieved at the end of cooling process for the overall body and for each body segment according to Berkeley model.

The Fanger model predication, in winter period, in terms of PMV is in figure 5.15. As the RH value decreases, the cabin can reach the human comfort zone ($PMV = \mp 0.5$) faster than the case with un-controlled RH. Table 5.4 determines the time needed to reach the human comfort zone (HCZ) that corresponds to a specific RH value during the cooling and the heating processes, and according to Fanger model in terms of PMV and PPD.

Table 5.3: The RH corresponding to maximum comfort achieved at the end of cooling and heating process according to Berkeley model.

Part	Summer Period-Cooing Process			Winter Period-Heating Process		
	RH %	Comfort	Sensation	RH %	Comfort	Sensation
Overall	60	0.901	0.276	20	1.233	-0.222
Head	30	2.344	-0.668	20	0.973	-1.148
Chest	60	0.456	1.069	50	2.881	0.213
Back	60	1.974	0.072	40	2.029	-0.222
R Hand	40	2.155	-0.233	20	2.03	0.044
L Hand	40	2.151	-0.227	20	2.036	0.051
R Foot	40	2.224	-0.072	20	1.887	-0.146
L Foot	40	2.24	-0.096	20	1.848	-0.168

Table 5.4: Determine the time needed to enter human comfort zone (HCZ) corresponding to specified RH during cooling and heating process according to Fanger model in terms of PMV and PPD. And determine the values of PMV and PPD and the end of cooling and heating process.

	RH %	@	Summer Period-Cooling Process			Winter Period-Heating Process		
			Time (min)	PMV	PPD %	Time (min)	PMV	PPD %
Overall	20	Enter HCZ	---	---	---	17	-0.42	9
		End Process	30	0.82	19	30	0.18	5
	30	Enter HCZ	29	0.49	10	20	-0.43	9
		End Process	30	0.49	10	30	-0.04	5
	40	Enter HCZ	18	0.5	10	23	-0.48	10
		End Process	30	0.14	5	30	-0.26	6
	50	Enter HCZ	17	0.47	10	30	-0.49	10
		End Process	30	-0.22	6	30	-0.49	10
	60	Enter HCZ	18	0.43	9	---	---	---
		End Process	30	-0.53	11	30	-0.73	16

5.5 Summary

This chapter analyzed the effect of controlling the RH along with the dry-bulb temperature on the Thermal comfort window and sensation, in vehicular cabins. Two different models were used to investigate the effect of relative humidity inside the

vehicle's cabin on local and overall sensation and comfort during the summer and winter periods. The study results can be usefully summarized into following points;

- The Berkeley comfort and sensation results can be used to help understand the physiological response of the human body in complex thermal scenarios such as asymmetric environments. So, the comfort and sensation results can be used to aid trade-off studies and test design changes for the HVAC parameters.

- At the beginning of a cooling process; the higher value of RH, the more dominant is the "hot" is thusly the more uncomfortable the body becomes. But at the end of cooling process; the higher value of RH, results in more comfortable state according to the Berkeley model simulation results. The RH has no effect on the PMV at the beginning of cooling process. But at the end, when the RH value is around 40%, the PMV becomes 0.14 with the percentage of people feeling uncomfortable as described by the PPD is around 5%.

- At the beginning of a heating process; the body feels uncomfortably cold, while at the end of a heating process the body becomes more comfortable, neutral especially at the lower RH values according to the Berkeley model. According to Fanger model, when the RH decreases, the cabin A/C system can reach the human comfort zone ($PMV = \mp 0.5$) faster. So, at the end of a cooling process, as the RH value becomes around 20%, the value of PMV is 0.18 and the percentage of people feeling uncomfortable as described by the PPD is around 5%.

Furthermore, this study analyzed the effect of the cabin's RH on all the environmental conditions including the DBT, DPT, WBT, H, vp, ω and ν during the summer and winter periods.

CHAPTER SIX

DESIGN FOR THERMAL SENSATION AND COMFORT STATES IN VEHICLE CABINS

This chapter investigates the analysis and modeling of vehicular thermal comfort parameters using a set of designed experiments aided by thermography measurements. The experiments are conducted using a full size climatic chamber to host the test vehicle, to accurately assess the transient and steady state temperature distributions of the test vehicle cabins. Further investigate the thermal sensation (overall and local) and the human comfort states under artificially created relative humidity scenarios. The thermal images are calibrated through a thermocouples network, while the outside temperature and relative humidity are manipulated through the climatic environmental chamber with controlled soaking periods to guarantee the steady state conditions for each test scenario. The relative humidity inside the passenger cabin is controlled using a Total Humidity Controller (THC). The simulation uses the experimentally extracted boundary conditions via a 3-D Berkeley model that is set to be fully transient to account for the interactions in the velocity and temperature fields in the passenger compartment, which included interactions from turbulent flow, thermal buoyancy and the three modes of heat transfer conduction, convection and radiation. The model investigates the human comfort by analyzing the effect of the in-cabin relative humidity from two specific perspectives; firstly its effect on the body temperature variation within the cabin. Secondly, the Local Sensation (LS) and Comfort (LC) are analyzed for the different body segments in

addition to the Overall Sensation (OS) and the Overall Comfort (OC). Furthermore, the human sensation is computed using the Fanger model in terms of the Predicted Mean Value (PMV) and the Predicted Percentage Dissatisfied (PPD) indices. The experimental and simulation results show that controlling the RH levels during the heating and the cooling processes (winter and summer conditions respectively) aid the A/C system to achieve the human comfort zone faster than the case if the RH value is not controlled. Also, the measured and predicted transient temperatures are compared and found to be in good agreement.

6.1   Introduction

Recently, more emphasis has been placed on optimizing the thermal comfort for vehicular occupants to provide better driving experience and more comfort features. Additionally, optimizing the cabin Air Conditioning A/C system can reduce the vehicle energy consumption; around 30% of the Mile Per Gallon (MPG) expenditure is related to the A/C system. Traditional climate control strategies classify the in-cabin modeling into; human physiological and psychological perspectives in addition to the compartment zone and the human thermal manikin approaches. However, the current experimental studies still deal with subjective observers and in rare cases thermal manikins. Experimental work aided with visualization tools such as infrared thermography can help in integrating the proposed models with the actual cabin conditions [2].

In this study, thermography or thermal imaging techniques will be used to measure the surface temperature distribution of an automobile cabin, which is subjected

to a set of controlled environmental forcing. The experimental work main objective is to analyze the effect of controlling the RH on the cabin's environment, and its role in achieving the thermal comfort range in lesser time. Infrared thermography has been mainly used in military, industrial, mechanical, electrical and medical applications [77]. Other potential HVAC applications for infrared (IR) thermography included the evaluation of heat exchangers subsystems (evaporator, condenser, and heater core) fin temperatures, in locating primary sources of heat loss from the cabin during winter, and in evaluating the ability of different window glazing to reduce summer cabin solar loading [42, 77]. Thermography has been used to evaluate various flaws, including leaks, cracks, debonding, corrosion, poor electrical wiring and contacts, and delaminations. They also can be used to assess overall thermal characteristics. The detection of discontinuities in a material is possible because the uniform diffusion of heat from the surface of a sample into its bulk is disrupted by such anomalies in the surface properties of the material [78].

During the past two decades infrared thermography has evolved into a powerful investigative means of thermo fluid-dynamic analysis to measure convective heat fluxes as well as to investigate the surface flow field behavior over complicated body shapes. Thermography is characterized by the use of thermal and infrared sensors to measure temperature variations in a variety of test objects.

Using IR thermography in an automobile during transient conditions enables the temperature measurement of solid surfaces, clothes and the visible body parts of human subjects [43]. The temperatures of these surfaces can then be used for thermal comfort

studies. Also through proper image analysis and data reduction, thermal images or thermograms can provide quantitative solid surface temperature assessments comparable in accuracy to thermocouple arrays, while adding the advantage of the full-field scanning [79]. At the same time, accurate temperature profiles can only be obtained if the surface emissivity, the ambient temperature, and the wavelength of radiation are known [79, 80].

The structure of this chapter starts by discussing the related research from the body of literature in section two in terms of thermography use in vehicles' climate control and RH control; while section three discusses the experimental approach and the 3D simulation model. Section four presents the results and the discussion; section five summarizes the study findings through the conclusion.

6.2   Literature Review

The body of literature contains limited number of research studies that discuss and address the use of IR thermal imaging to measure and evaluate the thermal conditions inside vehicular cabins, even though the IR thermography is a contact-less modality that can measure the global climatic conditions inside the passenger compartment in real-time. Burch et al. in [42] described the use of several infrared IR sensors for automotive climatic control analysis. Additionally, he proposed a different method for measuring ambient air temperature, using a thin (0.15 mm) layer of polyethylene plastic film that is mounted perpendicular to the air stream. Korukçu et al. reported in [43] the use of the IR thermal imaging through an un-cooled thermal detector to measure the front panel temperature and that of a human facial skin during the heating and the cooling periods.

This experiment validated the use of the thermal imager by showing that the acquired temperature profiles (spatial and temporal) from the thermal imagers and a network of thermocouples were in agreement.

The influence of high humidity levels on human comfort; specifically the response of sedentary human to high humidity exposure (RH between 60% - 90%) at a temperature range of $20 - 26\ ^{o}$C had been investigated by Fountain et al. in [28]. This study articulated the qualitative RH effect without distinguishing it from other variables mainly the Dry Bulb Temperature DBT. Alahmer et al. discussed the effect of manipulating the Relative Humidity RH on the in-cabin environment from the thermal comfort and human occupants' thermal sensation perspectives using thermo-dynamics and psychometric analyses in [30] in addition to using a Berkley simulation model in [81]. He also proposed a practical system implementation to control RH inside vehicle cabins using an evaporative cooler design. The results showed that controlling the RH along with the dry bulb temperature inside vehicular cabins can improve the air conditioning efficiency by reducing heat removed while improving the human comfort sensations [30, 81]. Another study of manipulating the effect of relative humidity and temperature on the human health in air conditioned buildings was presented by Sookchaiya et al. [82] in this study, two scenarios were discussed: scenario one is the assessment of the thermal environment (temperature and relative humidity) effects on the human comfort and health using Delphi technique. While, scenario two tackled the design and development of a temperature and relative humidity control system (precision inverter air conditioning system). The result showed that the inverter air conditioning has

distinguished advantages for the human comfort and health. Moreover, it saves electricity consumption by 7.5%.

Because, the experimental work associated with a thermal sensation rating approach is expensive, time consuming and difficult to standardize, the proposed experimental approach using thermography, coupled with thermal comfort predictions can be effective in guiding design directions during the early stages of the vehicle development process. Furthermore, simulating the in-cabin conditions using the experimental boundary conditions can serve not only as a visualization tool but also as a new way of evaluating the human local and overall comfort levels. In [63] a three-dimensional fluid flow and heat transfer scheme (commercial name RadTherm, product of Thermo-Analytics) was coupled with an in-house developed solar radiation code to simulate the passenger compartment cooling process. The analysis was fully transient and the computed velocity and temperature fields in the passenger compartment included the interactions from turbulent flow, thermal buoyancy, and the three modes of heat transfer, i.e. radiation, convection, and conduction.

6.3   Methodology

6.3.1   Experimental Setup

A series of experiments was carried out during the month of July 2011 using an MTS road-simulator, housed in a Weiss climatic environmental chamber. The chamber is equipped with a FlexTest IIm control module, capable of manipulating the inside temperature from -40 to 85°C, and the relative humidity range from 15 to 95%. The

chamber accommodates transient testing in both heating and cooling conditions at a rate of $1.3^{\circ}C$/ minute and a $0.9\ ^{\circ}C$/minute for a vehicle with up to 3000 kg in weight; the test setup is displayed in figure 6.1. The testing is done at the Clemson University International Center for Automotive Research CU-ICAR testing laboratories. The test vehicle used in this experimental study is a 2011 Toyota Camry sedan, with its Controlled Area Network CAN-Bus accessed through the On-Board Diagnostic OBD module.

The experimental work is set according to the following protocol; (i) surrounding environmental conditions are set to the desired values in terms of RH and DBT, through a 30 minutes soak period to guarantee the steady-state conditions. (ii) The vehicle inside conditions are continuously measured and assessed using the thermocouple network, the infrared detectors, and the OBD software; each experiment (data acquisition part) session lasts for 30 minutes.

Inside the vehicle, the air vents are directed on the feet and windshield mode. The tests utilized an uncooled, micro-bolometric, Vanadium Oxide VO_X coated, focal plane array in two different locations within the vehicle. At first mounting location; the detector is placed in front of the right passenger seat with its Field of View FoV focused on the driver's face to measure facial skin temperature as shown in figure 6.2; while the second mounting spot is placed in the middle of the back seat to measure the surface temperature of the front panel as shown in figure 6.3. In addition, thermocouple network are installed to have a reference signal to track transient and spatial temperature measurements in the different locations (windshield, vent outlet, forehead, hands and feet). During the

132

experiment, the relative humidity is continuously measured using a digital Hygro-thermometer (commercial name LAM880D), which is controlled using a Total Humidity Controller (THC). The THC is connected to humidifier/dehumidifier combination utilizing a duplex cord cap to alternate between the humidifier and dehumidifier; while the surrounding relative humidity and temperature are controlled by the climatic chamber. The outside RH is set to range between 20 to 60%, and the temperature is set at 55, -10 ℃ during the heating and the cooling periods respectively. Additionally, the air stream velocity is measured using a digital anemometer (commercial name DAF800). The accuracy and the measuring range of all previous equipment are tabulated in table 6.1 and table 6.2.

Figure 6.1: Heat- cold climatic test chamber.

Figure 6.2: Location of cooled IR camera to measure driver's face temperature.

Figure 6.3: Location of uncooled IR camera to measure side of cabin temperature.

Table 6.1: IR thermal detector specifications.

Description	Uncooled Camera
Model Name	FLIR A40M
Camera Images	
Camera Resolution	320x240
Focal Plane Array Cooling (FPA)	No Cooling
Thermal Sensitivity	0.08 ° C at 30 ° C
Frame Rate	7.5 Hz, 15 Hz, 30 Hz and 60 Hz
Temperature Range	-40 ° C to 500 ° C

Table 6.2: Specification of the experimental equipments.

Equipment	Parameter	Range	Accuracy
Cold-Heat Climatic Test Chamber Manufactured by Weiss	Control (T) Control (RH)	-40 º C 85 º C 10% to 90%	$\leq 1\ K$ $\leq 5\ \%$
Thermocouple Type K	T	-60 º C 175 º C	±0.1
Digital Anemometer (DAF800)	V	0.4- 30 m/s	0.1 m/s
Digital Hygro-Thermometer (LAM880D)	RH	0-100% RH	$\pm3\%$ at 25 ℃
Total humidity Control (THC)	Control RH	20-70% RH	$\leq 5\ \%$
Humidifier (VICS CM 1GA)	Increase RH	---	---
Dehumidifier (ADS-400)	Decrease RH	---	---

6.3.2　3-D Thermal Simulation

A virtual thermal manikin, based on the Berkeley model, is used in the simulation study to help predict the human thermal comfort within the different vehicle cabin environments. This manikin integrates a human thermal physiological model to predict the body core and skin temperatures for twenty one parts of the human body; the solver package relied on a Finite Differencing FD scheme commercial name RadTherm [63]. The solver uses a human comfort subroutine by creating nodal network to represent conduction in the human body while the radiation and convection are set at the surface using shell based geometry. Also, the human comfort library has the ability to perform thermoregulatory mechanisms, calculation of metabolic rates and blood perfusion energy rates, simultaneously.

This proposed simulation approach allows the computation of the human comfort levels, both local and overall comfort, while accounting for the localized thermoregulatory responses such as perspiration, respiration, and blood flow changes. The experimental results will aid the simulation in two folds; by providing the initial boundary conditions and by verifying the simulation findings. The proposed simulation study comprises the individual human body parts allowing the user to define separate layers of clothing and other local effects. Additionally, the environmental model supports full weather inputs, solar models, transparent glass with greenhouse effects, and all other significant in-cabin thermal variables.

The thermal sensation and comfort votes are calculated using the nine-point Berkeley comfort scale. On this scale, the higher positive sensation value indicates hotter feeling. On the other hand, the higher negative sensation value indicates cooler feeling, while a zero sensation indicates a neural thermal sensation. The higher comfort value indicates a better or a more comfortable feeling as shown in tables 3.4 and 3.6. The thermal manikin is placed inside the virtual model for the test vehicle cabin with a homogeneous environment over a range of relative humidity of (20-60%) as shown in figure 5.1. The manikin is simulated wearing short sleeve with long trousers with an approximate clothing insulation value of 0.5 clo or $0.078 \frac{m^2 K}{W}$ for the heating period, and wearing long thick sleeve, long thick trousers, hand-wear and footwear with approximate clothing insulation value of 1 clo ($0.155 \frac{m^2 K}{W}$) for the cooling period. The metabolic rate is set at 1.4 met ($81 \frac{W}{m^2}$), which is the standard value for a seated human metabolic rate as reported in [14, 48, 69].

Lastly, a Fanger-model based subroutine is incorporated to compute the; (i) The Predicted Mean Value (PMV) index, to describe the mean response of the thermal vote of a large group of people exposed to the same environment. (ii)The Predicted Percentage Dissatisfied (PPD), which calculates a prediction of the number of thermally dissatisfied people. Table 3 describes the seven-point thermal sensation scale as used by Fanger-based model relying on the PMV index of a large group of people [17 - 19].

6.4   Results and Discussion

6.4.1 Passenger Compartment, Skin Segments and Front Windshield Temperature Variation During Heating Period

The variation in the temperature-time history inside the cabin during the heating period is depicted in figure 6.4. As shown, as time passes, the temperature decreases for different values of RH, with the temperature curve passing through three stages specifically; (i) Rapid transient response due to the rapid changes and interactions between the cabin different heat sources, as the air conditioning process begins, where the A/C removes the cabin heat leading to a rapid decrease in the cabin temperature. This stage typically lasts for few minutes. (iii) Slow transient response; being slower than the first stage due to the lesser amounts of heat being removed from the cabin. Lastly, (iv) Steady state stage; where the heat added from the cabin generation sources is equal to the heat removed by the A/C system.

The RH effect causes the temperature variation (drop) to increase as the RH level increases, which can be explained by the variations in the airstream thermal energy content that is being absorbed through evaporative cooling, as a result, the air temperature decreases as its humidity increases [30, 67].
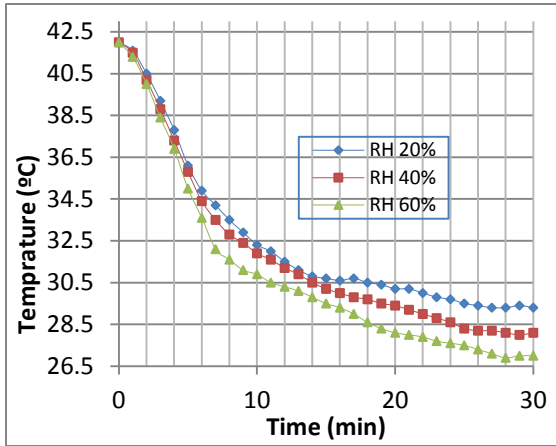
Figure 6.4: Temperature variation versus time inside passenger cabin under different relative humidity at heating period.

The thermo-grams (i.e. thermal images) of the front windshield, during the heating period, at different relative humidity levels are displayed in figure 6.5. As shown in this figure, the warmer the object, the brighter it appears on the thermography photos. Also, the all solid surfaces in the cabin will initially appear in bright color indicating high temperatures. As the time passes, the color of the surfaces become darker indicating the decrease in the surface temperatures. Also it can be noted that the all surfaces near the vent outlets are cooled down more rapidly. The temperature changes on the windscreen, temperature profiles provide the information about the air flow distribution on the windscreen; however the flowing air over all the surfaces injected by the inlet vents do not have the same value [43]. This information is used as boundary conditions of Berkeley simulation model to help evaluate the temperature variation of all human body segments and the overall and local comfort and sensation. It can be also seen that the temperature at any point in the thermography can be easily quantified at any instance and at any spot.

The temperature variation of the windshield using under different relative humidity level during the heating period are displayed in figure 6.6, as acquired by the uncooled thermal detector. It can be seen that the front side of the cabin temperatures have reached steady-state after 27 minutes. The effect of relative humidity on the temperature variation of the windshield front side leads to an increase in such variation as the RH levels increase.
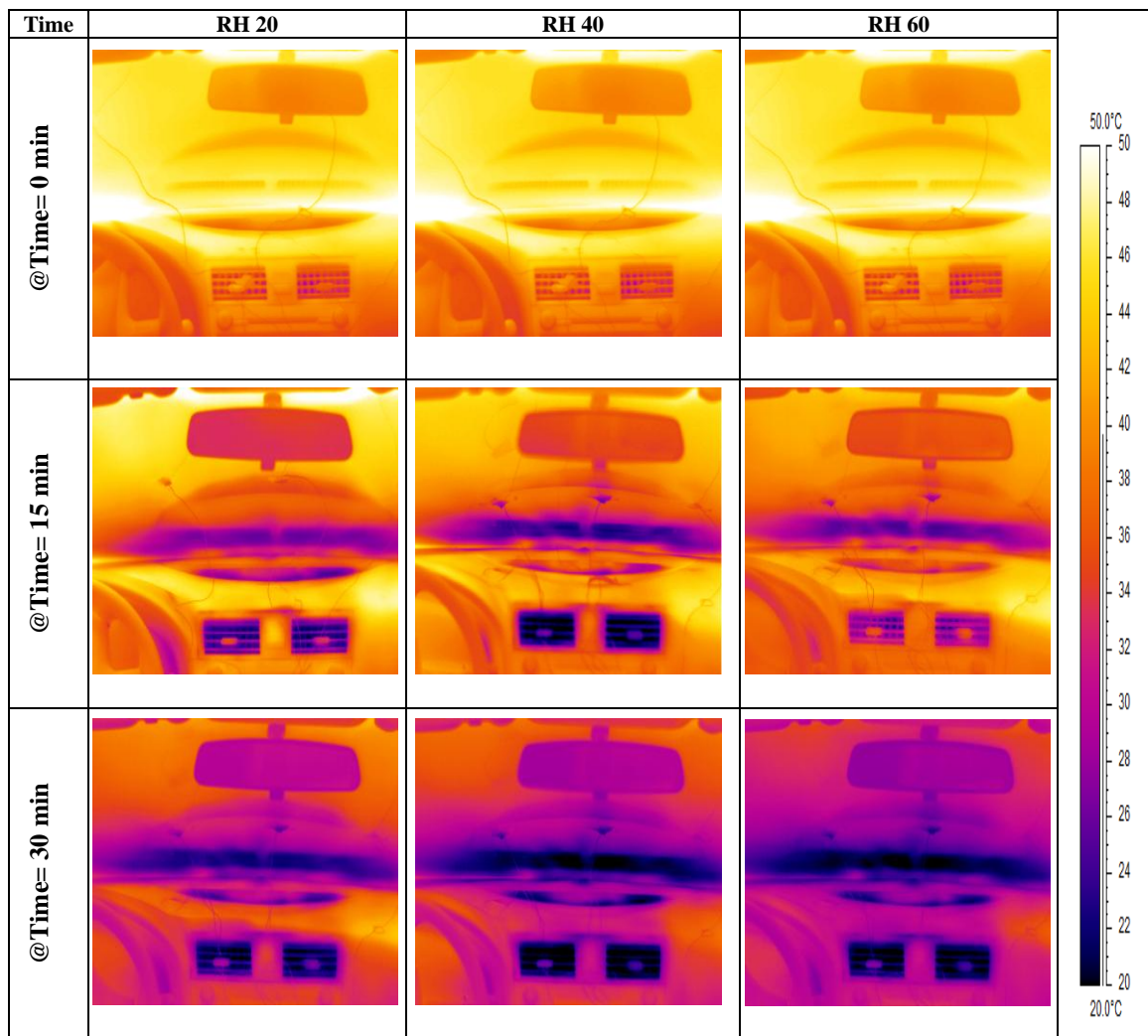
Figure 6.5: IR picture of front windshield inside passenger cabin at heating period for different relative humidity.
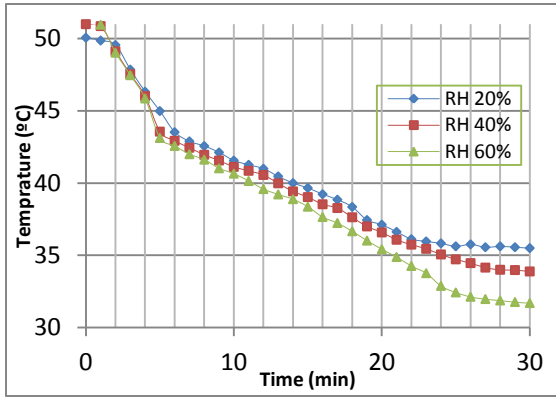
Figure 6.6: Temperature variation versus time of front windshield under different relative humidity at heating period.

The divers' face thermograms have been captured each 15 min interval for the different relative humidity scenarios during heating period and are presented in figure 6.7. While the temperature variation inside the passenger cabin decreases with time, the facial skin temperature also decreases. From the temperature scale, one can notice that the passenger's head and face temperature are lower than that of the compartment cabin.

The skin temperature variation for the different body segments such as the forehead, hand and driver's foot against time, and for the different relative humidity scenarios during the heating period, are also captured using the uncooled micro-bolometric array, the thermocouples network in addition to the Berkeley model, all are displayed in figure 6.8; with addition of the schematic of temperature variation at the end of cooling process from the simulation being shown in figure 6.9. While air condition was operated at third level, all segment temperature decreases during the time passes until reaches steady state. It can be seen that the temperature profiles are similar, and the largest differences between the measured and predicted temperatures of forehead, hand and foot are less than 0.9, 1.2 and 1.4 °C respectively at any time instance during the

141

heating period under different relative humidity. In general, the relative humidity has no effect on the temperature variation of the different segments during the heating process. The results agree with Wiley and Newburgh [73] who found no change in skin temperature when subjects were exposed to a relative humidity varying from 20 to 80% at a room temperature of 28ºC. Also, Winslow et al in [74] showed that the skin temperatures were in general the same for both low and high humidity levels.
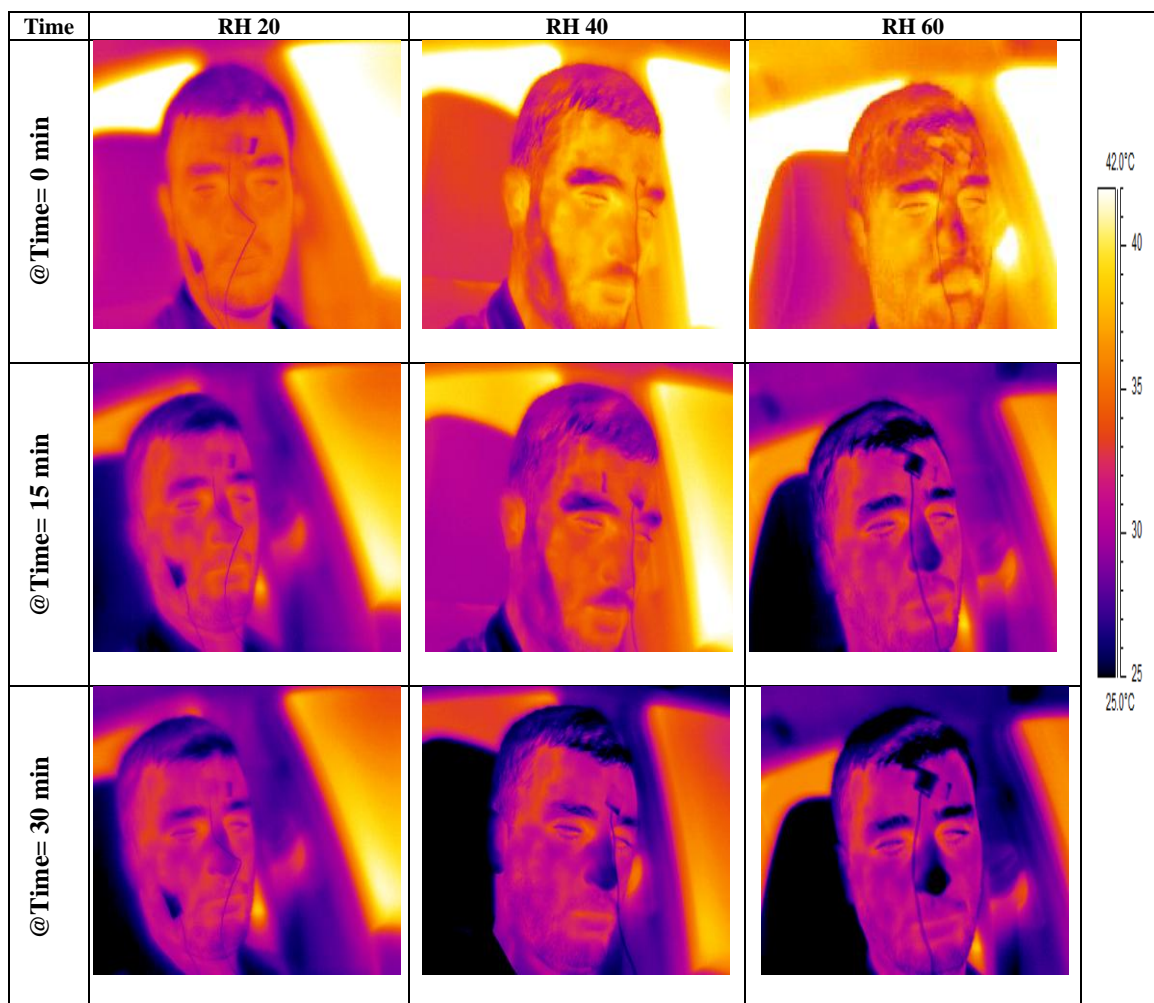
Figure 6.7: IR picture of the driver's face at heating period for different relative humidity scenarios.
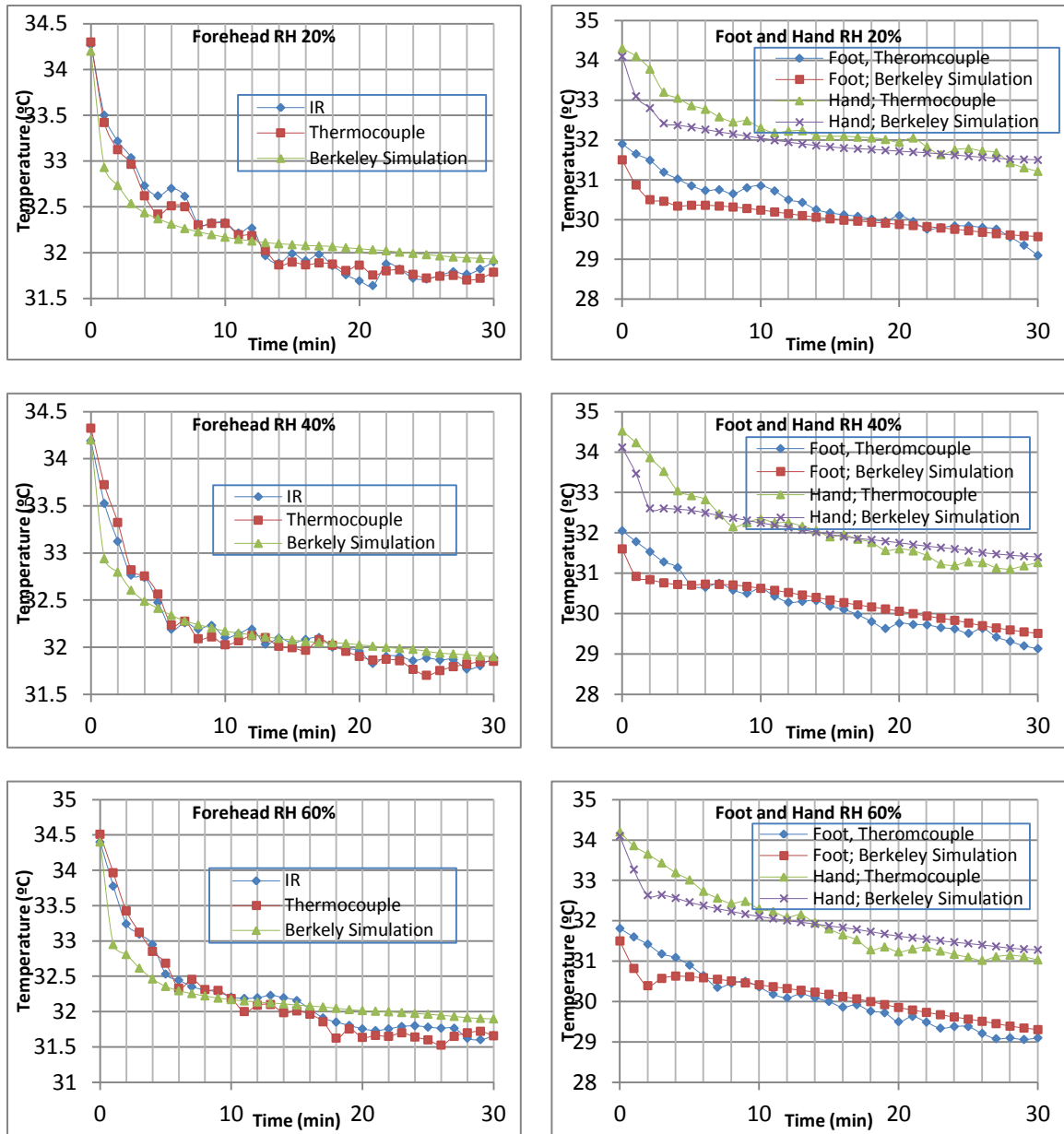
Figure 6.8: Temperature variation for different segment parts at different relative humidity scenarios during heating period.

RH 20%	RH 40%	RH 60%

26.5   27.3   28.0   28.8   29.5   30.3   31.0   31.8   32.5
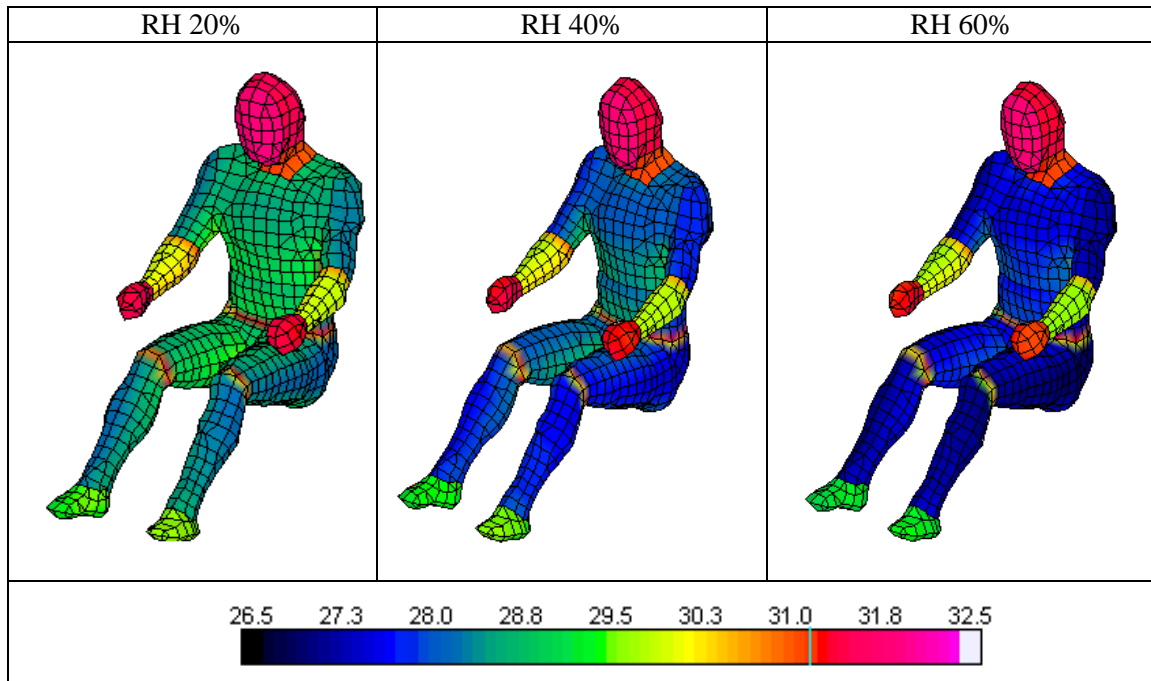
Figure 6.9: Schematic of body temperature variation inside passenger cabin at end of cooling process in heating period for different relative humidity.

6.4.2 Passenger Local, Overall Sensation and Comfort during Heating Period

The overall sensation and comfort variations as computed for the different relative humidity scenarios and during the heating period are depicted in figure 6.10. In the early stages, the thermal sensation increases rapidly -through the first few minutes- until it reaches a maximum value that to expresses the human body feeling of "very hot" and the human comfort decreases rapidly expressing uncomfortable feeling due to the high surrounding temperature. The heat is transferred from the cabin environment to the passenger body through conduction, convection and radiation. Also, the body has several thermal adjustment mechanisms to help adjust in high temperature environments. So, in a warm environment, vasodilatation increases the blood flow to the skin increasing the heat

transport, and the skin temperature thus increasing the heat dissipation. If there is an imbalance, the sweat production starts and an evaporative cooling mechanism help in cooling the body down [74].

Also, the impact of relative humidity on sensed temperature is more pronounced when the outside temperature increased. So, under humid conditions, the rate at which perspiration evaporates on the skin is lower than it would be under arid conditions. Because humans perceive the rate of heat transfer from the body rather than temperature itself, one feels warmer when the relative humidity is high than when it is low.

After this period, the overall thermal sensation starts decreasing due to decrease in cabin's air temperature. So, as time passes, the body becomes more neutral (i.e. more comfortable). At the beginning of the cooling process; the higher the value of RH, the feeling of "hot" conditions becomes more dominant and the more uncomfortable human body becomes. Because at the early stage, the passenger cabin temperature is nearly the same for the different RH scenarios as shown in figure 6.4, feeling warmer and uncomfortable when the relative humidity is higher than the case when it is low. But at the end of the cooling process; the higher the RH value, the more comfortable the body becomes, because the cabin temperature at the high relative humidity value is lower than that at a lower relative humidity level.

The local sensation and comfort exhibit the same of behavior; overall sensation and comfort are displayed in figure 6.11.

The RH has more influential effect at the beginning of the cooling process, when the RH increases, the feeling of "hot" and uncomfortable increases especially for the foot

145

segment. But at the end of cooling process; the effect of an increasing RH value on the comfort level becomes less pronounced especially for the hands and the feet segments. Although local thermal discomfort can be caused from wetness, the thermal comfort of the whole body will not be affected by the wetness of certain parts [75].

Computing the Fanger model indices PMV and PPD versus time and under different relative humidity scenarios, in the heating period, results in figure 6.12. As shown in this figure, at the initial stage i.e. before the 4 minute mark, the RH has an opposite effect on the human comfort on the PMV scale, as RH increases the more the uncomfortable feeling becomes more dominant due to the same reasoning mentioned previously. According to the PPD index, the predicted number of people likely to feel uncomfortable in these conditions is around 100% for all values of RH. In the next time stage, increasing the RH inside the cabin leads to more comfortable feelings. So, as the RH value increases, the A/C can achieve the human comfort zone ($PMV = \mp 0.5$) faster than the case if the RH value is not controlled. And according to PPD index, as the RH increases the predicted number of people likely to feel uncomfortable decreases with time. The difference in predictions between the Berkeley and the Fanger models, especially at the first stage, is caused by the fact that the PMV establishes the human thermal strain based on a steady-state heat transfer assumption between the human body and its thermal comfort ratings from a panel of subjects. Also the PMV has been proposed for homogenous conditions only, but when applied in non-homogenous conditions as the case of vehicular cabins, it did not provide accurate predictions [18, 20].
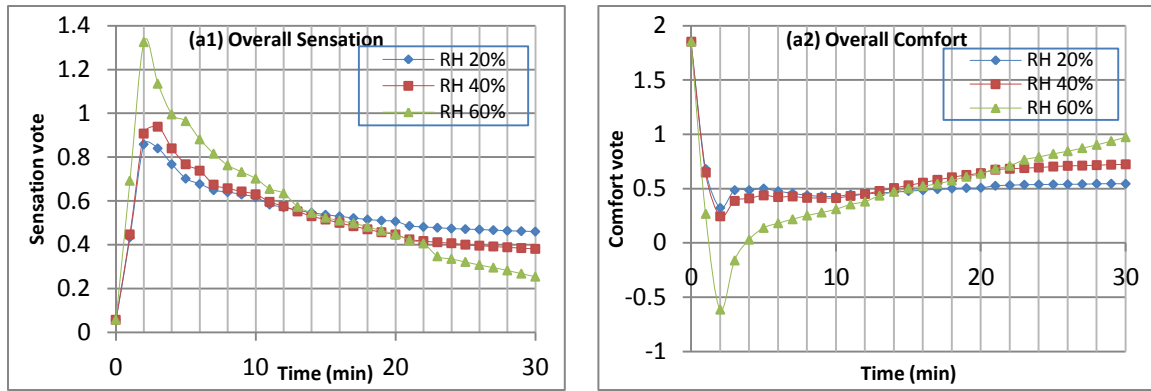
Figure 6.10: Overall sensation (OS) and overall comfort (OC) variation versus time at heating period for different RH scenarios; (a1) OS (a2) OC.
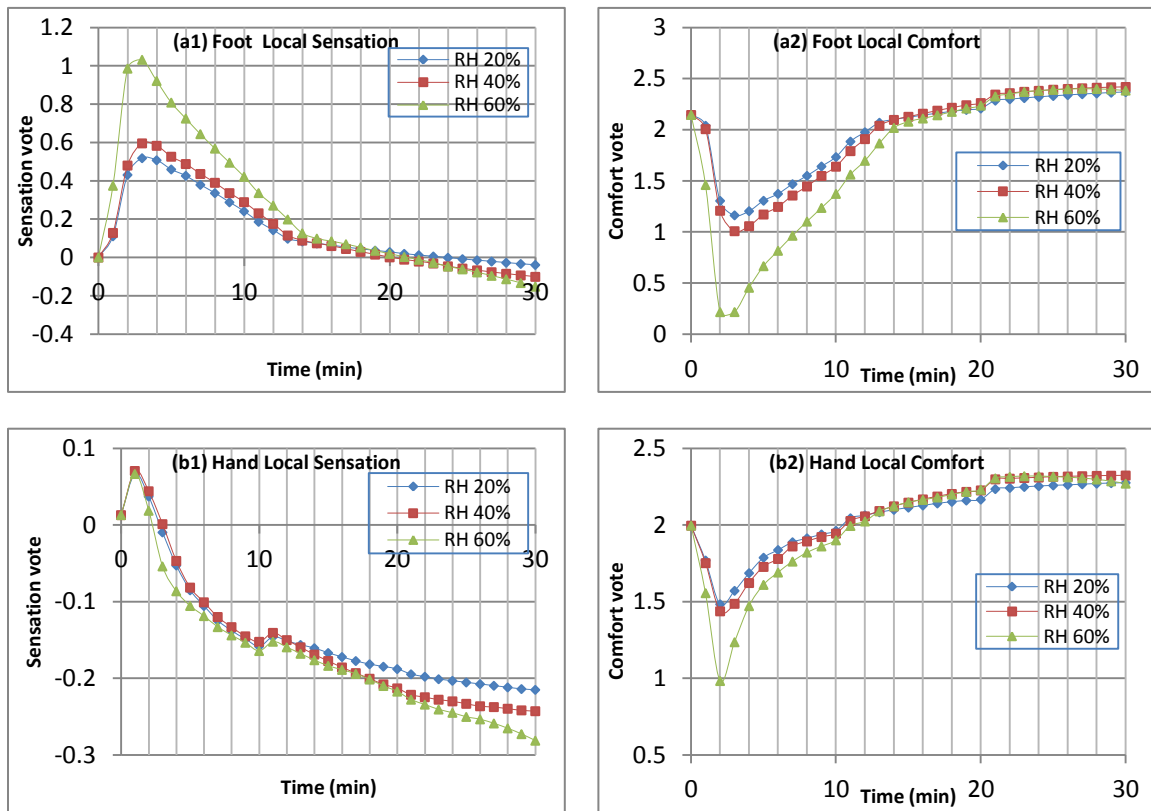
Figure 6.11: Local sensation (LS) and local comfort (LC) for different segment part at heating period; (a1) foot LS (a2) foot LC (b1) hand LS (b2) hand LC.
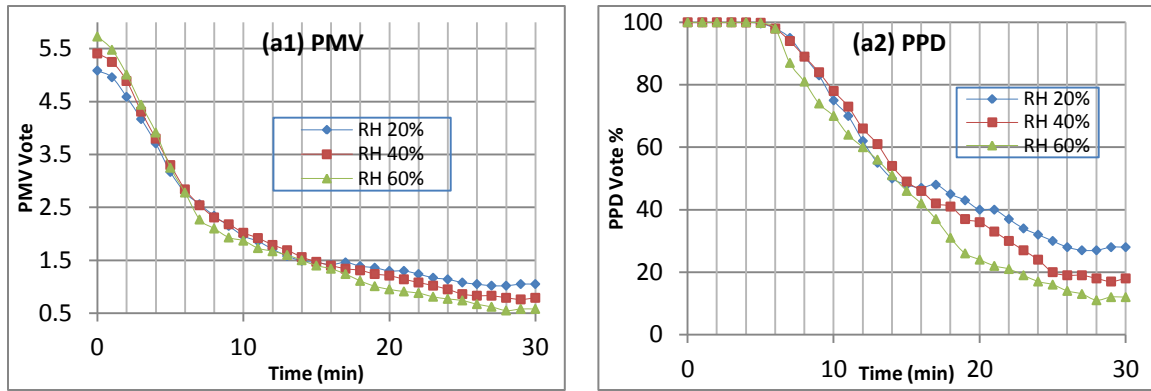
Figure 6.12: PMV and PPD versus time inside passenger cabin under relative humidity scenarios at heating period (a1) PMV (a2) PPD.

6.4.3 Passenger Compartment, Skin Segments and Front Windshield Temperature Variation during the Cooling Period

The temperature-time variation inside the passenger cabin during cooling period is depicted in figure 6.13. From this figure, as time passes the temperature increases for the different values of RH. The temperature variation curve passes through three stages specifically; (i) the rapid transient response period, through which the heat losses to the outside is lower than the heat added (by the cabin heated air), leading to a rapid increase in the cabin temperature. (ii) The second phase is the slow transient response period while the (iii) third period is the steady state or equilibrium state, at which the heat added to the cabin is equal to the heat lost to the outside. Now, when the RH value increases inside the cabin, the rate of change (an increase in this case) of the temperature variation decreases.

148

The thermograms of the front windshield as recorded during the cooling period for the different relative humidity levels are displayed in figure 6.14, based on a 15 minute interval.

The temperature variation of the windshield as extracted from the thermograms is shown in figure 6.15. It can be noted that the front side temperatures have reached steady-state after 28 minutes. The effect of relative humidity on the temperature variation of the windshield front side increases as the rate of temperature variation decreases.
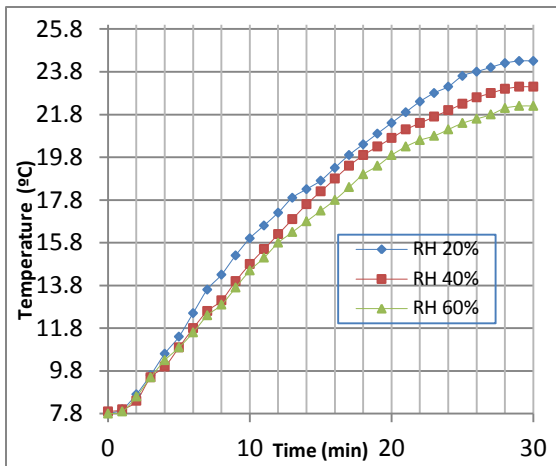
Figure 6.13: Temperature variation versus time inside passenger cabin under different relative humidity at cooling period.

Time	RH 20	RH 40	RH 60
@Time= 0 min			
@Time= 15 min			
@Time= 30 min			
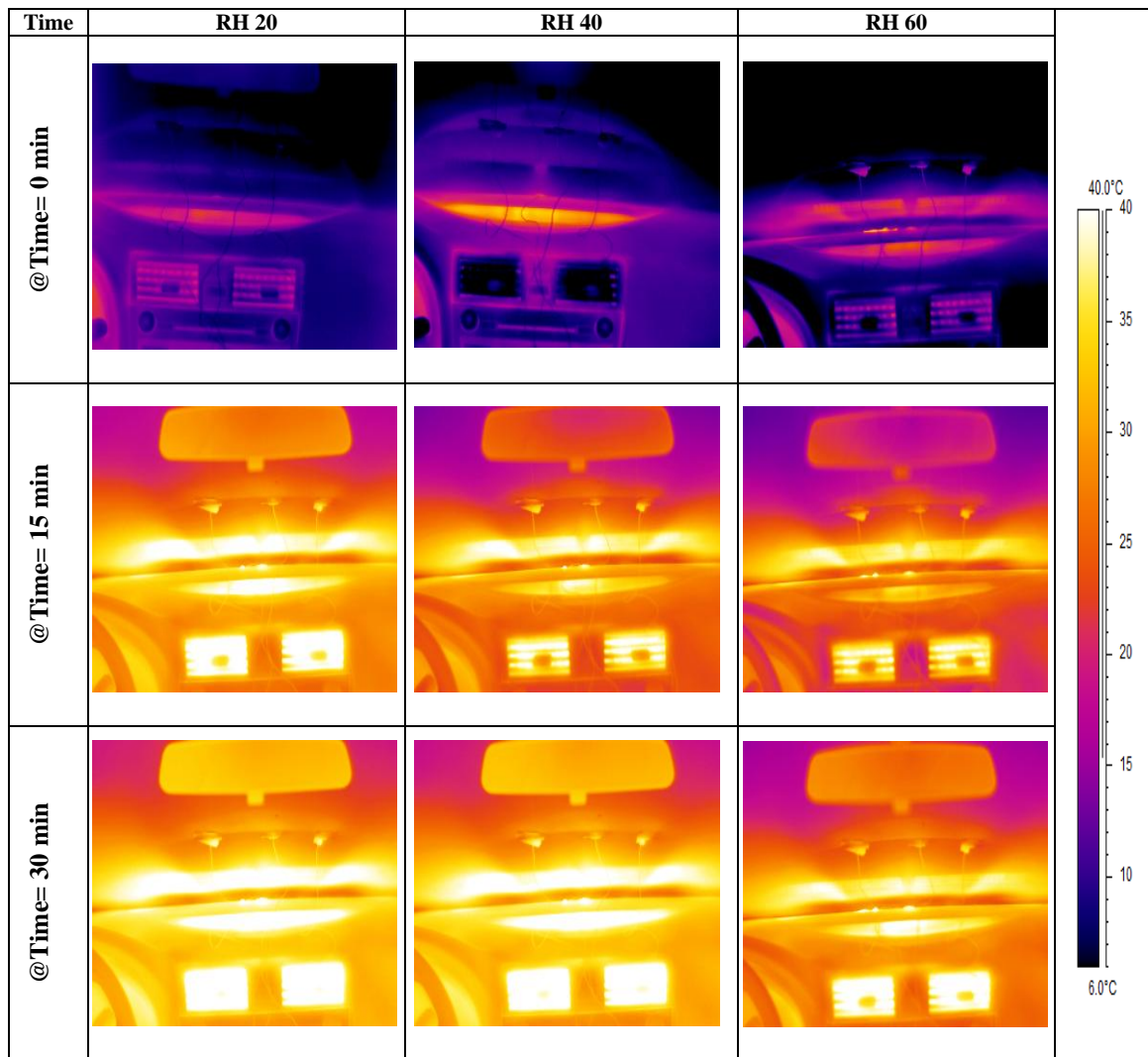
Figure 6.14: IR picture of front windshield inside passenger cabin at cooling period for different relative humidity.
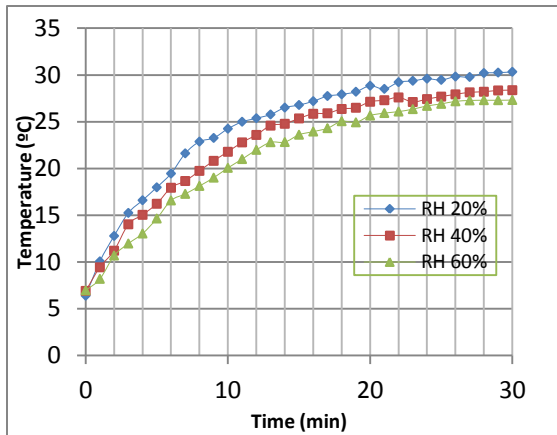
Figure 6.15: Temperature variation versus time of front windshield under different relative humidity at cold period.

Additionally, the driver's face thermograms for each 15 minute interval at different relative humidity scenarios, during cooling period, are presented in figure 6.16. While the temperature variation inside the cabin increases the facial skin temperature decreases.

The skin temperature variation for different body segments such as the forehead, hands and feet for the different relative humidity scenarios during the cooling period using the uncooled IR detector, the thermocouples network and the simulation model are were displayed in figure 6.17; with the simulation predictions for the temperature variation at the end of cooling process being shown in figure 6.18. At the beginning of the heating process, the skin temperature for different body segments decreases because of the big difference between the skin temperature and vehicle compartment temperature. As time passes, the air temperature surrounding the body increases such that all segments' temperature start to increase until it reach the steady state at the end of heating process. It can be seen that the temperature profiles are similar, and the maximum

differences between the measured temperatures values for forehead, hand and foot are less than 1, 1.8 and 1.6 °C respectively at any time instance, during the cooling period and under different relative humidity levels. In general, the relative humidity has little effect on the temperature variation of the different segments during the heating process, as the RH increases inside the cabin, the temperature variation of the skin segment (increases with time) decreases by a little. This is due to the difference in the surrounding air temperature for the different RH values, depicted in figure 6.13. So, the rise in skin temperature is related to the temperature surrounding the occupant body.
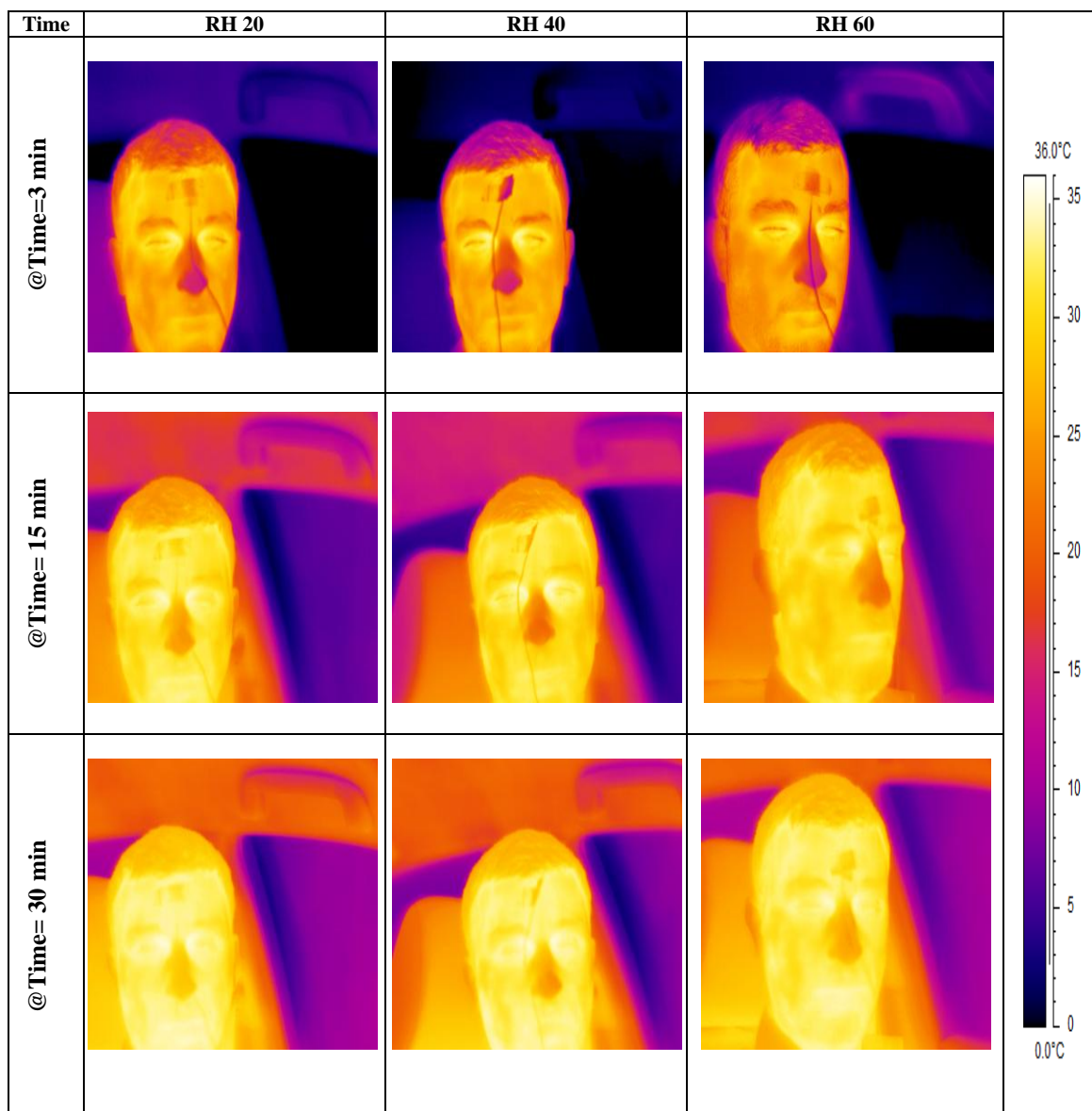
Figure 6.16: IR picture of the driver's face at cooling period for different relative humidity scenarios.
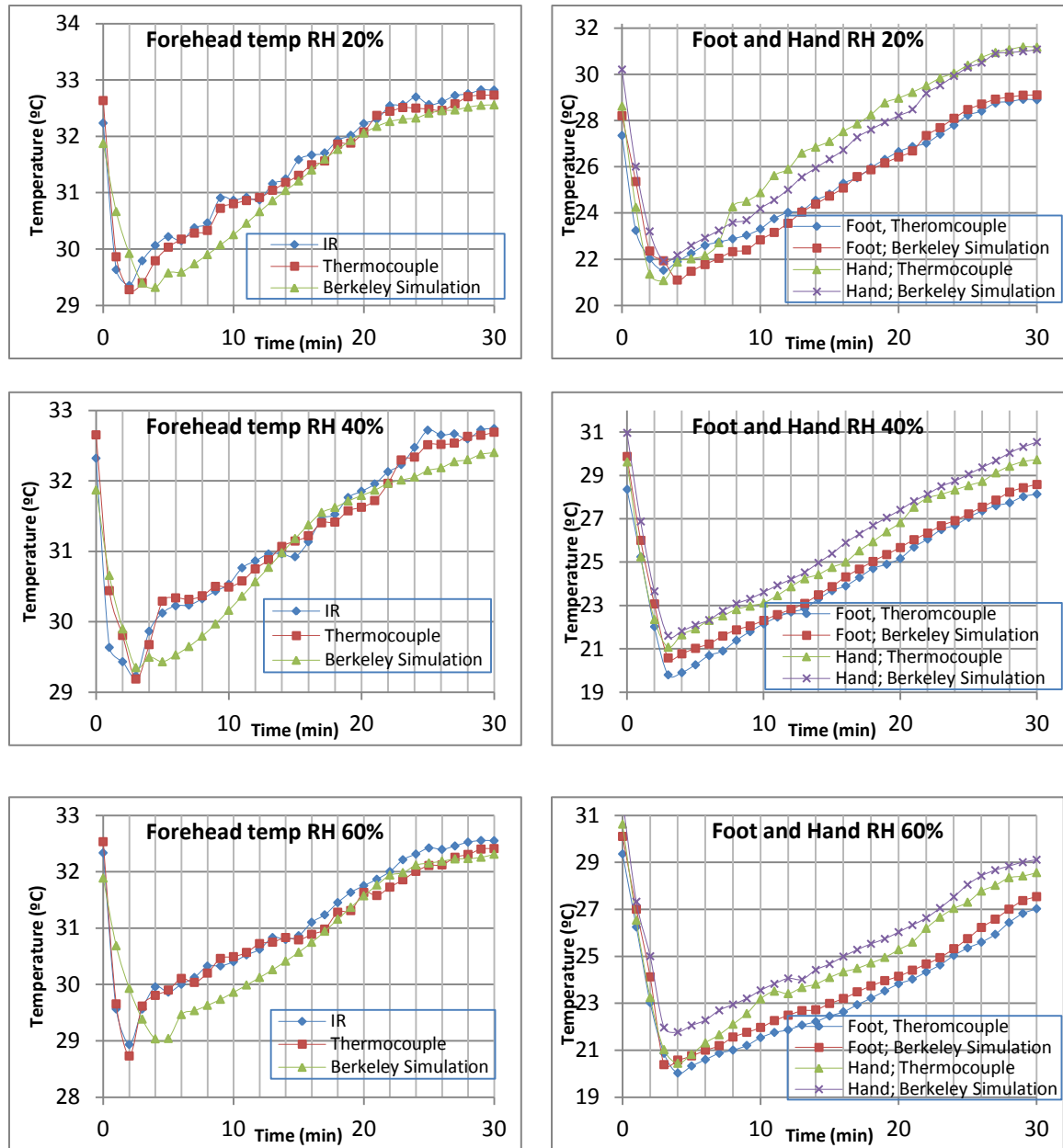
Figure 6.17: Temperature variation for different segment parts at different relative humidity scenarios during cooling period.

| RH 20% | RH 40% | RH 60% |

27.0 27.8 28.5 29.3 30.0 30.8 31.5 32.3 33.0
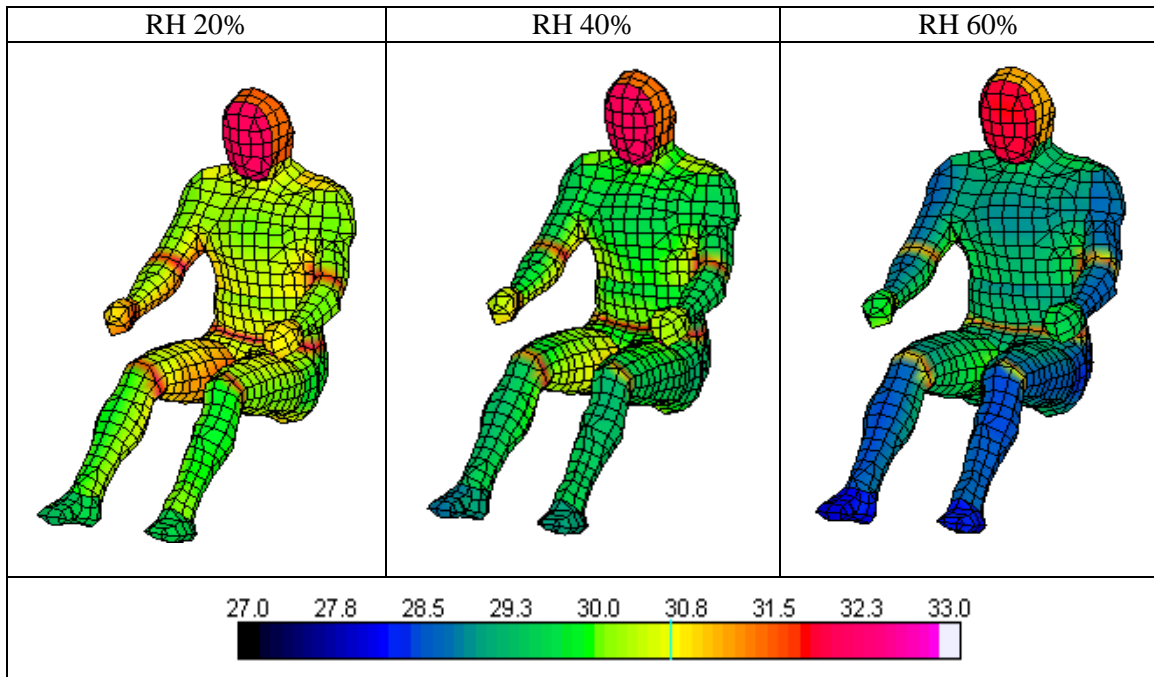
Figure 6.18: Schematic of body temperature variation inside passenger cabin at end of heating process in cooling period for different relative humidity.

6.4.4 Passenger Local, Overall Sensation and Comfort during Cooling Period

The overall sensation and comfort variations as computed using the Berkeley model for the different relative humidity scenarios, and during the cooling period are displayed in figure 6.19. In the early stages, the thermal sensation decreases rapidly for few minutes until it reaches minimum value. During this stage, the heat is transferred from the passenger body to the cabin environment through conduction, convection and radiation. On the other hand, the body has several thermal adjustment mechanisms to survive in cold environments; shivering will start, involuntarily forcing the muscles to work to increase the heat production [75].

After that the overall thermal sensation starts increasing due to the increase in the air temperature that surrounds the body; thusly the body becomes more neutral (i.e. more comfortable).

The local sensation and comfort vote of the different body segments are displayed in figure 6.20; which shows nearly the same behavior for the overall sensation and comfort values. The RH has no influential effect at beginning of the heating process. But as heating process progresses; the effect of an increasing RH value on the comfort level becomes more influential especially for the hands and the feet. As the RH decreases inside the passenger cabin, the feeling of more "comfort" increases.

Although local thermal discomfort can be caused from dryness, the thermal comfort of the whole body will not be affected by a localized dryness [75].

According to the Fanger model, the variation in the PMV and PPD indices versus time under the different relative humidity scenarios, in the cooling period, are depicted in figure 6.21. As shown in this figure, the RH has no effect on the PMV value at the beginning of the heating process. But as time passes, the RH effect becomes more pronounced on the predicted thermal sensation. So, as the RH value decreases, the heating system can achieve the human comfort zone ($PMV = \mp 0.5$) faster than the case if the RH value is not controlled. At the beginning of heating process, the percentage of people feeling uncomfortable is the same for all different RH. Then as the RH decreases the percentage of people feeling uncomfortable also decreases. At the end of the heating process, the RH does not have any main effect on the percentage of people feeling uncomfortable.
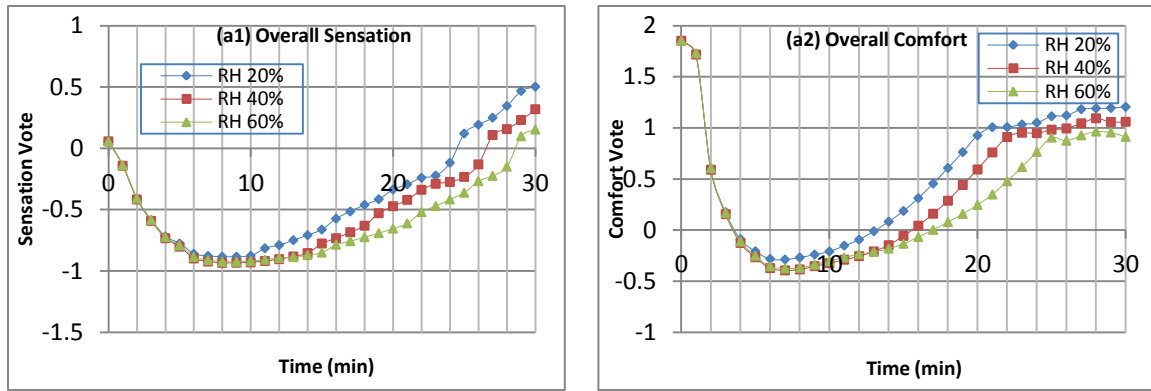
Figure 6.19: Overall sensation (OS) and overall comfort (OC) variation versus time at cooling period for different RH scenarios; (a1) OS (a2) OC.
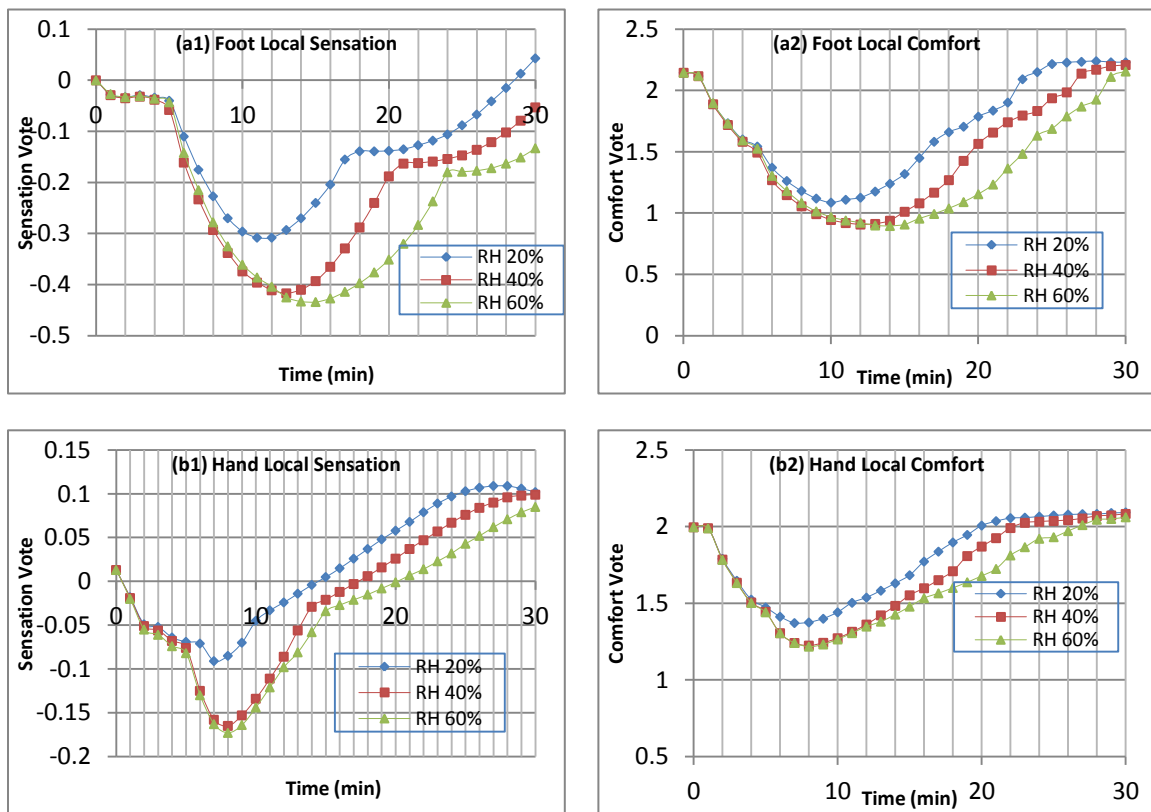
Figure 6.20: Local sensation (LS) and local comfort (LC) for different segment part at cooling period; (a1) foot LS (a2) foot LC (b1) hand LS (b2) hand LC.
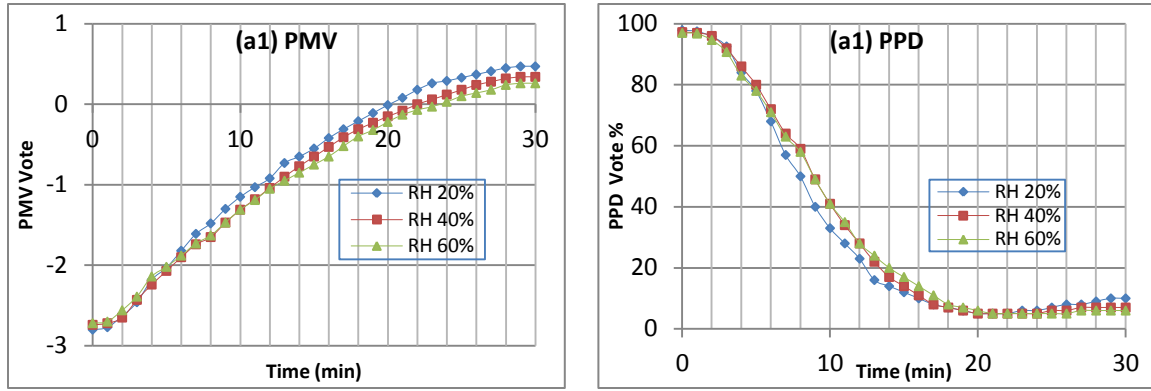
Figure 6.21: PMV and PPD versus time inside passenger cabin under relative humidity scenarios at cooling period (a1) PMV (a2) PPD.

6.5   Summary

This chapter evaluated the transient and non-uniform temperature variations inside passenger cabin and for driver's skin temperature variation for his/her different body segments mainly the forehead, the hands and the feet. These segments were monitored under different relative humidity scenarios using full-field thermography in addition to a discrete thermocouples network; additionally, a 3-D simulation model of the driver is developed. The measured and the predicted transient temperature-time profiles were compared and found to be in good agreement.

Two different models were used to investigate the effect of relative humidity inside the vehicle's cabin on the local and the overall sensation and comfort, during the heating and cooling periods. This study results can be usefully summarized into following points;

- At beginning of the cooling process; the higher the RH value, the more dominant the feeling of "hot" is. But at the end of the cooling process; the higher the RH value, the more comfortable the body feels.

- The local sensation and comfort vote as computed for the different body segments during the heating period have the same behavior as that of the overall sensation and comfort. The RH has more influential effect at beginning of the cooling process, when the RH increases, the feeling of hot and uncomfortable increases especially for the feet. But at the end of cooling process; the effect of an increasing RH value on the comfort level becomes less pronounced.

- At beginning of the heating process; the body feels uncomfortably cold, and during the heating process the body becomes more comfortable when the RH value is reduced.

- The local sensation and comfort votes of the different body segments during the cooling process have nearly the same behavior as that of the overall sensation and comfort. The RH has more influence at beginning of the cooling process, when the RH increases, the feeling of "uncomfortably hot" increases especially for the feet. But at the end of cooling process; the effect of an increasing RH value on the comfort level becomes less pronounced.

From the above discussion, controlling the RH value inside the cabin can benefit the A/C system by reducing its thermal load, i.e. amount of heat to be transferred in or out of the cabin. However, the RH control should be based on a transient scheme that is synchronized with the cabin temperature and outside forcing. Future work will investigate the RH control scheme and implement it into actual vehicle cabin.

CHAPTER SEVEN

PASSENGER THERMAL COMFORT ZONES

This chapter developed the passenger thermal comfort zones during summer and winter periods by using two different thermal models, Berkeley model in term of Overall thermal Sensation (OS) and Fanger model in term of predicted Mean Vote index (PMV). The boundary limits of the thermal comfort zone according to the Berkeley model was determined by the overall thermal sensation (OS is $\mp$ 0.5), while to Fanger model is by the Predicted mean vote index(PMV $\mp$ 0.5) . The virtual thermal Berkeley manikin was used in this study to predict the thermal comfort in different vehicle cabin environments. The Berkeley comfort manikin was placed inside a vehicle cabin with a homogeneous environment over a range of relative humidity of (20-60%). The manikin is simulated in standard form by wearing short sleeve with long trousers with approximate clothing insulation value of 0.5 clo for summer period, and wearing long thick sleeve, long thick trousers, hand-wear and footwear with approximate clothing insulation value of 1 clo for the winter period. The metabolic rate is set at 1.4 met which would be for a seated human metabolic rate. The air velocity around the thermal manikin was set at 0.4 m/s. The same conditions were applied to Fanger model except the range of a relative humidity (20-80%). The results show that the lower and upper temperature limits on the summer comfort window at standard conditions are 22.4 and 27.3°C respectively for Berkeley model and 23.1 and 27.4 °C respectively for Fanger model. While on the winter comfort window temperature limits are19.8 and 25.2°C respectively for Berkeley model and 18.6

and 24.6 °C respectively for Fanger model. Finally, the sensitivity analyses of increases/decreases of metabolism, air velocity and clothing insulation on the thermal comfort zones were investigated.

7.1   Introduction

Comfort zones describe the specific combinations of temperature and relative humidity (RH) ranges where statistical tests have shown 80% of the tested population to be comfortable [83]. These zones are different for winter and summer conditions. The human body are very sensitive to environmental condition that surrounding him. So, it is important to specify the comfort window that the human body feels comfortable. This is the main reason why automobiles have been fitted with both heating and air conditioning systems because in the absence of these systems it is inevitable that at some stage we are going to feel uncomfortable. The delineation of comfort windows will assist the designer to focus on achieving the most efficient and effective means toward a conditioned space that is within the human comfort zone.

The three primarily pillars that assist us to develop thermal comfort zones for passenger compartment: (i) determine the main sources of heating, cooling and relative humidity sources on in cabin; (ii) specify the main characteristics of the vehicular in-cabin environments that complicate the human thermal comfort determination and predictions; (iii) lastly, understanding of thermal comfort zone studies that concern on in door environment.

The first pillar, the passenger compartment of vehicles can become very uncomfortable since there are so many sources of heat radiating heat into it: (i) the outside temperature surrounding the vehicle, (ii) the sun (the main source of unwanted heat energy) in terms of green house effect, (iii) engine, transmission and exhaust system all radiate a large amount of heat energy that finds its way into the passenger compartment, (iv) also in summer time a hot road surface will radiate heat onto the body of a vehicle, which is conducted throughout the vehicle's body and is then radiated into the interior, (v) the vehicle occupants also add heat to the compartment due to thermoregulatory system, (vi) lastly, other heating sources include in-cabin electronics and infotainment systems. While the relative humidity recourses are based on the: (i) outside humidity, (ii) whatever heating or cooling is added by the HVAC system. Since the relative humidity depends on temperature, the relative humidity of cold air from the outside decreases as it is warmed up and refrigerated air conditioning often removes moisture from the air as it is cooled, so evaporative air conditioning adds moisture to the air, (iii) lastly, the vehicle occupants add considerable moisture to the room through exhaled air which is at 100% relative humidity.   All of these sources add to the uncomfortable feeling within the passenger compartment of a vehicle.

The next pillar to design thermal comfort zones for passenger compartment, the main characteristics of the vehicular in-cabin environments should be specifically determined, which are fast transient behavior that complicates predicting the optimum settings to achieve thermal comfort. Also the non-uniformities associated with the cabin thermal environment due to the air temperature distribution, the solar flux, and the

radiation heat flux from the cabin surrounding interior-trim surfaces, complicate the conditioning process. Furthermore, the multiple governing parameters of the cabin thermal comfort such as the solar incidence angle, the glass/glazing properties, the surrounding radiant heat and air velocity, affect the HVAC system performance [2, 3]. In addition, the psychological as well as physiological difference among the passengers is another challenge. Finally, the variation in passengers' thermal loads in terms of; thermal sensation, clothing, number of passenger, metabolism rate, hinders the system robustness. So, the vehicular climatic control systems suffer from previous distinct challenges.

Lastly, the most of thermal comfort zone studies concern on in door environment e.g. building. One of this study shows the higher RH necessitates cooler dry bulb temperatures to be in the comfort zone. It is more energy efficient for a facility to have a lower temperature with a more humid environment during the winter, and a dryer but higher dry bulb temperature during the summer [84, 85]. So, the temperature and humidity ranges defined as the comfort zone are rather wide. The winter comfort zone is between 20 ℃ with 90% RH and 24 ℃ with 25% RH. The summer conditions are between 23 ℃ with 90% RH to 27 ℃ with 25% RH. The American Society of Heating, Refrigerating and Air-Conditioning Engineers (ASHRAE) standard 55-2004 has an upper limit for humidity ratio of 0.012. This translates approximately to a relative humidity of 75% at a dry bulb temperature of 21°C and 53% at 27°C [86].The thermal comfort conditions - ASHRAE standard 55 (1992) during summer and winter comfort zone is depicted in figure 7.1 [6, 87]. Another approach for defining the comfort zone is done by the standard ISO 7730, it neglects the fact that higher temperatures can be borne at low

humidity. Therefore its upper and lower temperature limits are vertical. This approach can be used in less demanding applications for simpler implementation of air-conditioning algorithms. While simple temperature ranges are given per season the relative humidity is set between 30%RH and 70%RH in winter and summer time, respectively as displayed in figure 7.2. The limits are set to decrease the risk of unpleasantly wet or dry skin, eye irritation, static electricity, microbial growth and respiratory diseases [45, 87].

Tsutsumi et al. [88] tested the effect of low humidity on comfort and other results in participants under stable circumstance in summer. Yamtraipat et al. [89, 90] conducted a study of thermal comfort standards in air-conditioned buildings in Thailand and found that thermal comfort standards are that temperature is 26 ∘C, that relative humidity is 60% and that air velocity is 0.2 m/s. The influence of high humidity levels on human comfort; specifically the response of sedentary human to high humidity exposure (RH between 60% - 90%) at a temperature range of $20 - 26$ ^{o}C had been investigated by Fountain et al. in [28]. The study findings indicated the RH effect but did not quantify it independently. Ibamoto et al. [91] reported that low humidity was possible for thermal comfort in both transient and steady state. T. Lin et al. [92] shows the neutral temperatures for short- and long-haul vehicles are 26.2°C and 27.4°C, while the comfort zones are 22.4–28.9°C and 22.4–30.1°C, respectively. Silva et al. [93] performed a survey on a total of 28 pre-arranged subjects on a bus and examined, through artificial neural analysis, how these subjects' thermal sensations were affected by the physical

environment. Surveying the published literature shows limited number of studies that discussed the idea of discusses the thermal comfort zone inside passenger cabin.

In this chapter, the idea of design the passenger thermal comfort zones during summer and winter periods is introduced. The study starts by discussing the human thermal comfort in section 7.2; the sub-sections introduce the Fanger and Berkeley models. While section 7.3 discusses the research methodology, and section 7.4 specify the design consideration in terms of dry bulb temperature and relative humidity. In section 7.5, the results of summer and winter passenger thermal comfort zone in standard conditions with sensitivity analysis were presented followed by discussion. Finally, section 7.6 summarizes the entire paper and shows and shows the conclusion.
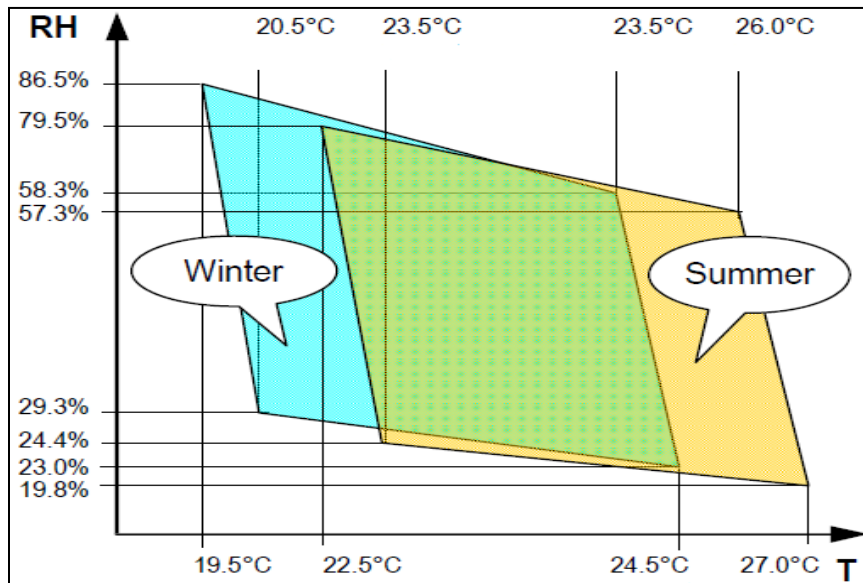
Figure 7.1: Relative humidity (RH) / temperature (T) diagram based on comfort zone according to ASHRAE 55-1992 [6, 87].
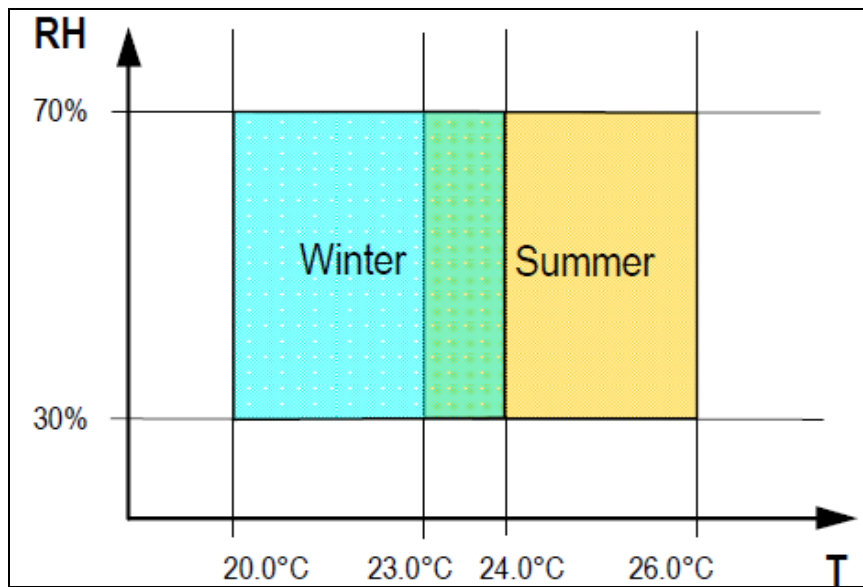
Figure 7.2: RH/T diagram showing the comfort zone according to ISO7730 [45, 87].

7.2 Human Thermal Comfort Models

Many researchers have been tried to predict the thermal sensation of people in their environment based on numbers of factors such as the personal, environmental and physiological variables that influence thermal comfort. From the research done, some mathematical models that simulate occupants' thermal response to their environment have been developed. The most notable models have been developed by P.O. Fanger (it is called Fanger Comfort Model), and Berkeley thermal comfort model. The main similarity of the two models is that two model apply an energy balance to a person and use the energy exchange mechanisms along with experimentally derived physiological parameters to predict the thermal sensation and the physiological response of a person due to their environment. The models differ somewhat in the physiological models that represent the human passive system (heat transfer through and from the body) and the

167

human control system (the neural control of shivering, sweating and skin blood flow). The models also differ in the criteria used to predict thermal sensation.

7.2.1   Fanger Model

Fanger (1970) defined thermal comfort as "The condition of mind which expresses satisfaction with the thermal environment" [48]. Fanger's model in term of Predicted Mean Value (PMV) index is based on thermoregulation and heat balance theories can be predicted the thermal comfort. The PMV model combines four physical variables (air temperature, air velocity, mean radiant temperature, and relative humidity) and two personal variables (clothing insulation and activity level). Figure 7.3 depicted the Physical parameters and heat transfer modes that effect on passenger compartment [94].

The PMV is based on the subjective seven-step scale [50, 52]. The value of the PMV index has a range from -3 to +3, corresponding to human sensations from cold to hot, respectively, where the null value of the PMV index means neutral.
Fanger model has limitations related to: (i) thermal steady state heat transfer between the human body and thermal comfort ratings from panel subject, (ii) non distinction between local and whole-body thermal comfort thermal, (iii) the PMV has been proposed and established for homogenous conditions only [32].
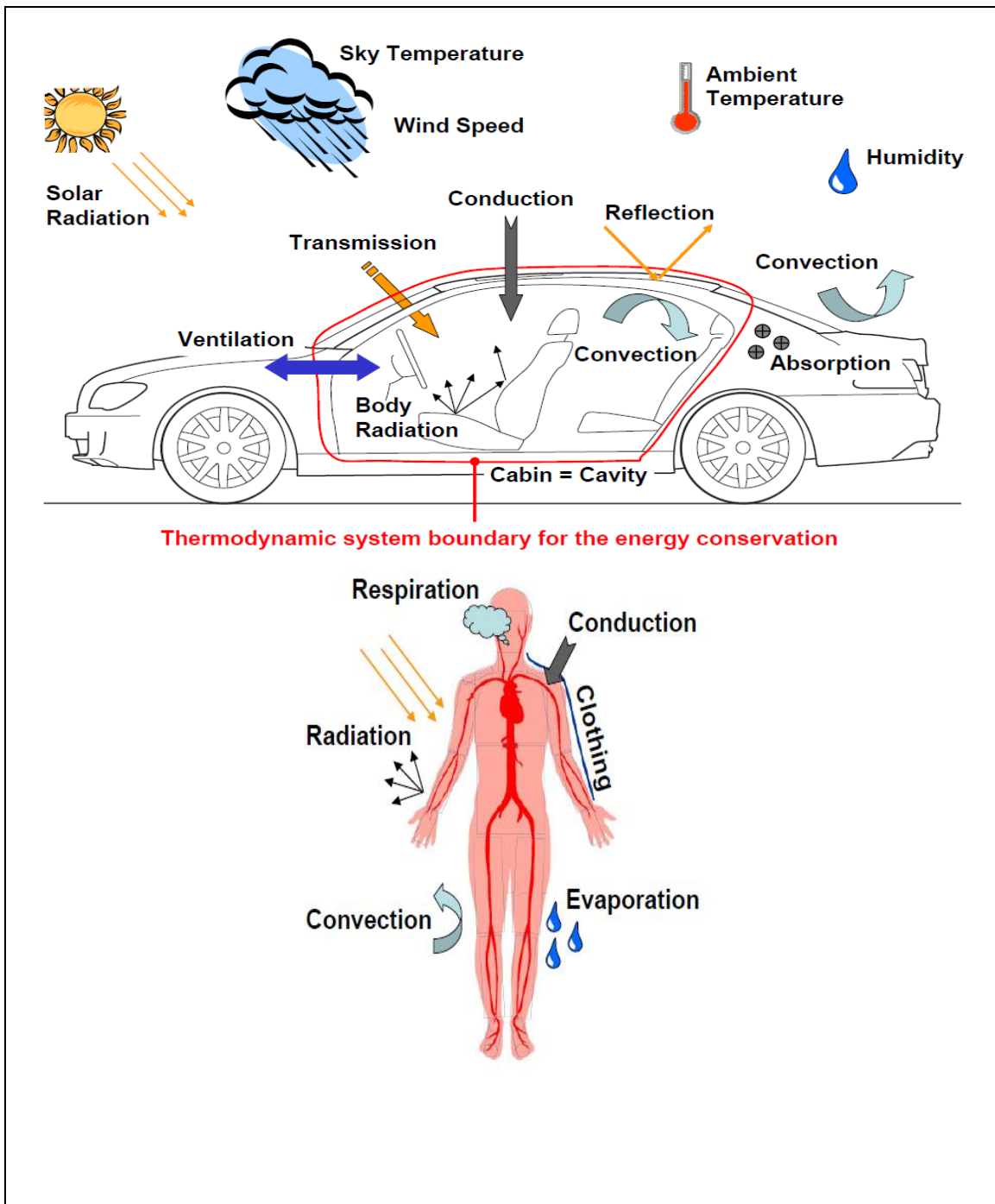
Figure 7.3: Physical parameters and heat transfer modes that effect on passenger compartment.

7.2.2   Berkeley Model

It is one of the most sophisticated thermal comfort models in existence. It is capable of analyzing human thermoregulation and comfort responses in non-uniform and transient conditions. The model has been under development at UC Berkeley since the early 90s.

The Berkeley Comfort Model [56-61] is based on the Stolwijk model of human thermal regulation but includes several significant improvements as (i) Increase in number of body segments; (ii) Introduce of a clothing node to model; (iii) introduce the conduction mode to surfaces that contact with the body; (iv) Improved convection and radiation heat transfer coefficients; (v) lastly, Introduce radiation heat flux model [95]. Each segment of Berkeley model is modeled as four body layers (core, muscle, fat, and skin tissues) and a clothing layer are depicted in figure 7.4 [94, 95]. Physiological mechanisms such as vasodilation, vasoconstriction, sweating, and metabolic heat production are explicitly considered. Convection, conduction (such as to a car seat or other surface in contact with any part of the body) and radiation between the body and the environment are treated independently. The model is capable of predicting human physiological response to transient, non-uniform thermal environments. The model has been implemented in an object-oriented C++ computer code. It simulates an arbitrary number of sequential sets of environmental and physiological factors called phases. Each phase consists of environmental and physical information such as duration of exposure, metabolic rate, clothing, physiological constants and the external environmental factors; all of which affect human comfort [95].

The Berkeley model uses temperature data from the physiological model to predict the local and global thermal comfort as a function of local skin and core temperatures and their rates of change. In addition, the physiological response uses to predict the local sensation and the local comfort of each body segment. The body thermal sensation in a given environment depends on the skin temperature (cold through hot). However, the thermal comfort depends on the desired physiological state (uncomfortable through comfortable). The sensation and comfort are interrelated but their interaction is of a complex nature, which includes the environment and the dynamic physiological conditions.
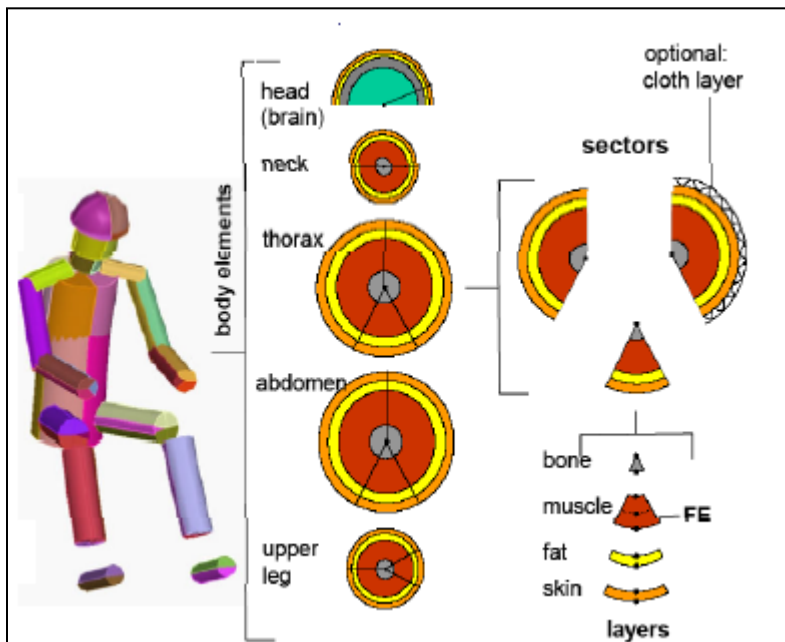
Figure 7.4: Human Berkeley layers [94].

7.3   Research Methodology

Two thermal models were used to create the thermal comfort windows, Berkeley model and Fanger model based on PMV index. According to Berkeley model the virtual thermal Berkeley manikin is composed of individual body parts that allow the user to define separate layers of clothing and other local effects. The environmental models support full weather inputs, solar models, transparent glass with greenhouse effects, and all other significant thermal variables, while the Fanger model (PMV index) required defining physical and personal parameters. The thermal sensation and comfort votes are calculated using the Berkeley comfort model and the Fanger model too. The sensation and comfort are then reported on the nine-point scale for the Berkeley model and the seven-point thermal sensation scale for the Fanger model based on PMV index. On both scale, the higher positive sensation value indicates hotter feeling. On the other hand, the higher negative sensation value indicates cooler feeling, while a zero sensation indicates a neural thermal sensation. The higher comfort value indicates a better or a more comfortable feeling. The Berkeley comfort manikin is placed inside a vehicle cabin with a homogeneous environment over a range of relative humidity of (20-60%) as shown in figure 5.1. The manikin is simulated in standard form by wearing short sleeve with long trousers with approximate clothing insulation value of 0.5 clo or 0.078 $\frac{m^2 K}{W}$ for summer period, and wearing long thick sleeve, long thick trousers, hand-wear and footwear with approximate clothing insulation value of 1 clo (0.155 $\frac{m^2 K}{W}$) for the winter period. The metabolic rate is set at 1.4 met (81 $\frac{W}{m^2}$) [14,69] which would be for a seated human

172

metabolic rate. The measured discharge temperatures at the A/C outlets are specified as the boundary conditions for the finite differencing processor, which relies on using a RadTherm solver package. The major five steps that the Berkeley thermal-manikin modeling employ are [63]; (i) firstly importing a human geometry into a finite differencing platform that includes the Berkeley sub-routine. Secondly, (ii) meshing the human geometry to discreatize it depending on the resolution needed. (iii) Setting the biological material properties and the thickness values to each individual part. (iv) Setting the environmental boundary conditions; including the environmental variables, the clothing properties, the surface conditions, and the convection settings. (v) Finally, solving the heat transfer balance equations using a finite differencing approach. While the PMV is derived from the physics of heat transfer combined with an empirical fit to human comfort; as described in equation (1).

$$PMV = [0.303 \exp\{-0.036\,M + 0.028\} \times E_{st}] \qquad (1)$$

Where; M: metabolic rate of body that provides energy, E_{st} is the rate of increase of the energy stored within the human body.

Lastly, the creation of thermal comfort windows depends on this condition, according to Berkeley model the overall thermal sensation (OS) inside the comfort zone or window (OS= $\mp$ 0.5) and according to Fanger model, the thermal comfort zone comfort zone ($PMV = \mp 0.5$).

173

7.4   Design Considerations

The comfort zones are usually expressed graphically as an overlay on the psychometric chart or other diagrams which shows the relation between temperature and relative humidity.

The air temperature defined as the temperature of the air surrounding the occupant that determines the net heat flow between the human body and its environment. This factor is considered important because of its narrow range within the comfort zone. An increase in temperature above the comfort level may prevent the body to dissipate heat to the surrounding air. This will lead to increase in body temperature, increased heart action, reduction of human performance, tired and sleepy. So it is need to increase the compartment ventilation, induct cool air and exhaust hot air. On a contrast, a decrease in temperature may the body loses too much heat to surrounding air. This will lead to make body shivering, reduced powers to concentration and restless. So, it is need to warm the air by using heating units [96].

Another important factor is humidity. The most body heat loss usually occurs through evaporation process. If the air has a high RH, the potential for evaporation to take place is greatly reduced because the air cannot easily absorb more moisture. And the growth and spread of unhealthy biological pollutants and to the damaging effect of moisture on the construction materials. While, the symptoms of at low relative humidity in passenger compartment are headache, irritated eyes, sore throat, and dry skin. Also, dry air lowers the natural defense against airborne infections and makes people vulnerable to the attack of viruses and other micro-organisms [96].

Typically humans are less sensitive to humidity than temperature. People generally fail to associate discomfort and potential health problems with variations in relative humidity. So, it needs to control a relative humidity to keep it within comfort limits.

Also, another advantage of controlling temperature and RH within comfort limits is the energy can be saved when indoor spaces are monitored for both humidity and temperature, because e.g. when humidity is low, a higher temperature is acceptable and cooling is not necessary. In a system which only is controlled by temperature, unnecessary heating or cooling may be done even if conditions still are within the comfort zone.

7.5   Results and Discussion

7.5.1   Fanger and Berkeley Models Simulation

Figures 7.5 and 7.6 display the changing of dry bulb temperature and relative humidity effects on the PMV index during summer and winter period respectively, with the relative humidity being the vertical axis, and dry bulb temperature the horizontal axis, and the diagonal lines represent the PMV index different values. According to the PMV index scale; humans will be thermally comfortable, if the PMV index ranges from -0.5 to 0.5. At summer period, figure 7.5, occupants will be more comfortable at higher temperatures with a lower humidity. As the temperature drops, higher humidity levels are required to attain the PMV comfort range. At winter period, figure 7.6, occupants will be

more comfortable at low temperatures with a high relative humidity. As the temperature increases, lower humidity levels are required to attain the PMV comfort range.

The Prediction of Overall Sensation (OS) during summer and winter periods according to Berkeley model at 20% RH are depicted in figures 7.7 and 7.8 respectively and at 60% RH are displayed in figures 7.9 and 7.10 respectively. The schematic of temperature variation at enter and leave of the thermal comfort zone for summer and winter periods under different relative humidity scenarios being shown in figures 7.11 and 7.12 respectively. According to the Berkeley OS index scale; humans will be thermally comfortable, if the OS index ranges from -0.5 to 0.5. The data generation in figures 6-11 will be used to develop thermal comfort zone. In [81] we presented a comprehensive study the effect of manipulating the Relative Humidity (RH) along with the Dry Bulb Temperature (DBT) on vehicular cabins' environment in terms of the overall thermal comfort and human occupants' thermal sensation by using Berkeley and Fanger model. Alahmer at el. showed that the temperature variation on in cabin passes through three stages specifically; (i) In the early stages, the thermal sensation increases rapidly through few minutes until reach a maxima to express the human body fells very hot and the human comfort decreases rapidly to express uncomfortable due to the high surrounding temperature. During this stage, the heat is transferred from the cabin environment to the passenger body through conduction, convection and radiation. After that the overall thermal sensation starts decreases due to air condition begins to reduce the in cabin temperature. So, as time passes, the temperature of air surrounding the body decreases and the body becomes more neutral (i.e. more comfortable). On winter period,

in the early stages, the thermal sensation decreases rapidly through few minutes until reaches minima to express the human body fells very cold and the human comfort decreases rapidly to express uncomfortable due to the lower surrounding temperature. After that the overall thermal sensation starts increases due to the air temperature surrounding the body increases and the body becomes more neutral (i.e. more comfortable), then neutrality or thermal comfort is achieved. Also, in this paper, the temperature variation, the cabin local sensation (LS) and comfort (LC) were analyzed for different body segments mainly; the head, chest, back, hands and feet with the addition of the overall sensation (OS) and the overall comfort (OC).
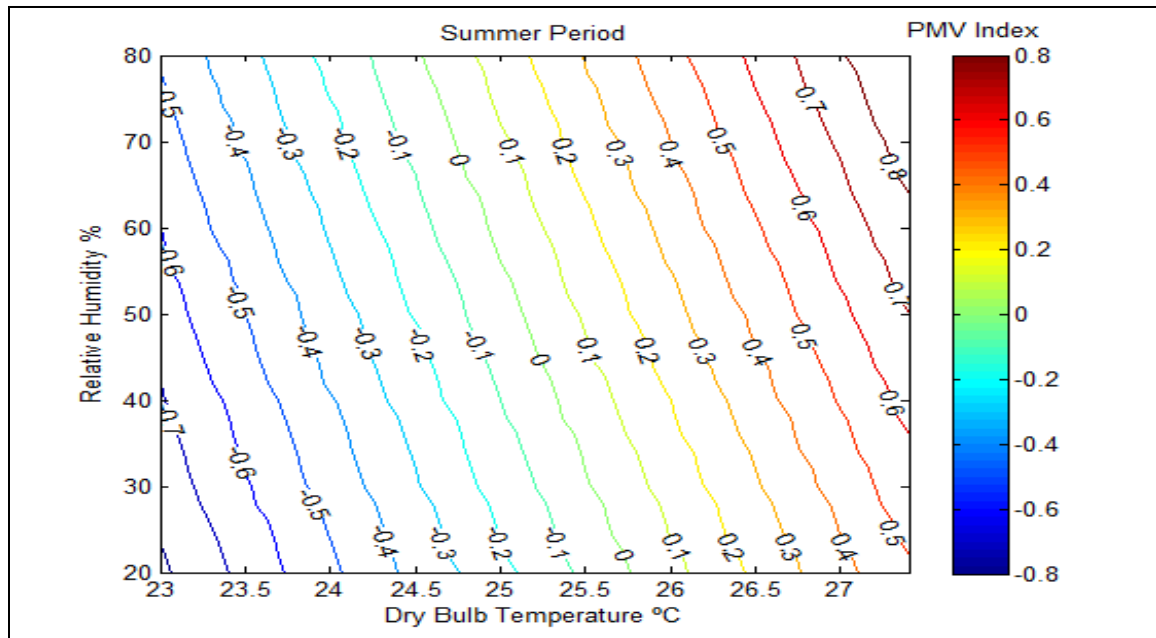
Figure 7.5: Effect of changing RH and dry bulb temperature on PMV index during summer period (air velocity 0.4 m/s, metabolic rate 1.4 met and insulation level 0.5 clo).
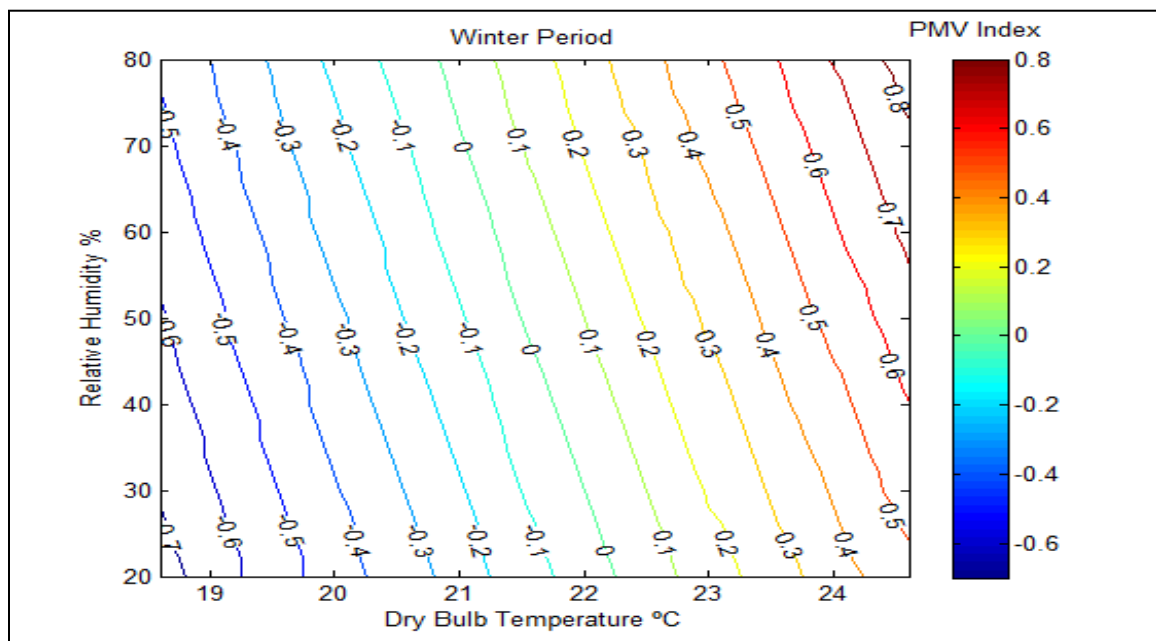
Figure 7.6: Effect of changing RH and dry bulb temperature on PMV index during winter period (air velocity 0.4 m/s, metabolic rate 1.4 met and insulation level 1 clo).
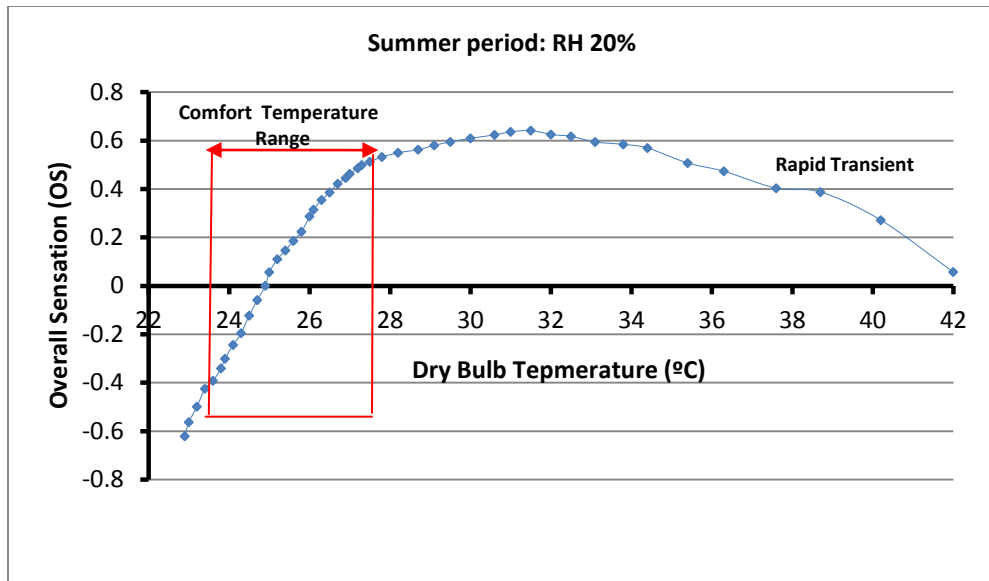
Figure 7.7: Prediction of Overall Sensation (OS) during summer period according to Berkeley model at 20% RH.
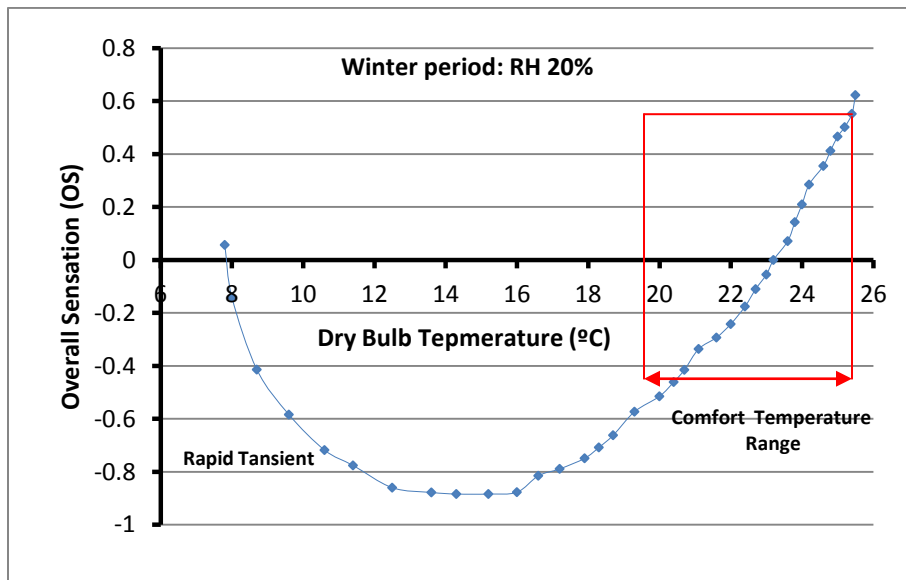
Figure 7.8: Prediction of Overall Sensation (OS) during winter period according to Berkeley model at 20% RH.
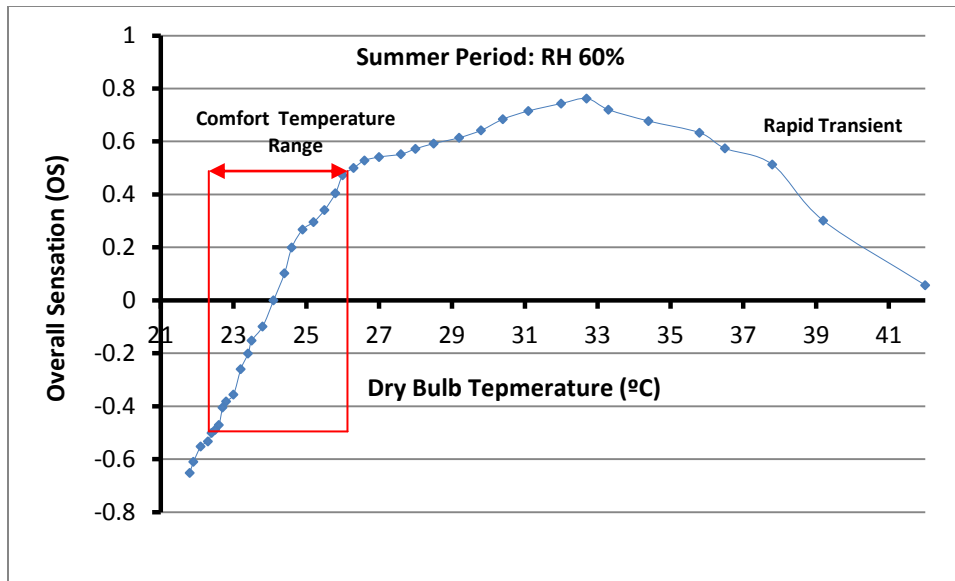
Figure 7.9: Prediction of Overall Sensation (OS) during summer period according to Berkeley model at 60% RH.
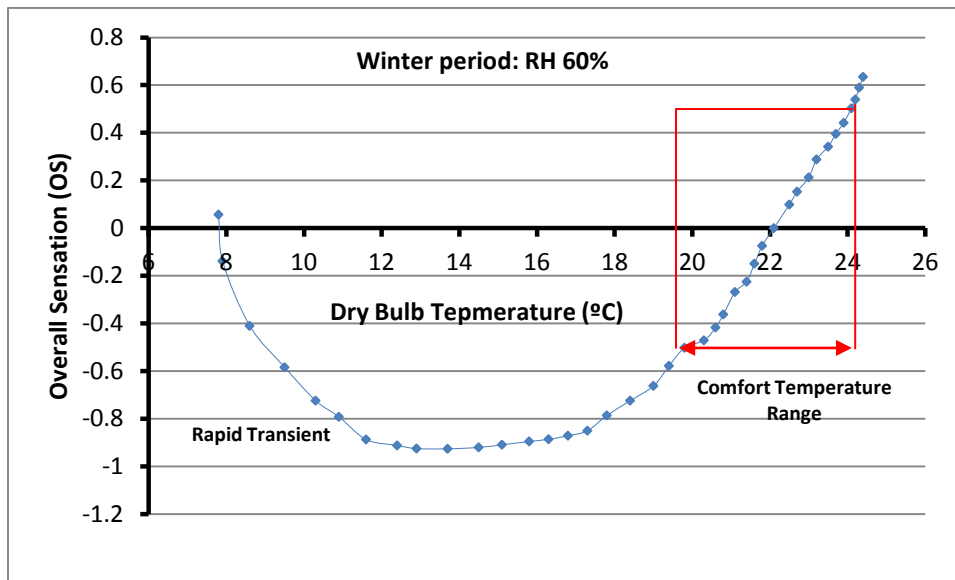
Figure 7.10: Prediction of Overall Sensation (OS) during winter period according to Berkeley model at 60% RH.

Summer Period			
RH Value %	**Enter**	**Leave**	**Temperature Scale**
20			
60			
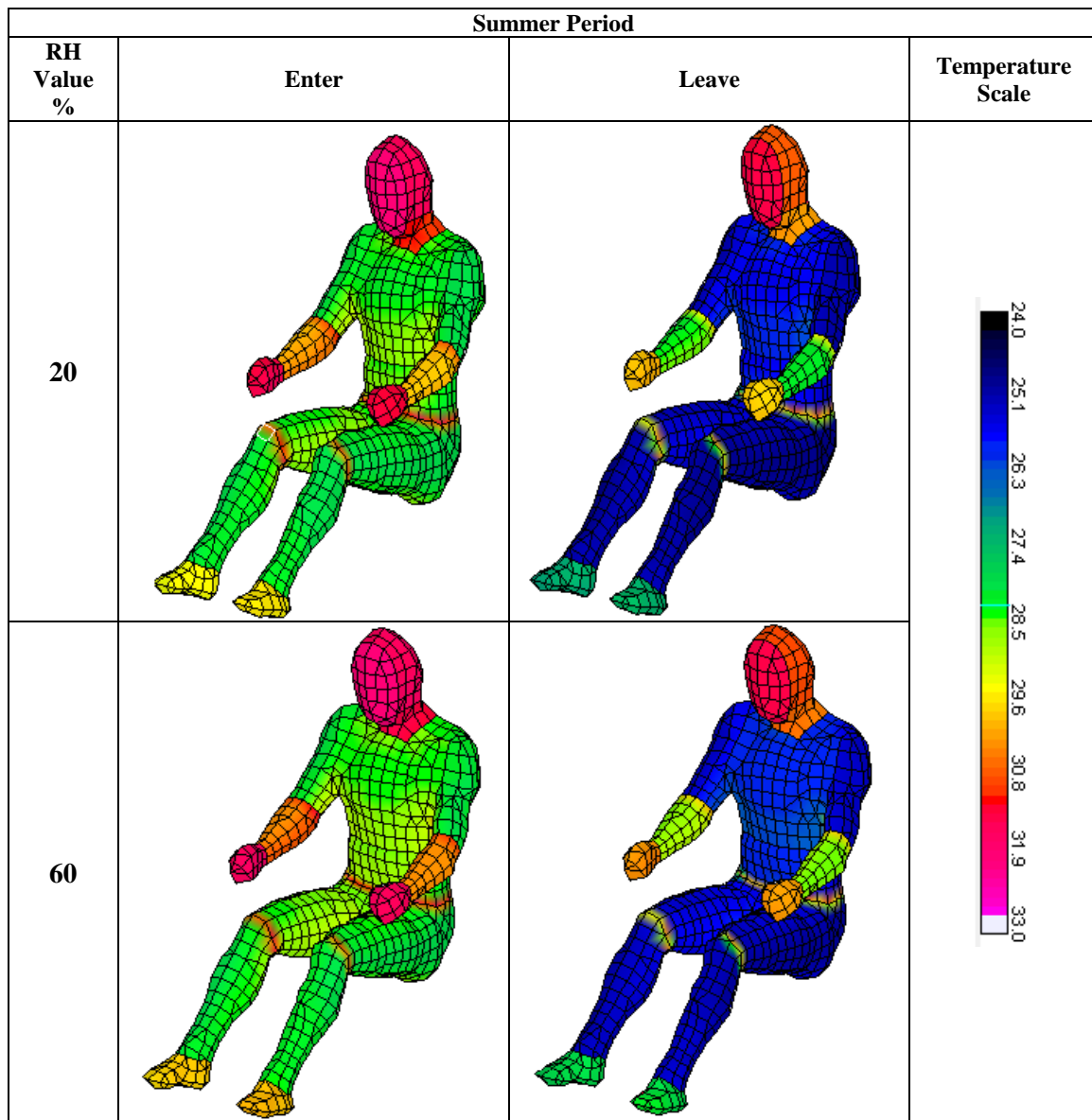
Figure 7.11: Schematic of body temperature variation on in cabin at enter and leave summer thermal comfort zone for different relative humidity scenarios.

Winter Period			
RH Value %	Enter	Leave	Scale temperature
20			
60			
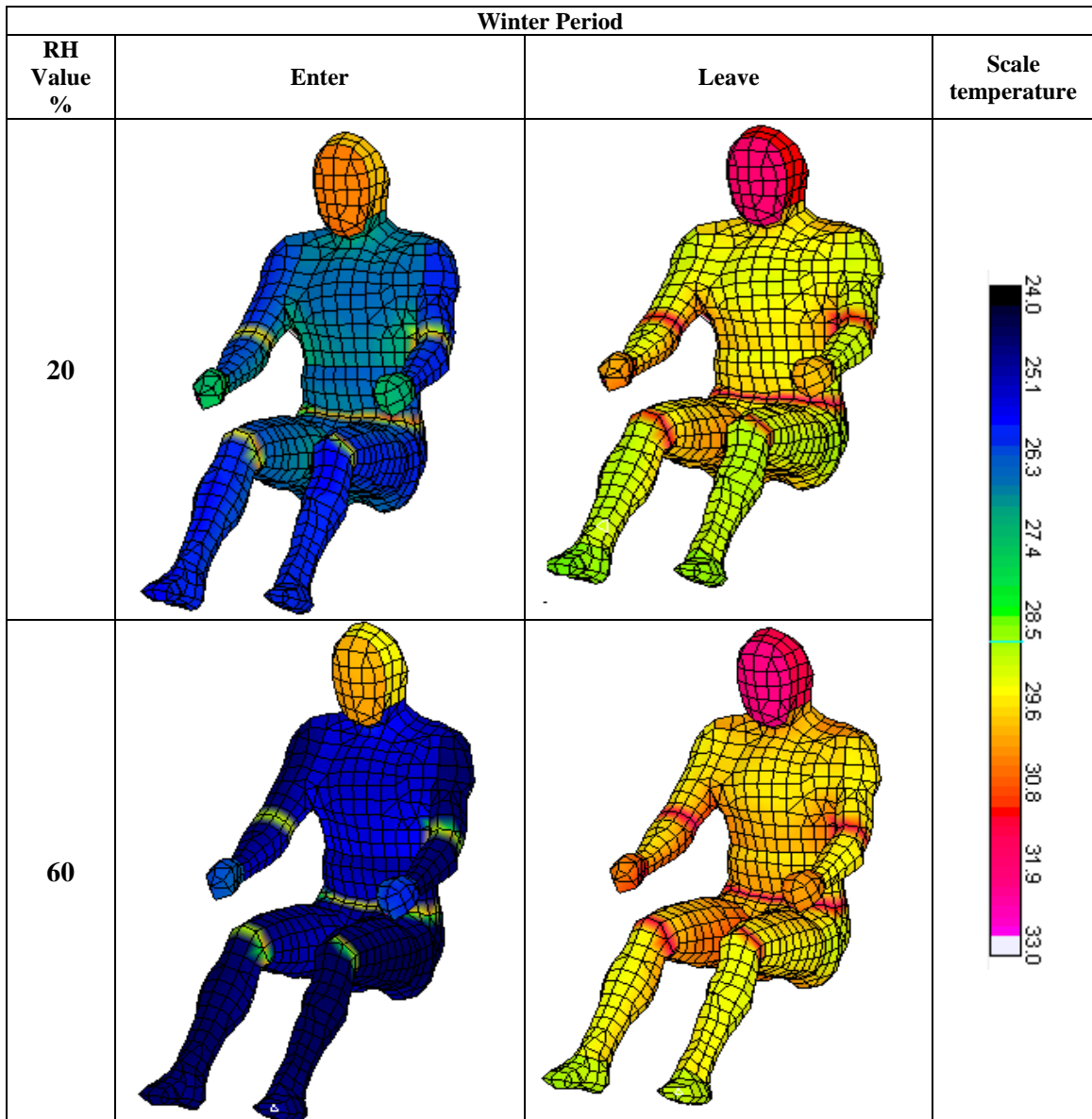
Figure 7.12: Schematic of body temperature variation on in cabin at enter and leave winter thermal comfort zone for different relative humidity scenarios.

7.5.2 Summer and Winter Passenger Thermal Comfort Zone-Standard Envelope

The comfort chart is useful for determining design conditions to be met by a passenger compartment envelope and its heating, ventilation, and air conditioning

(HVAC) equipment. The two models were used to design summer and winter passenger thermal comfort zone according to Fanger and Berkeley models as shown in figures 7.13 and 7.14 respectively.

Two comfort windows or zones are defined by the enclosed regions on the comfort chart—one for winter and one for summer. Their difference is primarily attributable to differences in normal clothing levels between winter and summer. The thermal conditions within these envelopes are estimated to be acceptable to 80 percent (Fanger model: $PMV = \mp 0.5$ or Berkely mode: $OS = \mp 0.5$) of the occupants when wearing the clothing ensemble indicated. To satisfy 90 percent of the people, the limits of the acceptable comfort zone are sharply reduced to one-third of the above ranges [34]. The lower and upper temperature limits on the summer comfort window 23.1 and 27.4 °C respectively for Fanger model, and 22.4 and 27.3°C respectively for Berkeley model. While on the winter comfort window temperature limits are18.6 and 24.6 °C respectively for Fanger model, and 19.8 and 25.2°C respectively for Berkeley model.

The upper and lower humidity limits on the comfort window of figure are based on achieved maximum comfort with take considerations of respiratory health, mold growth, and other moisture-related phenomena in addition to comfort. Humidification in winter must be limited at times to prevent condensation on cold windows. The zones overlap in the 23.6 to 24.6 °C range for Fanger model and 23.2 to 25.2 °C. In this region, people in summer dress tend to be slightly cool, while those in winter clothing feel a slightly warm sensation.

The limitation of proposed passenger comfort window is designed for overall comfort not for specific parts, in more explanation although a person may feel thermally neutral in general -preferring neither a warmer nor a cooler environment - thermal discomfort may exist if one part of the body is warm and another is cold.
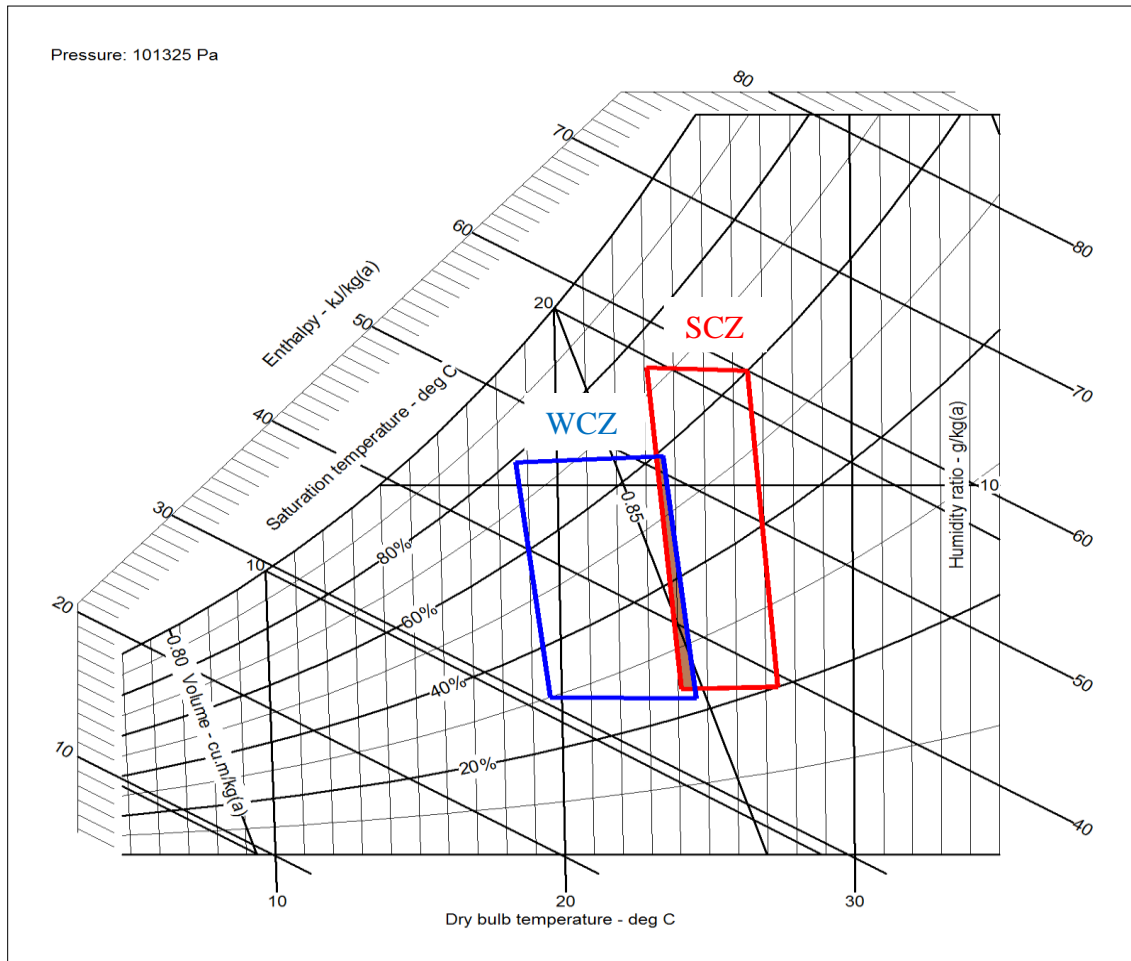
Figure 7.13: Summer and winter passenger thermal comfort zones (SCZ-WCZ) according to Fanger model.
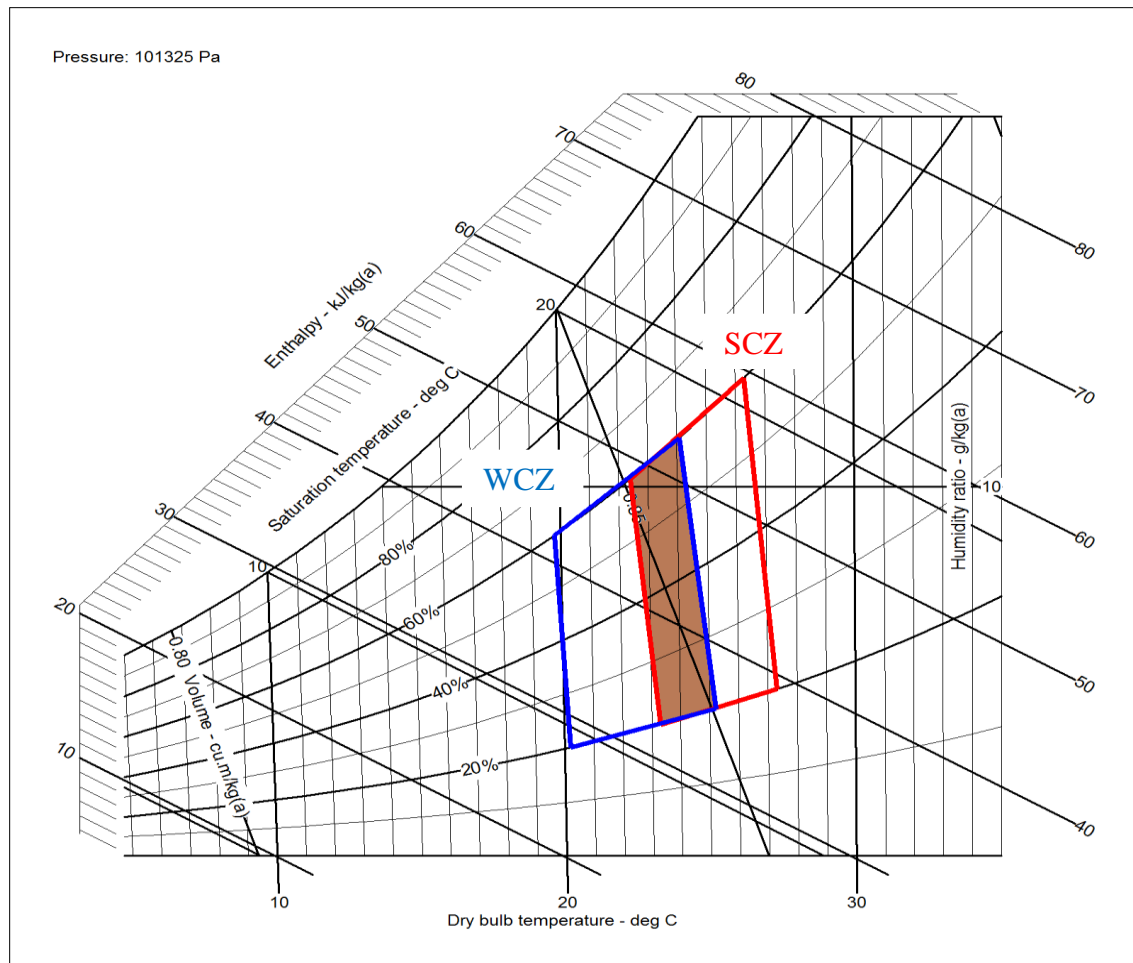
Figure 7.14: Summer and winter passenger thermal comfort zones (SCZ-WCZ) according to Berkeley model.

7.5.3 Passenger Thermal Comfort Zones Sensitivity Analysis

The importance of studying the sensitivity of environmental conditions on passenger comfort zone that when one of environmental conditions (dry-bulb temperature, humidity, Mean radiant temperature MRT, air movement, Metabolic rate and clothing) is out of the comfort range, adjusting one or more of the other conditions will restore comfort with the addition of little or no additional energy.

7.5.3.1 Metabolism and Activity Sensitivity Analysis

The Metabolism and activity sensitivity analysis of summer passenger thermal comfort zone according to Fanger and Berkeley models are depicted in figures 7.15 and 7.16 respectively. While it's the effect in winter period according to Fanger and Berkeley models are displayed in figures 7.17 and 7.18 respectively. The metabolic rate expresses the rate of transformation of chemical energy into heat and mechanical work by metabolic activities within an organism, usually expressed in terms of unit area of the total body surface. In this standard, this rate is expressed in met units [86]. Hence, the metabolic rate depends on the activity level and the fitness level.

When air temperature is low, convective heat loss increases with air motion associated with increased activity, thereby decreasing the heat load on the body evaporative system and resulting in a wider range of activity before discomfort is felt. The maximum range of activity in which people feel comfortable is therefore achieved by minimizing dry-bulb temperature and RH while compensating with an MRT sufficient to maintain comfort. In figures 7.15 to 7.18, as increases the metabolic rate, the thermal comfort zone will shift to the left, which leads the limits of the higher and lower temperature values will decrease. So, the new lower and upper temperature limits on the summer comfort window 21 and 26 °C respectively for Fanger model, and 20.8 and 25.6 °C respectively for Berkeley model. While on the winter comfort window temperature limits are15.9 and 22.7 °C respectively for Fanger model, and 18 and 24 °C respectively for Berkeley model.

So, with higher metabolic rates and/or with more clothing insulation, people are less thermally sensitive and consequently the risk of local discomfort is lower [86]. So, the greater the activity and the more clothing worn, the lower the effective temperature must be for comfort.

When the metabolic rate decreases, the thermal comfort zone will shift to the right, which leads the limits of the higher and lower temperature will increase values. So, the new lower and upper temperature limits on the summer comfort window 25.5 and 28.8 °C respectively for Fanger model, and 25.3 and 29.2 °C respectively for Berkeley model. While on the winter comfort window temperature limits are 21.4 and 26.5 °C respectively for Fanger model, and 21 and 26.5 °C respectively for Berkeley model. So, the people are more sensitive to local discomfort when the whole body is cooler than neutral and less sensitive to local discomfort when the whole body is warmer than neutral [86].

As metabolic rates increase above limit values, the evaporation of sweat becomes a more and more important factor for thermal comfort. The Fanger models in term of PMV method does not fully account for this factor.
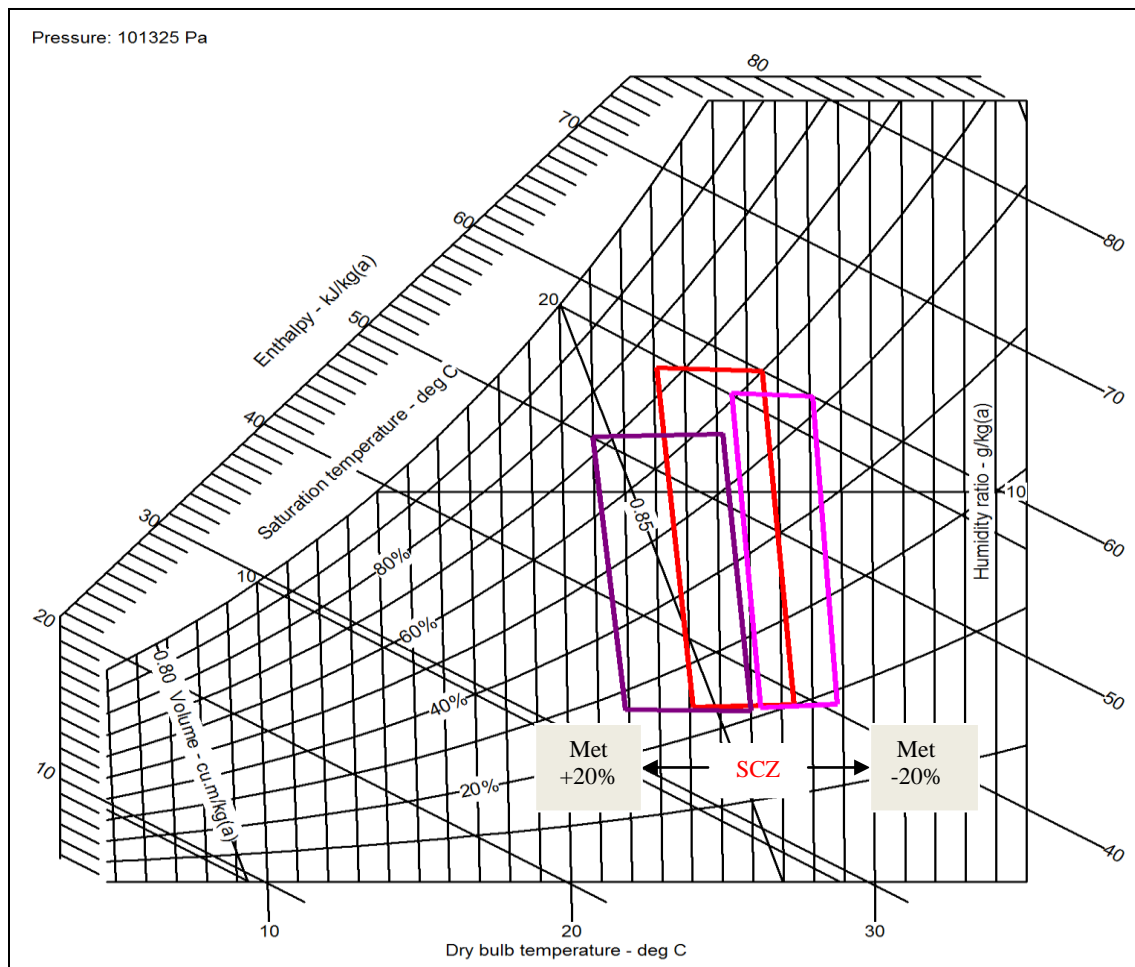
Figure 7.15: Metabolism sensitivity analysis of summer passenger thermal comfort zone according to Fanger model.

Figure 7.16: Metabolism sensitivity analysis of summer passenger thermal comfort zone according to Berkeley model.

Figure 7.17: Metabolism sensitivity analysis of winter passenger thermal comfort zone according to Fanger model.

Figure 7.18: Metabolism sensitivity analysis of winter passenger thermal comfort zone according to Berkeley model.

7.5.3.2 Air Velocity Sensitivity Analysis

The air velocity sensitivity analysis of summer passenger thermal comfort zone according to Fanger and Berkeley models are depicted in figures 7.19 and 7.20 respectively. While it's the effect in winter period according to Fanger and Berkeley models are displayed in figures 7.21 and 7.22 respectively. The air motion across the skin accomplished cooling through both convective energy transfer and latent energy transfer

(evaporative of perspiration from skin). Since skin temperature is relatively high, the air can carry some of excess heat. So, the comfort temperature is dependent on air velocity, particularly if light clothing is worn. Control of air movement with fans is an important opportunity to give individuals control over their climatic environment. Using air movement to control comfort is a delicate balance since too high an air velocity (or too large a temperature).

In figures 7.19 to 7.22, as increases the air velocity, the thermal comfort zone will shift to the right, which leads the limits of the higher and lower temperature values will a small increase. So, the new lower and upper temperature limits on the summer comfort window 23.4 and 27.6 °C respectively for Fanger model, and 22.7 and 27.6 °C respectively for Berkeley model. While on the winter comfort window temperature limits are 18.9 and 24.9 °C respectively for Fanger model, and 20.3 and 25.6 °C respectively for Berkeley model. On the contrast, when the air velocity decreases, the thermal comfort zone will shift to the left, which leads the limits of the higher and lower temperature values will small decrease. So, the new lower and upper temperature limits on the summer comfort window 22.8 and 27.2 °C respectively for Fanger model, and 22.1 and 27.1 °C respectively for Berkeley model. While on the winter comfort window temperature limits are 18.3 and 24.4 °C respectively for Fanger model, and 19.5 and 24.8 °C respectively for Berkeley model.

The studies show that occupant discomfort increased with increasing air velocity, and decreasing temperature [48].
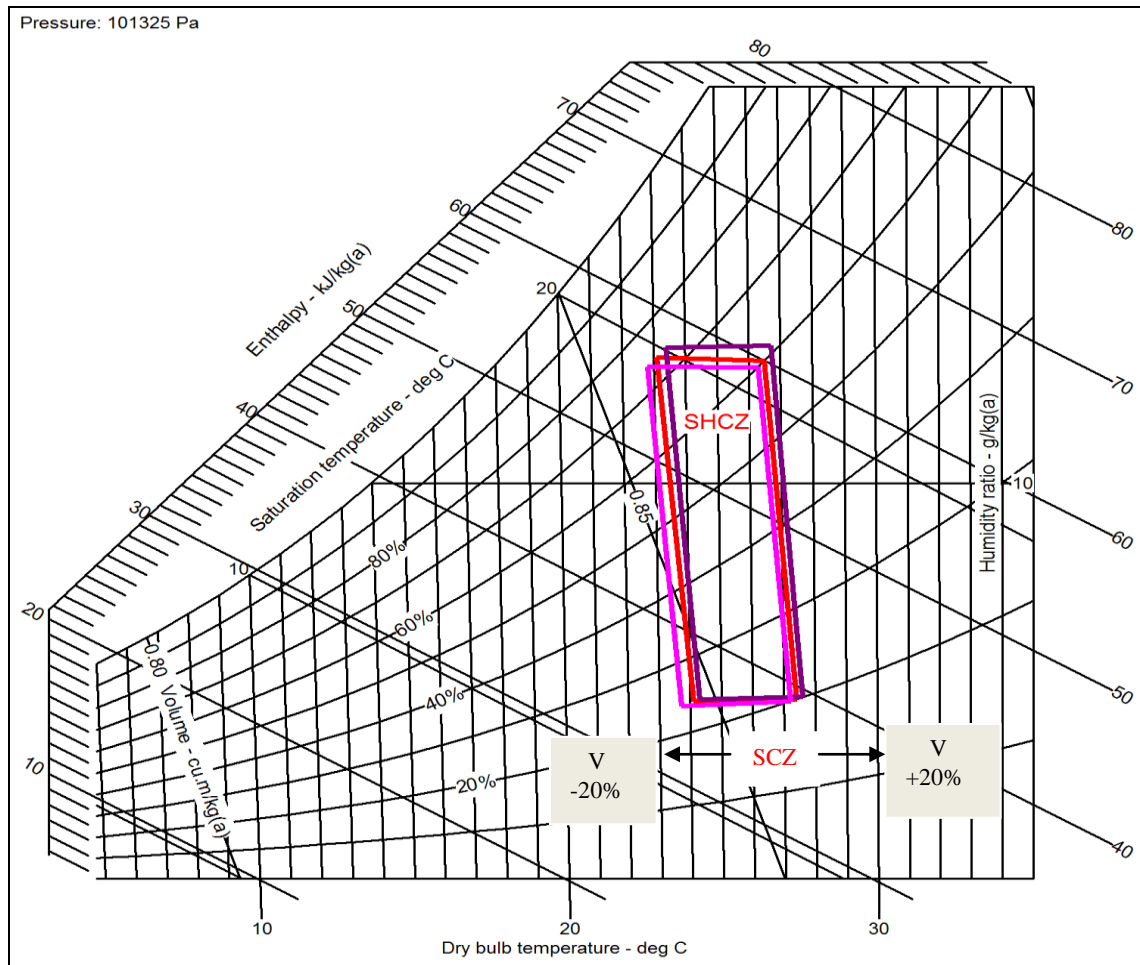
Figure 7.19: Air velocity sensitivity analysis of summer passenger thermal comfort zone according to Fanger model.
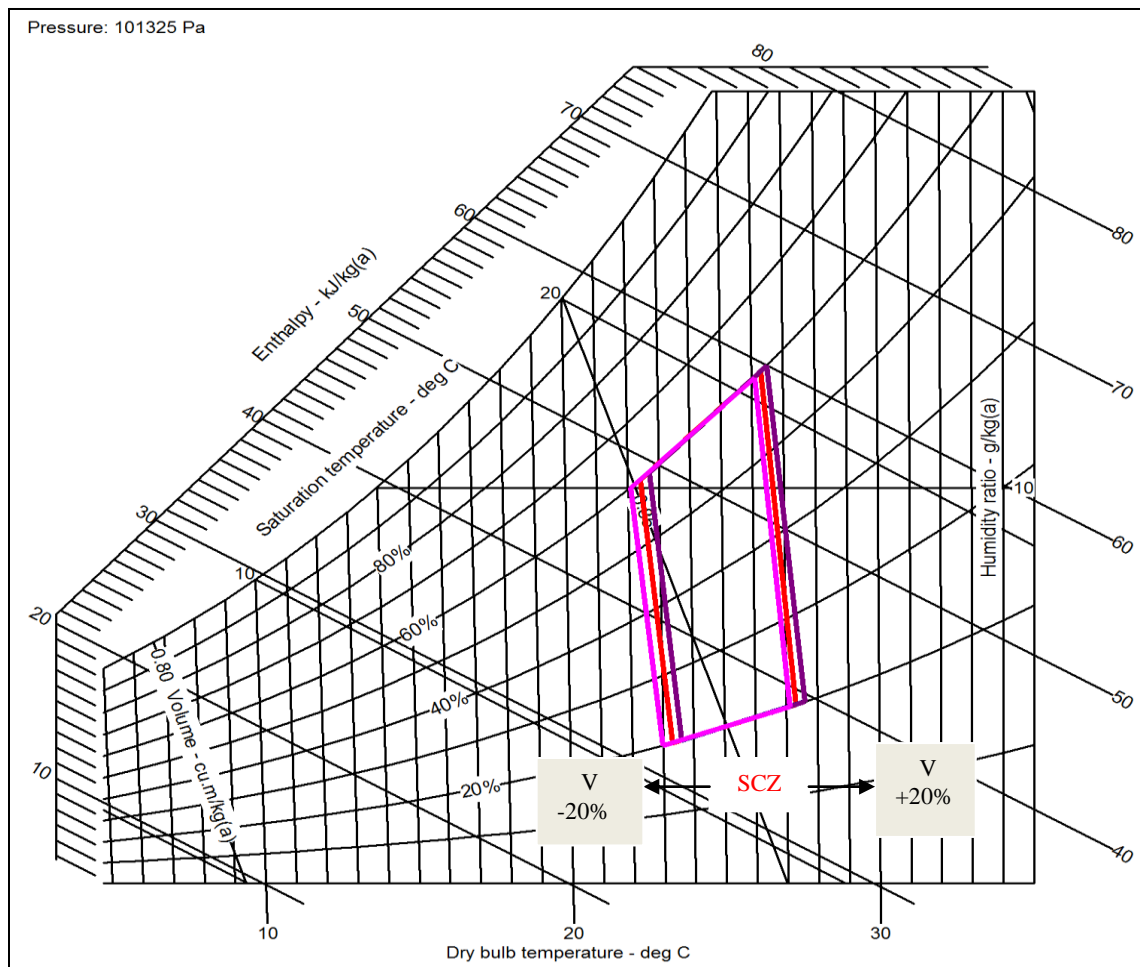
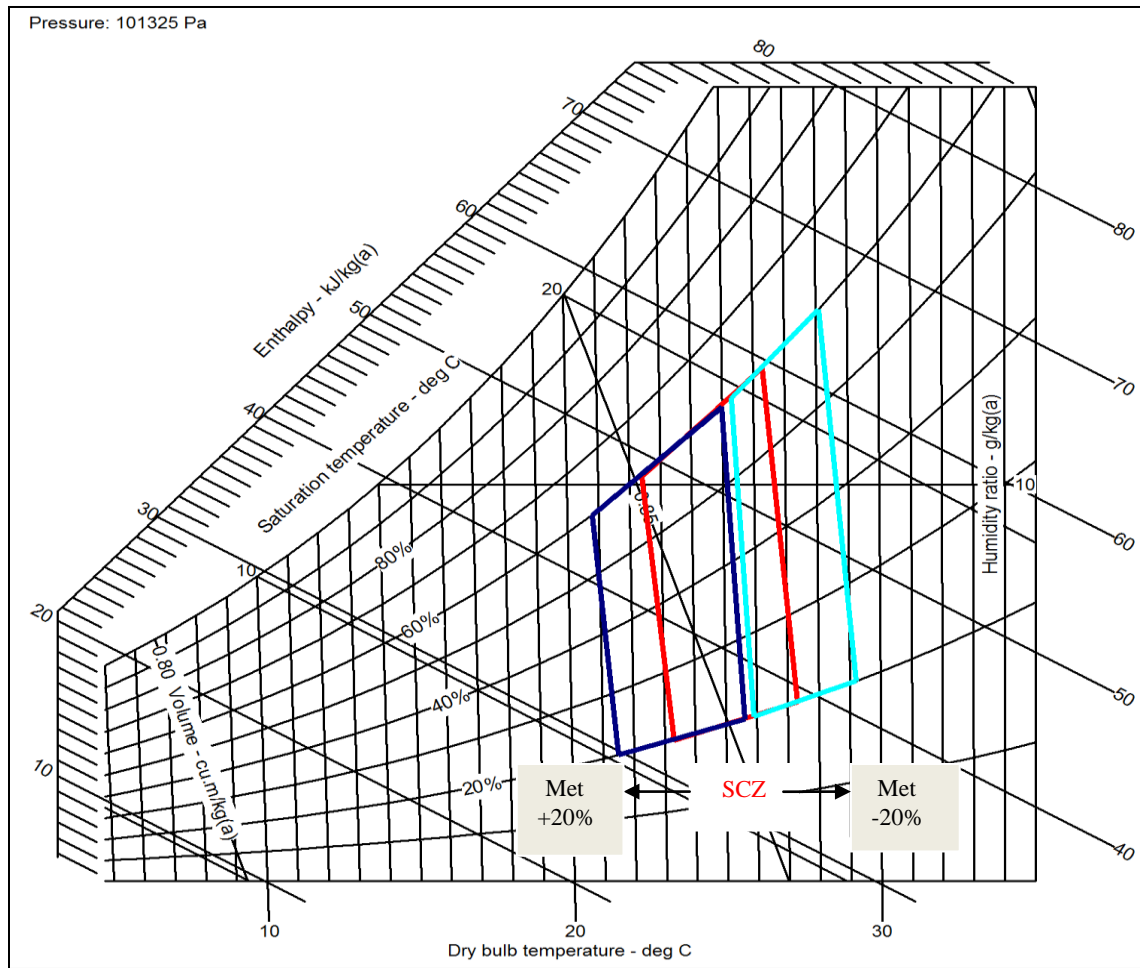**Figure 7.20:** Air velocity sensitivity analysis of summer passenger thermal comfort zone according to Berkeley model.

Figure 7.21: Air velocity sensitivity analysis of winter passenger thermal comfort zone according to Fanger model.

Figure 7.22: Air velocity sensitivity analysis of winter passenger thermal comfort zone according to Berkeley model.
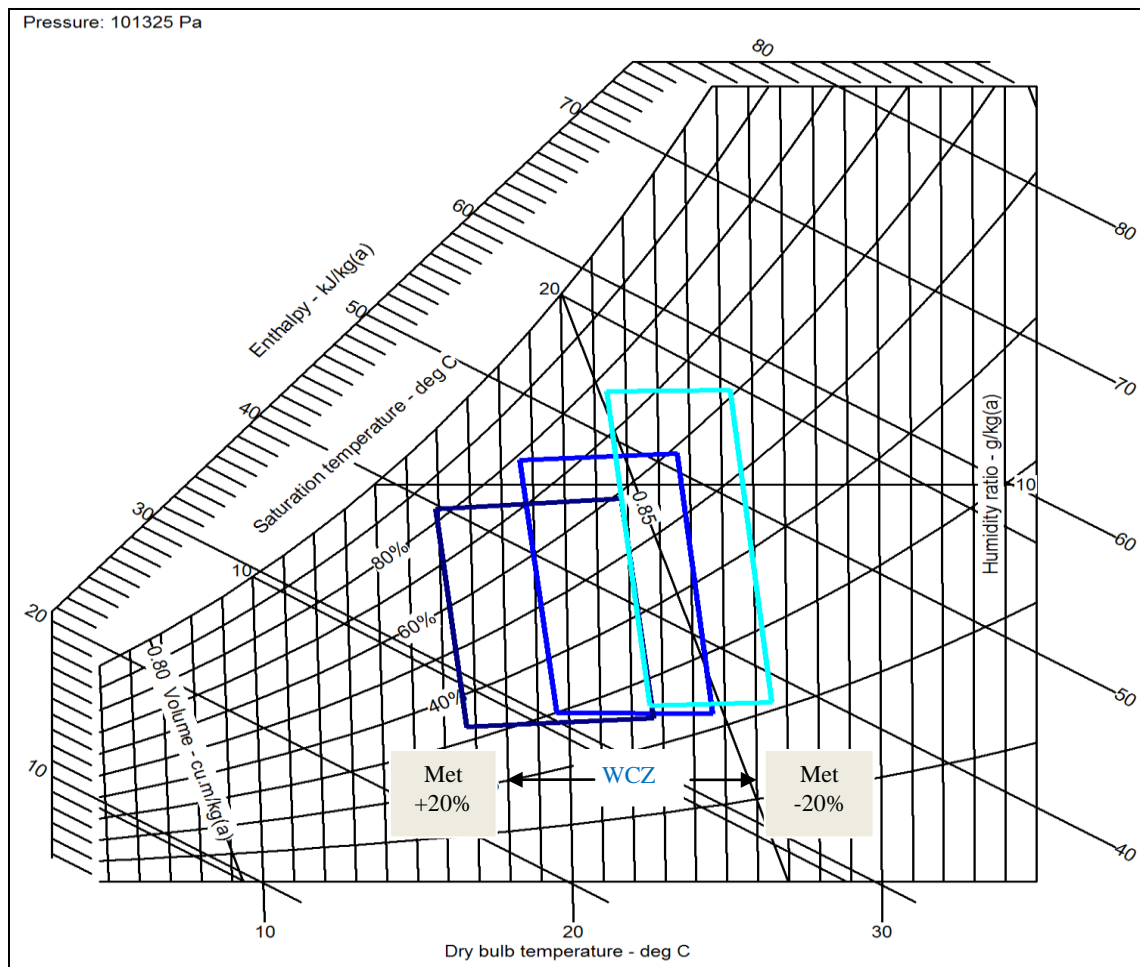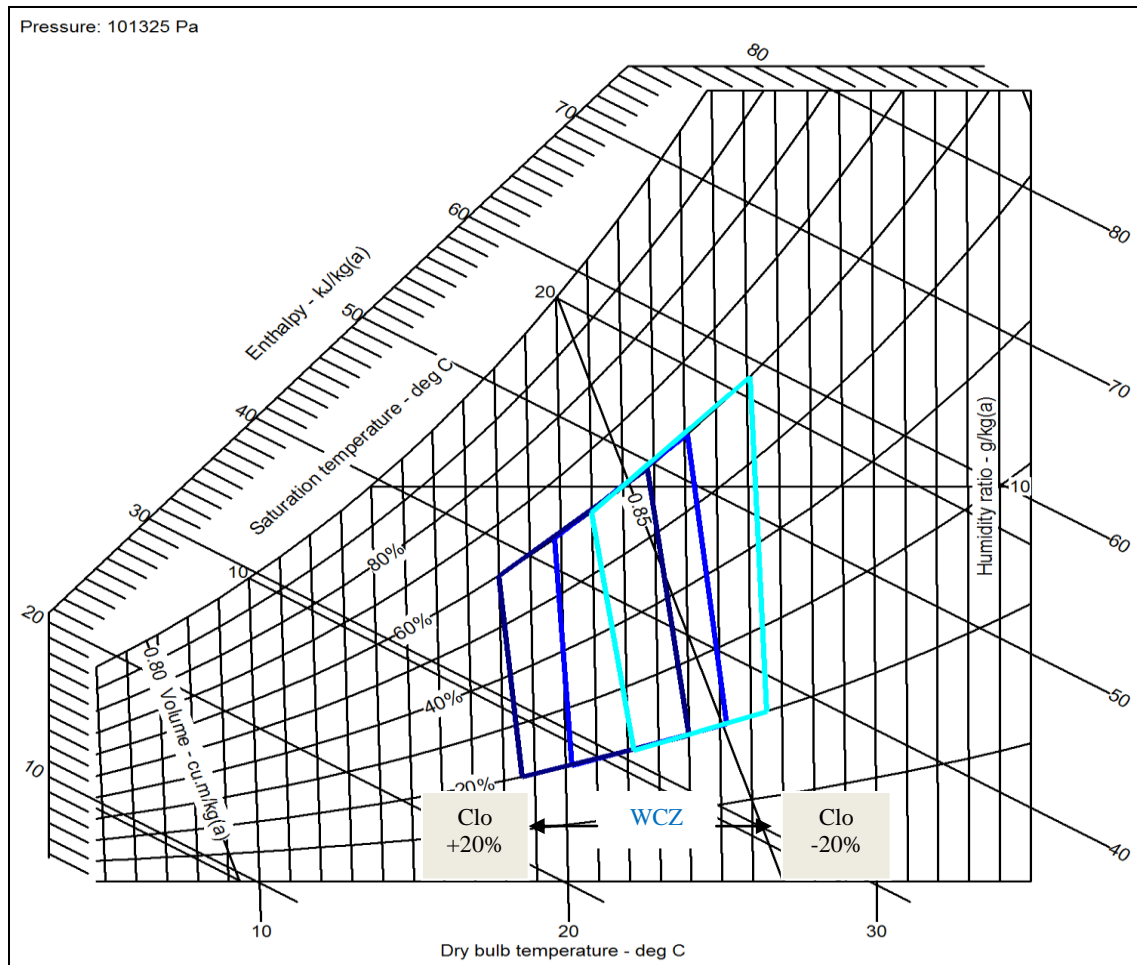
7.5.3.3 Clothing Insulation Sensitivity Analysis

The Clothing insulation sensitivity analysis of summer passenger thermal comfort zone according to Fanger and Berkeley models are depicted in figures 7.23 and 7.24 respectively. While it's the effect in winter period according to Fanger and Berkeley models are displayed in figures 7.25 and 7.26 respectively. During cold weather, layers of insulating clothing can help keep a person warm. At the same time, if the person is doing

a large amount of physical activity, lots of clothing layers can prevent heat loss and possibly lead to overheating. Generally, the thicker the garment is the greater insulating abilities it has. Depending on the type of material the clothing is made out of, air movement and relative humidity can decrease the insulating ability of the material. So, all the four mechanisms of heat transfer (Evaporation, convection, radiation and conduction) are greatly influenced by clothing. This can provide insulation to reduce mainly convective and radiant heat transfer (but also conductive – e.g. wearing gloves and protective clothing when hot or very cold surfaces/objects are handled. Shoes reduce heat loss/gain from the floor). Clothing can prevent air movement at the skin, which almost eliminates convective and evaporative heat transfer from the skin. The effect of clothing on evaporative heat transfer is dependent on the type of material. Clothing can also reduce radiant heat transfer, as the thermal resistance of the clothing will reduce the flow of heat from the body. In figures 7.23 to 7.26, as increases the clothing insulation, the thermal comfort zone will shift to the left, which leads the limits of the higher and lower temperature values will decrease. So, the new lower and upper temperature limits on the summer comfort window 22.1 and 26.8 °C respectively for Fanger model, and 22 and 26.8 °C respectively for Berkeley model. While on the winter comfort window temperature limits are 16.9 and 23.5 °C respectively for Fanger model, and 22.8 and 27.8 °C respectively for Berkeley model. On the opposite direction, when the air velocity decreases, the thermal comfort zone will shift to the right, which leads the limits of the higher and lower temperature values will increase. So, the new lower and upper temperature limits on the summer comfort window 24 and 28 °C respectively for Fanger

model, and 18.8 and 24.6 °C respectively for Berkeley model. While on the winter comfort window temperature limits are 20.4 and 25.7 °C respectively for Fanger model, and 20.8 and 26.1 °C respectively for Berkeley model.

The table 7.1 presented a concise of range of temperature and relative humidity for passenger thermal comfort zone with sensitivity analysis for summer and winter periods according to Fanger and Berkeley models.
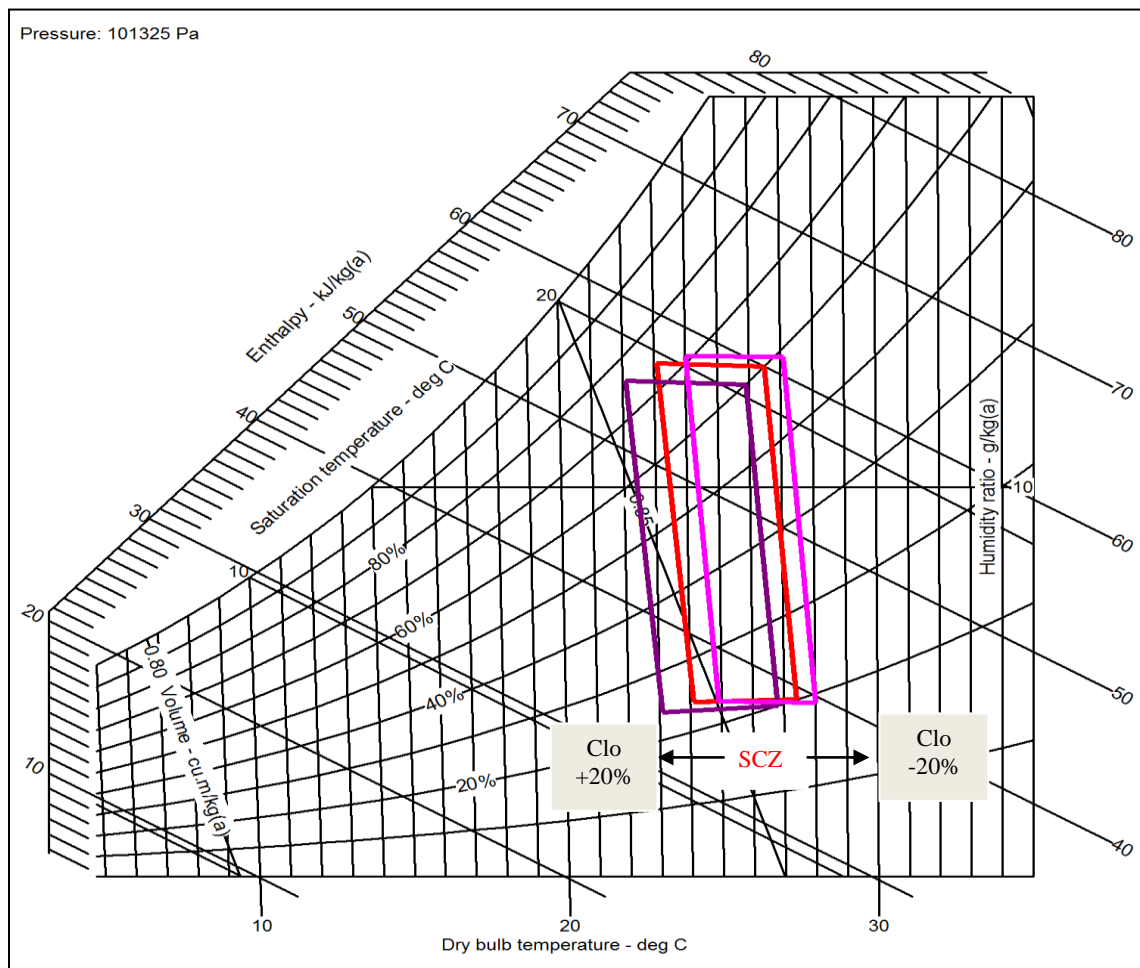
Figure 7.23: Clothing insulation sensitivity analysis of summer passenger thermal comfort zone according to Fanger model.
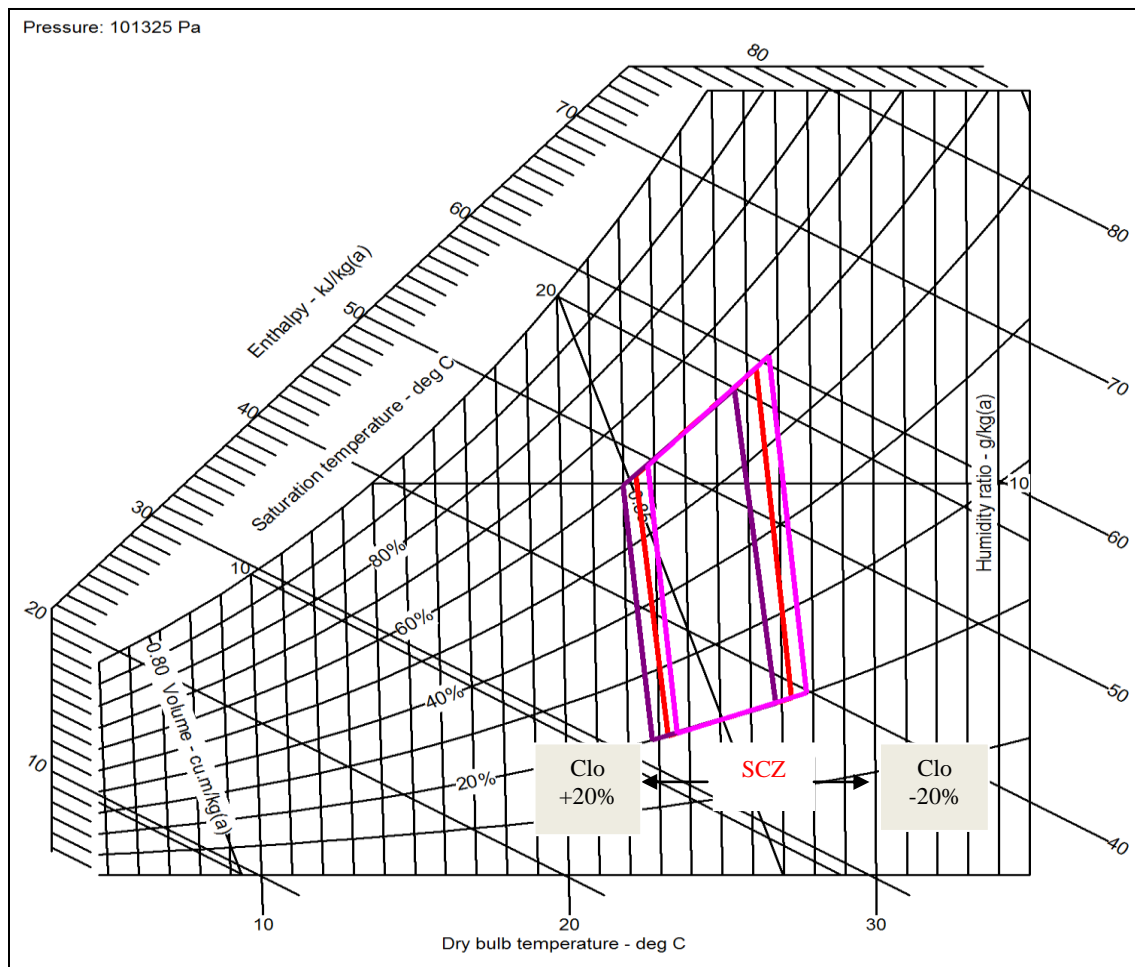
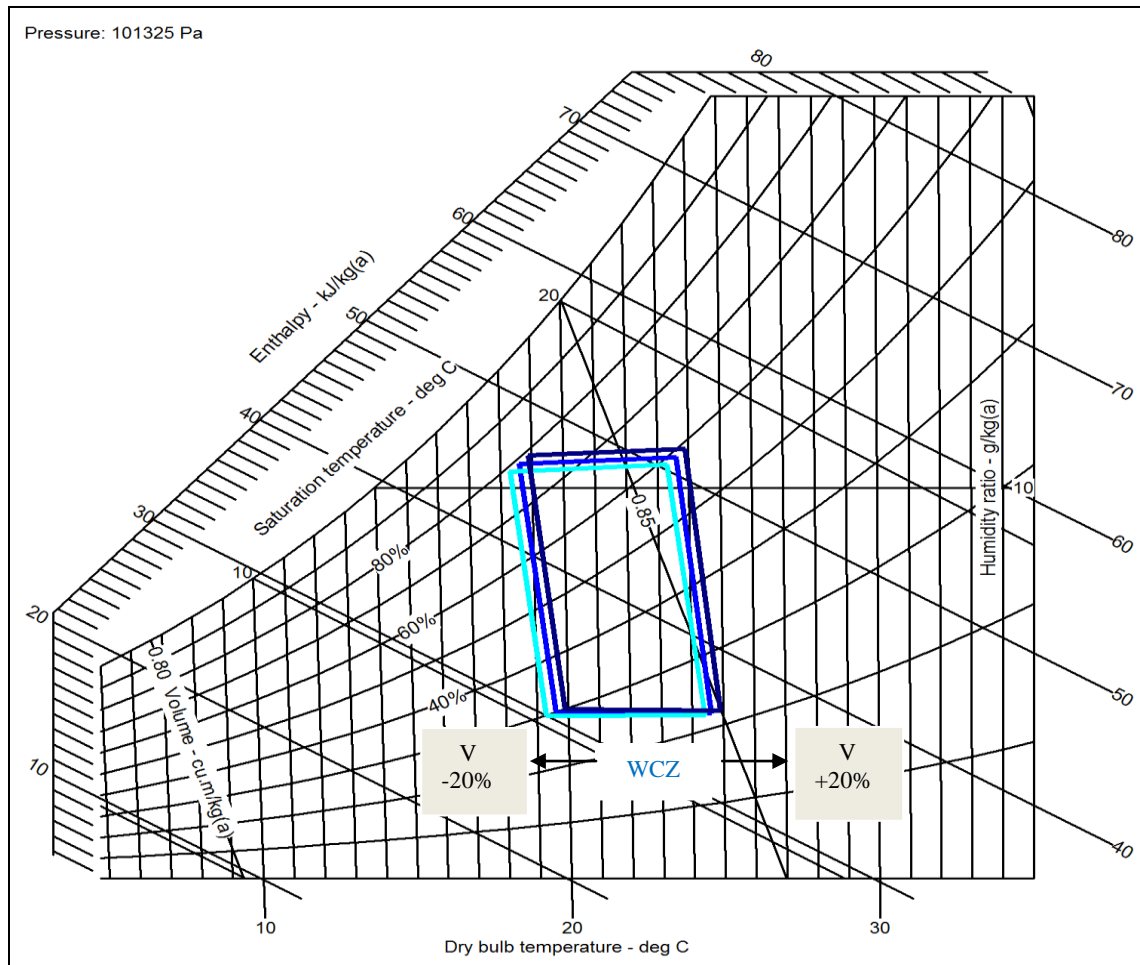**Figure 7.24:** Clothing insulation sensitivity analysis of summer passenger thermal comfort zone according to Berkeley model.
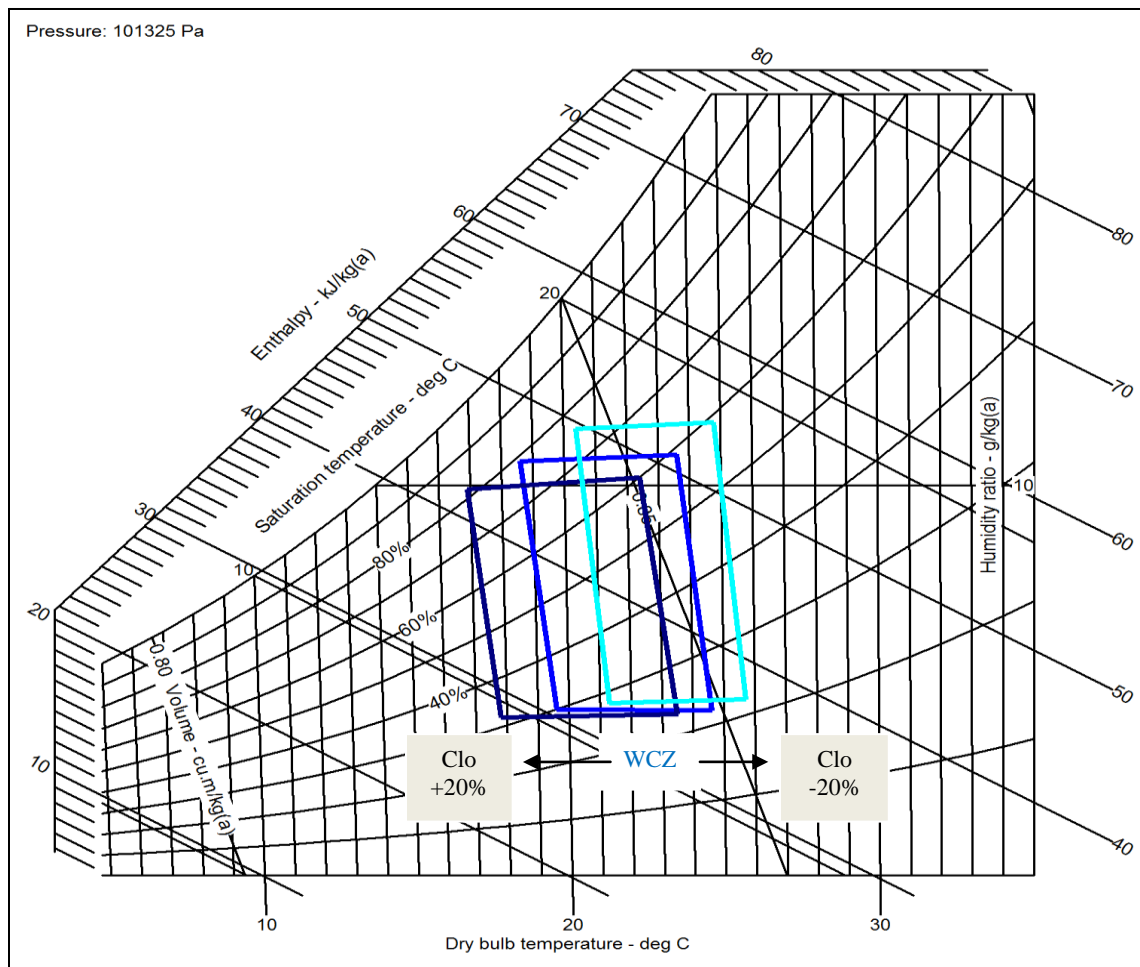
Figure 7.25: Clothing insulation sensitivity analysis of winter passenger thermal comfort zone according to Fanger model.
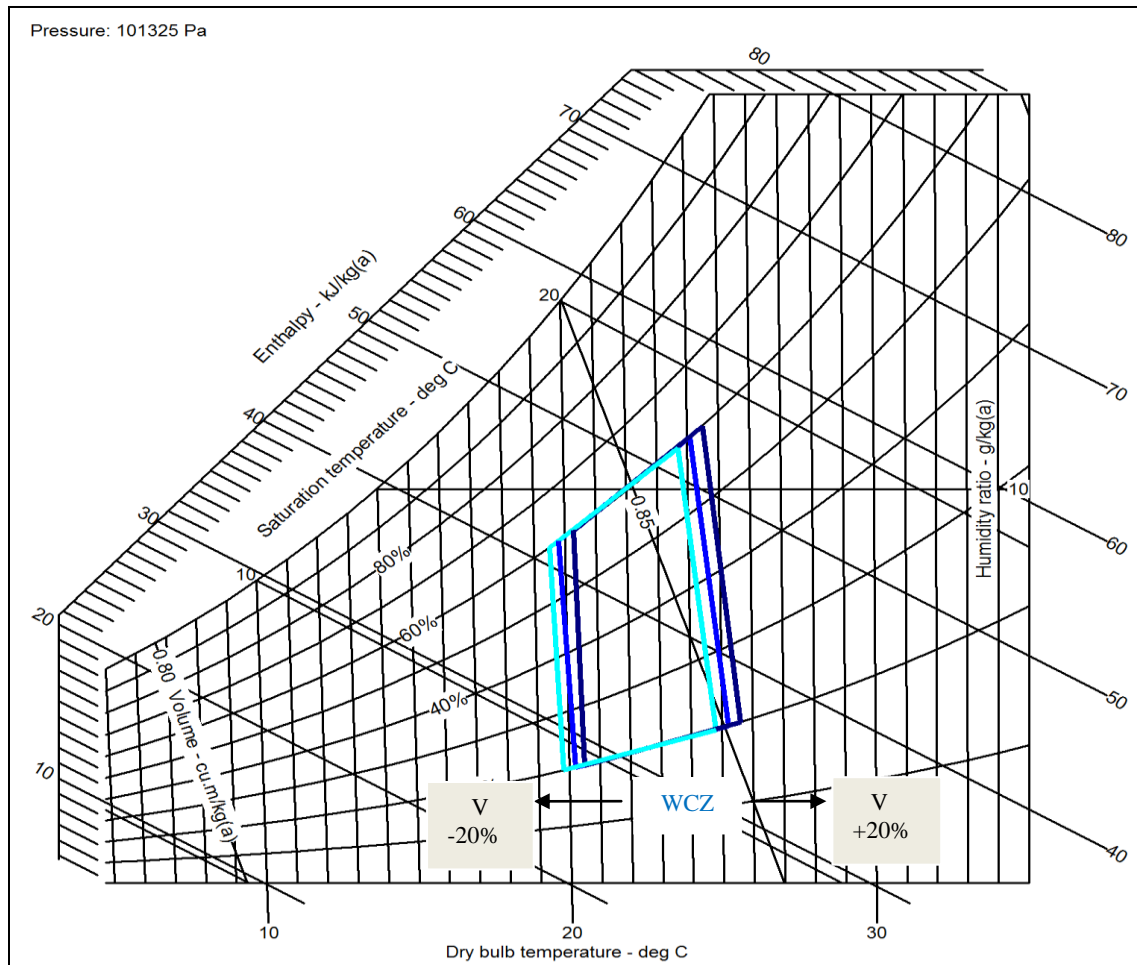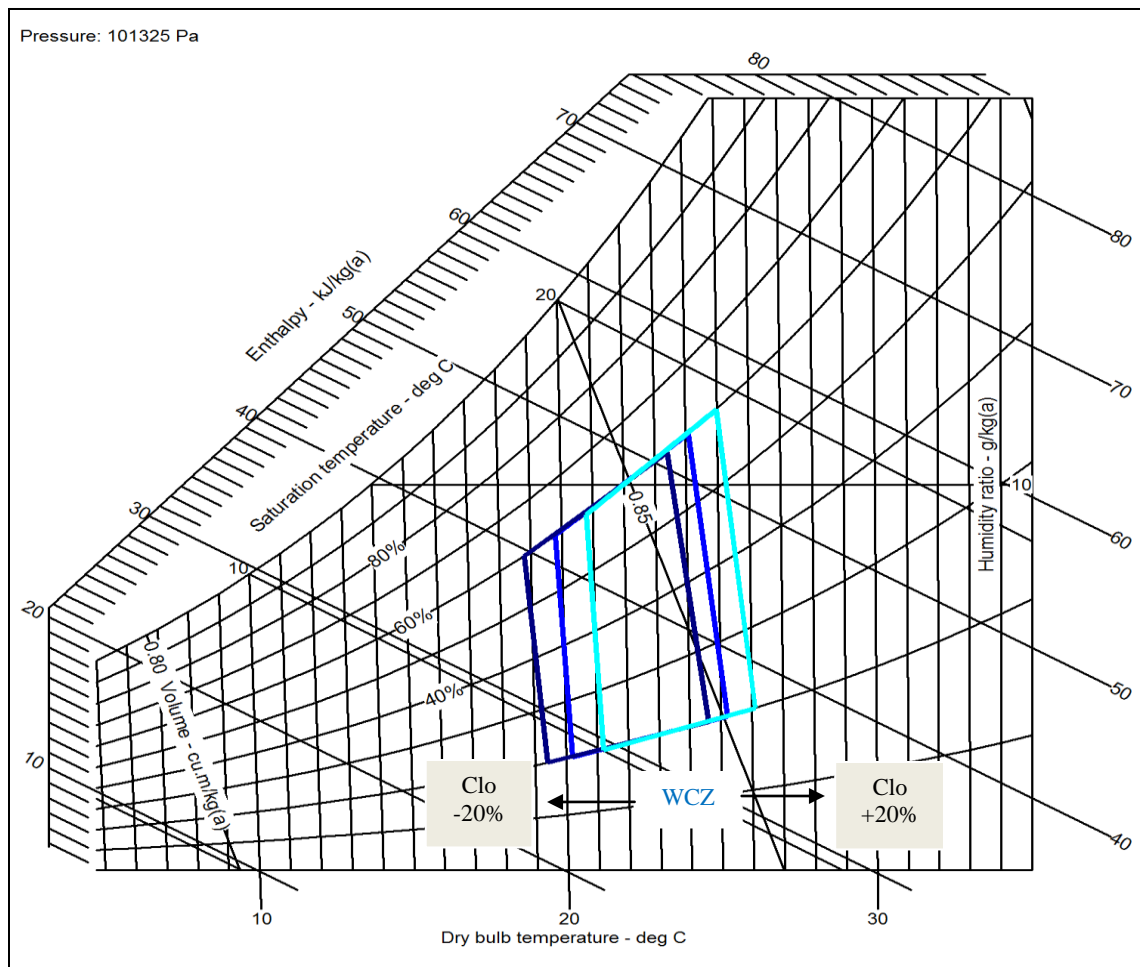
Figure 7.26: Clothing insulation sensitivity analysis winter passenger thermal comfort zone according to Berkeley model.

Table 7.1: Passenger thermal comfort zone limits with sensitivity analysis for summer and winter periods according to Fanger and Berkeley models.

	Summer Period			
	Fanger Model-PMV Index		**Berkeley Model**	
	T ºC-Range	**RH %- Range**	**T-Range**	**RH- Range**
*Standard	23.1-27.4	20-74 %	22.4-27.3	20-60 %
Metabolism (+ 20%)	21-26	21-73 %	20.8-25.6	20-60 %
Metabolism (-20%)	25.5-28.8	19-61 %	25.3-29.2	20-60 %
Velocity (+20%)	23.4-27.6	20-74 %	22.7-27.6	20-60 %
Velocity (-20%)	22.8-27.2	20-74 %	22.1-27.1	20-60 %
Clothing (+20%)	22.1-26.8	20-76 %	22-26.8	20-60 %
Clothing (-20%)	24-28	19-71 %	22.8-27.8	20-60 %
	Winter Period			
**Standard	18.6-24.6	22-79 %	19.8-25.2	20-60 %
Metabolism (+ 20%)	15.9-22.7	24-83 %	18-24	20-60 %
Metabolism (-20%)	21.4-26.5	21-77 %	21-26.5	20-60 %
Velocity (+20%)	18.9-24.9	22-79 %	20.3-25.6	20-60 %
Velocity (-20%)	18.3-24.4	22-79 %	19.5-24.8	20-60 %
Clothing (+20%)	16.9-23.5	23-82 %	18.8-24.6	20-60 %
Clothing (-20%)	20.4-25.7	22-76 %	20.8-26.1	20-60 %

*Metabolic rate: 1.4 met, Clothing insulation: 0.5 clo and Air velocity: 0.4m/s
**Metabolic rate: 1.4 met, Clothing insulation: 1 clo and Air velocity: 0.4m/s

7.6   Summary

This chapter developed the passenger thermal comfort zones during summer and winter periods. Two different models were used to generate the comfort windows Fanger and Berkeley models. The study results can be usefully summarized into following points;

-       The thermal conditions within these envelopes are estimated to be acceptable to 80 percent (Fanger model: $PMV = \mp 0.5$ or Berkely mode: $OS = \mp 0.5$) of the occupants when wearing the clothing ensemble indicated.

-        The temperature ranges on the summer comfort window are 23.1- 27.4 °C with 20-74 % RH for Fanger model, and 22.4 - 27.3°C with 20-60% RH for Berkeley model. While on the winter comfort window temperature limits are18.6- 24.6 °C with 22-79% RH for Fanger model, and 19.8- 25.2°C with 20-60% RH for Berkeley model.

-        When the metabolic rate increases, the thermal comfort zone will shift to the left, which leads the limits of the higher and lower temperature values will decrease and vice versa.

-        When the air motion across the skin increases, , the thermal comfort zone will shift to the right, which leads the limits of the higher and lower temperature values will a small increase and vice versa.

-        When the clothing insulation increases, the thermal comfort zone will shift to the left, which leads the limits of the higher and lower temperature values will decrease and vice versa.

CHAPTER EIGHT

CONCLUSION

8.1   Summary

This study analyzed the effect of controlling the RH along with dry-bulb temperature on the thermal comfort zone and sensation, in vehicular cabins. Three key techniques were used in this dissertation to validate our research; Firstly thermodynamic and psychometric analysis with practical implantation to investigated an actual embodiment of a system capable of RH manipulation through an evaporative cooling design. Additionally, the effect of each sub-system has been studied to quantify its effect on the sprayed water requirement, which affects the ultimate system size and accompanying accessories (tanks, etc). The thermal comfort has been also computed through the PMV and PPD indices using the Fanger model. The second technique is the use of a 3 dimensional finite differencing simulation, to predict the RH effect on the thermal local and overall sensation and comfort metrics during the summer and winter periods according to Berkeley model. Thirdly, the analysis and modeling of vehicular thermal comfort parameters using a set of designed experiments aided by thermography measurements. The experiments are conducted using a full size climatic chamber to host the test vehicle, to accurately assess the transient and steady state temperature distributions of the test vehicle cabins. Further investigate the thermal sensation and the human comfort under artificially created relative humidity scenarios. Finally, develop the passenger thermal comfort zones during summer and winter periods by using Berkeley

and Fanger models follows by sensitivity analysis. The study results can be usefully summarized into following points;

-        The presented study investigated the different challenges that exist in predicting and evaluating the thermal comfort for vehicular cabins when compared with thermal comfort in buildings i.e. static enclosures. These challenges are mainly related to the fast transient behaviors involved especially the cases of cooling the cabin after a hot soak condition, in addition to the non-uniformities in the thermal environment associated with the high localized air velocity, air temperature distribution, solar flux, and radiation heat flux from surrounding interior surfaces; in addition to other variations related to trip durations (driving distances) and passenger clothing levels.

-        Increasing the final relative humidity inside the passenger compartment reduces the amount of heat rejected thus making the AC system more efficient in terms of fuel consumption.

-        Starting the AC system under hot and dry air is more energy efficient than under hot and humid conditions.

-        Controlling the RH inside the cabin should take into consideration the initial RH value, because, as higher initial relative humidity values leads to higher amount of heat rejection.

-        Evaporative cooling system can be used to control the RH inside vehicles' cabin; however the sprayed water requirements will determine its packaging and weight constraints for automotive applications. The water requirements have been found in-

sensitive to the evaporative cooler and desiccant performances, but dependant on the amount of heat to be rejected.

-       At beginning of a cooling process; the higher the RH value, the more dominant the feeling of "hot" is. But at the end of the cooling process; the higher the RH value, the more comfortable the body feels.

-       The local sensation and comfort vote as computed for the different body segments during the heating period have the same behavior as that of the overall sensation and comfort. The RH has more influential effect at beginning of the cooling process, when the RH increases, the feeling of hot and uncomfortable increases especially for the feet. But at the end of cooling process; the effect of an increasing RH value on the comfort level becomes less pronounced.

-       At beginning of the heating process; the body feels uncomfortably cold, and during the heating process the body becomes more comfortable when the RH value is reduced.

-       The local sensation and comfort vote of the different body segments during the cooling process have nearly the same behavior as that of the overall sensation and comfort. The RH has no influential effect at beginning of the heating process. But during the heating process; the effect of an increasing RH value on the comfort level becomes influential for the hands and the feet. As the RH decreases inside the passenger cabin, so as the feeling of comfort.

The temperature ranges on the summer comfort window are 23.1- 27.4 °C with 20-74 % RH for Fanger model, and 22.4 - 27.3°C with 20-60% RH for Berkeley model. While on

the winter comfort window temperature limits are18.6- 24.6 °C with 22-79% RH for Fanger model, and 19.8- 25.2°C with 20-60% RH for Berkeley model.

8.2 Contribution

The main contributions of this dissertation as following;

- Proving that a dual control of RH along with DBT inside transient, non-homogenous vehicular cabins, can improve their air conditioning efficiency (in heating and cooling periods) in two folds; reducing the amount of heat removed (thermodynamics) to achieve comfort levels, and improving the human comfort sensation levels (psychometric) [30].

- The validation of a practical implementation; a system to manipulate RH and DBT inside vehicular cabins; through thermodynamic and psychometric calculations [30].

- Development of a simulation model that describes the human sensation and comfort states; LS, LC, OS and OC inside vehicular cabins; under transient, non-homogenous conditions [81, 98]

- Experimental and simulation studies generated optimized RH control plots for heating and cooling periods, inside non-homogenous and transient cabins [81, 98].

The thermal comfort windows for both summer and winter periods are developed using a combined approach of Fanger and Berkeley models [99].

- Analyses of Berkeley and Fanger models' sensitivities to personal condition and environmental conditions [99].

8.3   Future works

Following the investigations described in this thesis, a number of projects could be taken up, involving the modified human comfort on in cabin studied:

-    The building and testing of the evaporative cooling system is absolutely necessary because the economical and performance should be on a real system.

-    The thermal environment in an automobile is more difficult to control and evaluate compared to buildings environment due to the shape and size which may create considerable thermal asymmetry and inhomogeneous air temperature and velocity fields. Moreover, unlike air conditioned buildings, the climate of a car is more subjected to thermal transients than steady-state. So, for these reasons, more effort needed to develop of innovative methods and instruments able to predict the thermal sensation of driver and passengers under both transients and steady state conditions.

-    Develop a whole-body comfort index and dynamic comfort zone for Equivalent Homogenous Temperature (EHT) under transient conditions with non-uniform thermal environment.

-    Integrating previous models in vehicle applications to develop and evaluate fuel-saving, climate control systems (vapor compression system, cooling evaporative system).

-    Develop a method to determine on in-cabin temperature and on in-cabin relative humidity for minimum energy consumption regarding an adequate human thermal comfort level.

REFERENCES

[1]   J. Rugh, V. Hovland, National and world fuel savings and CO_2 emission reductions by increasing vehicle air conditioning COP, Proceedings from the 2003 Alternate Refrigerant Systems Symposium in Phoenix, AZ (2003).

[2]   A. Alahmer, Ahmed Mayyas, Abed Mayyas, M. Omar, D. Shan, Vehicular thermal comfort models; a comprehensive review, Applied Thermal Engineering 31 (6-7) (2011) 995-1002.

[3]   M. Cisternino, Thermal climate in cabs and measurement problems, Paper for the CABCLI seminar – EC Cost Contract No SMT4-CT98-6537 (DG12 BRPR), (1999), Dissemination of results from EQUIV – EC Cost Contract No SMT4-CT95-2017.

[4]   T. Han, L. Huang, A sensitivity study of occupant thermal comfort in a cabin using virtual thermal comfort engineering, Proc. of the SAE World Congress Detroit, Michigan, April 11-14, SAE (2005)-01-1509.

[5]   T. Han, L. Huang, S. Kelly, C. Huizenga, Z. Hui, Virtual thermal comfort engineering, Proc. of the SAE World Congress, Detroit, Michigan, March 5-8, SAE (2001) -01-0588.

[6]   ANSI/ASHRAE Standard 55-1992, Thermal environmental conditions for human occupancy, Atlanta: American Society of Heating, Refrigerating and Air Conditioning Engineering Inc; (1992).

[7]   J. Rugh, R. Farrington, D. Bharathan, A. Vlahinos, R. Burke, C. Huizenga, H. Zhang, Predicting human thermal comfort in a transient nonuniform thermal environment, Eur J Appl Physiol 92 (2004) 721–727.

[8]   T. Doherty, E. Arens, Evaluation of the physiological bases of thermal comfort models, ASHRAE Transactions 94 (1) (1988) 15.

[9]   N. Martinho1, M. Silva, J. Ramos, Evaluation of thermal comfort in a vehicle cabin, Proc. of InstnMech. Engrs 218 Part D: J. Automobile Engineering, (2004).

[10]   T. Madsen, B. Olesen, N. Kristensen, Comparison between operative and equivalent temperature under typical indoor conditions, ASHRAE Trans. 90 (1) (1984) 1077–1090.

[11]   O. Kaynakli, M. Kilic, An investigation of thermal comfort inside an automobile during the heating period, Applied Ergonomics 36 (3) (2005) 301-312.

[12]   O. Kaynakli, E. Pulat, M. Kilic, Thermal comfort during heating and cooling periods in an automobile, Heat Mass Transfer (2005) 41: 449–458.

[13]   O. Kaynakli, U. Unver, M. Kilic, Evaluating thermal environments for sitting and standing posture, Int Commun Heat Mass Transfer 30 (8) (2003) 1179–1188.

[14]   T. Han, L. Huang, A model for relating a thermal comfort scale to EHT comfort index, Proc. of the SAE World Congress Detroit, Michigan March 8-11, (2004), SAE 2004-01-0919.

[15]   F. Mattiello, C. Malvicin, S. Mola, M. Magini, Soft air diffusion to improve the thermal comfort - a design approach based on CFD tool and virtual thermal manikin, Proce. of the Automotive & Transportation Technology Congress & Exhibition October 1- 3, Barcelona, Spain, SAE (2001)-01-3439.

[16]   M. Kulkarni, F. Hong, An experimental technique for thermal comfort comparison in a transient pull down, Building and Environment 39 (2004) 189 – 193.

[17]   T. Cengiz, F. Babalık, An on-the-road experiment into the thermal comfort of car seats, Applied Ergonomics 38 (3) (2007) 337-347.

[18]   K. Shek, W. Chan, Combined comfort model of thermal comfort and air quality on buses in Hong Kong, Science of the Total Environment 389 (2008) 277 – 282.

[19]   W. Chakroun, S. Al-Fahed, Thermal comfort analysis inside a car, International Journal of Energy Research 21 (1997) 327-340.

[20]   A. Mezrhab, M. Bouzidi, Computation of thermal comfort inside a passenger car compartment, Applied Thermal Engineering 26 (2006) 1697–1704.

[21]   H. Zhang, L. Dai, G. Xu, Y. Li, W. Chen, W. Tao, Studies of air-flow and temperature fields inside a passenger compartment for improving thermal comfort and saving energy, Part I: Test/numerical model and validation, Applied Thermal Engineering 29 (2009) 2022–2027.

[22] H. Zhang, L. Dai, G. Xu, Y. Li, W. Chen, W. Tao, Studies of air-flow and temperature fields inside a passenger compartment for improving thermal comfort and saving energy, Part II: Simulation results and discussion, Applied Thermal Engineering 29 (2009) 2028–2036.

[23] Y. Zhang, R. Zhao, Relationship between thermal sensation and comfort in non-uniform and dynamic environments, Building and Environment 44 (2009) 1386–1391.

[24] T. Han, K. Chen, B. Khalighi, Assessment of various environmental thermal loads on passenger thermal comfort, SAE (2010)-01-1205.

[25] T. Han, K. Chen, Assessment of various environmental thermal loads on passenger compartment soak and cool-down analyses, SAE (2009)-01-1148.

[26] L. Huang, T. Han, A case study of occupant thermal comfort in a cabin using virtual thermal comfort engineering, EACC (2005), 2nd European Automotive CFD Conference, Frankfurt, Germany, 29 - 30 June 2005.

[27] G. Karimi, E. Chan, J. Culham, Experimental study and thermal modeling of an automobile driver with a heated and ventilated seat, Proc. of the SAE World Congress, SAE (2003)-01-2215.

[28] M. Fountain, E. Arens, T. Xu, F. Bauman, M. Oguru, An investigation of thermal comfort at high humidities, ASHRAE Transactions 105 (2) (1999) 94-103.

[29] Z. Guerra, Evaporative air conditioner for automotive application, Master Dissertation, Department of mechanical engineering, Massachusetts institute of technology, USA, (1994).

[30]   A. Alahmer, M. Omar, A. Mayyas, S. Dongri, Effect of relative humidity and temperature control on in-cabin thermal comfort state; thermodynamic and psychometric analyses, Applied Thermal Engineering 31 (14-15) (2011) 2636-2644.

[31]   I. Holmèr, Thermal manikin history and applications, Eur J Appl Physiol 92 (2004) 614–618.

[32]   R. Musat, E. Helerea, Parameters and models of the vehicle thermal comfort, Acta Universitatis Sapientiae, Electrical and Mechanical Engineering 1 (2009) 215-226.

[33]   S. Tanabe, E. Arens, F. Bauman, H. Zhang, T. Madsen, Evaluating thermal environments by using a thermal manikin with controlled skin surface temperature, ASHRAE Transactions 100 (1) (1994) 39-48.

[34]   H. Nilsson, Thermal comfort evaluation with virtual manikin methods, Building and Environment 42 (12) (2007) 4000–4005.

[35]   H. Nilsson, Comfort climate evaluation with thermal manikin methods and computer simulation models, Ph.D. Thesis, Department of Civil and Architectural Engineering Royal Institute of Technology, Sweden Department of Technology and Built Environment, University of Gävle, Sweden, (2004).

[36]   R. McGuffin, R. Burke, C. Huizenga, Z. Hui, A. Vlahinos, G. Fu, Human thermal comfort model and manikin, SAE (2002)-01-1955.

[37]   J. Rugh, D. Bharathan, Predicting human thermal comfort in automobiles, Vehicle Thermal Management Systems Conference and Exhibition, Toronto, Canada, SAE (2005)-01-2008.

[38]   K. Mahmoud, E. Loibner, B. Wiesler, C. Samhaber, Simulation-based vehicle thermal management system-concept and methodology, SAE world congress, Detroit, Michigan, SAE (2003)-01-0276.

[39]   A. Curran, S. Peck, T. Schwenn, M. Hepokoski, Improving cabin thermal comfort by controlling equivalent temperature, AeroTech Congress & Exhibition, Seattle, WA, USA, SAE (2009)-01-3265.

[40]   A. Arakawa, K. Saito, W. Gruver, Automated infrared imaging temperature measurement with application to upward flame spread studies: Part I, Combustion and Flame 92 (1993) 222-230.

[41]   C. Qian, H. Ishida, K. Saito, Upward flames spread along PMMA vertical corner walls: Part II, mechanism of "M" Shape pyrolsis front formation, Combustion and Flame 99 (1994) 331-338.

[42]   S. Burch, V. Hassani, T. Penney, Use of infra-red thermography for automotive climate control analysis, Proc. of the SAE World Congress, SAE (1993) - 921136.

[43]   M. Korukçu, M. Kilic, The usage of IR thermography for the temperature measurements inside an automobile cabin, International Communications in Heat and Mass Transfer 36 (8) (2009) 872-877.

[44]   J. Orosa, Research on general thermal comfort models, European Journal of Scientific Research 27 (2) (2009) 217-22.

[45] ISO 7730: 2005, Analytical determination and interpretation of thermal comfort using calculation of the PMV and PPD indices and local thermal comfort criteria, Ergonomics of the thermal environment, (2005).

[46] F. Butera, Chapter 3-Principles of thermal comfort, Renewable and Sustainable Energy Reviews 2 (1998) 39-66.

[47] K. Parsons, Human thermal environments: The effects of hot, moderate and cold environments on human health, comfort and performance, 2nd ed., Taylor and Francis, Washington, (2002).

[48] P. Fanger, Thermal comfort: Analysis and applications in environmental engineering, McGraw-Hill Co., New York, (1970).

[49] P. Fanger, Thermal comfort, McGraw-Hill Co., New York, (1973).

[50] K. Charles, Fanger's Thermal comfort and draught models, Institute for Research in Construction, Report RR-162, Ottawa, Oct. (2003).

[51] R. Nevins, Thermal comfort and drafts, Journal de Physiologie 13 (1971) 356-358.

[52] ISO 7730, Moderate thermal environments-Determination of the PMV and PPD indices and specification of the conditions for thermal comfort, Geneva, (1994).

[53] D. DuBois, E. DuBois, A formula to estimate surface area if height and weight are known, Archive s of internal medicine 17 (1916) 863.

[54] ASHRAE 1989a, Physiological principles, comfort and health, Fundamentals handbooks, Atlanta, (1989).

[55]   E. McCullough, B. Jones, A comprehensive data base for estimating clothing insulation, Institute for environmental research, Kansas state university, IER technical report 84-01, December (1984).

[56]   H. Zhang, Human thermal sensation and comfort in transient and non-uniform thermal environments, Ph.D. Thesis, University of California Berkeley (2003).

[57]   E. Arens, H. Zhang, C. Huizenga, Partial- and whole body thermal sensation and comfort, Part I: uniform environmental conditions, Journal of Thermal Biology 31 (2006) 53-59.

[58]   E. Arens, H. Zhang, C. Huizenga, Partial- and whole body thermal sensation and comfort, Part II: non-uniform environmental conditions, Journal of Thermal Biology 31 (2006) 60-62.

[59]   H. Zhang, E. Arens, C. Huizenga, T. Han, Thermal sensation and comfort models for non-uniform and transient environments: Part I: local sensation of individual body parts, Building and Environment 45 (2) (2010) 380-388.

[60]   H. Zhang, E. Arens, C. Huizenga, T. Han, Thermal sensation and comfort models for non-uniform and transient environments: Part II: local comfort of individual body parts, Building and Environment 45 (2) (2010) 389-398.

[61]   H. Zhang, E. Arens, C. Huizenga, T. Han, Thermal sensation and comfort models for non-uniform and transient environments: Part III: whole body sensation and comfort, Building and Environment 45 (2) (2010) 399-410.

[62]   T. Han, K. Chen. Assessment of various environmental thermal loads on Vehicular compartment soak and cool-down analyses, SAE (2009)-01-1148.

216

[63] RadTherm 10.0.0, Commercial thermal analysis code. ThermoAnalytics Inc. (2010).

[64] A. Auliciems, S. Szokolay, Thermal comfort, Passive and Low Energy Architecture International in association with Department of Architecture, The University of Queensland Brisbane 4072, (2007).

[65] F. Rohles, J. Woods, R. Nevins, The influence of clothing and temperature on thermal comfort, ASHRAE Transactions 79 (1973) 71-78.

[66] R. Sonntag, C. Borgnakke, G. Wylen, Fundamentals of thermodynamics, 6th ed., John Wiley & Sons Inc, New York, (2002).

[67] Y. Çengel, M. Boles, Thermodynamics an engineering approach, 6th ed., Mc Graw/Hill, (2008).

[68] F. Incropera, D. Dewitt, Fundamentals of heat and mass transfer, 4th ed., John Wiley & sons Inc, New York, (1996).

[69] Karimi G., Chan E.C., Culham J.R., Linjacki I., Brennan L. Thermal comfort analysis of an automobile driver with heated and ventilated seat. Proc. of the SAE World 2002; 2002-01-0222.

[70] J. Hensen, Literature review on thermal comfort in transient conditions, Building and Environment 25 (1990) 309–316.

[71] The Animal protection institute, "How hot do cars get?", Available : http://mydogiscool.com/x_car_study.php , last cited:August 8, 2011.

[72] I. Atmaca, A. Yigit, Predicting the effect of relative humidity on skin temperature and skin wettedness, Journal of Thermal Biology 31 (2006) 442–452.

[73]   F. Wiley, L. Newburgh, The relationship between the environment and the basal insensible loss of weight, J. Clin. Inves. 10 (1931) 689.

[74]   C. Winslow, L. Herrington, A. Gauge, Physiological reactions of the human body to various atmospheric humidities, Am. J. Physiol. 120 (1937) 288.

[75]   S. Szokolay, Introduction to architectural science, the basis of sustainable design, 2nd ed., Elsevier, 2008.

[76]   W. Woodson, Barry Tillman, Peggy Tillman, Human Factors Design Handbook, 2nd ed., McGraw-Hill Book Company; 1992.

[77]   C. Balaras, A. Argiriou, Infrared thermography for building diagnostics, Energy and Buildings 34 (2002) 171−183.

[78]   S. Chu, Studies of using infrared flash thermography (FT) for detection of surface cracks, subsurface defects and water-paths in building concrete structures, Master of philosophy thesis, Department of manufacturing engineering management, City university of Hong Kong, Hong Kong, July 2008.

[79]   T. Astarita, G. Gardone, G. Carlomango, Infrared thermography: an optical method in heat transfer and fluid flow visualisation, Optics and Lasers in Engineering 44 (2006) 261−281.

[80]   A. Moropoulou, N. Avdelidis, The role of emissivity in infrared thermographic imaging and testing of building and structural materials, in: X.P.V. Maldague (Ed.), Thermosense XXIV, SPIE Press, Orlando, Florida, USA, (2002) 281−287.

[81]   A. Alahmer, M. Omar, A. Mayyas, A. Qattawi, Analysis of vehicular cabins'
         thermal sensation and comfort state, under relative humidity and temperature
         control, using Berkeley and Fanger models, Building and Environment 48 (2012)
         146-163.

[82]   Sookchaiya, V. Monyakul, S. Thepa, Assessment of the thermal environment
         effects on human comfort and health for the development of novel air
         conditioning system in tropical regions, Energy and Buildings 42 (10) (2010)
         1692-1702.

[83]   ASHRAE Standard 62-2001: ventilation for acceptable indoor air quality,
         American Society of Heating, Refrigerating and Air Conditioning Engineers Inc.,
         Atlanta, GA, (2001).

[84]   Honeywell, Engineering manual of automatic control for commercial buildings
         Minneapolis: Honeywell, 1997.

[85]   D. Stipanuk, Hospitality facilities management and design, 2nd ed., Lansing, MI:
         Educational Institute of the American Hotel and Lodging Association, 2002.

[86]   ASHRAE Standard 55-2004, Thermal environmental conditions for human
         occupancy, American Society of Heating, Refrigerating and Air-Conditioning
         Engineers Inc., Atlanta, 2004.

[87]   Sensirion Co., "Conditions of thermal comfort influence of humidity and
         temperature on personal well-being", Available:
         http://www.sensirion.com/en/pdf/product_information/Conditions_Thermal_Com
         fort_V2.0_C1.pdf ,   last cited: September 8, 2011.

[88]   H. Tsutsumi, T. Akimoto , T. Suzuki, Effects of low humidity on sensation of eye dryness caused by using different type of contact lenses in summer season, Proceedings of Indoor Air (2002) 394–399.

[89]   N. Yamtraipat, J. Khedari, J. Hirunlabh, Thermal comfort standards for air conditioned buildings in hot and humid Thailand considering additional factors of acclimatization and education level, Solar Energy 78 (2005) 504–517.

[90]   N. Yamtraipat, J. Khedari, J. Hirunlabh, J. Kunchornrat, Assessment of Thailand indoor set-point impact on energy consumption and environment, Energy Policy 34 (7) (2006) 765–770.

[91]   T. Ibamoto, Study on higher temperature and low humidity air conditioning (Part1-Part4), Annual Meeting of SHASE, (2000) (2001):Part1-2: 821-828:Part3-4: 1325-1332.

[92]   T. Lin , R. Hwang , K. Huang , C. Sun , Y. Huang, Passenger thermal perceptions, thermal comfort requirements, and adaptations in short- and long-haul vehicles, Int J Biometeorol 54 (2010) 221–230 .

[93]   M. Silva, C. Alcobia, N. Martinho, J. Ramos, Indoor environment in vehicles, Int J Veh Des 42 (1–2) (2006) 35–48.

[94]   S. Paulke, M. Ellinger, S. Wanger, Air conditioning cabin simulation with local comfort rating of passenger, 2nd European Workshop on Mobile Air Conditioning and Auxiliary System-ATA/CRF, 29- 30 November 2007, Torino-Italy.

[95]   C. Huizenga, Z. Hui, E. Arens, A model of human physiology and comfort for assessing complex thermal environments. Build Environ 36 (6) (2001) 691–699.

[96]   Ergonomics 4 schools, "The learning zone-temperature", Available: http://www.ergonomics4schools.com/lzone/temperature.htm last cited: September 8, 2011.

[97]   "Human Comfort and health requirements", Chapter 1, Available: http://courses.washington.edu/me333afe/Comfort_Health.pdf, last cited: September 8, 2011.

[98]   A. Alahmer, M. Abed-Al hameed, M. Omar, Design for thermal sensation and comfort states in vehicles cabins, Accepted, Applied thermal Engineering.

[99]   A. Alahmer, M. Omar, Develop of passenger thermal comfort zones during summer and winter periods with sensitivity analysis, Under Review, Building and Environment.